Aspects of Modelling Solid Tumours

James W. Schofield

Balliol College
University of Oxford

A thesis submitted for the degree of
Doctor of Philosophy

Trinity Term 2010

Abstract

This thesis considers aspects of modelling solid tumours. We begin by considering the common assumption that nutrient or drug concentrations in avascular tumour spheroids are radially symmetric. We derive a simple Poisson equation for biomolecular diffusion into an avascular tumour, but with highly oscillatory boundary conditions due to the surrounding capillary network. We find that the assumption of radial symmetry is legitimate for biomolecules that are taken up in sufficient quantities by proliferating cancer cells; however radially symmetric profiles need not be observed otherwise.

We then investigate how the gap between an avascular tumour and the neighbouring vasculature varies as the tumour grows. This is explored by (i) using scaling arguments based on ordinary differential equations, (ii) coupling the rate of oxygen flux from the vasculature to oxygen evolution within the tumour, and (iii) deriving a system of six coupled nonlinear partial differential equations modelling the tumour evolution. It is found that as the tumour grows any initial gap between the tumour and neighbouring vasculature closes since there is no mechanism which would sufficiently up-regulate non-cancerous cell proliferation. This is in contrast to the intra-cornea implantation observations, upon which several mathematical models are based.

Finally, we study the growth and treatment of a vascular tumour subjected to chemotherapies, particularly when the therapies can exhibit an anti-angiogenic effect and resistance to the therapy is incorporated. A multi-compartment model is derived for the evolution of a tumour undergoing treatment and parameters are estimated, with extensions to incorporate numerous different therapy protocols in the literature. We find that anti-angiogens can be effective, though the appropriate scheduling is counter-intuative and contradicts many standard therapy rules. We conclude that

chemotherapy protocol design is very sensitive to the mode of action of the drug and simple general strategies will, in many cases, not be the most effective.

Acknowledgements

There are many people whose contribution to my thesis, and the last four years of my life, should be acknowledged.

As a supervisor, Professor Philip Maini has been a source of tireless support and encouragement. I am indebted to him for the immense contribution he has made to my thesis. I do not think the task of guiding me through a DPhil was an enviable one and the fact that he has managed to do so is testament to how good a supervisor he has been. Furthermore, his ability to proof read hundreds and hundreds of pages of (often poorly written) mathematics and always provide attentive, constructive comment is quite simply staggering.

I am equally indebted to my other co-supervisor, Dr Eamonn Gaffney. He has provided me with unwavering guidance and direction throughout the duration of my DPhil, at all hours of the day and night, and his input has been invaluable. Furthermore, his perseverance at trying to get me to understand the difference between "effect" and "affect" have been admirable; I am sorry I was a slow learner.

Thanks too should go to Dr Bob Gatenby, from the H. Lee Moffitt Cancer Center and Research Institute, and Dr. T. Velpandian, from the All India Institute of Medical Sciences, for their help with papers which are in the process of being born from my thesis.

Further back in my academic career there are many people I should acknowledge, but Dr Peter Howell, Miss Hooton, and Mr Oates especially so. Whilst they have not contributed to my thesis directly, without them this thesis would not exist.

I should also thank all the people who have helped make my Oxford career a largely healthy and happy one.

To all my colleagues in the CMB who became my friends, particularly Charlotte, Stevie, Matt, Alex, Phil, Natasha, and Ruth, thank you. Copa and then the PT will never be the same again.

To all the friends and acquaintances I have made elsewhere, thank you. I hope that you have enjoyed it all at least as much as I did. Particular mention should go to Xav, Robin, Megan, and Spooley, who have put up with more than their fair share of grief from me, Simon, who has kept me warm and dry for the past 4 years, and Emily, who made a brief cameo at the end of my Oxford career and was an exemplary housemate, things are so different now you're gone, I thought it'd be easy, I was wrong. Recognition should also go to the house of boys, Stevie, Neelio, Robbie, and Sinapinos, for supplying me with what is likely to be the funnest year of my life, and all the other friends I made at Univ. Deep down I know that's going to be what I remember when I reminisce about Oxford.

Also, I can't not mention the massive part that OUTriC has played in my Oxford career. Although, I'm not sure what has been more significant, the part that it's played in my life or the part that I've played in its. Either way I hope that it's been symbiotic.

Finally, I should acknowledge all the bodies who've allowed me to remain solvent during my DPhil. Thank you to the Engineering and Physical Sciences Research Council for my funding. Thank you also to the Mathematical Institute, Balliol College, and sweet Univ, for paying me for various forms of teaching.

Contents

List of Figures

Chapter 1

Introduction

In this thesis we will be considering aspects of modelling solid tumours. In particular we will consider avascular tumour growth and how avascular tumour spheroids interact with the neighbouring vasculature as they grow. We will also be considering the evolution of vascular tumours and their response to drugs, and in particular their response to drugs which exhibit some anti-angiogenic effect. The mathematical modelling of solid tumours is an extensive field with much active research. It is not feasible to introduce the entire field here and the mathematical modelling specifically relevant to each chapter will be presented in the introduction to that chapter. However we now provide a brief overview of the biological background that is relevant throughout this thesis.

1.1 Motivation

In 2007 cancer caused 7.9 million deaths worldwide (around 13% of all deaths) (www.who.int). Specifically in England, more than one in three people will be diagnosed with cancer at some point of their lives and one in four people will die of the disease (Donnellan, 2003). In a bid to overcome the disease, cancer therapy has been an area of intense research for a number of years. Since 1971, when the American President declared "war on cancer", America has invested over $200 billion into cancer research (Begley, 2008), yet despite this cancer deaths are expected to continue rising with a projected 13 million deaths world wide in 2030 (www.who.int). The war on cancer remains intense.

1.2 What is Cancer?

Throughout this section we use Hanahan and Weinberg (2000), and Kleinsmith (2006) as sources of information.

Cancer is actually a generic term used to describe over 100 chronic diseases which can affect any part of the body. It is difficult to define cancer in a way which characterises every variant of the disease, but the following six traits are common to most, if not all, types of human cancers:

1. Cancer cells can proliferate in the absence of the mitogenic growth signals which normal cells require for proliferation.
2. Cancer cells are insensitive to the anti-growth signals which inhibit proliferation in normal cells.
3. Cancer cells can evade apoptosis, which is a form of programmed cell death which contributes to regulating normal cell growth.
4. Cancer cells can replicate a limitless number of times.
5. Cancer cells can cultivate their own blood supply, via a process called angiogenesis.
6. Cancer cells can invade neighbouring tissues and spread via metastasis, which is the process by which some diseased cells separate from the primary diseased tissue and invade healthy tissue elsewhere in the body.

The unrestrained division of cancer cells will cause a growth, or swelling, of tissue[1]. Any swelling caused by abnormal tissue growth is known as a tumour, however not all tumours are cancerous. A tumour which is cancerous is called malignant, whereas a tumour which does self-limit its growth and does not invade healthy tissue is called benign.

[1]Note that leukaemias are cancers which develop from blood-forming cells in bone marrow. These cancers are characterised by the accumulation of abnormal white blood cells in the patient's bloodstream and do not arise as solid growths of tissue.

1.3 The "Life Cycle" of a Malignant Tumour

Throughout this section we use Carmeliet and Jain (2000), Michor et al. (2004), and Kleinsmith (2006), as sources of information.

It is widely accepted that cancer is initiated by mutations in cancer-susceptible genes. These genes are typically those which regulate cell growth in some way, either by controlling cell birth or death directly, or by suppressing tumours, or by controlling the cell environment in a way which affects cell division. If these genes mutate then it can become possible for cells to grow and divide without restraint. The mutation of a single gene is usually not sufficient to cause full-blown cancer; for malignancy to occur a number of mutations are necessary. For example, the initiation of colorectal cancer requires a sequence of four or five mutations (Knudson, 2001). These gene mutations can be the result of carcinogens, or can be randomly acquired through errors in DNA replication, or can be inherited.

If a malignant tumour becomes established then the net proliferation rate within the tumour is typically higher than the surrounding tissue and this causes the tumour to grow in size. As the tumour gets bigger its surface area to volume ratio decreases. Eventually this ratio will become so small that not enough nutrients can diffuse into the tumour to adequately feed it and this lack of nutrients will begin to inhibit tumour growth. Eventually the tumour will reach a maximum size where the amount of nutrient diffusing into the tumour is only just enough to sustain its size and it cannot continue to grow. This regulation process is called diffusion-limited control. The maximum volume a tumour spheroid can reach in this way is typically $1\text{mm}^3 - 2\text{mm}^3$ (Bicknell et al., 1997). A tumour of this size will not be fatal for its host.

For a tumour to grow to a larger size than this it must increase the quantity of nutrients available to it. To do this the tumour releases numerous growth factors which induce capillary growth into the tumour. Once the capillaries have grown into the tumour it has more nutrients available to it and can continue to grow in size.

The process by which a tumour cultivates its own capillaries is known as tumour angiogenesis. Tumours which have yet to undergo angiogenesis are known as avascular and tumours which have undergone angiogenesis are known as vascular.

Once angiogenesis has taken place tumour cells from the primary tumour can travel to different parts of the body via the circulatory system and establish secondary tumours in different parts of the body; this process is known as metastasis. Before angiogenesis

has taken place a tumour will be too small to kill its host, but after angiogenesis, and then metastasis, the host is likely to end up suffering from multiple tumours, any of which could grow to a fatal size. This makes the process of angiogenesis a critical step in malignant tumour growth.

1.4 The Structure of an Avascular Malignant Tumour

Throughout this section we use Carmeliet and Jain (2000), Michor et al. (2004), and Kleinsmith (2006) as sources of information.

A tumour will begin as a single cancerous cell. This cell will divide into two cells and these cells will then in turn divide and so on and a small clump of cancerous cells will develop. At this stage of tumour development the tumour cells divide in a roughly uniform manner which causes most tumours to grow in a comparatively spherical way, unless constrained by the local environment, in which case spherical growth will not be possible.

Once a tumour spheroid has grown to a large enough size, typically 150 μm in diameter, cells at the centre of the tumour stop dividing. The cells which have stopped dividing are called quiescent cells and the cells which are still dividing are known as proliferating cells. Despite its importance to tumour growth little is known about the onset of quiescence. It is known that it is not simply driven by nutrient depletion at the centre of the tumour and instead a combination of other factors, including cell-cell interaction and the availability of growth factors, are likely to be important (Freyer, 1998; Mueller-Klieser, 2000).

As the tumour continues to grow the proliferating rim on the surface of the tumour will maintain an approximately constant thickness, typically 2-4 cells deep (LaRue et al., 2004) and the tumour core remains quiescent. When the tumour reaches a certain size, typically 600 μm or so in diameter, cells at the centre of the tumour begin to die. The region of the tumour where cells have died is known as the necrotic core. Whilst the precise reason for this cell death is currently unknown it is often analogised, with some success, that the cells at the centre of the tumour die when the radius of the tumour exceeds the diffusion distance of a critical factor, which is typically taken to be oxygen (Mueller-Klieser, 2000).

As the tumour continues to grow the region consisting of the proliferative rim and the quiescent region, known as the viable rim, maintains an approximately constant depth and the necrotic core increases in size.

An illustration of the structure of a well-developed avascular tumour is shown in Figure 1.1.

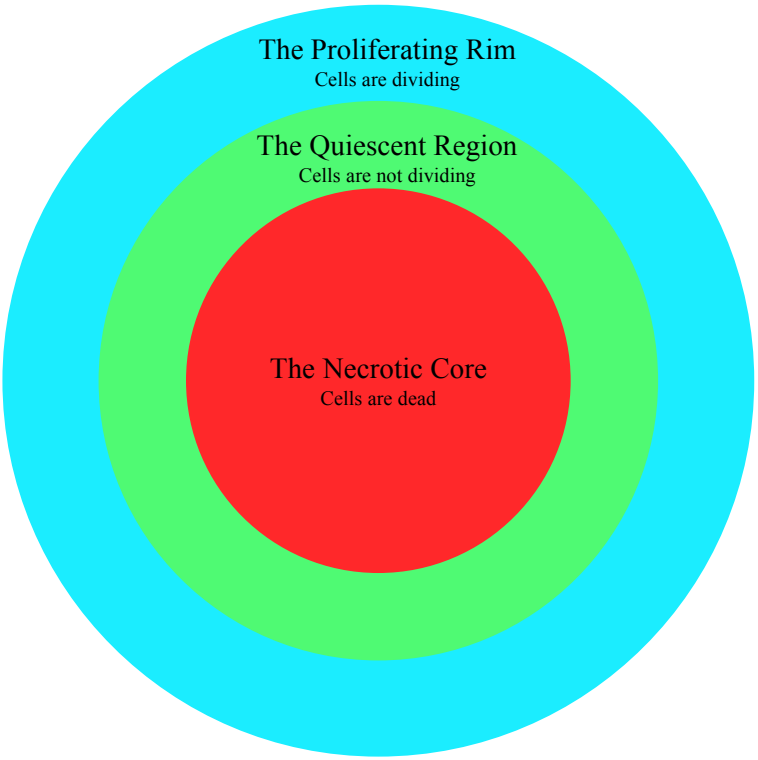

Figure 1.1: A schematic cross-section of a well-developed avascular tumour (not to scale).

1.5 The Cell Cycle

Throughout this section we use Murray and Hunt (1994), Andreef et al. (2000), and Alberts et al. (2002) as sources of information.

Cancer cells characteristically exhibit different proliferation dynamics to non-cancerous cells. As such a basic understanding of the cell cycle is necessary for understanding the evolution of cancer cells.

Immediately following a cell division the new daughter cells enter the G_1 phase of the cell cycle. This is a growth phase where the newly formed cells increase in size and synthesise the proteins required for the next phase of the cell cycle.

Following the G_1 phase there is a checkpoint where the cell monitors the progress of the cell cycle and if the cell has grown suitably, and conditions are appropriately favourable, then the cells enter the S phase of the cell cycle. During the S, or synthesis, phase all the DNA in the cell is replicated.

Following the S phase the cell undergoes the G_2 phase, a second growth phase, which prepares the cell for division.

Following the G_2 phase there is another cell cycle checkpoint and if conditions are suitably favourable then it enters the M phase where it undergoes mitosis and divides. The M phase begins with the cell's nucleus dividing into two identical nuclei and then the cell also divides into two identical cells. Each of these new daughter cells then enter the G_1 phase of the next cell cycle.

If conditions are not favourable during the G_1 phase, then cells can arrest from the cell cycle and enter the G_0 phase. During this phase the cells are quiescent, and are not dividing nor preparing to divide. Cells in the G_0 phase can rejoin the cell cycle when conditions become more favourable, but can arrest in the G_0 phase for a limitless amount of time before doing so.

The G_1, S, and G_2 phase of the cell cycle are collectively known as the interphase portion of the cell cycle.

A diagram illustrating the cell cycle is shown in Figure 1.2.

1.6 Cancer Therapies

Throughout this section we use Carmeliet and Jain (2000), www.cancer.gov (2002), Michor et al. (2004), www.cancer.gov (2005), and Kleinsmith (2006) as sources of information.

1.6.1 Current Therapies

The ultimate goal of cancer therapy is the complete removal of the cancerous tissue without damage to the rest of the body. In theory it is possible to cure the patient by

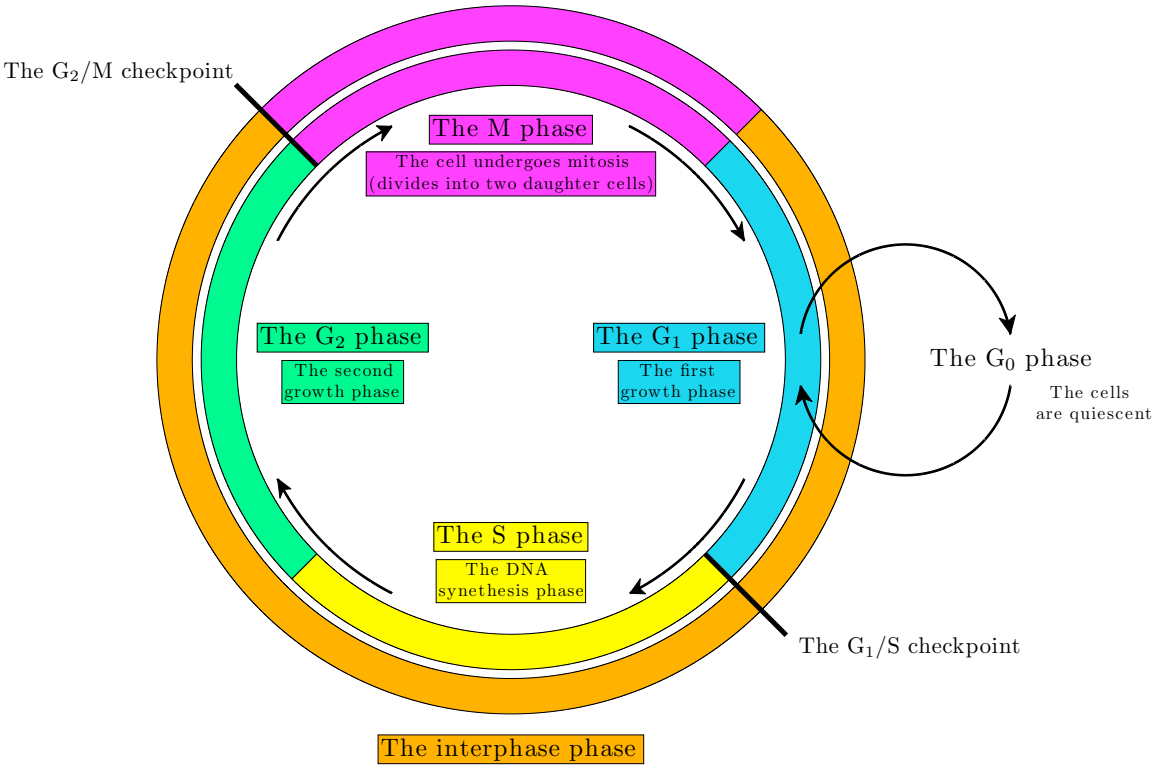

Figure 1.2: A schematic of the cell cycle.

surgically removing all cancerous tissues. However tumours are not always accessible and a cancer's ability to invade adjoining tissue and metastasise to other parts of the body often makes the complete removal of all cancerous tissue impossible. Also, many tumours will not be detectable until they are too big to be removed surgically.

Instead it is often necessary to treat the tumour by attempting to poison it without fatally damaging healthy tissues. The two most common cancer therapies which do this are radiotherapy, which uses ionising radiation to poison the tumour, and chemotherapy, which uses drugs to poison the tumour.

The radiation used in radiotherapy damages the affected cell's genetic material in a way which makes it impossible for the cells to grow and divide. The radiation can either come from an internal source, where radioactive material is placed within the host's body, or an external source, where radiation waves are passed through the host. The radiation used in radiotherapy will also damage healthy cells, although a larger proportion of healthy cells than diseased cells will recover once radiotherapy has ceased. In an attempt to minimise the damage to healthy cells the dose of

radiation is focused upon the tumour cells, but side-effects are still inevitable. Cells are more sensitive to radiotherapy in the presence of oxygen and if a tumour becomes hypoxic (deficient in oxygen) then it can become relatively resistant to the effects of the radiation. If the tumour is particularly resilient to radiation then it might not be possible to successfully treat the tumour without using a dose of radiation which would be fatal for the patient, even if the radiotherapy were given in many small doses to encourage healthy tissue recovery between doses.

The drugs used in chemotherapy typically target cells which are dividing and impair cell division. Cancer cells tend to divide more quickly than non-cancerous cells and so chemotherapy will target cancer cells; however healthy cells which are dividing will also be destroyed and healthy cells with a high replacement rate will be particularly affected. These healthy cells will typically recover once the chemotherapy has ceased. Chemotherapy aims to deliver a high dose of the drug to the tumour, whilst also delivering a dose of the drug to the rest of the patient which is low enough to prevent major side-effects yet high enough to destroy any metastases present. Typically this will involve delivering the drug intravenously but the drug can also be delivered in a number of different ways, including orally. If the tumour is particularly resilient to the chemotherapeutic agent then it might not be possible to successfully treat the tumour without using a dose which would be fatal for the patient, even if the chemotherapy were given in many small doses to allow healthy tissue to recover between doses.

Surgery, radiotherapy and chemotherapy are the three well established cancer treatments and usually a combination of the three will be used to treat a patient. Alternative therapies do exist for cancer treatment, although these are generally specific to a particular type of cancer or are newer therapies which have yet to become well established.

Hormonal therapy can be used to treat cancers in hormonally responsive tissue such as breast or prostrate. The growth of these cancers can be controlled by altering the hormone levels in the surrounding tissue and in some cases it is even possible to induce tumour cell death.

Immunotherapy is any therapy which attempts to use the patient's own immune system to destroy cancer cells. This typically involves either vaccinating the patient so that their immune system can recognise tumour cells as cells to be destroyed, or giving the patient therapeutic antibodies which use their own immune system to destroy cancer cells. Immunotherapy is currently used as a treatment for some forms

of cancer, including cancer of the sympathetic nervous system and small cell lung cancer, but it is not yet an effective treatment for all types of cancer.

An anti-angiogenic therapy is any therapy which attempts to control tumour growth by preventing or rescinding angiogenesis. The first study concerning the potential use of anti-angiogenic therapies was conducted in 1998 when angiostatin and endostatin were successfully used to make tumours shrink and disappear in mice. Since then dozens of angiogenesis inhibiting drugs have undergone clinical trials to try and reproduce these results in humans.

The early trials on humans showed that anti-angiogenic drugs exhibit much milder side-effects than chemotherapy or radiotherapy and tumours did seem to stop growing in a few patients, but results were generally disappointing. The trials have so far only used patients with well-developed tumours, but it has been suggested that anti-angiogenic drugs might be more effective at treating patients with early stage tumours and that this may have contributed to the disappointing results. It is hoped that the use of anti-angiogenic drugs to treat human cancers will become much more effective once the optimal treatment schedules have been found.

In 2004 Avastin become the first anti-angiogenic drug to be approved by the U.S. Food and Drug Administration (FDA) for routine medical use in cancer patients. This was after clinical trials showed that patients with metastatic colon cancer who received chemotherapy in conjunction with Avastin lived longer than patients who received chemotherapy alone. Avastin works by targeting and inhibiting the action of a natural protein called vascular endothelial growth factor (VEGF) which tumours excrete to induce angiogenesis. Avastin binds to VEGF and blocks its ability to stimulate capillary growth.

Avastin is currently used in conjunction with chemotherapy for the treatment of metastatic colon cancer and most forms of metastatic non-small cell lung cancer. However Avastin is prone to resistance and the mechanisms by which tumours become resistant to Avastin are not currently well understood (Schneider and Sledge Jr., 2007). There are several clinical studies currently underway to determine the effectiveness of Avastin in treating several other forms of cancer.

1.6.2 Future Therapies

Cancer therapy is an area of intense active research. Whilst established therapies are continuing to be improved there are new therapies being developed which could potentially provide more effective cancer treatments.

Targeted therapy refers to any treatment which targets the molecules which are specifically needed for tumour growth, rather than simply targeting cells which are dividing. Certain cancers have a palpable "molecular driver" which encourages cancer progression and targeted therapies act to inhibit the action of such drivers (www.cancer.gov, 2006a). In early clinical trials targeted therapies were found which caused a dramatic response in most patients with a dose of therapeutic below the maximum dose the patient could tolerate (Green, 2004). However, many common solid tumours have no overriding single molecular driver, which makes the development of targeted therapy for these types of cancer much more challenging.

Most targeted therapies under development are currently undergoing pre-clinical animal testing, some are undergoing clinical trials and a few have been approved for use by the FDA (www.cancer.gov, 2005).

Gene therapy refers to any treatment which introduces genetic material into a patient's cells with the aim of fighting disease; typically a virus is used to insert the genetic material. Gene therapy has several possible applications to cancer treatment. One approach involves treating cancers caused by missing or mutated genes by replacing the problem gene with a healthy copy. Another approach involves inserting genes into a patient's white blood cells to help the white blood cells identify and kill tumour cells. It is also possible to insert genes into cancer cells which make them more susceptible to chemotherapy or radiotherapy, or insert genes into the cancer cells to make them undergo apoptosis, which is a form of programmed cell death (www.cancer.gov, 2006b).

Gene therapy is not without its risks. Viruses will insert the new gene into healthy cells as well as cancer cells, and when the new gene is inserted it can cause mutations to the patient's DNA. These mutations could actually cause new cancers. It is also possible that the virus used to insert the new gene could cause an adverse immune reaction.

The first trial for human gene therapy has been approved for patients with adenosine deaminase (ADA) deficiency, which is a rare genetic condition. There are cur-

rently no trials for human gene therapy with direct applications to treating cancer (www.cancer.gov, 2006b).

Developing targeted or gene therapies is a very slow process and such drugs typically need a long-term administration to adequately trial them. Furthermore, early clinical trials are often ineffective because the optimal therapy dose is not known, which means several trials can be required to adequately test the therapies. It is also difficult to quantify the effectiveness of a new therapy. A standard measure for the effectiveness of a therapy is the extent to which the therapy regresses the tumour. However, many targeted therapies are designed to prevent tumour growth without causing a significant amount of tumour regression and such measures underestimate the effectiveness of these therapies. The combination of these factors means that targeted therapies and gene therapies are many years away from being a viable and widespread cancer treatment.

1.7 Thesis Outline

In this chapter we have provided a brief overview of the biology relevant to our study. In particular we have motivated why cancer is a worthwhile area of investigation, what cancer is, and provided a brief introduction into cancer therapies.

In Chapter 2 we consider the validity of the often made assumption that the nutrient and drug concentrations within an avascular tumour spheroid are radially symmetric. To test this we derive a model for the radially averaged mean nutrient or drug concentration within an avascular tumour, which after some simplification consists of a one-dimensional Poisson equation, and the perturbation of the nutrient or drug concentration away from this mean value, which after some simplification consists of Laplace's equation, which is solved by introducing a Laplace series. Our model contains some freedom and so we test this assumption for a number of parameter values and configurations which encompass a range of relevant situations.

In Chapter 3 we utilise our work of Chapter 2 to construct a multi-compartment model for avascular tumour growth and interaction with the surrounding vasculature, which after some simplification consists of six coupled non-linear differential equations. We also use a simple scaling argument, and an oxygen delivery argument to consider what the correct interaction between a growing avascular tumour spheroid and the

surrounding vasculature is and in particular what size gap should exist between the tumour and neighbouring capillaries.

In Chapter 4 we derive a multi-compartment model for vascular tumour growth and estimate the parameters in this model, which consists of four coupled non-linear ordinary differential equations. To estimate the parameters we make a temporary simplifying assumption, which is expected to be valid when modelling tumour growth in the absence of therapy but not when modelling a tumour's response to therapy. To estimate the parameters in this simplified model we perform a literature search, an asymptotic analysis, a steady state analysis, and also ensure that parameter values are chosen so that the behaviour of our model is consistent with observed tumour growth. We then use this parameter estimation for the simplified model to obtain a parameter estimation for the corresponding general model, and then compare the behaviour of the simplified and general models to ensure than the parameter estimation for the general model also provides realistic tumour growth.

In Chapter 5 we generalise the model of Chapter 4 by including the application of chemotherapy, and in particular a chemotherapy which can exhibit an anti-angiogenic effect. We then use this model to consider by what mechanisms the therapy can treat the tumour and test the Norton-Simon hypothesis for discrete and continuous applications of therapy. We then attempt to use our model to reproduce the experimental work of Browder et al. (2000), who found that chemotherapy can be used effectively as an angiogenesis inhibitor, and finally we consider the behaviour of the tumour when the action of the chemotherapy saturates.

In Chapter 6 we generalise the work of Chapters 4 and 5 further by considering the effect of resistance to obtain a system of six coupled non-linear ordinary differential equations when the resistance to a single therapy is considered, and a system of ten coupled non-linear ordinary differential equations when the resistance to a double therapy is considered. Again we consider by what mechanisms the therapy can treat the tumour when resistance is included, and investigate whether the Norton-Simon hypothesis is altered by the inclusion of resistance. We also consider the application of double therapies and test the Goldie-Coldman hypothesis and Day's worst drug first rule and consider whether even better therapy schedules can be obtained. We also determine if the resistance of endothelial cells has a significant effect on our results.

Finally in Chapter 7 we summarise our work and discuss possible future extensions.

Chapter 2

The Radial Symmetry of Nutrients and Drugs in an Avascular Tumour Spheroid

2.1 Introduction

2.1.1 The Assumption of Radial Symmetry

Many models for the growth of avascular tumour spheroids, particularly early models, assume that the growth of the tumour and the concentration of any nutrient, or drug, within the tumour are radially symmetric. For example, Casciari et al. (1992) models the evolution of an avascular tumour spheroid and implicitly assumes that the concentrations of oxygen, glucose, carbon dioxide, lactate ions, bicarbonate ions, chlorine ions, and hydrogen ions are all radially symmetric with no explicit justification of why this assumption is reasonable. Assuming radial symmetry like this with little or no explicit justification is common.

The justification for assuming that the concentration of any nutrient, or drug, within an avascular tumour is radially symmetric typically stems from the fact that solid tumours are generally observed to grow as spheroids, like the tumour shown in Figure 2.1 for example, unless they are inhibited by the local geometry. However, this need not imply that the concentration of all nutrients and drugs within the tumour are also radially symmetric. Any such substance must diffuse into the tumour from the capillary network. This capillary network is not perfectly uniform and typically forms a mesh like structure, such as that shown in Figure 2.2. Throughout this mesh we

would expect the concentration of any nutrient, or drug, to be relatively high in the vicinity of a capillary and relatively low away from the capillaries. Whether or not this expected difference in concentrations in the vicinity of the capillary network causes significant variations in concentrations within the tumour has not been explicitly considered. Therefore a detailed understanding of whether, and indeed when, it is legitimate to invoke radial symmetry is lacking and motivates further study.

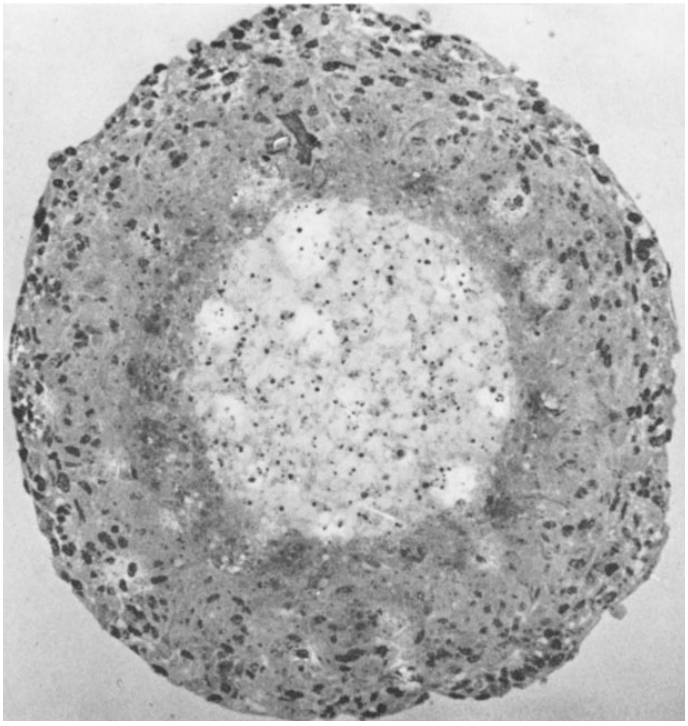

Figure 2.1: A cross-section of a tumour spheroid, which is 1mm in diameter and has been grown *in vitro* (reproduced with permission from Folkman and Hochberg, 1973).

2.1.2 The Aims of this Chapter

In this chapter we will consider the assumption that the concentration of any nutrient, or drug, in an *in vivo* avascular tumour spheroid is radially symmetric and can be approximated by the radially averaged mean nutrient concentration.

To consider this assumption we will model the diffusion of a particular nutrient, or drug, out of the capillary network and into an *in vivo* tumour spheroid. We will then calculate the magnitude of the radially averaged mean nutrient, or drug, concentration and the magnitude of the perturbation away from this mean concentration throughout

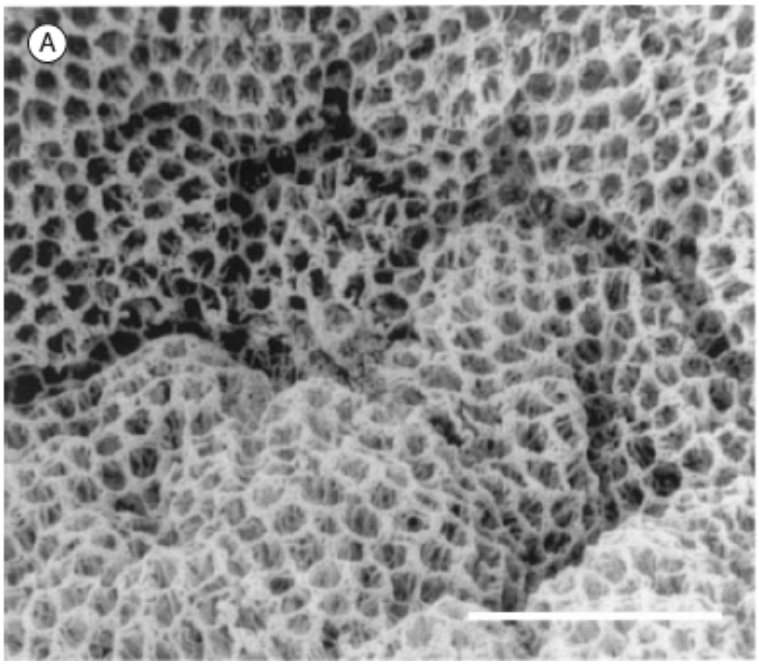

Figure 2.2: An *in vivo* scanning tunnelling microscope illustration of the capillary network of a mucosal fold of the human colon with a 1mm scale bar shown (reproduced with permission from Konerding et al., 2001).

the tumour. From this we will determine whether or not the perturbation away from the mean is significant. If we find that it is valid to approximate the concentration of nutrients, and drugs, in an avascular tumour spheroid by their radially averaged mean value then we will be justified in utilising this assumption in future models.

2.1.3 The Use of the Term Nutrient

Note that throughout this chapter we will be considering the concentration of any substance which could diffuse into an *in vivo* avascular tumour spheroid; although cell nutrients and cancer therapy drugs will be of particular relevance. For ease of reference rather than discussing the nutrient, or drug, concentration we will simply refer to the nutrient concentration. However unless specified otherwise this will refer to the concentration of any nutrient or drug which may be present in the tumour. Whenever our discussion specifically considers either a nutrient or a drug we will explicitly state this.

2.2 Modelling Nutrient Diffusion Into An Avascular Tumour Spheroid

2.2.1 The Model

We now derive a model for the diffusion of a nutrient out of the capillary network and into an avascular tumour spheroid.

Spherical Polar Co-ordinates

We begin by assuming that the tumour grows as a spheroid and work in spherical polar co-ordinates, where the origin lies at the centre of the tumour, as defined by

$$x = r\cos\theta\sin\phi, \qquad y = r\sin\theta\sin\phi, \qquad z = r\cos\phi,$$

where $$r \in [0, \infty), \qquad \theta \in [0, 2\pi), \qquad \phi \in [0, \pi].$$

The Mutual Dependency of Nutrient Concentration and Tumour Evolution

Before deriving our model we first consider the interaction between the tumour and the nutrient concentration. Any nutrient present in the tumour must diffuse out of the capillary network and into the tumour; hence the nutrient concentration within the tumour will depend upon the size of the tumour and the evolution of cells within the tumour. However, if the nutrient being considered is required for cell division, or is a drug which kills cells, then the evolution of the tumour will depend upon the local nutrient concentration. Hence the evolution of the tumour and the nutrient concentration within the tumour will be mutually dependent.

This mutual dependency is likely to be too complex for it to be desirable to model it explicitly. To simplify our model we will assume a particular form for the distribution of the rate of nutrient uptake by the tumour and then build a model based upon this assumption. We now consider what properties this nutrient uptake must exhibit to be realistic.

The Distribution of the Rate of Nutrient Uptake

The cells within the necrotic core of the tumour are all dead and so there can be no nutrient uptake in this region. Outside the necrotic core and at relatively low nutrient concentrations we would expect the rate of nutrient uptake to be an increasing function of the nutrient concentration. Finally, it would be unphysical for the rate of nutrient uptake to increase without bound as the nutrient concentration is increased and hence the rate of nutrient uptake must reach a saturation level, whereby any further increase in the nutrient concentration does not increase the rate of nutrient uptake.

Whether the uptake of a particular nutrient or drug actually saturates in any given tumour will depend upon which nutrient or drug is being considered. Cells have evolved to be very efficient at uptaking oxygen and so the rate of oxygen uptake is likely to saturate in a tumour, even if the oxygen concentration is relatively low (Guzy and Schumacker, 2006). Also, the most common site for metastases of colorectal tumours is the liver and such metastases are treated by delivering a highly concentrated dose of chemotherapeutic directly into the liver via the portal vein (Midgley and Kerr, 2000). The corresponding concentration of the chemotherapeutic is so high that the rate of chemotherapeutic uptake would be expected to saturate. However other chemotherapies, particularly those which cannot be delivered as efficiently, do not saturate at clinically relevant concentrations (Mistry et al., 1992; Hromas et al., 1987; Johnson et al., 1996).

In this chapter we limit the possible choices for the distribution of the rate of nutrient uptake by only considering the case where the rate of nutrient uptake saturates. We then assume that the distance over which the nutrient uptake increases from zero to its saturated rate is small compared to the width of the tumour (this assumption is later justified in Section 2.4 of this chapter). Hence, if we denote the radius of the tumour by R and the distance over which the rate of nutrient uptake increases from 0 to its saturated rate by ε then we have assumed that $\frac{\varepsilon}{R} \ll 1$. Given the existence of this small parameter we proceed by taking $\varepsilon = 0$ and consider the leading order approximation to the nutrient concentration; in which case the leading order distribution of the rate of nutrient uptake is

$$\mu H(r - r_*),$$

where μ is the saturated rate of nutrient uptake, r_* is the distance from the centre of the tumour at which nutrient first uptake saturates (which we will refer to as the radius of saturation) and $H(x)$ is the Heaviside function.

Conservation of Nutrients

We now derive our model for the evolution of the leading order nutrient concentration in an avascular tumour which has reached its maximum size as given by diffusion-limited control. Our model will explicitly consider the two main mechanisms which affect the local nutrient concentration: nutrient diffusion, and nutrient uptake by the tumour cells. Our model will not explicitly consider the advection of the nutrient with the movement of the cells, but in Section 2.2.2 it is shown that the Péclet number of our system, which is a non-dimensional constant relating the rate of advection to the rate of diffusion (Schetz, 1999), is small so that it is legitimate to neglect any advection dynamics. If we assume that the diffusive flux of the nutrient satisfies Fick's law, then a simple conservation of nutrient argument yields the following equation for the local nutrient concentration

$$\frac{\partial c}{\partial t} = D\nabla^2 c - \mu H(r - r_*) \qquad \text{in} \qquad r < R, \tag{2.1}$$

where $c(r, \theta, \phi, t)$ is the local nutrient concentration, D is the diffusion coefficient of the nutrient, and R is the radius of a typical avascular tumour at its maximum size as given by diffusion-limited control.

The Radius of Saturation

Having considered the distribution of the leading order rate of nutrient uptake and derived an equation governing the conservation of nutrients we now consider how the radius of saturation, r_*, must relate to the structure of the tumour and the nutrient concentration for it to be viable. This will then give us a value, or range of values, for r_* which we should consider in our later analysis.

As discussed in Section 2.2.1 we are considering the leading order system where there is no nutrient uptake for $r < r_*$ and nutrient uptake at the saturated rate for $r \geq r_*$. For nutrient uptake to occur at the saturated rate for $r > r_*$ we require the nutrient concentration to be suitably high and cells which consume the nutrient to be present. Hence we require that

$$c(r, \theta, \phi, t) > c_{\text{thres}} \quad \forall\, r > r_*, \forall\, \theta, \phi, t, \qquad \text{AND} \qquad r_* \geq r_i, \tag{2.2}$$

where $c(r, \theta, \phi, t)$ is the concentration of the nutrient at position (r, θ, ϕ) and time t, c_{thres} is the threshold nutrient concentration necessary to sustain nutrient uptake at the saturated rate, and r_i is the radius of the region of the tumour which cannot consume the nutrient. For $i = 1$ we consider cell cycle non-specific nutrients, which are consumed by both quiescent and actively proliferating cells, and then $r_1 = r_{\text{nec}}$, the radius of the necrotic core. For $i = 2$ we consider cell cycle specific nutrients, which are only consumed by proliferating cells, and then $r_2 = r_{\text{prof}}$, the radius from the centre of the tumour to the inner surface of the proliferating rim.

A schematic showing r_{nec}, r_{prof}, and R, is presented in Figure 2.3.

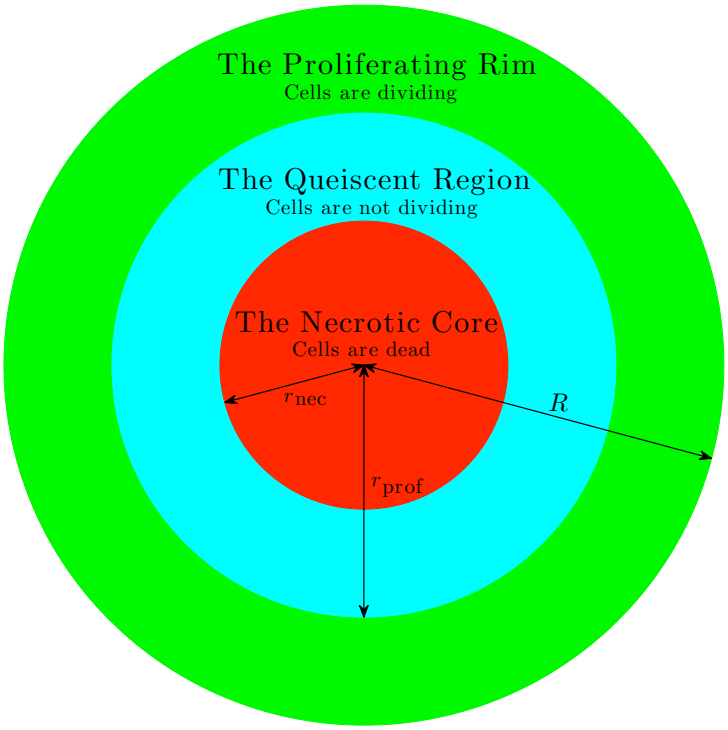

Figure 2.3: A schematic cross-section of the tumour spheroid we are considering with the different regions of the tumour and the parameters r_{nec}, r_{prof}, and R highlighted (not to scale).

Similarly, for there to be no nutrient uptake for $r < r_*$ we require there to either be a lack of nutrient or a lack of cells which can consume the nutrient, so that

$$c(r, \theta, \phi, t) < c_{\text{thres}} \quad \forall\, r < r_*, \forall\, \theta, \phi, t, \qquad \text{OR} \qquad r_* \leq r_i. \tag{2.3}$$

Note that for r_* to be realistic it must satisfy both Conditions (2.2) and (2.3). This then gives two different pairs of conditions for r_* to be a viable radius of saturation,

namely:

$$\begin{aligned} & c(r_*,\theta,\phi,t) = c_{\text{thres}} \quad \forall\,\theta,\phi,t \qquad \text{AND} \qquad r_* \geq r_i, \qquad \text{(CASE 1)} \\ \text{OR} & \\ & c(r_*,\theta,\phi,t) \geq c_{\text{thres}} \quad \forall\,\theta,\phi,t \qquad \text{AND} \qquad r_* = r_i. \qquad \text{(CASE 2)} \end{aligned} \tag{2.4}$$

Condition (2.4) then defines two different cases for the radius of saturation to be realistic for each value of r_i, and r_i can take two different values depending upon whether we are considering a cell cycle specific of cell cycle non-specific nutrient. So we actually have four separate conditions for the radius of saturation, r_*, and if any one of them is satisfied then our value of the radius of saturation is viable, subject to correctly considering either a cell cycle specific or cell cycle non-specific nutrient. Given these conditions we will later consider a range of values for the radius of saturation which will consider a wide range of biologically reasonable situations.

To close our model we now derive a corresponding boundary condition.

A Boundary Condition

For our boundary condition we will consider the outward nutrient flux across the surface of the tumour spheroid, which we denote by the currently unknown function $h(\theta,\phi,t)$. This nutrient flux will be the flux due to diffusion and assuming again that this satisfies Fick's law we obtain the following boundary condition

$$h(\theta,\phi,t) = -D\nabla c \cdot \underline{n} \qquad \text{on} \qquad r = R, \tag{2.5}$$

where $\underline{n}$ is the outward unit normal across the surface of the tumour.

Note that for ease of notation we will now refer to the outward nutrient flux across the surface of the tumour spheroid simply as the flux.

We couple this with the behaviour inside the tumour by integrating Equation (2.1) over the volume of the tumour and then appealing to the divergence theorem and Equation (2.5) to obtain

$$\begin{aligned} \iiint_V \frac{\partial c}{\partial t} + \mu H(r - r_*)\,\mathrm{d}V &= \iiint_V D\nabla^2 c\,\mathrm{d}V, \\ &= -\iint_{\partial V} h\,\mathrm{d}S, \end{aligned} \tag{2.6}$$

which the flux must satisfy for the system to be well posed. We obtain a further condition on the flux by noting that we expect the nutrient flux to be strictly towards the tumour, so that

$$\max_{\theta,\phi} h(\theta,\phi,t) \leq 0 \quad \forall\, t. \tag{2.7}$$

Note that the actual form of the flux, $h(\theta,\phi,t)$ is still unknown, but for a given form of $h(\theta,\phi,t)$ we have derived two conditions to check that $h(\theta,\phi,t)$ is biologically reasonable and a corresponding boundary condition for the nutrient concentration.

2.2.2 Non-Dimensionalising the Model

Non-Dimensionalisation

We now non-dimensionalise the model using the following rescalings

$$c = \frac{\mu R^2}{D}\widehat{c}, \qquad \underline{r} = R\,\underline{\widehat{r}}, \qquad t = T\,\widehat{t},$$

where T is the doubling time of the tumour, R is the radius of a the tumour, and the carets denote dimensionless variables. We then find that Equation (2.1) for the conservation of nutrients non-dimensionalises to become

$$P_e \frac{\partial \widehat{c}}{\partial \widehat{t}} = \widehat{\nabla}^2 \widehat{c} - H(\widehat{r} - \widehat{r}_*), \tag{2.8}$$

where $P_e = \frac{R^2}{DT}$ is the Péclet number of the system and the corresponding boundary condition, Equation (2.5), becomes

$$\widehat{h}\left(\theta,\phi,\widehat{t}\right) = -\widehat{\nabla}\widehat{c}\cdot\underline{n} \qquad \text{on} \qquad \widehat{r} = 1, \tag{2.9}$$

where $\widehat{h}(\theta,\phi,\widehat{t}) = \frac{R}{DC}h(\theta,\phi,t)$ is the non-dimensional nutrient flux across the surface of the tumour spheroid. The solvability condition on our system, Equation (2.6), becomes

$$\iint_{\partial\widehat{V}} \widehat{h}\,\mathrm{d}\widehat{S} = -\frac{4\pi}{3}(1-\widehat{r}_*^3) - \frac{R^2}{DT}\iiint_{\widehat{V}} \frac{\partial \widehat{c}}{\partial \widehat{t}}\,\mathrm{d}V, \tag{2.10}$$

and the direction of flux condition, Inequality (2.7), becomes

$$\max_{\theta,\phi} \widehat{h}\left(\theta,\phi,\widehat{t}\right) \leq 0 \quad \forall\, \widehat{t}. \tag{2.11}$$

Finally the viability conditions on the radius of saturation, Conditions Equation (2.4), become

$$\begin{aligned} &\widehat{c}(\widehat{r}_*, \theta, \phi, \widehat{t}\,) = \widehat{c}_{\text{thres}} \quad \forall\, \theta, \phi, \widehat{t} \qquad \text{AND} \qquad \widehat{r}_* \geq \widehat{r}_i, \qquad \text{(CASE 1)} \\ &\text{OR} \qquad\qquad\qquad\qquad\qquad\qquad\qquad\qquad\qquad\qquad\qquad\qquad\qquad\qquad (2.12) \\ &\widehat{c}(\widehat{r}_*, \theta, \phi, \widehat{t}\,) \geq \widehat{c}_{\text{thres}} \quad \forall\, \theta, \phi, \widehat{t} \qquad \text{AND} \qquad \widehat{r}_* = \widehat{r}_i, \qquad \text{(CASE 2)} \end{aligned}$$

where $\widehat{r}_* = \dfrac{r_*}{R}$, $\widehat{c}_{\text{thres}} = \dfrac{Dc_{\text{thres}}}{\mu R^2}$, and $\widehat{r}_i = \dfrac{r_i}{R}$.

Parameter Estimation

We now evaluate as many of the non-dimensional parameters in our model as possible by performing a literature search.

Avascular tumours typically saturate at a radius of between 0.5 mm and 2 mm (Folkman and Hochberg, 1973; Haji-Karim and Carisson, 1978) and here we consider a tumour at saturation and take $R = 1\,\text{mm}$.

The diffusion coefficient of the nutrient will depend upon which specific nutrient is being considered. To estimate its likely magnitude we now consider the diffusion coefficient of oxygen, which has been recorded in DS-Carcinosarcoma tumour cells to be $D = 1.75 \times 10^{-5}\,\text{cm}^2\,\text{s}^{-1}$ (Grote et al., 1977).

The time scale of tumour growth will depend upon what tumour type is being considered and again we estimate the likely magnitude of T by considering a specific example. Kusama et al. (1972) analysed the results of 199 patients with breast cancer and calculated their mean doubling time to be 3.5 months. Given this we take $T = 9 \times 10^6$ seconds.

Using these values we find that

$$P_e \approx 6 \times 10^{-5} \ll 1.$$

So for oxygen in breast cancer the non-dimensional parameter P_e is a small parameter. We generalise this result by assuming that P_e will be negligibly small for an arbitrary nutrient in an arbitrary tumour, which justifies our original neglection of advection from our model in Section 2.2.1.

The parameter $\widehat{c}_{\text{thres}}$, which is the non-dimensional threshold nutrient concentration required to sustain nutrient uptake at the saturated rate, is also going to vary depending upon which particular nutrient is being considered. To estimate its likely

magnitude we evaluate it when the nutrient being considered is glucose. Weiss (1965) showed that varying the glucose concentration from 1mM to 5mM did not appreciably affect metabolic activity in bacteria. This suggests that once the glucose concentration reaches 1mM the rate of glucose uptake has already reached its saturated rate. Non-dimensionalising with the diffusion coefficient of glucose in a multicellular tumour spheroid, $5 \times 10^{-6}\text{cm}^2\text{s}^{-1}$ (Groebe et al., 1994), and the saturated rate of glucose uptake in rats, 40 μmol $\text{g}^{-1}\text{min}^{-1}$ (Groebe et al., 1994), we find that for glucose

$$\widehat{c}_{\text{thres}} \approx 7.5 \times 10^{-4} \ll 1.$$

So for glucose $\widehat{c}_{\text{thres}}$ is a small parameter and we generalise this by assuming that $\widehat{c}_{\text{thres}}$ is a small parameter for an arbitrary nutrient. A relaxation of this assumption, which is not guaranteed to be valid for drugs the cells have not evolved to be efficient at uptaking, could be a future generalisation of our work.

Finally we consider the values of $\widehat{r}_1$ and $\widehat{r}_2$, which are the non-dimensional radius of the necrotic core and the non-dimensional radius from the centre of the tumour to the inner surface of the proliferating rim respectively. Mueller-Klieser (2000) recorded the diameter of necrosis and spheroid diameter of 46 human colon tumour spheroids and a linear regression through the data points found the radius of the necrotic core to be given by $r_{\text{nec}} = 1.03 \times r_{\text{tum}} - 203.5\,\mu\text{m}$, where r_{tum} is the radius of the tumour. Hence we take the non-dimensional radius of the necrotic core to be

$$\widehat{r}_{\text{nec}} = \frac{1.03 \times 1000\,\mu\text{m} - 203.5\,\mu\text{m}}{1000\,\mu\text{m}} = 0.83 \quad (2 \text{ s.f.}).$$

Similarly, LaRue et al. (2004) found that for a tumour of diameter 1200 μm only the outer two or three cells on the surface of the tumour are proliferating. Taking the mean diameter of an animal cell to be 25 μm (Alberts et al., 2002) and the cell volume fraction to be 0.66 (Freyer and Sutherland, 1986) this gives the non-dimensional distance from the centre of the tumour to the inner surface of the proliferating rim to be:

$$\widehat{r}_{\text{prof}} = \frac{1000\,\mu\text{m} - 2 \times \dfrac{25\,\mu\text{m}}{0.66}}{1000\,\mu\text{m}} = 0.92 \quad (2 \text{ s.f.}).$$

The Non-Dimensional System

Having evaluated some of the non-dimensional parameters in our model we now re-consider the non-dimensional system. Having found that $\frac{R^2}{DT}$ and $\widehat{c}_{\text{thres}}$ are both small

parameters we neglect these terms and consider a leading order approximation. Note that neglecting the $O\left(\frac{R^2}{DT}\right)$ terms removes all the time derivatives from our system and hence we make the quasi-steady state assumption that to leading order the nutrient concentration within our avascular spheroid tumour exhibits no time dependency; which is equivalent to assuming that the time scale for nutrient diffusion is much faster than the time scale for tumour growth. As part of this quasi-steady state assumption we have assumed that $R(t)$, the tumour radius, is a constant, and hence r_i

After neglecting these terms and dropping carets we obtain the following leading order non-dimensional system. Equation (2.8) for the conservation of nutrients becomes

$$\nabla^2 c = H(r - r_*), \tag{2.13}$$

with the corresponding boundary condition, Equation (2.9), becoming

$$\underline{n} \cdot \nabla c = -h(\theta, \phi) \qquad \text{on} \qquad r = 1. \tag{2.14}$$

Also, for this system to be well defined it must satisfy the non-dimensional solvability Condition (2.10), which becomes

$$\iint_{r=1} h \, \mathrm{d}S = -\frac{4\pi}{3}\left(1 - r_*^3\right), \tag{2.15}$$

and the flux Condition (2.11), which becomes

$$\max_{\theta,\phi} h(\theta, \phi) \leq 0. \tag{2.16}$$

Finally the criteria for the location of the radius of saturation, r_*, Conditions (2.12), become

$$\begin{aligned} & c(r_*, \theta, \phi) = 0 \qquad \text{AND} \qquad r_* \geq r_i, \qquad \text{(CASE 1)} \\ \text{OR} & \\ & c(r_*, \theta, \phi) \geq 0 \qquad \text{AND} \qquad r_* = r_i. \qquad \text{(CASE 2)} \end{aligned} \tag{2.17}$$

Despite having simplified our model to obtain the leading order system our system still contains significant freedom. In particular the precise form of the flux, $h(\theta, \phi)$, and the values of the radius of saturation, r_*, and nutrient concentration at the radius of saturation, $c(r_*, \theta, \phi)$, are unknown for an arbitrary nutrient. However we can remove some of this freedom from our system by deliberately considering the worst case scenario with regard to our problem.

Recall that we are investigating when the perturbation away from the mean nutrient concentration is much smaller than the mean nutrient concentration. The worst case scenario corresponding to our problem will consider the largest possible perturbation and the smallest possible mean. Hence we remove some of the freedom from our system by deliberately only considering the smallest possible mean.

The smallest value of the mean nutrient concentration will correspond to the lowest value of the nutrient concentration at the radius of saturation, as allowed by Condition (2.17), and so we take

$$c(r_*, \theta, \phi) = 0. \tag{2.18}$$

The radius of saturation, r_*, will depend upon which nutrient is being considered, and it could possibly take one of an infinite number of values subject to Condition (2.17). We limit this freedom by only considering a finite number of values for r_*, which will encompass a range of situations for both cell cycle specific and non-specific nutrients. Recalling the values of $\widehat{r}_{\text{nec}}$ and $\widehat{r}_{\text{prof}}$ found earlier when performing our parameter estimation we will consider each of the following values of r_* in turn

$$r_* \in \big\{0.83, 0.92, 0.85, 0.9, 0.95\big\}.$$

2.3 Considering Radial Symmetry

We now calculate the magnitude of the radially averaged mean nutrient concentration and the perturbation away from this mean. We begin by considering the magnitude of the radially averaged nutrient concentration.

2.3.1 Quantifying Radial Symmetry

The Mean Nutrient Concentration

We define the leading order radially averaged mean non-dimensional nutrient concentration, $\overline{c}(r)$, by

$$\overline{c}(r) = \frac{1}{4\pi r^2} \int_0^{\pi} \int_0^{2\pi} c(r, \theta, \phi) r^2 \sin\phi \, \mathrm{d}\theta \, \mathrm{d}\phi.$$

Note that for brevity we will refer to the leading order radially averaged mean non-dimensional nutrient concentration simply as the mean nutrient concentration, or just the mean.

We obtain a model for the mean by radially averaging the equation for the conservation of nutrients, Equation (2.13), and the corresponding boundary conditions, Equations (2.14) and (2.18), to obtain the following system for the mean

$$\frac{1}{r}\frac{\mathrm{d}^2\left(r\overline{c}(r)\right)}{\mathrm{d}r^2} = H(r-r_*) \qquad \text{in} \quad r<1, \tag{2.19}$$

$$\begin{aligned} \frac{\mathrm{d}\overline{c}(r)}{\mathrm{d}r} &= \frac{1-r_*^3}{3} \qquad \text{on} \quad r=1, \\ \overline{c}(r_*) &= 0. \end{aligned} \tag{2.20}$$

This system of equations can be explicitly solved and ensuring that the mean is continuous at r_* and is bounded at the origin yields

$$\overline{c}(r) = \begin{cases} \dfrac{r^2}{6} + \dfrac{r_*^3}{3r} - \dfrac{r_*^2}{2} & \text{for} \quad r_* \leq r \leq 1, \\ 0 & \text{for} \quad 0 \leq r < r_*. \end{cases} \tag{2.21}$$

The Perturbation Away from the Mean Nutrient Concentration

We now consider the perturbation of the leading order non-dimensional nutrient concentration away from its radially averaged mean value, $\widetilde{c}(r,\theta,\phi)$, as defined by

$$\widetilde{c}(r,\theta,\phi) = c(r,\theta,\phi) - \overline{c}(r).$$

For brevity we will refer to this simply as the perturbation.

We obtain a model for the perturbation by recalling the full system, given by Equations (2.13) and (2.14), and subtracting the radially averaged system, given by Equations (2.19) and (2.20), to obtain:

$$\nabla^2\widetilde{c}(r,\theta,\phi) = 0 \qquad \text{in} \quad r<1, \tag{2.22}$$

$$\underline{n}\cdot\nabla\widetilde{c}(r,\theta,\phi) = \widetilde{h}(\theta,\phi) \qquad \text{on} \quad r=1, \tag{2.23}$$

where $\widetilde{h}(\theta,\phi)$ is the perturbation of the leading order flux away from its radially averaged mean value as defined by

$$\widetilde{h}(\theta,\phi) = h(\theta,\phi) + \frac{1-r_*^3}{3}.$$

Note that for brevity we will refer to the perturbation of the leading order flux away from its radially averaged mean value simply as the perturbed flux.

To close our model for the perturbation we recall the solvability condition on the flux, Condition (2.15), which gives the following solvability condition on the perturbed flux:

$$\int_0^{\pi}\int_0^{2\pi} \widetilde{h}(\theta,\phi) r^2 \sin\phi \, \mathrm{d}\theta \, \mathrm{d}\phi = 0. \tag{2.24}$$

Hence for our system to be well posed the mean perturbed flux must be zero. We also recall the flux condition, Inequality (2.16), which gives the following bound on the magnitude of the perturbed flux

$$\max_{\theta,\phi} \widetilde{h}(\theta,\phi) \leq \frac{1-r_*^3}{3}. \tag{2.25}$$

Before choosing a particular form for the perturbed flux, which must satisfy Conditions (2.24) and (2.25), we now consider what further properties the perturbed flux must exhibit to be realistic.

2.3.2 The Required Properties of the Perturbed Flux

We begin by considering what properties the perturbed flux should inherit from the capillary network in the vicinity of the tumour. The capillary network will consist of a criss-crossing mesh of capillaries, such as that shown in Figure 2.2, and it can be seen that this capillary mesh is quite regular. In the vicinity of the capillaries we would expect the nutrient flux to be relatively high and in between the capillaries we would expect the nutrient flux to be relatively low, which suggests that the nutrient flux across the surface of the tumour will consist of regions of relatively high and low flux which are regularly distributed and the number of regions of high and low flux will depend upon the relative length scales of the tumour radius and the inter-capillary distance.

The mean inter-capillary distance in different segments of the human large intestine has been measured to be 101.9 μm (Fait et al., 1998), with the minimum and maximum inter-capillary distance observed by Fait et al. being 41.7 μm and 196.3 μm respectively.

Fait et al. measured the inter-capillary distance in tissue which was tumour free. It could be conjectured that as a tumour grows it displaces the surrounding tissue in a way which might alter the inter-capillary distance in the vicinity of the tumour. Whilst there has been little research specifically considering how the inter-capillary distance in the vicinity of a tumour varies as the tumour grows, papers by Carmeliet

and Jain (2000), and Fukmura and Jain (2007) do present images of the vessels in the vicinity of a tumour at different stages of its growth. These images show no noticeable change in the inter-capillary distance in the vicinity of the tumour as the tumour grows. Given this we assume that the average inter-capillary distance in the vicinity of the tumour is $100\,\mu$m irrespective of the size of the tumour.

Recalling that we are considering a tumour with a radius of 1 mm we find that this mean intercapillary distance implies that around any circumference of the tumour there will be approximately 63 capillaries, which in turn implies that our nutrient flux should exhibit approximately 63 regions of high flux and 63 regions of low flux around any circumference of the tumour spheroid.

Having shown that the flux will be highly oscillatory and recalling that the perturbed flux averages to zero, as given by Equation (2.24), we assume that we can generalise the upper bound in Condition (2.25) and assume that

$$\max_{\theta,\phi} \left|\widetilde{h}(\theta,\phi)\right| \leq \frac{1-r_*^3}{3}. \tag{2.26}$$

As before we can remove some of the freedom from our system by deliberately considering the worst case scenario for our investigation. The worst case scenario here corresponds to having the largest possible perturbation and so we will only consider perturbed fluxes which achieve the upper bound given by Condition (2.26).

Having derived this bound for the magnitude of the perturbed flux and considered how oscillatory it should be, we are now in a position to assume a realistic form for the distribution of the perturbed flux. However, there is still considerable freedom concerning the form the perturbed flux can take. To ensure generality we will consider a number of different forms for the distribution of the for the perturbed flux, each of which will be known as a test function.

Having derived criteria which ensure that the perturbed flux is realistic, we now consider how to evaluate the perturbation given a particular form of the perturbed flux.

2.3.3 Introducing a Laplace Series

To aid us in evaluating the perturbation for a given form of the perturbed flux we now introduce a Laplace series.

We have just shown that the perturbed flux must be bounded and to be biologically realistic it must also be continuous. Hence the perturbed flux must be square integrable and can therefore be expressed as a Laplace series thus

$$\widetilde{h}(\theta,\phi)=\sum_{n=0}^{\infty}\sum_{m=0}^{n}\underbrace{\alpha_{n,m}Y_{C_{n,m}}(\theta,\phi)+\beta_{n,m}Y_{S_{n,m}}(\theta,\phi)}_{\psi_{n,m}(\theta,\phi)}, \tag{2.27}$$

where

$$\begin{aligned} Y_{C_{n,m}}(\theta,\phi)&=\sqrt{\tfrac{(2n+1)}{2\pi}\tfrac{(n-m)!}{(n+m)!}}P_n^m(\cos\phi)\cos(m\theta),\\ Y_{S_{n,m}}(\theta,\phi)&=\sqrt{\tfrac{(2n+1)}{2\pi}\tfrac{(n-m)!}{(n+m)!}}P_n^m(\cos\phi)\sin(m\theta), \end{aligned} \tag{2.28}$$

where $P_n^m(x)$ is the associated Legendre polynomial of degree n and order m (Hobson, 1955). The functions $Y_{C_{n,m}}(\theta,\phi)$ and $Y_{S_{n,m}}(\theta,\phi)$ are known as the real spherical harmonics of degree n and order m. The $\sqrt{\frac{2n+1}{2\pi}\frac{(n-m)!}{(n+m)!}}$ coefficients are normalisation factors which are chosen so that each of the spherical harmonics are $O(1)$.

The real spherical harmonics are orthogonal with respect to the L^2 inner product with integration taken over the surface of a unit sphere, as defined by

$$\langle f(\theta,\phi),g(\theta,\phi)\rangle=\int_0^{\pi}\int_0^{2\pi}f(\theta,\phi)g(\theta,\phi)\sin\phi\,\mathrm{d}\theta\,\mathrm{d}\phi,$$

(Arfken and Weber, 2005). In fact these spherical harmonics satisfy the following orthogonality relationships

$$\begin{aligned} \left\langle Y_{C_{n,m}}(\theta,\phi),Y_{C_{n',m'}}(\theta,\phi)\right\rangle&=(1+\delta_{m,0})\,\delta_{n,n'}\,\delta_{m,m'} && \forall\, n,\, n',\, m,\, m',\\ \left\langle Y_{C_{n,m}}(\theta,\phi),Y_{S_{n',m'}}(\theta,\phi)\right\rangle&=0 && \forall\, n,\, n',\, m,\, m',\\ \left\langle Y_{S_{n,m}}(\theta,\phi),Y_{S_{n',m'}}(\theta,\phi)\right\rangle&=(1-\delta_{m,0})\,\delta_{n,n'}\,\delta_{m,m'} && \forall\, n,\, n',\, m,\, m'. \end{aligned}$$

These orthogonality relationships can then be used to relate the coefficients in our Laplace series, as defined by Equation (2.27), to the perturbed flux to give

$$\alpha_{n,m}=\frac{1}{1+\delta_{m,0}}\left\langle\widetilde{h}(\theta,\phi),Y_{C_{n,m}}(\theta,\phi)\right\rangle \qquad \forall\, n,\, m, \tag{2.29}$$

$$\beta_{n,m}=(1-\delta_{m,0})\left\langle\widetilde{h}(\theta,\phi),Y_{S_{n,m}}(\theta,\phi)\right\rangle \qquad \forall\, n,\, m. \tag{2.30}$$

Notice that in the Laplace series (2.27) the spherical harmonic $Y_{S_{n,0}}$ is zero for all n and so without loss of generality we have taken $\beta_{n,0}=0$ for all n.

Given a particular form for the perturbed flux Equations (2.29) and (2.30) allow us to calculate the corresponding Laplace series. In order to calculate the perturbation corresponding to a particular form for the perturbed flux we now consider how to solve for the perturbation in terms of this Laplace series.

Solving for the Perturbation

The Laplace series (2.27) can be substituted into the boundary condition for the perturbation, Equation (2.23), to give

$$\frac{\partial \widetilde{c}}{\partial r} = -\sum_{n=0}^{\infty}\sum_{m=0}^{n} \psi_{n,m}(\theta,\phi), \qquad \text{on} \quad r=1. \tag{2.31}$$

We now seek a quasi-separable solution to Laplace's equation, Equation (2.22), which satisfies this boundary condition of the form

$$\widetilde{c}(r,\theta,\phi) = \sum_{n=0}^{\infty}\sum_{m=0}^{n} f_{n,m}(r)\psi_{n,m}(\theta,\phi). \tag{2.32}$$

From the definition of the spherical harmonics in Equations (2.28) it can be shown that

$$\nabla^2 \psi_{n,m} = -\frac{n(n+1)}{r^2}\psi_{n,m},$$

(Arfken and Weber, 2005) and after exploiting this property Laplace's equation for the perturbation, Equation (2.22), becomes

$$\left(\nabla^2 f_{n,m} - \frac{n(n+1)}{r^2} f_{n,m}\right) \langle \psi_{n,m}, \psi_{n,m} \rangle = 0 \qquad \forall\, n,\, m.$$

Without loss of generality we can assume that the inner product in this equation is strictly positive to obtain the following ordinary differential equation for $f_{n,m}(r)$

$$\frac{1}{r}\frac{\mathrm{d}^2\left(r f_{n,m}\right)}{\mathrm{d}r^2} - \frac{n(n+1) f_{n,m}}{r^2} = 0 \qquad \forall\, n,\, m.$$

This differential equation is simply an Euler equation with general solution

$$f_{n,m}(r) = C_{n,m} r^n + \frac{D_{n,m}}{r^{n+1}}.$$

We require $f_{n,m}(r)$ to be bounded at the origin and recalling the boundary condition, Equation (2.31), we find that

$$f_{n,m}(r) = -\frac{r^n}{n} \qquad \forall\, n,\, m.$$

Substituting this back into Equation (2.32) we find that the perturbation is given by

$$\widetilde{c}(r,\theta,\phi) = -\sum_{n=0}^{\infty}\sum_{m=0}^{n}\sqrt{\tfrac{2n+1}{2\pi}\tfrac{(n-m)!}{(n+m)!}}\frac{r^n}{n}P_n^m(\cos\phi)\left\{\alpha_{n,m}\cos(m\theta)+\beta_{n,m}\sin(m\theta)\right\}, \tag{2.33}$$

where $\alpha_{n,m}$ and $\beta_{n,m}$ are the coefficients in the Laplace series expansion for the perturbed flux in Equation (2.27). The coefficients $\alpha_{n,m}$ and $\beta_{n,m}$ are unique to each perturbed flux, but given a particular form for the distribution of the perturbed flux the corresponding Laplace coefficients can be calculated using Equations (2.29) and (2.30) and then the corresponding perturbation is given by Equation (2.33).

2.3.4 The Decay of the Perturbation

We now review our analysis so far and use it to suggest that the perturbation will decay to zero quickly as r tends to zero.

Recall that when considering the properties of the perturbed flux in Section 2.3.2 we reasoned that it should be a highly oscillatory function. It follows from this that the dominant terms in the Laplace series in Equation (2.27) will be the higher order modes with relatively high values of n. However, Equation (2.33) for the perturbation shows that the contribution these higher order terms make to the perturbation will decay like $\frac{r^n}{n}$ as r tends to zero. The fact that the terms which dominate the perturbation on the edge of the tumour are expected to quickly decay away from the edge of the tumour suggests that the perturbation is likely to be small inside the tumour.

This gives us an indication that we are on course to show that it is valid to approximate the nutrient concentration by its radially averaged mean value. To confirm this we now quantify and compare the magnitudes of the mean and perturbation. Before doing this we use our initial analysis to perform a consistency check and justify some of the assumptions made in deriving our model.

2.4 A Consistency Check

With our initial analysis complete we are now able to perform a consistency check to show that an assumption made in Section 2.3.2 when considering the distribution of the rate of nutrient uptake is consistent with the behaviour of our modelled tumour. In particular we check the assumption that when the rate of nutrient uptake saturates,

the distance over which the nutrient uptake increases from zero to its saturated rate is small compared to the width of the tumour.

For there to be no nutrient uptake there must either be no nutrient or no cells which consume the nutrient. Equally, for nutrient uptake to occur at the saturated rate the nutrient must be present in a suitably high concentration and all cells must be able to consume the nutrient. So, for our assumption to be true in all possible situations we require that the transition from the necrotic core to the quiescent region, and then from the quiescent region to the proliferating rim, both be sharp transitions, and we also require that the nutrient concentration quickly increases from zero to the concentration required for saturation.

It can be seen that the tumour shown in Figure 2.1 exhibits a clean boundary between the necrotic core and the quiescent region, although the location of the proliferating rim is less clear. The tumour shown in Figure 2.1 has been grown *in vitro*, but tumours grown *in vivo* have been observed to exhibit similar structures. Furthermore, it has been shown mathematically that if the different cell populations exhibit a different chemotactic response to the local nutrient concentration then shocks can form, which results in the transitions between the different compartments of the tumour being sharp (Tindall and Please, 2007; Tindall et al., 2008). The combination of these effects suggest that it is reasonable to assume that the boundary between the necrotic core and the quiescent region and the boundary between the quiescent region and the proliferating rim will both be sharp boundaries.

The distance over which the nutrient concentration increases from zero to the concentration required for saturation will vary depending upon which nutrient is being considered. To suggest the likely magnitude of this distance we now estimate it for glucose. Recall that during our parameter estimation of Section 2.2.2 we found that a non-dimensional mean of $\overline{c}(r) = 7.5 \times 10^{-4}$ is sufficient for the rate of glucose uptake to be at its saturated rate. Recalling Equation (2.21) for the mean and taking the radius of saturation to be $r_* = 0.83$ we find that the non-dimensional distance over which the nutrient concentration increases from zero to its saturated rate is 0.039 (2 s.f.), where a non-dimensional distance of 1 corresponds to the radius of our tumour.

This shows that for glucose the distance over which the nutrient concentration increases from zero to its saturated rate is small compared to the width of the tumour. Given this we assume that this distance is small for any arbitrary nutrient for which the rate of nutrient uptake saturates.

This demonstrates that the assumption that the distance over which the nutrient uptake increases from zero to its saturated rate is small compared to the width of the tumour is consistent with the results of our model.

2.5 Results

We are now in a position to choose some suitable test functions for the perturbed flux and evaluate the corresponding maximum value of the perturbation.

2.5.1 Test Function 1

We choose our first test function so that it is simple to calculate the corresponding perturbation analytically. To do this we take our test function to be a simple sum of spherical harmonics and in particular we consider a sum of spherical harmonics which exhibits the required distribution of regions of high and low flux. We do this by taking the distribution of the perturbed flux to be

$$\widetilde{h}(\theta,\phi) = \left(\frac{1-r_*^3}{3}\right)\frac{g(\theta,\phi)}{\max\limits_{\theta,\phi}|g(\theta,\phi)|}, \tag{2.34}$$

where $$g(\theta,\phi) = \frac{{}^{Y}c_{91,63}(\theta,\phi)}{\max\limits_{\phi}|Y_{c_{91,63}}(\theta,\phi)|} + \frac{{}^{Y}c_{91,12}(\theta,\phi)}{\max\limits_{\phi}|Y_{c_{91,12}}(\theta,\phi)|} + \frac{{}^{Y}c_{91,1}(\theta,\phi)}{\max\limits_{\phi}|Y_{c_{91,1}}(\theta,\phi)|}.$$

Then the distribution of the nutrient flux across the surface of the tumour spheroid is shown in Figure 2.4.

For this choice of test function we can use the uniqueness of the Laplace series to evaluate the coefficients $\alpha_{n,m}$ and $\beta_{n,m}$ analytically and it is found that

$$\alpha_{n,m} = \left(\frac{1-r_*^3}{3}\right)\frac{1}{\max\limits_{\theta,\phi}|g(\theta,\phi)|}\frac{1}{\max\limits_{\theta,\phi}|Y_{c_{n,m}}(\theta,\phi)|},$$

for $(n,m) \in \big\{(91,1),(91,12),(91,63)\big\}$, and $\alpha_{n,m} = \beta_{n,m} = 0$ otherwise.

The corresponding perturbation can then be evaluated explicitly and is

$$\widetilde{c}(r,\theta,\phi) = -\left(\frac{1-r_*^3}{3}\right)\frac{r^{91}}{91}\frac{g(\theta,\phi)}{\max\limits_{\theta,\phi}|g(\theta,\phi)|},$$

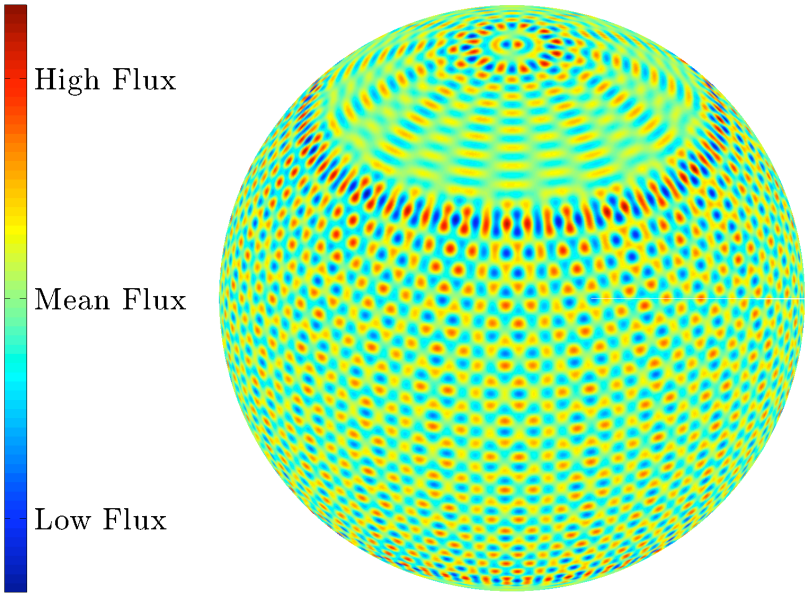

Figure 2.4: The distribution of the nutrient flux across the surface of the tumour when the perturbation away from the mean nutrient flux is given by Equation (2.34).

and hence for a given value of r the maximum value of the perturbation is

$$\max_{\theta,\phi}|\widetilde{c}(r,\theta,\phi)| = \left(\frac{1-r_*^3}{3}\right)\frac{r^{91}}{91}. \tag{2.35}$$

Having bounded the perturbation we plot this bound and the corresponding mean, as given by Equation (2.21), for the radii of saturation $r_* = 0.83,\ 0.92,\ 0.85,\ 0.9$, and 0.95 in Figure 2.5.

It can be seen in Figure 2.5(a) that when the radius of saturation is $r_* = 0.83$, which is the non-dimensional radius of the necrotic core, the bound on the nutrient concentration is extremely tight in most of the tumour. In fact for a dimensional radius of $r < 950\,\mu$m the difference between the mean nutrient concentration and the bound on the nutrient concentration cannot readily be seen. However for a dimensional radius of $r > 950\,\mu$m the difference between the nutrient concentration and the bound on the nutrient concentration is observable, but still small.

For the larger values of r_* we again see that for dimensional radii of $r < 950\,\mu$m the difference between the mean nutrient concentration and the bound on the nutrient

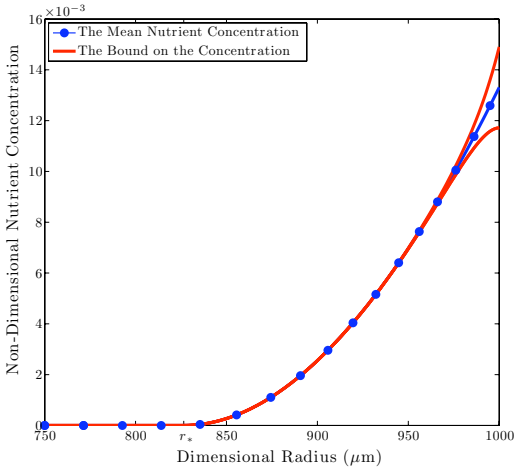

(a) $r_* = 0.83$

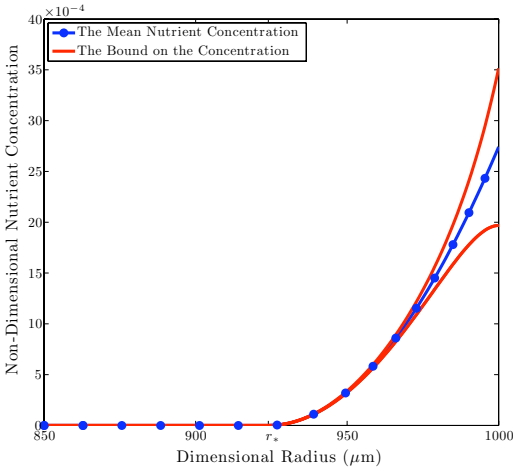

(b) $r_* = 0.92$

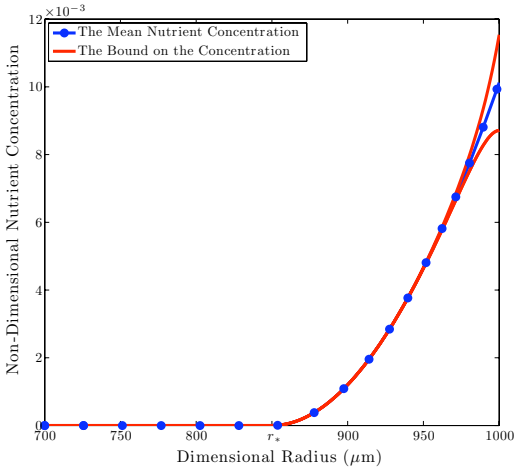

(c) $r_* = 0.85$

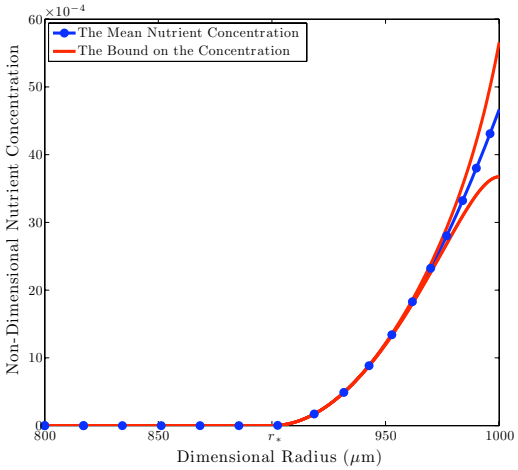

(d) $r_* = 0.9$

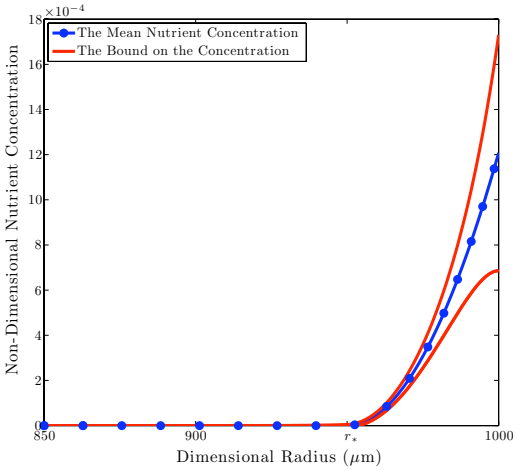

(e) $r_* = 0.95$

Figure 2.5: The radially averaged mean nutrient concentration and the bound on the nutrient concentration, as given by Equations (2.21) and (2.33), in an avascular tumour of radius 1000 μm as a function of the radius from the centre of the tumour when the perturbed flux is as given by Equation (2.34) for different values of r_*, the radius of saturation, as defined in Section 2.2.1. See text for details.

concentration is so small that it cannot be resolved, but for dimensional radii of $r > 950\,\mu$m a difference between the mean and the nutrient concentration can be observed, the relative magnitude of which appears to be getting larger with increasing values of r_*. To see how large this difference might become for extreme values of r_* we now consider the limit as r_* tends to one.

2.5.2 The Limit as r_* Tends to One

Our results suggest that for this test function increasing the value of r_*, which moves the radius of saturation closer to the edge of the tumour, results in a more significant relative difference between the mean and perturbation on the surface of the tumour. To consider how significant this difference could become we consider the limit as r_* tends to one. We do this by recalling Equation (2.21) for the mean and Equation (2.35) for the bound on the perturbation and then using l'Hopital's rule we find that

$$\lim_{r_*\to 1} \frac{\max_{\theta,\phi}|\widetilde{c}(1,\theta,\phi)|}{|\overline{c}(1)|} = \lim_{r_*\to 1} \frac{1}{91}\left(\frac{2(1-r_*^3)}{1+2r_*^3-3r_*^2}\right) = \infty.$$

Hence as r_* tends to one the relative difference between the mean and perturbation blows up to infinity, which implies that when $r_* \approx 1$ the relative difference between the mean and the perturbation will be large. However, when $r_* \approx 1$ the radius of saturation is very close to the surface of the tumour, which means that the nutrient is only penetrating a very small distance into the tumour. Hence this very large relative difference in nutrient concentration only occurs over a very small region of the tumour so that the overall effect of the nutrient on the tumour may only be slight.

2.6 Numerically Approximating the Perturbation

We deliberately chose our first test function so that the perturbation could be evaluated analytically, however many other forms for the perturbed flux are possible. To consider other forms for the perturbed flux we will consider different test functions and calculate the corresponding perturbations. However, analytically calculating the perturbation for an arbitrary test function will be non-trivial. So we now outline a numerical scheme to approximate the perturbation for a given test function.

Approximating the Perturbation

Our solution series for the perturbation, as given by Equation (2.33), contains the Laplace coefficients $\alpha_{n,m}$ and $\beta_{n,m}$. These coefficients are related to the original test function by the integral Equations (2.29) and (2.30). These integrals can be evaluated numerically to obtain approximations to the coefficients $\alpha_{n,m}$ and $\beta_{n,m}$, which we denote by $\alpha'_{n,m}$ and $\beta'_{n,m}$ respectively. This can be done using any quadrature method, of which there are many, and our choice of quadrature method will be optimised to suit the particular test functions being considered.

We now consider what criteria should be placed on the approximations to $\alpha_{n,m}$ and $\beta_{n,m}$ to ensure that the corresponding approximation to the perturbation is suitably accurate. It will only be possible to numerically approximate a finite number of Laplace coefficients, but our solution series, given by Equation (2.33), contains a doubly infinite number of Laplace coefficients. It will therefore be necessary to consider a truncated approximation to the solution series and if we truncate the solution series at order N then we obtain the following approximation to the perturbation

$$\widetilde{c}'(r,\theta,\phi) = -\sum_{n=0}^{N}\sum_{m=0}^{n}\frac{r^n}{n}\psi'_{n,m}(\theta,\phi), \tag{2.36}$$

where $\psi'_{n,m}(\theta,\phi)$ is the numerical approximation to $\psi_{n,m}(\theta,\phi)$ as defined by

$$\psi'_{n,m}(\theta,\phi) = \alpha'_{n,m}Y_{c_{n,m}}(\theta,\phi) + \beta'_{n,m}Y_{s_{n,m}}(\theta,\phi).$$

The corresponding numerical approximation to the perturbed flux is then given by

$$\widetilde{h}'(\theta,\phi) = \sum_{n=0}^{N}\sum_{m=0}^{n}\psi'_{n,m}(\theta,\phi), \tag{2.37}$$

To ensure that the error in the approximation to the perturbation is acceptably small we consider the relative mean square error in our numerical approximation to the perturbed flux. In particular, we ensure that $\alpha'_{n,m}$, $\beta'_{n,m}$ and N are chosen so that the relative mean square error in our approximation to the perturbed flux is less than 1%, i.e. we ensure that $\alpha'_{n,m}$, $\beta'_{n,m}$ and N are chosen so that

$$\frac{1}{4\pi}\int_0^{2\pi}\int_0^{\pi}\left(\frac{\widetilde{h}'(\theta,\phi)-\widetilde{h}(\theta,\phi)}{\max\limits_{\theta,\phi}\left|\widetilde{h}(\theta,\phi)\right|}\right)^2\sin\phi\,\mathrm{d}\phi\,\mathrm{d}\theta < 10^{-2}. \tag{2.38}$$

We then assume that when Condition (2.38) is satisfied the numerical error in the approximation to the perturbation, as defined by Equation (2.36), will be acceptably small. There are two ways of justifying this assumption. Firstly, if our numerical approximation only introduces a "small" error into the perturbed flux then by the continuous dependence of Laplace's equation the error introduced into the perturbation should also be "small". Furthermore, the terms discarded when truncating our solution series are all $O(\frac{r^{N+1}}{N+1})$ where N is expected to be large and so for r less than one these terms will contribute less to the perturbation than the corresponding terms contribute to the perturbed flux. So if discarding the corresponding terms from the perturbed flux gives an acceptable approximation to the perturbed flux, then discarding these terms from the perturbation should give an acceptable approximation to the perturbation.

Alternatively, we can justify this numerical approximation differently. Suppose that $\widetilde{h}(\theta,\phi)$ is a suitable test function for the perturbed flux and that Condition (2.38) is satisfied. Then the relative difference between $\widetilde{h}(\theta,\phi)$ and $\widetilde{h}'(\theta,\phi)$ is small, which implies that $\widetilde{h}'(\theta,\phi)$ will also be a suitable test function for the perturbed flux. If we take $\widetilde{h}'(\theta,\phi)$ to be the test function in its own right then the corresponding perturbation is exactly $\widetilde{c}'(r,\theta,\phi)$ and is subject to no numerical errors. So rather than numerically approximating the perturbation it can be viewed that the test function has been approximated to obtain a new, but equally valid, test function and the corresponding perturbation corresponding to this approximated test function has been calculated exactly.

Either way we assume that given a test function for the perturbed flux and having ensured that $\alpha'_{n,m}$, $\beta'_{n,m}$ and N are chosen so that the relative mean square error in our numerical approximation for the perturbed flux is less than 1%, then $\widetilde{c}'(r,\theta,\phi)$ is a numerical approximation to the perturbation which is subject to acceptably small numerical errors.

To ensure Condition (2.38) is satisfied we must evaluate a double integral. It is expected that it will not be possible to evaluate this integral analytically and so when necessary we will approximate it numerically. To do this we will use a repeated trapezium rule quadrature method using $(63k)^2$ quadrature points as defined by

$$(\theta,\phi) \in \left\{ \left(\frac{2\pi p}{63k}, \frac{\pi q}{63k} \right) \middle| \, 0 \leq p \leq 63k, 0 \leq q \leq 63k \right\}.$$

Note that we have used $(63k)^2$ quadrature points because our test functions will exhibit 63 regions of high and low flux around any of its circumferences and so we will be using k quadrature points for each peak and trough in the θ and ϕ direction.

To ensure that this repeated trapezium quadrature method gives a suitably accurate approximation to the integral in Condition (2.38) we will increase the number of quadrature points until the relative change in the numerical approximation of the integral is less than 10^{-4}, so if I_k is the value of the approximated integral using the repeated trapezium rule with $(63k)^2$ equally spaced quadrature points, then we increase k until

$$\left| \frac{I_{k+1} - I_k}{I_{k+1}} \right| < 10^{-4},$$

and then take I_{k+1} to be an appropriate numerical approximation of the double integral in Condition (2.38)

Bounding the Perturbation

Having calculated our numerical approximation to the perturbation we now consider how to find the maximum value of this approximation at any given radius. If possible we will bound the perturbation analytically, but it is likely we will have to approximate this maximum value numerically.

To numerically approximate the maximum value of the perturbation at a given radius we will evaluate the numerical approximation to the perturbation, $\widetilde{c}'$, at $(63k)^2$ equally spaced θ and ϕ values and consider the maximum observed value as defined by

$$M_k(r) = \max \left\{ \left| \widetilde{c}' \left(r, \frac{2\pi p}{63k}, \frac{\pi q}{63k} \right) \right| \middle| 0 \leq p \leq 63k, 0 \leq q \leq 63k \right\}, \tag{2.39}$$

and then increase k until the change in value of $M_k(r)$ is acceptably small. Note that we are calculating the maximum value of the perturbation so that we can compare it to the mean and so any error in the bound on the perturbation need only be small compared to the mean. Hence we increase k until the error in the approximation to the maximum value of the perturbation is small compared to the magnitude of the mean, and so we increase k until

$$\max_{0 \leq r \leq 1} |M_{k+1}(r) - M_k(r)| < \frac{\overline{c}(1)}{10^4}. \tag{2.40}$$

Summarising the Numerical Scheme

To approximate the magnitude of the perturbation we have performed several numerical approximations and some of these numerical approximations depend upon previously calculated numerical approximations. A summary of all these numerical approximations is presented in Table 2.1.

Details of how these numerical scheme is actually implemented for our test functions are presented in the Appendix and referenced in the section discussing that test function.

2.7 Further Results

2.7.1 Test Function 2

For our second test function we consider a simple test function which exhibits the necessary properties discussed in Section 2.3.2 and take the perturbed flux to be

$$\widetilde{h}(\theta,\phi) = \left(\frac{1-{r_*}^3}{3}\right)\sin(63\theta)\sin(63\phi). \tag{2.41}$$

The distribution of the nutrient flux across the surface of the tumour spheroid corresponding to this test function is shown in Figure 2.6.

To quantify the magnitude of the perturbation corresponding to this test function we utilise the numerical scheme derived in the previous section, Section 2.6, but here we are able to make some simplifications to the general scheme. These simplifications and details of how the scheme are actually implemented are outlined in Appendix A.1. Then our bound on the nutrient concentration and the corresponding mean, as given by Equation (2.21), for $r_* = 0.83,\ 0.92,\ 0.85,\ 0.9$, and 0.95 are shown in Figure 2.7.

As with the first test function it can be seen that for all values of r_*, for dimensional radii $r < 950\,\mu$m the difference between the mean nutrient concentration and the bound on the nutrient concentration is so small that it cannot be resolved, but for dimensional radii $r > 950\,\mu$m a difference between the mean and the nutrient concentration can be seen for all values of r_*, and this difference appears to get relatively larger with increasing values of r_*.

Quantity being approximated	**Approximated by**	**How approximation is calculated**	**Criteria for approximation being valid**
$\alpha_{n,m}$	$\alpha'_{n,m}$	Any standard quadrature method.	Choose in conjunction with $\beta'_{n,m}$ and N so that Condition (2.38) is satisfied.
$\beta_{n,m}$	$\beta'_{n,m}$	Any standard quadrature method.	Choose in conjunction with $\alpha'_{n,m}$ and N so that Condition (2.38) is satisfied.
The order of the truncated solution series.	N	Increase N until Condition (2.38) is satisfied.	Choose in conjunction with $\alpha'_{n,m}$ and $\beta'_{n,m}$ so that Condition (2.38) is satisfied.
The perturbed flux $\left(\widetilde{h}(\theta,\phi)\right)$.	$\widetilde{h}'(\theta,\phi)$.	From Equation (2.37) using the values of $\alpha'_{n,m}$, $\beta'_{n,m}$ and N.	Ensure that Condition (2.38) is satisfied.
The integral in Condition (2.38).	I_k	Using repeated Trapezium rule quadrature method with $(63k)^2$ quadrature points.	Increase the number of quadrature points until $\left\lvert\frac{I_{k+1}-I_k}{I_{k+1}}\right\rvert < 10^{-4}$.
The perturbation $(\widetilde{c}(r,\theta,\phi))$.	$\widetilde{c}\,'(r,\theta,\phi)$	From Equation (2.33) using the values of $\alpha'_{n,m}$, $\beta'_{n,m}$ and N.	Ensure that Condition (2.38) is satisfied.
$\max_{\theta,\phi}\lvert\widetilde{c}(r,\theta,\phi)\rvert$	$M_k(r)$	Evaluate the perturbation at $(63k)^2$ points and take the maximum observed value.	Increase the number of evaluation points until Condition (2.40) is satisfied.

Table 2.1: A summary of the numerical scheme used to evaluate and bound the perturbation, which outlines the quantities being approximated, how these approximations are denoted, how the approximations are calculated, and the criteria used to ensure the approximations are valid.

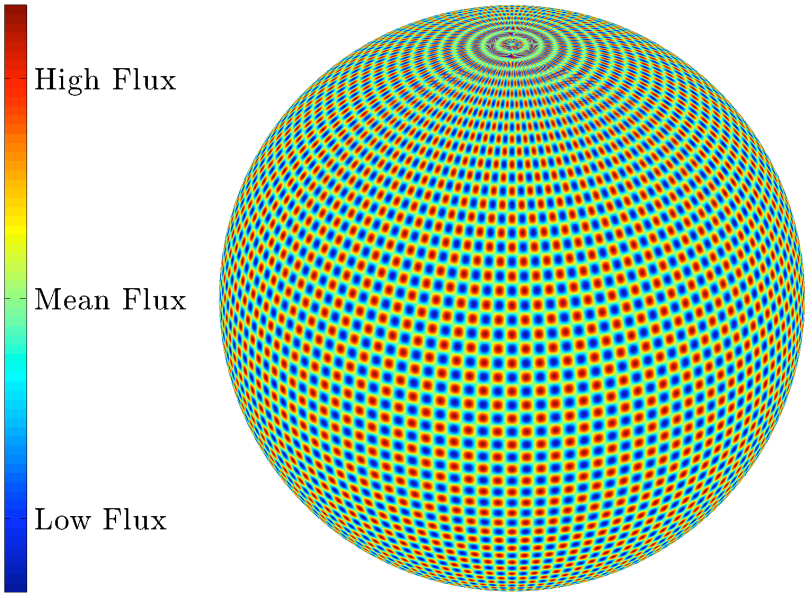

Figure 2.6: The distribution of the nutrient flux across the surface of the tumour when the perturbation away from the mean nutrient flux is given by Equation (2.41).

2.7.2 Test Function 3

For our third test function we consider the fact that the regions of high and low flux across the surface of the tumour will not all be perfectly evenly distributed. Fait et al. (1998) found that the mean inter-capillary distance in the human large intestine is approximately $100\,\mu$m, but a range of inter-capillary distances from $41.7\,\mu$m to $196.3\,\mu$m was observed. To capture this we take our third test function to be

$$\widetilde{h}(\theta,\phi) = \left(\frac{1-r_*^3}{3}\right)\sin\left\{63\left(\theta+\frac{\sin(10\theta)}{20}\right)\right\}\sin\left\{63\left(\phi+\frac{\sin(10\phi)}{20}\right)\right\}. \quad (2.42)$$

Then the distribution of the nutrient flux across the surface of the tumour spheroid is shown in Figure 2.8, and it can be seen that the regions of high and low flux vary in size.

We approximate the perturbation associated with this test function using the methodology outlined in the previous section, Section 2.6, but again we are able to simplify the general procedure. These simplifications and details of how the numerical scheme are actually implemented are outlined in Appendix A.2. Having bounded

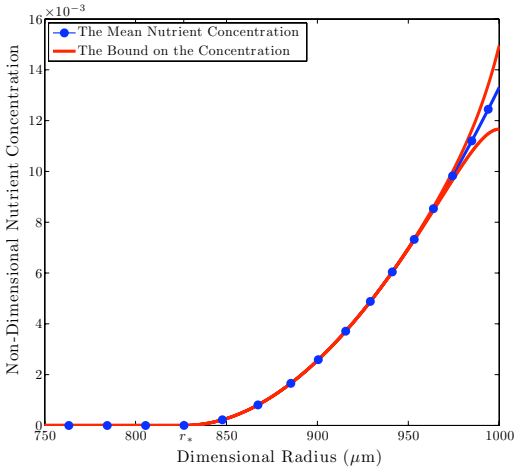

(a) $r_* = 0.83$

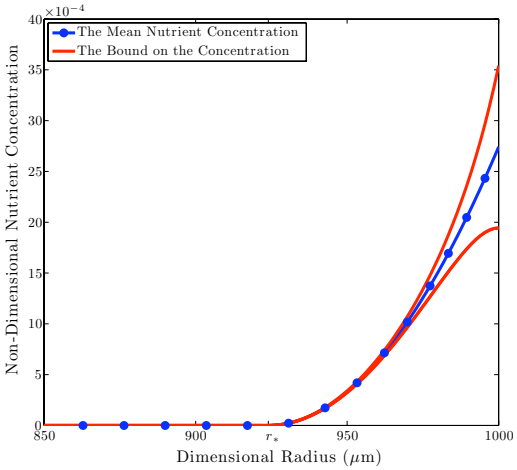

(b) $r_* = 0.92$

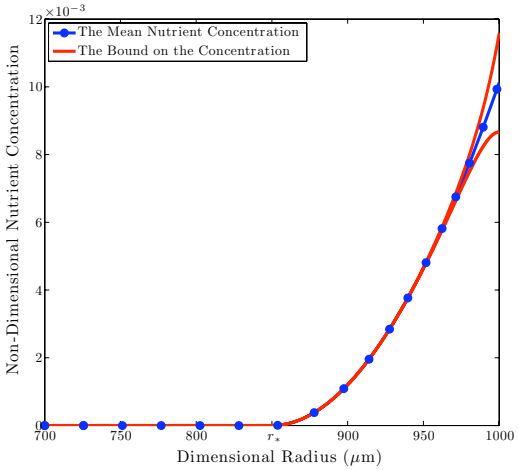

(c) $r_* = 0.85$

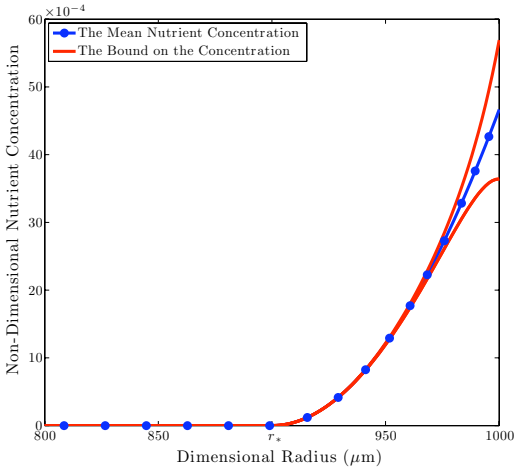

(d) $r_* = 0.9$

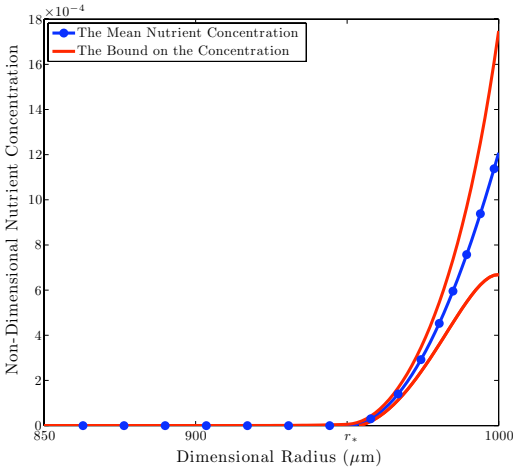

(e) $r_* = 0.95$

Figure 2.7: The radially averaged mean nutrient concentration and the bound on the nutrient concentration, as given by Equations (2.21) and (2.33), in an avascular tumour of radius 1000 μm as a function of the radius from the centre of the tumour when the perturbed flux is as given by Equation (2.41) for different values of r_*, the radius of saturation, as defined in Section 2.2.1. See text for details.

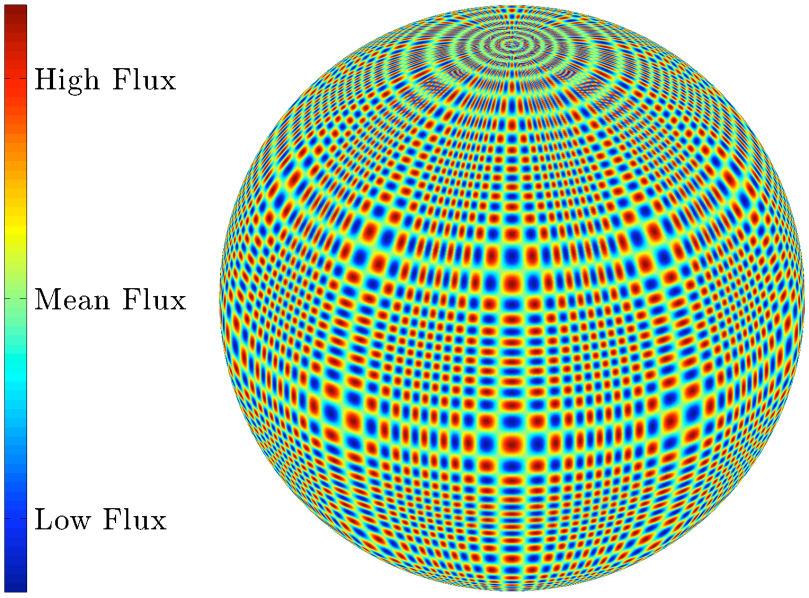

Figure 2.8: The distribution of the nutrient flux across the surface of the tumour when the perturbation away from the mean nutrient flux is given by Equation (2.42).

the perturbation we plot this bound and the mean, as given by Equation (2.21), for $r_* = 0.83,\ 0.92,\ 0.85,\ 0.9$, and 0.95 in Figure 2.9.

Our third test function behaves similarly to those considered previously, although the bound on the perturbation is looser for this third test function. It can be seen here that for all values of r_* for dimensional radii $r < 925\,\mu$m the difference between the mean nutrient concentration and the bound on the nutrient concentration is small, but for dimensional radii of $r > 925\,\mu$m a difference between the mean and the nutrient concentration becomes significant and this difference appears to become relatively larger with increasing values of r_*.

2.8 Conclusions

In this chapter we were aiming to compare the magnitudes of the radially averaged mean nutrient concentration in an avascular tumour spheroid and the perturbation away from the mean nutrient concentration. We were doing this to investigate the

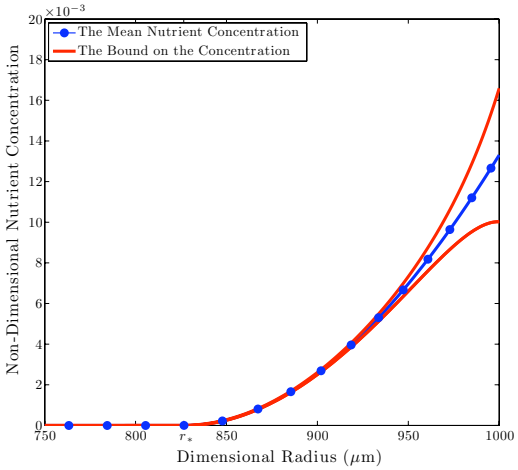

(a) $r_* = 0.83$

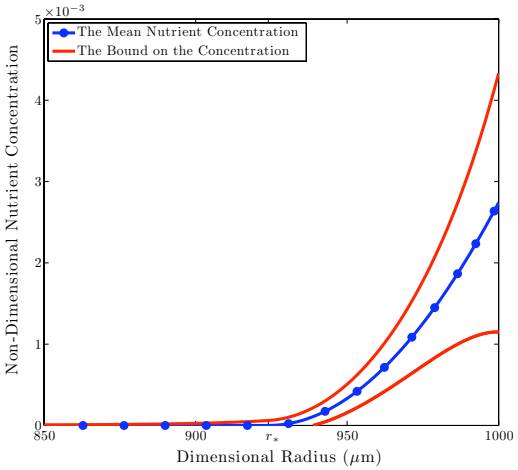

(b) $r_* = 0.92$

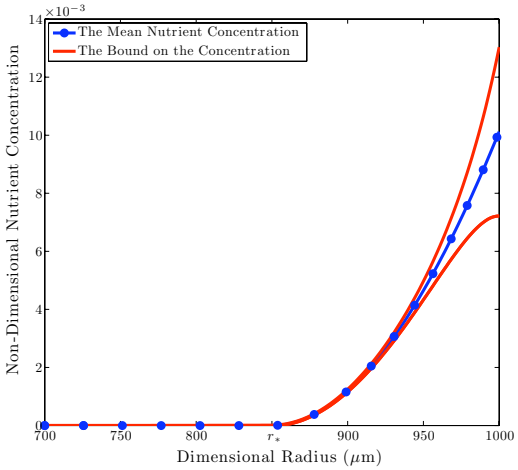

(c) $r_* = 0.85$

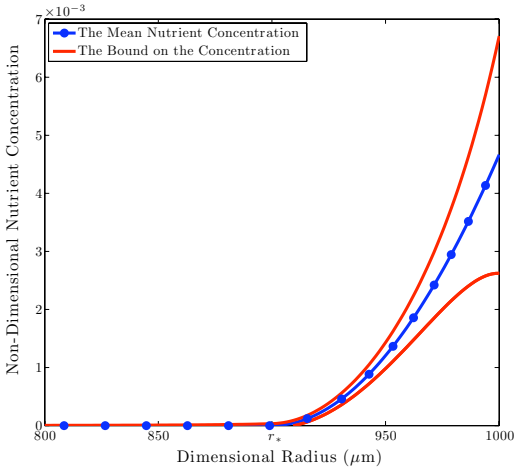

(d) $r_* = 0.9$

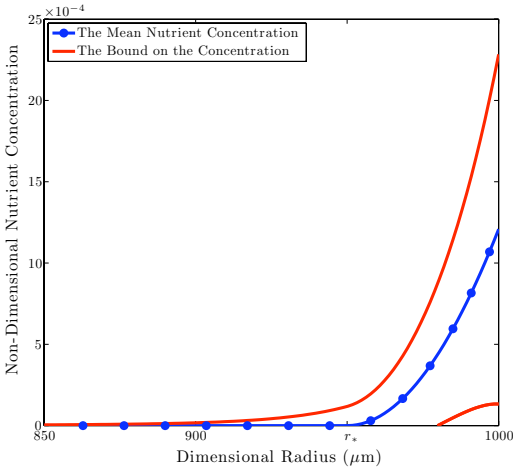

(e) $r_* = 0.95$

Figure 2.9: The radially averaged mean nutrient concentration and the bound on the nutrient concentration, as given by Equations (2.21) and (2.33), in an avascular tumour of radius 1000 μm as a function of the radius from the centre of the tumour when the perturbed flux is as given by Equation (2.42) for different values of r_*, the radius of saturation, as defined in Section 2.2.1. See text for details.

assumption that the concentration of any nutrient of drug within an avascular tumour spheroid is radially symmetric.

We achieved this by deriving a model for the diffusion of an arbitrary nutrient out of the capillary network and into an avascular tumour spheroid. In deriving our model we assumed that the rate of nutrient uptake saturates and does so quickly, although we later justified this assumption using a consistency check. Having justified this assumption for glucose we would expect it to be valid for any nutrient which is required for cell growth, because cells have evolved to be efficient at uptaking such nutrients. However, this assumption may not be true for nutrients, or drugs, which the cell has not evolved to take up efficiently, such as an arbitrary chemotherapeutic.

From this model we obtained a lower estimate for the radially averaged mean nutrient concentration within the tumour, and an upper bound on the perturbation away from this mean. These quantities still exhibited some freedom and to consider their general behaviour we considered a number of different distributions for the nutrient flux into the tumour and a number of different radii of saturation in each case.

Comparing the magnitudes of our lower estimated mean and the bound on the perturbation we found that the test functions all behaved similarly. For smaller values of r_*, which corresponds to the radius of saturation being a larger distance into the tumour, the bound on the perturbation was suitably tight for the mean nutrient concentration to be a valid approximation of the nutrient concentration.

As r_* increases, which corresponds to the radius of saturation moving closer to the edge of the tumour, the bound on the nutrient concentration loosens until eventually the difference between the mean and the nutrient concentration may become significant. In fact, for our first test function we showed analytically that as r_* tends to one, so that the radius of saturation moves to the edge of the tumour, the possible relative difference between the nutrient concentration and the mean tends to infinity.

So the expected value of r_* is fundamental to our conclusions. Our model is most applicable to nutrients which are required for cell growth and it would be expected that such nutrients would diffuse a significant distance into the tumour. In which case the largest value applicable value of r_* will be $r_* = 0.92$, which corresponds to a cell cycle specific nutrient being considered and the radius of saturation being the inner surface of the proliferating rim.

Figures 2.5(b), 2.7(b), and 2.9(b) show the mean nutrient concentration and bound on the nutrient concentration for the different test functions when $r_* = 0.92$. It can

be seen that the bound on the nutrient concentration is suitably tight to the mean, except for in a thin region of width approximately 25 μm on the edge of the tumour. The behaviour in such a thin region is unlikely to have a significant effect on the entire tumour. Furthermore we have demonstrated that for nutrients required for cell growth, which are the nutrients to which our model is most applicable, the nutrient uptake saturates and does so quickly. Hence even if the nutrient concentration cannot be assumed to be radially symmetric on the edge of the tumour, it may be valid to assume that the rate of nutrient uptake on the edge of the tumour is radially symmetric there.

Given this we conclude that for nutrients required for cell growth it is valid to assume that the nutrient concentration within the tumour is radially symmetric. Note that this conclusion is further supported by the fact that we deliberately considered a lower estimate for the mean and obtained a maximum bound for the perturbation so that our results represent the worst case scenario for our problem.

However for nutrients not required for cell growth, such as chemotherapeutic drugs, this conclusion may not apply. Either because the rate of nutrient uptake does not saturate, in which case our model does not apply, or because the nutrient only penetrates a small distance into the tumour. However if a nutrient does not even penetrate across the entire proliferating rim, then the nutrient will only be present in a region of the tumour which is less than two cell widths across. In which case a continuum model for the evolution of the tumour is unlikely to be appropriate anyway.

Given these conclusions we will assume that the concentration of any nutrient required for cell growth is radially symmetric, and we utilise this assumption in our model for the evolution of an avascular tumour spheroid in Chapter 3.

Chapter 3

The Interaction Between an Avascular Tumour Spheroid and the Surrounding Vasculature

3.1 Introduction

In this chapter we consider the interaction between an avascular tumour spheroid and the surrounding vasculature. In particular we consider how the distance between an avascular tumour spheroid and the surrounding vasculature varies as the tumour grows. We begin by carrying out a review of the relevant biological and mathematical literature.

3.1.1 Literature Summary

There is little information in the literature concerning the interaction between avascular tumours and the surrounding vasculature. Our literature review will therefore gather some information from implicit statements in the literature and previous mathematical models for angiogenesis. We begin by reviewing the biological literature.

Biological Literature

Most biological research into angiogenesis concerns the mechanisms which cause and drive angiogenesis and any interaction between the tumour and vasculature before the onset of angiogenesis is often overlooked. However, there is a prevailing implicit assumption in the literature that a significant gap exists between the tumour and the

vasculature at the onset of angiogenesis. Kerbel (2000) typifies this by describing the process of angiogenesis thus: "host blood vessels begin sprouting new blood capillaries which grow toward and eventually infiltrate the tumour masses". To have the literature discuss capillaries growing **toward** the tumour suggests that before the initiation of angiogenesis there is a significant gap between the tumour and vasculature for the capillaries to grow into.

One paper which does explicitly consider the movement of the vasculature surrounding an avascular tumour is an early paper by Warren and Shublik (1966), who implanted mammary carcinoma and viewing chambers into the cheeks of hamsters and observed the evolution of the tumour and the movement of the surrounding vasculature over a period of ten days. It was observed that, "As the tumour expanded it carried its vasculature with it, as well as pushing existing vessels ahead of the leading edge", which would appear to suggest that the capillaries ahead of the tumour move so that a gap between the tumour and the surrounding capillaries is maintained as the tumour grows. However, this work was not specifically investigating the distance between the capillaries and the tumour; instead it was considering the broad behaviour of the vasculature as the tumour grows. Their observation could equally be describing a growing tumour which pushes the surrounding vasculature ahead of it at a slower speed than that of the tumour front, so that the distance between the tumour and surrounding vasculature still decreases as the tumour grows. So we cannot be certain what their observation means for the interaction between an avascular tumour and surrounding vasculature. To further confuse things the sketch accompanying this work appears to show the distance between the tumour and capillaries decreasing as the tumour grows so that the capillaries eventually lie on the surface of the tumour whilst it is still avascular.

Note that some primary carcinomas, as opposed to metastases, can initiate with a basement membrane separating the tumour and capillaries, for example breast ductal carcinomas. In such tumours the basement membrane has the potential to form a restrictive barrier if it withstands the physical pressures of adjacent tumour growth without deforming into the capillary bed. Under such circumstances there will be a gap between the tumour and neighbouring capillaries of at least the lengthscale of the basement membrane thickness, possibly more. Here we will only consider the growth of tumours which are not inhibited by the presence of such a basement membrane, which is particularly relevant for modelling the growth of micrometastases.

Whilst it is widely accepted that most avascular tumours grow to their maximum size as given by diffusion limited control and then belatedly cultivate a blood supply, it has been shown that a subset of tumours obtain their vasculature via vessel co-option (Leenders et al., 2002; Wesseling et al., 1997; Dome et al., 2002). Holash et al. (1999) in particular considered vessel co-option in rat gliomas. They implanted gliomas into rat brains and observed them for four weeks and concluded that, "a subset of tumours rapidly co-opts existing host vessels to form an initially well vascularized tumour mass. There is wide spread regression of these initially co-opted vessels, leading to a secondarily avascular tumour and massive tumour cell loss. The remaining tumour is ultimately rescued by robust angiogenesis at the tumour margin".

Whilst the growth phase of co-opting tumours is very different to that of traditional avascular tumours, such tumours eventually cultivate their own blood supply by normal angiogenesis. Furthermore, in such tumours only the co-opted vessels are observed to regress and the vessels immediately outside the tumour are left intact. Hence when a co-opting tumour initiates angiogenesis the surrounding capillaries will be expected to lie on the surface of the tumour.

So a tumour that grows by vessel co-option would be expected to have the surrounding capillaries lie on its surface at the onset of angiogenesis. However, for a traditional avascular tumour which is not inhibited by the presence of the basement membrane or some other aspect of the local geometry is not clear what gap, if any, should exist between the surface of the tumour and the surrounding vasculature at the onset of angiogenesis.

Mathematical Literature

We now consider previous mathematical models for angiogenesis to see if there is a consensus as to whether a significant gap exists between the tumour and the capillaries at the onset of angiogenesis.

Mathematical models of angiogenesis often assume that there is a significant gap between the capillaries and the tumour at the onset of angiogenesis, but are not clear about how wide this gap should be and what mechanisms might maintain it. For example, Chaplain and Stuart (1993) and Chaplain (1995) both implicitly assume there is a gap between the tumour and the capillaries and then non-dimensionalise this gap to unity without explicitly evaluating it or considering why such a gap would exist.

Many other mathematical papers considering angiogenesis (including Balding and McElwain, 1985; Chaplain et al., 1995; Byrne and Chaplain, 1995; Holmes and Sleeman, 2000; Chaplain, 2000) take parameters from experiments where tumours have been implanted into a rat cornea. Motivated by these experiments, which exhibit a large gap between the newly implanted tumour and the surrounding vasculature, such papers assume that a significant gap exists between the tumour and the capillaries at the onset of angiogenesis, and is at least 2 mm wide. However, the cornea is a completely and uniquely avascular region of tissue and it is not clear whether this framework would be applicable to tumours growing in normally vascularised tissue.

The overall implicit consensus of the mathematical literature is that a significant gap between the tumour and neighbouring capillaries exists. However the existence of such a gap has not been verified experimentally, except in the context of intra-cornea tumour implantation, and the potential mechanisms which might maintain this gap are not known.

Summary

We have found that much of the mathematical and biological literature suggests that there is a significant gap between an avascular tumour and the surrounding capillaries, but the mechanism which might maintain this gap as the tumour grows is not known. This highlights a lack of understanding of how a tumour and the surrounding capillaries might interact as the tumour grows.

3.1.2 The Aims of this Chapter

In this chapter we aim to investigate the interaction between the tumour and the surrounding capillaries as the tumour grows. Of particular interest will be whether or not a significant gap exists between the tumour and surrounding vasculature, and what mechanisms might maintain or close this gap.

3.2 A Scaling Argument

The net rate of proliferation of tumour cells is typically faster than non-cancerous cells and hence cancerous tissue would be expected to increase in volume at a faster rate than non-cancerous tissue. We now consider whether this difference in proliferation

rates is consistent with the presence of a significant gap between the tumour and the surrounding vasculature, which our literature review suggested should exist. In particular, we consider whether the difference in proliferation rates can maintain a gap of constant width as the tumour grows.

Consider a tumour spheroid of radius $r(t)$, which is a function of time, then the corresponding tumour volume, $V_{\text{tum}}(t)$, is

$$V_{\text{tum}} = \frac{4\pi r^3}{3}.$$

From this we can use the chain rule to obtain an expression for the net growth rate per unit volume of the tumour

$$\frac{1}{V_{\text{tum}}}\frac{\mathrm{d}V_{\text{tum}}}{\mathrm{d}t} = \frac{3}{r}\frac{\mathrm{d}r}{\mathrm{d}t}. \tag{3.1}$$

Now assume that a gap of constant width is maintained between the tumour and the surrounding capillaries as the tumour grows. Then to be consistent with the mean inter-capillary distance this gap should be approximately $50\,\mu$m wide (Fait et al., 1998) and the volume of healthy tissue in this gap, $V_{\text{gap}}(t)$, is

$$V_{\text{gap}} = \frac{4\pi}{3}\big\{(r + 50\,\mu\text{m})^3 - r^3\big\}.$$

Again, we can use the chain rule to obtain an expression for the net growth rate per unit volume of healthy tissue in this gap

$$\frac{1}{V_{\text{gap}}}\frac{\mathrm{d}V_{\text{gap}}}{\mathrm{d}t} = \frac{3\big\{(r + 50\,\mu\text{m})^2 - r^2\big\}}{(r + 50\,\mu\text{m})^3 - r^3}\frac{\mathrm{d}r}{\mathrm{d}t}. \tag{3.2}$$

Taking the ratios of Equations (3.1) and (3.2) then gives an expression for the relative net growth rate per unit volume of each compartment:

$$\frac{\dfrac{1}{V_{\text{gap}}}\dfrac{\mathrm{d}V_{\text{gap}}}{\mathrm{d}t}}{\dfrac{1}{V_{\text{tum}}}\dfrac{\mathrm{d}V_{\text{tum}}}{\mathrm{d}t}} = \frac{r(r + 50\,\mu\text{m})^2 - r^3}{(r + 50\,\mu\text{m})^3 - r^3}. \tag{3.3}$$

Note that the right hand side of Equation (3.3) contains no time derivatives, so that the ratio of net growth rates of the different tissue types is actually independent of the growth rate of the tumour.

For large tumours the quantity $\frac{1}{V_{\text{tum}}}\frac{\mathrm{d}V_{\text{tum}}}{\mathrm{d}t}$ will be a poor estimate of the proliferation rate of individual tumour cells. This is because large tumours possess significant quiescent and necrotic regions and so the net doubling rate of the tumour will be significantly slower than the doubling rate of individual proliferating tumour cells. However, for a tumour of radius less than $80\,\mu$m all the cells within the tumour can be expected to be proliferating (LaRue et al., 2004). For such a tumour we can use Equation (3.3) to estimate the ratio of growth rates of proliferating tumour cells to non-cancerous cells and substituting in $r = 80\,\mu$m we find that

$$\frac{\dfrac{1}{V_{\text{gap}}}\dfrac{\mathrm{d}V_{\text{gap}}}{\mathrm{d}t}}{\dfrac{1}{V_{\text{tum}}}\dfrac{\mathrm{d}V_{\text{tum}}}{\mathrm{d}t}} = 0.499 \quad (3\,\text{s.f.}).$$

So to maintain a uniform gap between the tumour and capillaries we require non-cancerous cells to proliferate on average approximately half as quickly as proliferating tumour cells. However tumour cells usually proliferate much faster than non-cancerous cells; for example in healthy liver tissue only one cell in 10,000 to 20,000 is typically undergoing mitosis at any given time (Strain and Diehl, 1998) whereas in tumour tissue typically at least one cell in every ten is undergoing mitosis at any given time (McKinell et al., 1998). Hence this relative rate of proliferation is unrealistically high, except for tumours which are particularly slow growing or are growing in non-cancerous tissue which is particularly fast cycling.

This simple scaling argument shows that the maintenance of a uniform gap between the tumour and vasculature initially requires an unfeasibly high relative rate of proliferation of non-cancerous cells. This suggests that as the tumour begins to grow any gap between the tumour and surrounding vasculature will initially close and further highlights the non-triviality of the problem of whether a significant gap exists between the tumour and surrounding vasculature at the onset of angiogenesis.

However, our scaling argument does not imply that a significant gap between the tumour and surrounding vasculature cannot exist at the onset of angiogenesis. Our scaling argument only applies to small tumours and it could be hypothesised that the gap between the tumour and the vasculature might initially shrink when all the tumour cells are proliferating, but later recover once the growth fraction of the tumour has reduced.

To further investigate whether it is feasible for a significant gap to exist between the tumour and surrounding vasculature we now consider whether the capillaries could

supply enough oxygen to sustain an avascular tumour with a significant region of non-cancerous cells between the tumour and surrounding capillaries.

3.3 An Oxygen Delivery Argument

A solid avascular tumour at saturation places a considerable burden on the local vasculature and the addition of a region of healthy cells between the tumour and vasculature will place an even greater burden on the vasculature. We now consider whether it is feasible for the local vasculature to support this extra burden.

The Capacity of the Local Vasculature

We first estimate the maximum rate at which oxygen can be drawn out of the local vasculature. In particular we consider how much faster oxygen can be drawn out of the vasculature in extreme compared to regular conditions.

Oxygen extraction from the vasculature is often quantified by measuring a subject's arteriovenous oxygen difference (A-V O_2 difference), which measures how much oxygen the body extracts from the blood by considering the difference in oxygen content in the arterial and venous blood. Saltin et al. (1968) measured the A-V O_2 difference in five college students and found their mean resting A-V O_2 difference to be 4.2ml/100ml and their mean maximum A-V O_2 difference during exercise to be 16.2ml/100ml. So the oxygen extraction was found to increase almost fourfold in extreme compared to resting conditions. This is the average increase in oxygen extraction throughout the subject's body, but it is the muscles being exercised which experience the highest oxygen demand and so it could be hypothesised that the increase in oxygen extraction in the exercised tissue will be slightly higher than this.

This suggests that the oxygen flux out of the capillaries can increase by a factor of slightly more than four in extreme compared to normal conditions and gives us an indication of how much extra oxygen can be drawn out of the capillaries to support an avascular tumour. We now consider whether this observed increase in oxygen extraction is consistent with the presence of a region of healthy cells between the tumour and vasculature.

3.3.1 The Rate of Oxygen Supply in the Absence of a Tumour

We begin by quantifying the rate of oxygen extraction from the capillaries in the absence of a tumour and we will compare this to the corresponding oxygen extraction in the presence of a tumour.

We begin by considering the largest possible sphere of healthy tissue, in the absence of any tumour, which contains no capillaries. We label this sphere R_1 and let it have radius r_1, which will be determined by the inter-capillary distance. We assume that the cells in R_1 are homogeneous and that the oxygen uptake in R_1 takes place at the constant rate Γ_1. Such a system is as shown in Figure 3.1.

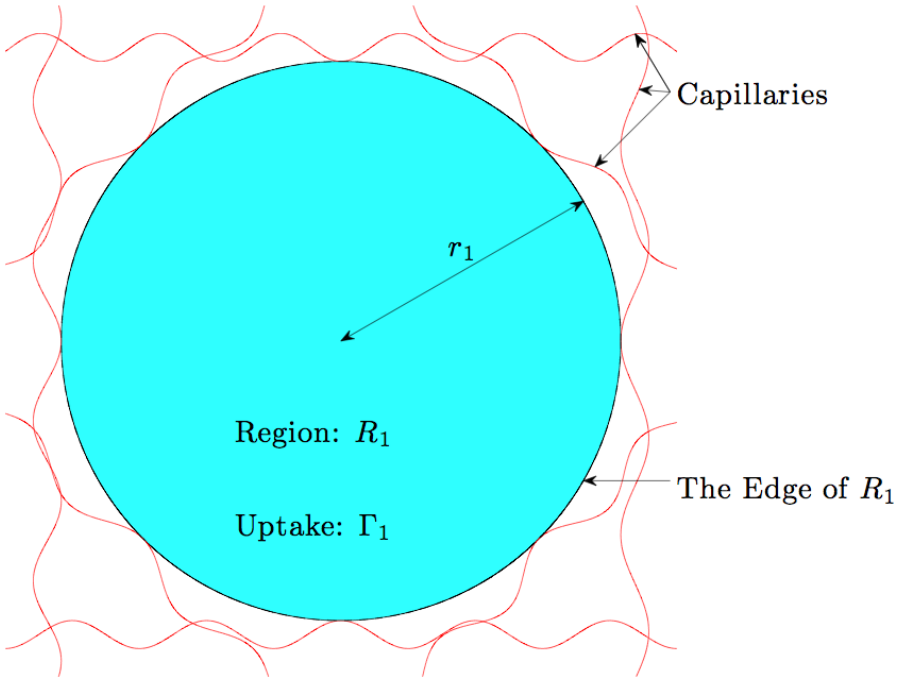

Figure 3.1: The region of non-cancerous cells considered to estimate the oxygen flux out of the vasculature in the absence of a tumour (not to scale).

As explicitly justified when performing the non-dimensionalisation in Section 2.2.2 of the previous chapter we assume that advection is negligible and make a quasi-steady state assumption, then the following simple diffusion equation can be derived for the evolution of the oxygen concentration

$$D\nabla^2 c = \Gamma_1 \qquad \text{in} \quad R_1,$$

where D is the diffusion coefficient of oxygen in healthy tissue and c is the local oxygen concentration. By integrating this equation over R_1, and using the divergence theorem, we can couple the total rate of oxygen uptake in R_1 to the total flux across ∂R_1 to obtain

$$\iint_{\partial R_1} D\nabla c \cdot \underline{n}\, \mathrm{dS} = \frac{4\pi\Gamma_1}{3} r_1^3.$$

where $\underline{n}$ is the outward unit normal. Denoting the mean oxygen flux out of the capillaries across ∂R_1 by μ_1, as defined by

$$\mu_1 = \frac{1}{4\pi r_1^2} \iint_{\partial R_1} D\nabla c \cdot \underline{n}\, \mathrm{dS},$$

we then obtain the following expression for μ_1

$$\mu_1 = \frac{\Gamma_1 r_1}{3}. \tag{3.4}$$

Hence the mean oxygen flux out of the capillaries is prescribed by the rate of oxygen uptake in the tissue. We now apply a similar argument to obtain an estimate for the mean oxygen flux in the presence of a tumour.

3.3.2 The Rate of Oxygen Supply in the Presence of a Tumour

We now consider the oxygen flux out of the vasculature in the presence of an avascular tumour spheroid which has grown to its maximum size as given by diffusion-limited control. Our system will consist of a tumour spheroid at saturation of radius r_2, which we label R_2. It is not expected that oxygen will penetrate all the way to the centre of the tumour and so we assume that there is a region on the edge of the tumour spheroid where oxygen uptake is homogeneous and occurs at a constant rate Γ_2, but within a distance a of the centre of the tumour the rate of oxygen uptake is zero, where a is to be estimated later.

We also assume the existence of a region of non-cancerous cells between the tumour and vasculature of width $\widetilde{r}_1$ which we label $\widetilde{R}_1$. As before we assume that the non-cancerous cells uptake oxygen homogeneously at a constant rate Γ_1. The system we are considering is then as shown in Figure 3.2.

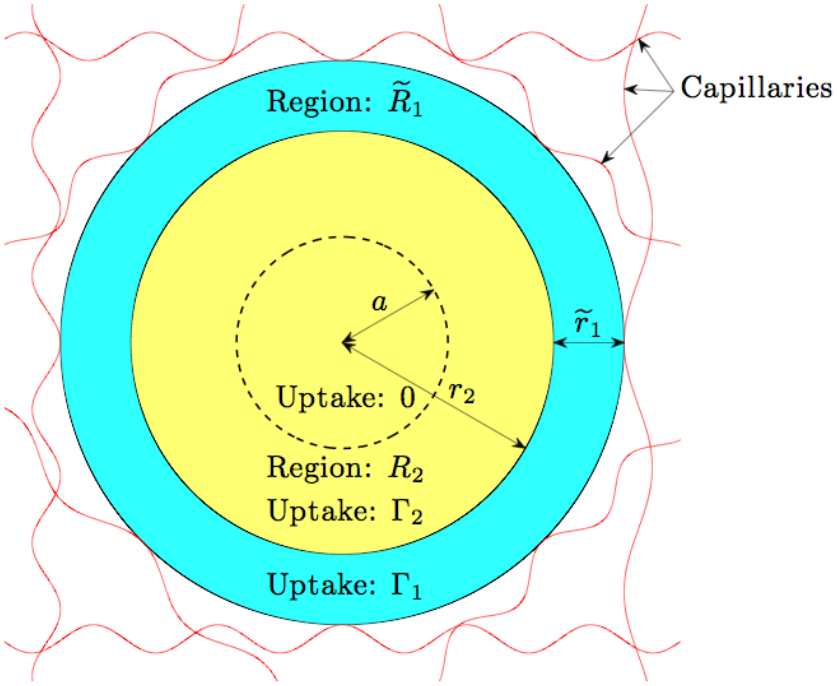

Figure 3.2: The regions of cancerous and non-cancerous cells considered to estimate the oxygen flux out of the vasculature in the presence of an avascular tumour at saturation (not to scale).

As before we assume that advection is negligible and make a quasi-steady state assumption to obtain a simple diffusion equation for the evolution of the oxygen concentration

$$D\nabla^2 c = \begin{cases} 0 & \text{if} \quad r \leq a, \\ \Gamma_2 & \text{if} \quad a < r \leq r_2, \\ \Gamma_1 & \text{if} \quad r_2 < r \leq \widetilde{r}_1 + r_2, \end{cases}$$

where D is the diffusion coefficient of oxygen and c is the local oxygen concentration. As before integrating this equation over $\widetilde{R}_1 \cup R_2$ allows us to couple the total rate of oxygen uptake in $\widetilde{R}_1 \cup R_2$ to the total flux across the surface of $\widetilde{R}_1 \cup R_2$ thus

$$\iint_{\partial(\widetilde{R}_1 \cup R_2)} D\nabla c \cdot \underline{n} \, \mathrm{dS} = \frac{4\pi\Gamma_1}{3}\left((\widetilde{r}_1 + r_2)^3 - r_2^3\right) + \frac{4\pi\Gamma_2}{3}\left(r_2^3 - a^3\right).$$

If we denote the mean oxygen flux out of the capillaries by μ_2, as defined by

$$\mu_2 = \frac{1}{4\pi\left(\widetilde{r}_1 + r_2\right)^2} \iint_{\partial(\widetilde{R}_1 \cup R_2)} D\nabla c \cdot \underline{n} \, \mathrm{dS},$$

then we obtain the following expression for μ_2

$$\mu_2 = \frac{\Gamma_1\left((\widetilde{r}_1 + r_2)^3 - r_2^3\right) + \Gamma_2\left(r_2^3 - a^3\right)}{3((\widetilde{r}_1 + r_2)^2}. \tag{3.5}$$

Taking the ratio of Equation (3.4) to Equation (3.5) then gives the following expression for the relative increase in oxygen flux out of the vasculature required to support the extra burden of the tumour:

$$\frac{\mu_2}{\mu_1} = \frac{\left(\widetilde{r}_1 + r_2\right)^3 - r_2^3}{r_1\left(\widetilde{r}_1 + r_2\right)^2} + \frac{\Gamma_2}{\Gamma_1}\frac{\left(r_2^3 - a^3\right)}{r_1\left(\widetilde{r}_1 + r_2\right)^2}. \tag{3.6}$$

Evaluating the Length Scales

To quantify the right hand side of Equation (3.6) we must evaluate the relevant length scales.

As in Chapter 2 we take r_1, half the inter-capillary distance, to be $50\,\mu$m (Fait et al., 1998) and r_2, the radius of an avascular tumour at saturation, to be $1000\,\mu$m (Folkman and Hochberg, 1973; Haji-Karim and Carisson, 1978).

To calculate the value of a, the radius of the sphere containing no oxygen, we consider the diffusion distance of oxygen in tumours. Olive et al. (1992) recorded the mean oxygen diffusion distance in mice tumours and found it to be $121 \pm 34\,\mu$m and Gunduz (1981) states that oxygen can only diffuse $80 - 90\,\mu$m into mouse mammary tumour tissue. This suggests that we would expect oxygen to diffuse approximately $100\,\mu$m into the tumour.

However, for the tumour's viable rim to be maintained oxygen must be present throughout the majority of the rim, with some of the rim also obtaining energy from glycolysis. Mueller-Klieser (2000) estimates that the viable rim on the surface of a $1000\,\mu$m radius tumour will be $174\,\mu$m (3 significant figures) deep, although this calculation extrapolates the trends of Mueller-Klieser's results beyond the range of tumour sizes explicitly considered.

Given these findings we take the penetration distance of oxygen into the tumour to be $120\,\mu$m, which is consistent with both the diffusion distance of oxygen and the width of the viable rim of our tumour. This then implies that $a = 880\,\mu$m.

To consider the width of any potential gap between the tumour and vasculature we will consider three different values for $\widetilde{r}_1$, the width of the gap between the tumour and vasculature at saturation. We will consider $\widetilde{r}_1 = 0\,\mu$m, which corresponds to no gap existing, $\widetilde{r}_1 = 50\,\mu$m, which corresponds to a gap of constant width being maintained as the tumour grows, and $\widetilde{r}_1 = 2000\,\mu$m, which corresponds to the width of gap seen in cornea implant experiments.

Finally, to evaluate the right hand side of Equation (3.6) we must consider the likely magnitude of the ratio $\frac{\Gamma_2}{\Gamma_1}$, which is the ratio of the rate of oxygen consumption in tumour tissue to the rate of oxygen consumption in non-cancerous tissue. The higher proliferation rate of tumour cells might cause them to exhibit higher metabolic activity than non-cancerous cells, however tumour cells obtain a significant proportion of their energy from glycolysis (Warburg, 1956) which suggests the ratio $\frac{\Gamma_2}{\Gamma_1}$ will be lower than the metabolic activity would suggest. Anticipating that Γ_1 and Γ_2 will be of similar magnitudes we consider a range of possible values for $\frac{\Gamma_2}{\Gamma_1}$, namely $0 < \frac{\Gamma_2}{\Gamma_1} < 2$, and consider how the right hand side of Equation (3.6) depends upon the ratio $\frac{\Gamma_2}{\Gamma_1}$.

3.3.3 Results

The relative oxygen supply, $\frac{\mu_2}{\mu_1}$, as a function of the relative oxygen uptake, $\frac{\Gamma_2}{\Gamma_1}$, for the different width gaps between the tumour and vasculature, $\widetilde{r}_1$, is shown in Figure 3.3.

It can be seen that when $\widetilde{r}_1 = 0\,\mu$m, so that the neighbouring capillaries lie on the surface of the tumour, the ratio of oxygen fluxes is an increasing function of the ratio of oxygen uptakes. In particular, when the rates of oxygen uptake are equal, so that $\frac{\Gamma_2}{\Gamma_1} = 1$ we have that the ratio of oxygen fluxes out of the vasculature is $\frac{\mu_2}{\mu_1} = 6.37$ (3 s.f.). This is larger than the relative increase of 4 seen in the maximum A-V O_2 difference experiments, but plausible for very extreme conditions. This is particularly plausible given that the tumour is at its maximum size as given by diffusion limited control and so the oxygen flux out of the vasculature would be expected to be at its absolute maximum.

Also note that when $\frac{\Gamma_2}{\Gamma_1} = 2$ we have $\frac{\mu_2}{\mu_1} = 12.7$ (3 s.f.). This is considerably larger than the relative increase of 4 seen in the maximum A-V O_2 difference experiments. The fact that the capillary network cannot supply enough oxygen to sustain this relative rate of oxygen uptake, even in the absence of any gap between the tumour and the vasculature, suggests that the relative oxygen uptake of the tumour cells must be less than 2, which validates the range of values of $\frac{\Gamma_2}{\Gamma_1}$ being considered.

Allowing the maintenance of a constant width gap between the tumour and vasculature, which corresponds to taking $\widetilde{r}_1 = 50\,\mu$m, the same trends are observed and the ratio of oxygen fluxes remains an increasing function of the ratio of oxygen uptakes. However the ratio of oxygen fluxes is higher than the case where no gap existed between the tumour and vasculature, and in particular when $\frac{\Gamma_2}{\Gamma_1} = 1$ we now have

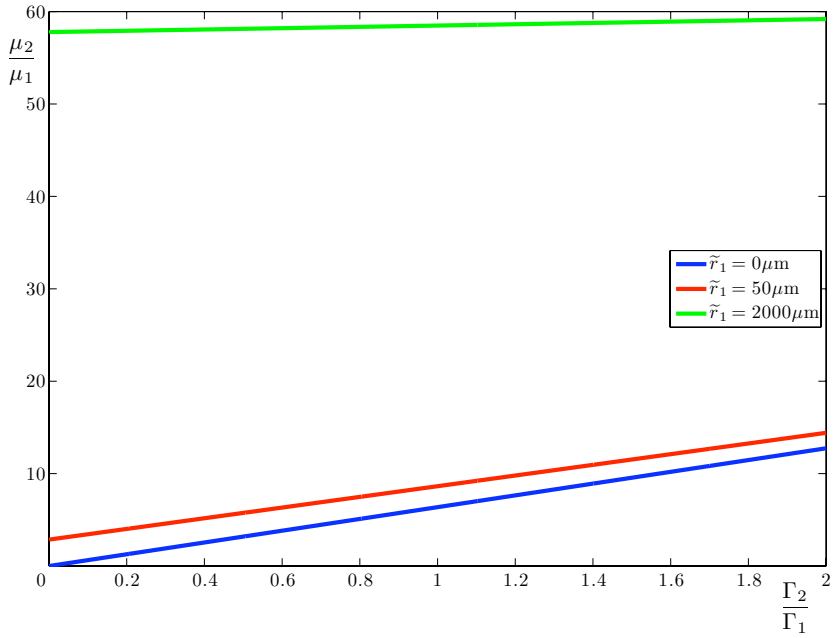

(a) The cases where $\widetilde{r}_1 = 0\mu$m, $\widetilde{r}_1 = 50\mu$m, and $\widetilde{r}_1 = 2000\mu$m.

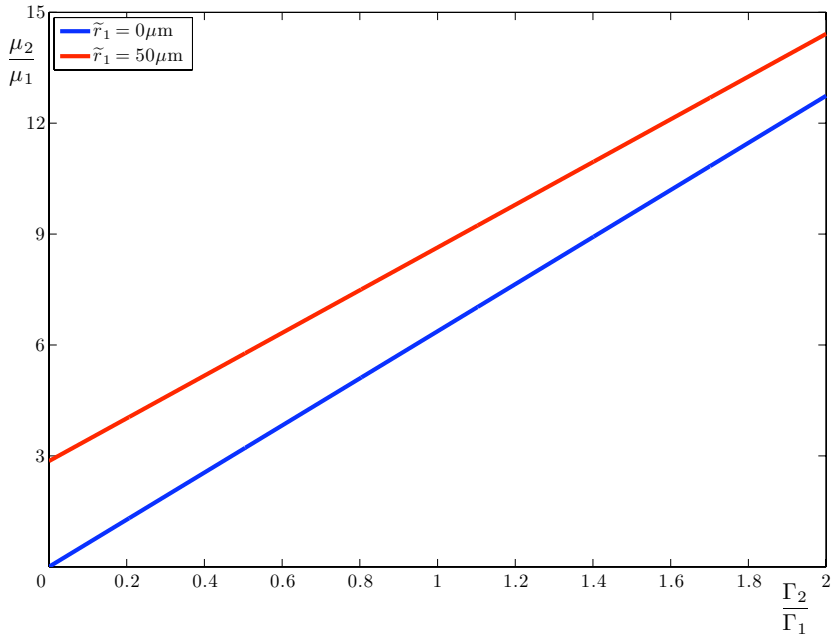

(b) The cases where $\widetilde{r}_1 = 0\mu$m, and $\widetilde{r}_1 = 50\mu$m in more detail.

Figure 3.3: The ratio of mean oxygen fluxes out of the vasculature in the presence of a tumour versus in the absence of a tumour, $\frac{\mu_2}{\mu_1}$, as a function of the ratio of the rate of oxygen uptake per unit volume in tumour versus non-cancerous tissue, $\frac{\Gamma_2}{\Gamma_1}$, for different widths of the gap between the tumour and the vasculature, $\widetilde{r}_1$, as governed by Equation (3.6).

$\frac{\mu_2}{\mu_1} = 8.64$ (3 s.f.). Such an increase in oxygen supply is not impossible, however it is twice that seen during maximal exercise, which is a very high demand for the vasculature to meet.

Finally, we see that taking $\widetilde{r}_1 = 2000\,\mu$m, which corresponds to the size of gap between the tumour and vasculature considered by models motivated by the cornea implant experiments, requires approximately 60 times as much oxygen supply than the case where no tumour is present. This is obviously much larger than is possible. In particular it is unfeasible for the local vasculature to supply enough oxygen to support such a system.

3.3.4 Conclusions

This rate of oxygen supply argument has shown that the presence of a 2 mm gap between a tumour and surrounding vasculature is unique to tumours implanted into the cornea, where nutrient supply is uniquely not contingent on vasculature, and cannot be representative of tumours growing in other tissue. So whilst the 2 mm gaps seen in the intra-cornea implant experiments are relevant to that setting, such a configuration cannot represent a tumour growing in vascularised tissue. It has also shown that the existence of a gap of constant width between the tumour and vasculature as the tumour grows would require a very high rate of oxygen supply, but our analysis was inconclusive concerning whether such a gap is plausible.

Similarly, our previous scaling argument showed that in general the distance between the tumour and the surrounding vasculature must reduce when the tumour first starts to grow, but was equivocal concerning whether gaps could exist on the surface of larger tumours. Since these simple models have proved inconclusive at investigating whether a small gap can exist between an avascular tumour at saturation and the surrounding vasculature we now utilise a full multi-compartment model for the growth of a avascular tumour spheroid to consider this problem in more detail.

3.4 A Multi-Compartment Model for Avascular Tumour Growth

In our multi-compartment model we consider the tumour and surrounding tissue to be a continuum of cells. Our model will consist of healthy non-cancerous cells,

proliferating cancerous cells, quiescent cancerous cells and necrotic cells and we now derive an equation governing the evolution of each class of cell and close our model by coupling these equations together and deriving the appropriate initial and boundary conditions.

3.4.1 The Model

Preliminary Assumptions

We assume that the tumour grows as a spheroid and given the results of the previous chapter we also assume that the distribution of the different cell compartments and the concentration of any nutrients in our system are radially symmetric. We derive our model in spherical polar co-ordinates, with the origin taken to be the centre of the tumour, as defined by

$$x = r\cos\theta\sin\phi, \qquad y = r\sin\theta\sin\phi, \qquad z = r\cos\phi,$$

where $$r \in [0, \infty), \qquad \theta \in [0, 2\pi), \qquad \phi \in [0, \pi].$$

The Domain

The domain of our system will consist of a tumour spheroid of radius S_{tum} and the region of non-cancerous cells outside the tumour up to and including the capillaries which are closest to the edge of the tumour. The boundary of our domain will be the largest sphere which is concentric with the tumour spheroid but contains no capillaries. This spheroid will be referred to as the capillary spheroid and will have radius S_{cap}. A schematic cross-section of our domain is shown in Figure 3.4.

Healthy Non-Cancerous Cells

We assume that in the absence of any tumour the healthy non-cancerous cells (hereby simply referred to as healthy cells) will exist in a steady state where the density of healthy cells is constant and uniform. We note that whilst healthy cells do proliferate as part of the natural turnover of cells, this proliferation occurs rarely and in many tissues the vast majority of healthy cells are in a quiescent state (Strain and Diehl, 1998). So whilst individual cells may be undergoing mitosis or necrosis, we

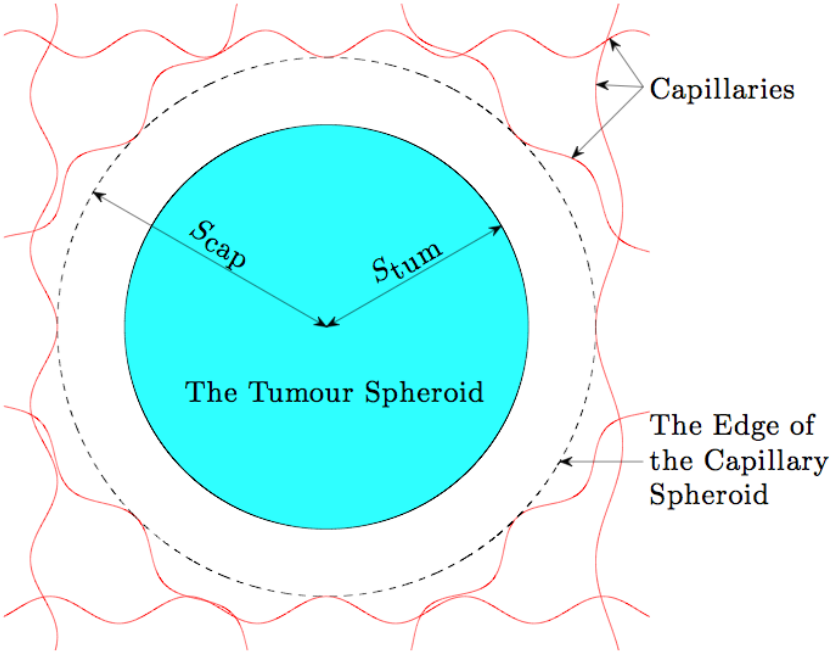

Figure 3.4: The domain of our multi-compartment model for avascular tumour growth (not to scale).

assume that we can neglect these processes in a leading order approximation. Then a conservation of cells argument gives the evolution of healthy cells to be governed by

$$\frac{\partial h}{\partial t} + \nabla \cdot (\underline{v} h) = 0, \tag{3.7}$$

where $h(r,t)$ is the density of healthy cells at radius r at time t, and $\underline{v}(r,t) = v(r,t)\underline{e}_r$ denotes the local cell velocity.

Proliferating Tumour Cells

We now consider the evolution of the tumour cells which are proliferating (hereby simply referred to as proliferating cells). It is possible that crucial nutrients required for cell growth will not adequately diffuse to all the proliferating cells. A lack of any such nutrient could then inhibit mitosis and/or drive cell necrosis. To model this we assume there is a single crucial nutrient, which we analogise to be oxygen, and make the often made assumption that the rates of cell mitosis and necrosis are functions of the local nutrient concentration (Lin, 1976; McElwain, 1978).

We denote the rates of mitosis and necrosis per proliferating cell by $k_m(c)$ and $k_d(c)$ respectively, where $c(r,t)$ is the local oxygen concentration. The rate of mitosis must

be a non-decreasing function of the local oxygen concentration, where the cells cannot proliferate in the complete absence of oxygen and the cells can only proliferate at a finite rate given an unlimited oxygen supply. To capture this behaviour we take $k_m(c)$ to be given by a first order Michaelis-Menten kinetic:

$$k_m(c) = \frac{Ac}{c + c_c}, \tag{3.8}$$

where A and c_c are constants. Michaelis-Menten uptake kinetics are often used to model cell kinetics (Casciari et al., 1992; McElwain, 1978); in particular Lin (1976) considered the data of Amberson (1928) for the oxygen consumption rate in a cell and showed Michaelis-Menten uptake kinetics to be a good fit to the data and White et al. (1978) have also observed that oxygen consumption in tissue often follows Michaelis-Menten kinetics.

Similarly, we expect the rate of cell death to be a non-increasing function of the local oxygen concentration, where the cell death rate is non-zero in an unlimited oxygen supply. To capture this behaviour we take $k_d(c)$ to also be given by a Michaelis-Menten based kinetic:

$$k_d(c) = B\left(1 - \frac{\sigma c}{c + c_d}\right),$$

where B, $\sigma < 1$ and c_d are constants.

As well as proliferating and dying, the density of proliferating cells will vary as proliferating cells become quiescent and quiescent cells recover the ability to proliferate. It is often suggested that proliferating cells become quiescent when the concentration of oxygen falls below some threshold level, and that quiescent cells can recover the ability to proliferate if the oxygen concentration increases again. For example, Casciari et al. (1992) makes this assumption when modelling the growth of an avascular tumour based upon the local concentration of oxygen and glucose. Whilst this is a popular analogy it has been shown in a number of studies that the onset of quiescence is not exclusively driven by hypoxia. For example, it has been shown that quiescent cells exist at the centre of small spheroids where there is only a slight difference in oxygen and nutrient concentration between the centre and edge of the tumour (Mueller-Klieser, 1997; Durand and Sham, 1998). In fact, Mueller-Klieser (2000) showed experimentally that the onset of quiescence is a complex process and as well as local hypoxia "other factors such as cell-cell and cell-matrix interaction, availability of growth factors, expression and accessibility of growth factor receptors, adhesion molecules and their receptors etc. may be involved in the emergence of

cell cycle arrest in spheroids". Furthermore, the observed distribution of proliferating and quiescent cells can be recreated mathematically by assuming transfer rates between the proliferating and quiescent populations which depend linearly upon the local nutrient concentration and allowing the different cell types to exhibit different chemotactic responses to the local nutrient concentration (Tindall and Please, 2007). Currently the exact mechanisms which cause proliferative cells to become quiescent and quiescent cells to become proliferative are not well understood.

Rather than attempting to model a system which is not well understood we will instead capture the observation that proliferating cells are generally observed in the outer region of the tumour and quiescent cells are generally seen further towards the centre of the tumour (LaRue et al., 2004). To do this we assume that proliferating cells become quiescent at a rate α if they exceed some distance R from the edge of the tumour and quiescent cells become proliferative at a rate β within a distance R of the edge of the tumour.

After applying a conservation of cells argument we find the density of proliferating cells to be governed by

$$\begin{aligned}\frac{\partial p}{\partial t} + \nabla \cdot (\underline{v} p) = [k_m(c) - k_d(c)]\, p - \alpha p H\left([S_{\text{tum}} - R] - r\right) \\ + \beta q H\left(r - [S_{\text{tum}} - R]\right),\end{aligned} \tag{3.9}$$

where $p(r,t)$ is the density of proliferating cells, $q(r,t)$ is the density of quiescent tumour cells, $S_{\text{tum}}(t)$ is the radius of the tumour and $H(x)$ is the Heaviside function.

Quiescent Tumour Cells

We now consider the evolution of the tumour cells which are quiescent (hereby simply referred to as quiescent cells). If we assume that the onset of quiescence merely prevents a cell from proliferating and does not affect the cell's death rate, then recalling the rate of cell transfer between the proliferating and quiescent compartments we find the evolution of quiescent cells to be governed by

$$\frac{\partial q}{\partial t} + \nabla \cdot (\underline{v} q) = -k_d(c) q + \alpha p H\left([S_{\text{tum}} - R] - r\right) - \beta q H\left(r - [S_{\text{tum}} - R]\right). \tag{3.10}$$

Necrotic Cells

We have already considered the rate at which living cells become necrotic, and we also assume that necrotic cells undergo linear degradation at a rate ν. Then the evolution of necrotic cells is governed by

$$\frac{\partial n}{\partial t} + \nabla \cdot (\underline{v} n) = k_d(c)(p+q) - \nu n. \tag{3.11}$$

where $n(r,t)$ is the density of necrotic cells.

Cell Volume Fraction

We also assume that the total cell volume fraction of the tissue is constant. We take the mean volume of the living cells to be V_L, independently of the state of the cell, and we take the mean volume of necrotic cells to be V_N. Then assuming that the mean cell volume fraction is constant gives

$$V_L(h+p+q) + V_N n = \mathcal{V} \leq 1, \tag{3.12}$$

where $\mathcal{V}$ is the mean cell volume fraction of the tissue.

The Oxygen Concentration

We now consider the evolution of the local oxygen concentration. Oxygen will move throughout our system by diffusion and we assume that the diffusion of oxygen follows Fick's law. As well as spreading via diffusion it is possible that some oxygen will be advected within cells as they move. It is not known to what extent oxygen will be carried in this way, so to deliberately overestimate this affect we will assume that oxygen is completely advected with the movement of cells. It is then shown in Section 3.4.2 that the Péclet number of our system, which is a non-dimensional constant relating the rate of advection to the rate of diffusion (Schetz, 1999), will be small so that any advection dynamics can be neglected anyway.

As well as moving via diffusion and advection the oxygen concentration will also depend upon the rate at which the cells consume oxygen. We split oxygen consumption into two separate components; the oxygen required for the normal processes which keep the cell alive, and the additional oxygen required for mitosis.

It has been shown that the rate of oxygen consumption in tissue fits well with Michaelis-Menten kinetics (Lin, 1976; Hlatky and Alpen, 1985) and so we denote the rate at which oxygen is utilised for normal processes by $k_n(c)$ and assume that

$$k_n(c) = \frac{Cc}{c + c_n},$$

where C and c_n are constants.

We previously assumed that cell proliferation occurs at a rate $k_m(c)p$ and so we assume that oxygen is also utilised for mitosis at a rate $\gamma k_m(c)p$. Then the evolution of the local oxygen concentration is governed by

$$\frac{\partial c}{\partial t} + \nabla \cdot (\underline{v}c) = \nabla \cdot (D\nabla c) - \gamma k_m(c)p - k_n(c)\left(h + p + q\right), \tag{3.13}$$

where D is the diffusion coefficient of oxygen.

The Tumour and Capillary Spheroids

We are using our model to consider the gap between the tumour and surrounding vasculature and to do this we must explicitly track the edge of the capillary spheroid. In particular, we are considering whether a significant gap can be maintained between the tumour and surrounding vasculature. Our scaling argument suggested that such a gap cannot be maintained and with a view to confirming this we will deliberately overestimate any such gap which might exist. To do this we neglect any inertia or elastic effects which may resist the movement of the capillaries and assume that the edge of the capillary spheroid moves at the local cell velocity.

Additionally, the governing equations for the local proliferating and quiescent cell densities, Equations (3.9) and (3.10), contain an S_{tum} term which denotes the edge of the tumour spheroid, and so we must also explicitly track the edge of the tumour spheroid. By definition the edge of the tumour spheroid will move with the local cell velocity, so that

$$\frac{\mathrm{d}S_{\text{cap}}}{\mathrm{d}t} = v(S_{\text{cap}}, t), \qquad \text{and} \qquad \frac{\mathrm{d}S_{\text{tum}}}{\mathrm{d}t} = v(S_{\text{tum}}, t), \tag{3.14}$$

where S_{cap} and S_{tum} are the radius of the capillary and tumour spheroids respectively.

The Initial and Boundary Conditions

We complete our model by deriving the corresponding initial and boundary conditions.

To consider how the gap between an avascular tumour and surrounding vasculature varies as the tumour grows we initiate our model starting from the smallest tumour which can be modelled as a continuum of cells. However, we must also start with a tumour where the distribution of proliferating, quiescent, and necrotic cells is known empirically.

LaRue et al. (2004) found the proliferating rim on the surface of avascular tumours to be typically two or three cells deep, so we take our tumour to have an initial radius corresponding to three cell widths and assume that this tumour only consists of proliferating cells. The initial tumour radius is then

$$S_{\text{tum}}(0) = \frac{6}{\mathcal{V}}\left(\frac{3V_L}{4\pi}\right)^{\frac{1}{3}},$$

and the initial distribution of the cell densities is

$$h(r,0) = \begin{cases} 0 & r \leq S_{\text{tum}}(0) \\ \dfrac{\mathcal{V}}{V_L} & r > S_{\text{tum}}(0) \end{cases}, \qquad p(r,0) = \begin{cases} \dfrac{\mathcal{V}}{V_L} & r \leq S_{\text{tum}}(0) \\ 0 & r > S_{\text{tum}}(0) \end{cases},$$

$$q(r,0) = 0, \qquad n(r,0) = 0.$$

We now consider the initial radius of the capillary spheroid. Recalling that Fait et al. (1998) observed the mean inter-capillary distance in the human large intestine to be $101.9\,\mu$m we assume that initially the capillary spheroid is $50\,\mu$m larger than the tumour spheroid, so that

$$S_{\text{cap}}(0) = \frac{6}{\mathcal{V}}\left(\frac{3V_L}{4\pi}\right)^{\frac{1}{3}} + 50\,\mu\text{m}.$$

We now derive the boundary conditions which apply at the centre of the tumour. The assumption of radial symmetry implies that the local cell velocity and the oxygen flux at the centre of the tumour must both be zero, so that

$$v(0,t) = 0 \quad \forall\, t, \qquad \text{and} \qquad \frac{\partial c(0,t)}{\partial r} = 0 \quad \forall\, t.$$

For our final boundary condition we assume that the capillary network is a constant source of oxygen so that

$$c(S_{\text{cap}}, t) = \widetilde{c} \qquad \forall\, t,$$

where $\widetilde{c}$ is the external oxygen concentration.

This boundary condition is used in the Krogh cylinder model (Krogh, 1919) for oxygen diffusion out of the capillary network and assumes that the oxygen permeability of the capillaries is high. A full boundary condition for the transfer of oxygen across the membrane of a capillary was considered by Tsoukais et al. (2007) and non-dimensionalising their condition with their parameter values shows that to leading order the oxygen concentration is constant on the surface of the capillary spheroid, which validates our assumption that to leading order the oxygen permeability of the capillaries can be taken to be high.

3.4.2 Non-Dimensionalisation

The Re-Scalings

With our model derived we now non-dimensionalise the system using the following re-scalings (where carets denote dimensionless variables)

$$h(r,t) = \frac{\mathcal{V}}{V_L}\widehat{h}\big(\widehat{r},\widehat{t}\big), \quad p(r,t) = \frac{\mathcal{V}}{V_L}\widehat{p}\big(\widehat{r},\widehat{t}\big), \quad q(r,t) = \frac{\mathcal{V}}{V_L}\widehat{q}\big(\widehat{r},\widehat{t}\big), \quad n(r,t) = \frac{\mathcal{V}}{V_N}\widehat{n}\big(\widehat{r},\widehat{t}\big),$$
$$r = L\widehat{r}, \qquad t = \frac{\widehat{t}}{A}, \qquad c(r,t) = \widetilde{c}\,\widehat{c}\big(\widehat{r},\widehat{t}\big), \qquad \underline{v}(r,t) = LA\underline{\widehat{v}}\big(\widehat{r},\widehat{t}\big),$$
$$S_{\text{cap}}(t) = L\widehat{S}_{\text{cap}}\big(\widehat{t}\big), \qquad S_{\text{tum}}(t) = L\widehat{S}_{\text{tum}}\big(\widehat{t}\big), \qquad v_{\text{tum}}(t) = LA\widehat{v}_{\text{tum}}\big(\widehat{t}\big),$$

where A is the maximum rate of mitosis in Equation (3.8) and L is the diameter of a living cell as given by

$$L = 2\left(\frac{3V_L}{4\pi}\right)^{\frac{1}{3}}.$$

Upon applying these re-scalings the system governed by Equations (3.7), (3.9), (3.10), (3.11), (3.12), and (3.13) non-dimensionalise to become

$$\frac{\partial\widehat{h}}{\partial\widehat{t}} + \widehat{\nabla}\cdot\left(\underline{\widehat{v}}\widehat{h}\right) = 0,$$
$$\frac{\partial\widehat{p}}{\partial\widehat{t}} + \widehat{\nabla}\cdot\left(\underline{\widehat{v}}\widehat{p}\right) = \left[\widehat{k}_m(\widehat{c}) - \widehat{k}_d(\widehat{c})\right]\widehat{p} - \widehat{\alpha}\widehat{p}H\left(\left[\widehat{S}_{\text{tum}} - \widehat{R}\right] - \widehat{r}\right) + \widehat{\beta}\widehat{q}H\left(\widehat{r} - \left[\widehat{S}_{\text{tum}} - \widehat{R}\right]\right),$$

$$\frac{\partial \widehat{q}}{\partial \widehat{t}} + \widehat{\nabla} \cdot \left(\underline{\widehat{v}}\widehat{q}\right) = -\widehat{k}_d(\widehat{c})\widehat{q} + \widehat{\alpha}\widehat{p}H\left(\left[\widehat{S}_{\text{tum}} - \widehat{R}\right] - \widehat{r}\right) - \widehat{\beta}\widehat{q}H\left(\widehat{r} - \left[\widehat{S}_{\text{tum}} - \widehat{R}\right]\right),$$

$$\frac{\partial \widehat{n}}{\partial \widehat{t}} + \widehat{\nabla} \cdot \left(\underline{\widehat{v}}\widehat{n}\right) = \delta\widehat{k}_d(\widehat{c})(\widehat{p} + \widehat{q}) - \widehat{\nu}\widehat{n},$$

$$\widehat{h} + \widehat{p} + \widehat{q} + \widehat{n} = 1,$$

$$P_e\left[\frac{\partial \widehat{c}}{\partial \widehat{t}} + \widehat{\nabla} \cdot \left(\underline{\widehat{v}}\widehat{c}\right)\right] = \widehat{\nabla}^2\widehat{c} - \widehat{\gamma}\widehat{k}_m(\widehat{c})\widehat{p} - \widehat{k}_n(\widehat{c})(\widehat{h} + \widehat{p} + \widehat{q}). \tag{3.15}$$

where

$$\widehat{k}_m(\widehat{c}) = \frac{\widehat{c}}{\widehat{c} + \widehat{c}_c}, \qquad \widehat{k}_d(\widehat{c}) = \widehat{B}\left(1 - \frac{\sigma\widehat{c}}{\widehat{c} + \widehat{c}_d}\right), \qquad \widehat{k}_n(\widehat{c}) = \frac{\widehat{C}\widehat{c}}{\widehat{c} + \widehat{c}_n},$$

$$\widehat{B} = \frac{B}{A}, \qquad \widehat{\alpha} = \frac{\alpha}{A}, \qquad \widehat{\beta} = \frac{\beta}{A}, \qquad \delta = \frac{V_N}{V_L},$$

$$\widehat{\nu} = \frac{\nu}{A}, \qquad P_e = \frac{AL^2}{D}, \qquad \widehat{\gamma} = \frac{\mathcal{V}A\gamma L^2}{V_L D\widetilde{c}}, \qquad \widehat{C} = \frac{\widehat{\gamma}C}{\gamma A}.$$

Here $\widehat{B}$ is the relative maximum rate of cell necrosis compared to the maximum rate of cell proliferation, $\widehat{\alpha}$ and $\widehat{\beta}$ are the relative maximum transfer rates compared to the maximum rate of cell proliferation, δ is the relative volume of a necrotic cell compared to a living cell, $\widehat{\nu}$ is the relative rate of necrotic cell decay compared to the maximum rate of proliferation, and P_e is the Péclet number of the system.

The equations governing the movement of the edges of the capillary and tumour spheroids, as given by Equation (3.14), also non-dimensionalise to become

$$\frac{\mathrm{d}\widehat{S}_{\text{cap}}}{\mathrm{d}\widehat{t}} = \widehat{v}\big(\widehat{S}_{\text{cap}}, \widehat{t}\big), \qquad \text{and} \qquad \frac{\mathrm{d}\widehat{S}_{\text{tum}}}{\mathrm{d}\widehat{t}} = \widehat{v}\big(\widehat{S}_{\text{tum}}, \widehat{t}\big),$$

and our initial and boundary conditions non-dimensionalise to become

$$\widehat{S}_{\text{tum}}(0) = \frac{3}{\mathcal{V}}, \qquad \widehat{S}_{\text{cap}}(0) = \frac{3}{\mathcal{V}} + \frac{50\,\mu\text{m}}{L}, \qquad \widehat{h}(\widehat{r}, 0) = \begin{cases} 0 & \widehat{r} \le \widehat{S}_{\text{tum}}(0), \\ 1 & \widehat{r} > \widehat{S}_{\text{tum}}(0), \end{cases}$$

$$\widehat{q}(\widehat{r}, 0) = 0, \qquad \widehat{n}(\widehat{r}, 0) = 0, \qquad \widehat{p}(\widehat{r}, 0) = \begin{cases} 1 & \widehat{r} \le \widehat{S}_{\text{tum}}(0), \\ 0 & \widehat{r} > \widehat{S}_{\text{tum}}(0), \end{cases}$$

$$\widehat{v}\big(0, \widehat{t}\big) = 0, \qquad \frac{\partial \widehat{c}\big(0, \widehat{t}\big)}{\partial \widehat{r}} = 0, \qquad \widehat{c}\big(\widehat{S}_{\text{cap}}, \widehat{t}\big) = 1.$$

Parameter Estimation

We now evaluate as many of our non-dimensional parameters as possible from the literature. If we are unable to evaluate any of the non-dimensional parameters, then we will estimate them using an analysis of parameters by ensuring that the growth of our modelled tumour is consistent with observed tumour growth.

We begin by trying to estimate the Péclet number, $P_e = \frac{AL^2}{D}$ where A is the maximum rate of tumour cell mitosis, L is the width of a live cell, and D is the diffusion coefficient of oxygen. Grote et al. (1977) measured the diffusion coefficient of oxygen in DS-Carcinosarcoma tumour cells and found it to be $1.75 \times 10^{-5}\,\mathrm{cm}^2 s^{-1}$ and Hlatky and Alpen (1985) took the diffusion coefficient of oxygen in tumour tissue to be $2 \times 10^{-5}\,\mathrm{cm}^2 s^{-1}$. Given these two results we take

$$D = 2 \times 10^{-5}\,\mathrm{cm}^2 s^{-1}.$$

Casciari et al. (1992) found the number of cells per unit volume of tumour in EMT6/Ro tumours to be 2.01×10^8 cells cm^{-3}. Before converting this into an estimate for the average volume of a live tumour cell we must take account of the extracellular space. Whilst there is little data concerning the cell volume fraction specifically in tumours, Buckley et al. (1999) found the cell volume fraction in parts of a rat forebrain to be 0.66 ± 0.04. Taking $\mathcal{V}$ to be 0.66 gives the average volume of a tumour cell to be approximately $3 \times 10^{-9}\,\mathrm{cm}^3$. In addition to this, Li (2006) found the median volume of rat brain tumour cells to be $1.2 \times 10^{-9}\,\mathrm{cm}^3$ and Landry et al. (1982) analysed the data of Landry et al. (1981) to conclude that the mean volume of exponentially growing tumour cells is $3 \times 10^{-9}\,\mathrm{cm}^3$.

Given these results we take $V_L = 3 \times 10^{-9}\,\mathrm{cm}^3$, which corresponds to

$$L = 9 \times 10^{-4}\,\mathrm{cm}.$$

To estimate the maximum rate of mitosis we use the work of Marini et al. (2006) who measured the median doubling time of untreated colorectal cancer cells to be 135 hours. Given this we can estimate the maximum rate of mitosis of colorectal cancer (as outlined in Appendix B.1) to be

$$A = 1.4 \times 10^{-6} s^{-1}.$$

Combining these values of D, A and L allows us to estimate the Péclet number and we find that

$$P_e \approx 5.6 \times 10^{-8} \ll 1.$$

Hence the Péclet number is a small parameter and to leading order we can neglect the left hand side of Equation (3.15) for the evolution of the non-dimensional oxygen concentration. This is equivalent to making the quasi-steady state assumption that the diffusion of oxygen occurs on a much faster time scale than the growth of the tumour and that the advection of oxygen with the movement of cells is negligible.

In Section 3.4.1, when deriving our model, we were unsure to what extent oxygen would be carried by advection. Having shown that the case where oxygen is completely carried by advection is negligible we can be certain that the actual advection of oxygen in the tumour will be negligible.

Having found the Péclet number to be small we now attempt to evaluate the other non-dimensional parameters in our model.

Landry et al. (1982) analysed the data of Landry et al. (1981) to estimate the mean volume of both living and necrotic cells. The mean volume of living cells was found to be $3 \times 10^{-9}\,\mathrm{cm}^3$ and the mean volume of necrotic cells was found to be $1.5 \times 10^{-9}\,\mathrm{cm}^3$. Given this we take δ, the ratio of the volume of a necrotic cell to the volume of a live cell volume, to be

$$\delta = 0.5.$$

As noted previously, LaRue et al. (2004) states that the proliferating rim is typically two or three cells thick. We take the proliferating rim to be three cells thick and including the extra-cellular space this gives the non-dimensional thickness of our proliferating rim, $\widehat{R}$, to be

$$\widehat{R} = \frac{3L}{\mathcal{V}L} = 4.5.$$

These are all the non-dimensional parameters it is possible to estimate from the literature and these parameters are given in Table 3.1.

We have not been able to determine all the parameters in our model. In particular the rates at which live cells change state, $\widehat{\alpha}$ and $\widehat{\beta}$, the necrotic cell decay rate, $\widehat{\nu}$, the rate at which oxygen is consumed for proliferation, $\widehat{\gamma}$, and the parameters in the Michaelis-Menten type kinetics, $\widehat{c}_c$, $\widehat{c}_d$, $\widehat{c}_d$, $\widehat{B}$, $\widehat{C}$, and σ, remain unknown. These remaining parameters will be estimated using an analysis of parameters where we will

Parameter	Description	Value	Reference
P_e	The Péclet number	5.6×10^{-8}	(Grote et al., 1977; Hlatky and Alpen, 1985; Casciari et al., 1992; Buckley et al., 1999; Li, 2006; Landry et al., 1982, 1981; Marini et al., 2006)
δ	The ratio of necrotic cell volume to live cell volume	0.5	(Landry et al., 1981, 1982)
$\widehat{R}$	The non-dimensional thickness of the proliferating rim	4.5	(LaRue et al., 2004; Buckley et al., 1999)

Table 3.1: The non-dimensional parameters in our model which can be estimated from the literature.

simulate the growth of our tumour for different parameter values and use a system of trial and improvement to find parameter values which yield realistic growth dynamics. To do this we must first consider how to numerically simulate the evolution of our non-dimensional model. We begin by recapping our non-dimensional model.

3.4.3 The Non-Dimensional Model

Upon dropping carets and having evaluated some of the non-dimensional parameters we have the following non-dimensional system

$$\frac{\partial h}{\partial t} + \nabla \cdot (\underline{v} h) = 0. \tag{3.16}$$

$$\frac{\partial p}{\partial t} + \nabla \cdot (\underline{v} p) = \left[k_m(c) - k_d(c)\right] p - \alpha p H\left(-\overline{r}\right) + \beta q H\left(\overline{r}\right), \tag{3.17}$$

$$\frac{\partial q}{\partial t} + \nabla \cdot (\underline{v} q) = -k_d(c) q + \alpha p H\left(-\overline{r}\right) - \beta q H\left(\overline{r}\right), \tag{3.18}$$

$$\frac{\partial n}{\partial t} + \nabla \cdot (\underline{v} n) = 0.5 k_d(c)(p+q) - \nu n, \tag{3.19}$$

$$h + p + q + n = 1, \tag{3.20}$$

$$\nabla^2 c = \gamma k_m(c) p + k_n(c)(h+p+q), \tag{3.21}$$

where

$$k_m(c) = \frac{c}{c+c_c}, \qquad k_d(c) = B\left(1 - \frac{\sigma c}{c+c_d}\right), \qquad k_n(c) = \frac{Cc}{c+c_n},$$
$$\overline{r} = r - [S_{\text{tum}} - 4.5] \qquad \frac{\mathrm{d}S_{\text{tum}}}{\mathrm{d}t} = v(S_{\text{tum}}, t), \qquad \frac{\mathrm{d}S_{\text{cap}}}{\mathrm{d}t} = v(S_{\text{cap}}, t).$$

To close our non-dimensional model we use the following initial and boundary conditions

$$h(r,0) = H(r-4.5), \qquad p(r,0) = 1 - H(r-4.5), \qquad q(0,t) = 0,$$
$$n(r,0) = 0, \qquad S_{\text{tum}}(0) = 4.5, \qquad S_{\text{cap}}(0) = 7.3,$$
$$c(S_{\text{cap}}, t) = 1, \qquad \frac{\partial c(0,t)}{\partial r} = 0, \qquad v(0,t) = 0.$$

3.4.4 Analysing the Non-Dimensional System

We will now simulate the growth of the tumour by numerically approximating the evolution of our system. Before doing this we will manipulate our system to make the calculation of this numerical approximation as efficient as possible.

The Local Cell Velocity

First we derive an equation governing the local cell velocity. Considering the sum of Equations (3.16) to (3.19) for the evolution of the different cell types and recalling that the cell volume fraction is constant, as given by Equation (3.20), gives the first order partial differential equation for the local cell velocity

$$\begin{aligned}\nabla \cdot \underline{v} &= \left[k_m(c) - 0.5k_d(c)\right] p - 0.5k_d(c)q - \nu n, \\ &= f^v(p,q,n,c),\end{aligned}$$

where for ease of notation we have denoted the right hand side of this equation by f^v.[1]

Recalling that $\underline{v} = v(r,t)\underline{e}_r$ we extract the following differential equation for v

$$\frac{1}{r^2}\frac{\partial(r^2 v)}{\partial r} = f^v(p,q,n,c) \tag{3.22}$$

[1]The superscript v represents this function denoting the right hand side of the partial differential equation for v. It does not denote f to the power of v.

The Characteristic Equations

We now manipulate Equations (3.16) to (3.19) for the evolution of the different cell types to make the numerical approximation of these equations as efficient as possible.

Note that expanding the equation for the evolution of healthy cells, Equation (3.16), and utilising the equation for the local cell velocity, Equation (3.22), gives the following partial differential equation for h

$$\begin{aligned}\frac{\partial h}{\partial t} + v\frac{\partial h}{\partial r} &= -hf^v(p,q,n,c),\\ &= f^h(h,p,q,n,c),\end{aligned}$$

where for ease of notation we have denoted the right hand side of this differential equation by f^h.

We simplify this equation further still by using the method of characteristics. We define the characteristics of our system to be the lines which follow the movement of the cells, which are the parameterised lines, $(r(s), t(s))$, which satisfy

$$\frac{\mathrm{d}r(s)}{\mathrm{d}s} = v(r(s),t(s)), \qquad \text{and} \qquad \frac{\mathrm{d}t(s)}{\mathrm{d}s} = 1, \tag{3.23}$$

and we define our parameterisation so that $t = 0$ when $s = 0$. The evolution of h along the characteristics is then given by the ordinary differential equation

$$\frac{\mathrm{d}h}{\mathrm{d}s} = f^h(h,p,q,n,c). \tag{3.24}$$

Similarly, the equations for the evolution of the other cell types, Equations (3.17) to (3.19), can be expanded and written in terms of the characteristic variable to give

$$\begin{aligned}\frac{\mathrm{d}p}{\mathrm{d}s} &= \left[k_m(c) - k_d(c)\right]p - \alpha pH\left(-\overline{r}\right) + \beta qH\left(\overline{r}\right) - pf^v(p,q,n,c),\\ &= f^p(\overline{r},p,q,n,c),\end{aligned} \tag{3.25}$$

$$\begin{aligned}\frac{\mathrm{d}q}{\mathrm{d}s} &= -k_d(c)q + \alpha pH\left(-\overline{r}\right) - \beta qH\left(\overline{r}\right) - qf^v(p,q,n,c),\\ &= f^q(\overline{r},p,q,n,c),\end{aligned} \tag{3.26}$$

$$\begin{aligned}\frac{\mathrm{d}n}{\mathrm{d}s} &= 0.5k_d(c)(p+q) - \nu n - nf^v(p,q,n,c),\\ &= f^n(p,q,n,c),\end{aligned} \tag{3.27}$$

where for ease of notation the right hand sides of these equations have been denoted by f^p, f^q and f^n respectively.

Finally for ease of notation we denote the right hand side of the equation for the oxygen concentration, Equation (3.21), by f^c to give

$$\frac{1}{r}\frac{\partial^2(rc)}{\partial r^2} = f^c(h, p, q, c). \tag{3.28}$$

Equations (3.22) to (3.28) now completely describe the evolution of the tumour and each equation only contains derivatives with respect to a single variable. This makes the numerical approximation of these equations simpler than solving the original system of coupled partial differential equations, however computing a numerical solution to our system remains non-trivial. In particular all the differential equations are coupled and we cannot use a predefined set of mesh points for our numerical scheme because Equations (3.24) to (3.27) must be integrated along along the characteristics. The details of the numerical scheme are discussed in the following section.

3.4.5 The Numerical Scheme

We now define the numerical scheme which we will use to simulate our system of non-dimensional equations. We will define this scheme iteratively and begin by calculating the numerical approximation at the initial time step.

We define r_i^j to be the mesh point which lies at $r = r_i$ when $t = t_j$. We also define H_i^j, P_i^j, Q_i^j, N_i^j, V_i^j, and C_i^j to be the numerical approximations to h, p, q, n, v, and c respectively at $r = r_i$ when $t = t_j$ and define S_{tum}^j and S_{cap}^j to be the numerical approximations of S_{tum}, and S_{cap} at $t = t_j$.

The Initial Approximation

From the initial conditions we have

$$\begin{array}{lll} H_i^1 = \begin{cases} 1 & \text{if } r_i^1 \geq 4.5, \\ 0 & \text{if } r_i^1 < 4.5, \end{cases} & P_i^1 = \begin{cases} 0 & \text{if } r_i^1 \geq 4.5, \\ 1 & \text{if } r_i^1 < 4.5, \end{cases} & Q_i^1 = 0 \ \ \forall\, i, \\ N_i^1 = 0 \quad \forall\, i, & S_{\text{tum}}^1 = 4.5, & S_{\text{cap}}^1 = 7.3, \end{array} \tag{3.29}$$

but the initial distribution of the local oxygen concentration and the local cell velocity are unknown.

To find the initial distribution of the local oxygen concentration we approximate the solution of its governing equation, Equation (3.28), subject to the boundary conditions

$$\frac{\partial c(0,0)}{\partial r} = 0, \qquad \text{and} \qquad c(S_{\text{cap}}(0), 0) = 1.$$

To do this we implement a shooting method where we approximate the solution subject to the modified boundary conditions

$$\frac{\partial c(0,0)}{\partial r} = 0, \qquad \text{and} \qquad c(0,0) = a,$$

and then find the value of a required to give $c(S_{\text{cap}}(0), t) = 1$.

These modified boundary conditions imply that $C_1^1 = C_2^1 = a$ and we calculate the remaining values of C_i^1 using a simple forward quadrature method where the integrand can be evaluated using the previous values of C_i^1 and the initial conditions for the other variables. To find a suitable value of a we initially consider the cases where $a = 0$ and $a = 1$ and then refine our estimate of a using the Newton-Raphson method.

Having approximated the initial oxygen concentration we find the initial local cell velocity by approximating the solution to its governing equation, Equation (3.22), subject to the condition that $v(0,0) = 0$. First we rewrite Equation (3.22) as

$$\frac{\partial v}{\partial r} = f^v(p, q, n, c) - \frac{2v}{r}$$

and then we integrate using the backward Euler method defined by

$$\begin{gathered} V_1^1 = 0, \\ V_{i+1}^1 = V_i^1 + \left(r_{i+1}^1 - r_i^1\right) \left\{ f^v(P_{i+1}^1, Q_{i+1}^1, N_{i+1}^1, C_{i+1}^1) - \frac{2V_{i+1}^1}{r_{i+1}^1} \right\}. \end{gathered} \tag{3.30}$$

Note that even though we are using a backward quadrature method the linearity of the integrand in v means that Equation (3.30) can be rewritten to obtain the following explicit scheme

$$\begin{gathered} V_1^1 = 0, \\ V_{i+1}^1 = \left(\frac{r_{i+1}^1}{3r_{i+1}^1 - 2r_i^1} \right) \left\{ V_i^1 + \left(r_{i+1}^1 - r_i^1\right) f^v(P_{i+1}^1, Q_{i+1}^1, N_{i+1}^1, C_{i+1}^1) \right\}. \end{gathered}$$

Having calculated the numerical approximation at the initial time step we now assume that we have calculated the numerical approximation up to and including the j^{th} time step and then show how to calculate the numerical approximation at the $(j+1)^{\text{th}}$ time step.

The Iterative Step

We begin by defining the mesh points we must take at the $(j+1)^{\text{th}}$ time step. Our mesh points must follow the path of the characteristics and given the mesh points $r = r_i^j$ for $i \in I$ at the j^{th} time step we calculate the new mesh points by integrating the characteristic equation, Equation (3.23), using a forward Euler method. This gives the mesh points at the $(j+1)^{\text{th}}$ time step to be

$$r_i^{j+1} = r_i^j + (t_{j+1} - t_j)V_i^j \qquad \text{for } i \in I.$$

Next we calculate the density of the different cell types at these mesh points. To do this we integrate the corresponding governing equations, Equations (3.24) to (3.27), from the old mesh points to the new mesh points using a forward Euler method to obtain

$$\begin{aligned}
H_i^{j+1} &= H_i^j + (t_{j+1} - t_j)f^h(H_i^j, P_i^j, Q_i^j, N_i^j, C_i^j),\\
P_i^{j+1} &= P_i^j + (t_{j+1} - t_j)f^p(\overline{r}_i^j, P_i^j, Q_i^j, N_i^j, C_i^j),\\
Q_i^{j+1} &= Q_i^j + (t_{j+1} - t_j)f^q(\overline{r}_i^j, P_i^j, Q_i^j, N_i^j, C_i^j),\\
N_i^{j+1} &= N_i^j + (t_{j+1} - t_j)f^n(P_i^j, Q_i^j, N_i^j, C_i^j).
\end{aligned}$$

With the values of H_i^{j+1}, P_i^{j+1}, Q_i^{j+1} and N_i^{j+1} calculated we must approximate the values of the local oxygen concentration and the local cell velocity. This is done in the same way as when calculating the initial state of the tumour, albeit with the necessary generalisation.

We calculate the values of C_i^{j+1} using a shooting method, whereby we approximate the solution to Equation (3.21) using a simple forward quadrature method subject to the boundary conditions

$$\frac{\partial c(0,t)}{\partial r} = 0, \qquad \text{and} \qquad c(0,t) = a.$$

We then find the value of a which gives $c(S_{\text{cap}}, t) = 1$ by a Newton-Raphson method with the starting values $a = 0$ and $a = C_1^j$.

We calculate the values of V_i^{j+1} by integrating Equation (3.22) using a backward Euler method. As before the approximations to the local cell velocity at the $(j+1)^{\text{th}}$ time step are given by the recursive relationship

$$V_1^{j+1} = 0,$$

$$V_{i+1}^{j+1} = \left(\frac{r_{i+1}^{j+1}}{3r_{i+1}^{j+1} - 2r_i^{j+1}}\right)\left\{V_i^{j+1} + \left(r_{i+1}^{j+1} - r_i^{j+1}\right) f^v(P_{i+1}^{j+1}, Q_{i+1}^{j+1}, N_{i+1}^{j+1}, C_{i+1}^{j+1})\right\}.$$

This completes our approximation of the tumour dynamics at the $(j+1)^{\text{th}}$ time step.

The Insertion and Deletion of Characteristics

To complete the numerical scheme we now consider the step sizes in our numerical scheme. The time step size can be prescribed, but our mesh points follow the paths of the characteristics and at any given time point the spatial step size is determined by the distance between adjoining characteristics.

Is it possible that as the system evolves some of the characteristics will diverge so that the corresponding spatial step sizes become unacceptably large. To prevent this we prescribe a maximum relative spatial step size. If any spatial step between two mesh points exceeds this maximum size, then we insert an additional mesh point midway between the original two. We approximate the values of the variables at this new mesh point by linearly interpolating the values of the adjacent mesh points. We then track the evolution of this new characteristic and include it at all future time steps.

It is also possible that some characteristics will converge so that some of the spatial steps become unnecessarily small. This would needlessly slow our computation and could possibly even result in the accumulation of significant rounding errors. To prevent this we prescribe a minimum relative step size. If at any point a spatial step is smaller than this minimum step size then we delete the second mesh point and will not consider its evolution at future time points.

Ensuring an Accurate Approximation

Having presented our numerical scheme we now discuss how to ensure that the numerical errors in it are suitably small. In particular, our quadrature scheme utilises quite simple explicit quadrature methods and so we must ensure that our scheme is both stable and convergent.

Given the complex nature of our coupled system of differential equations it is not desirable to analytically bound the error in our quadrature scheme. So instead we will use the results of the numerical scheme to self-validate.

Firstly, if our numerical scheme were to lose stability then a rapid breakdown of the results would be observed. It is therefore simple to prescribe step sizes that are small enough to ensure that such a breakdown does not occur.

Secondly, we must ensure that our numerical scheme is convergent and converges with an acceptably small numerical error. To verify this we will run the numerical scheme

with decreasingly small step sizes. Once decreasing the step sizes leads to only a negligible change in the results of our numerical scheme then we will assume that the scheme has suitably converged. Furthermore, the constancy of the cell volume fraction, as given by Equation (3.20), implies that the non-dimensional cell volume fraction, $h+p+q+n$, should be equal to unity and we can use this condition to ensure that the numerical errors in our scheme only accumulate at an acceptable rate. To do this we will consider the sum $H_i^j + P_i^j + Q_i^j + N_i^j$ at every mesh point and ensure that this sum diverges away from one at an acceptably slow rate and in a manner which is consistent with the tolerances of our numerical scheme. Any divergence quicker than this will highlight an unacceptably poor level of accuracy in our numerical scheme.

A further *a posteriori* check of our numerical scheme is discussed in Section 3.7.1.

3.5 Results

3.5.1 Analysis of Parameters

We now estimate the remaining parameter values using an analysis of parameters. To do this we will make an initial estimate of the values of the unknown parameters and then vary each parameter in turn whilst observing the corresponding tumour growth. From this we will consider which aspects of tumour growth each parameter affects and to which parameters the tumour is most sensitive. We will then refine our parameter estimation by a sequence of trial and improvement until the growth dynamics of our modelled tumour suitably match observed tumour growth. In particular we will ensure that our simulated tumour's growth curve, size at saturation, relationship between necrotic core radius and tumour radius, and oxygen diffusion distance are all realistic.

Doing this we find that the parameter with largest influence upon how long it takes the tumour growth to saturate is ν, the dead cell decay rate. Folkman and Hochberg (1973) considered the growth curves of several *in vitro* tumour lines and found that the time taken to reach saturation was of the order of a hundred days and we choose ν to match this time scale.

The parameters with the largest influence upon the distance that oxygen diffuses into the tumour are γ and C, the maximum oxygen consumption rates. We expect that the uptake of oxygen required for normal processes and the additional uptake

of oxygen for mitosis will both be significant and so we choose γ and C to be of similar magnitudes. We then choose these parameters in tandem so that the oxygen concentration remains significant until approximately 100 μm from the edge of the tumour (Olive et al., 1992; Gunduz, 1981).

The primary parameters determining the onset of necrosis are B, the maximum cell death rate, and σ, a parameter in the cell death kinetics. We choose these parameters so that the relationship between the necrotic core radius and tumour radius in our modelled tumour is realistic. To do this we use the work of Mueller-Klieser (2000) who considered the relationship between the diameter of necrosis and the tumour diameter in human colon carcinoma spheroids; the results of which are shown in Figure 3.5.

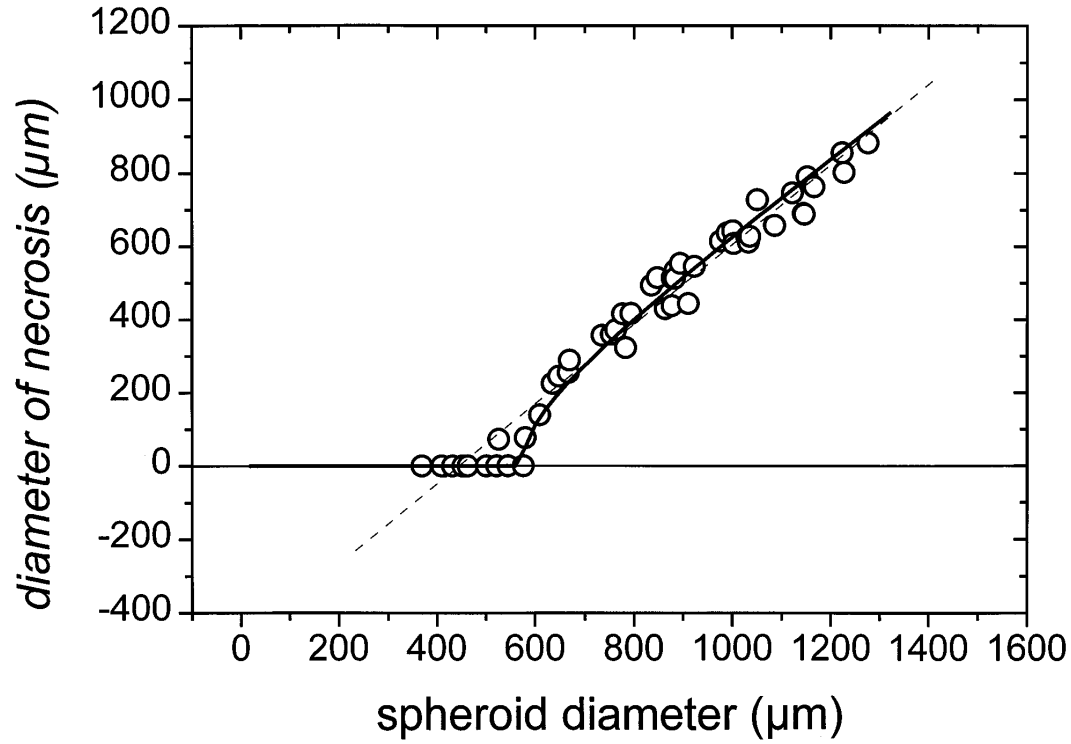

Figure 3.5: The diameter of necrosis as a function of spheroid diameter in WiDr human colon carcinoma spheroids (reproduced with permission from Mueller-Klieser, 2000). The dashed line is a linear best fit to the data and the solid line is obtained from Mueller-Klieser's modelling of the onset of necrosis.

The primary parameters determining the size the tumour reaches at saturation are B, the maximum cell death rate, and α, the rate at which proliferative cells become quiescent. Avascular tumours typically saturate at a radius between 0.5 mm and 2 mm

(Folkman and Hochberg, 1973; Haji-Karim and Carisson, 1978) and so we choose these parameters so that our modelled tumour saturates at a radius of approximately 1 mm.

Altering β, the rate at which quiescent cells recover the ability to proliferate inside the proliferating rim, had no effect on the behaviour of our modelled tumour. This is because our initial conditions assume there are initially no quiescent cells inside our tumour and as a consequence of this our proliferating rim never actually contains any quiescent cells. Hence the rate at which these cells might become proliferative is irrelevant. However, if our initial conditions were altered so that our tumour did initially contain some quiescent cells then the value of β may become influential. Here we estimate β by assuming that quiescent cells can become proliferative at a similar rate to which proliferating cells become quiescent.

Finally, the nutrient saturation parameters, c_c, c_d and c_n, are chosen so that the cell kinetics saturate over the range of nutrient concentrations observed in our model.

This analysis of parameters leads to the parameter values summarised in Table 3.2.

Non-Dimensional Parameter	**Symbol**	**Value Taken**
Maximum death rate	B	1.5
Maximum rate of oxygen consumption for normal processes	C	0.018
Rate of dead cell degradation	ν	0.2
Critical parameter in cell mitosis kinetic	c_c	0.1
Critical parameter in cell necrosis kinetic	c_d	0.1
Critical parameter in rate of oxygen consumption for normal processes kinetic	c_n	0.1
Rate of transfer from proliferating to quiescent compartment	α	1
Rate of transfer from quiescent to proliferating compartment	β	1
Rate of oxygen consumption per proliferating cell	γ	0.018
Parameter in cell necrosis kinetic	σ	0.9

Table 3.2: The non-dimensional parameters chosen by our analysis of parameters which result in our modelled tumour exhibiting realistic growth.

The radius of our modelled tumour as a function of time for the parameter values outlined in Table 3.2 is shown in Figure 3.6. It can be seen that the tumour undergoes the expected growth dynamics. There is an initial period of exponential like growth, then the growth slows, and eventually the tumour growth saturates at a radius of approximately 1000 μm. Furthermore it takes our modelled tumour a few hundred days to reach saturation, which is consistent with the results of Folkman and Hochberg (1973).

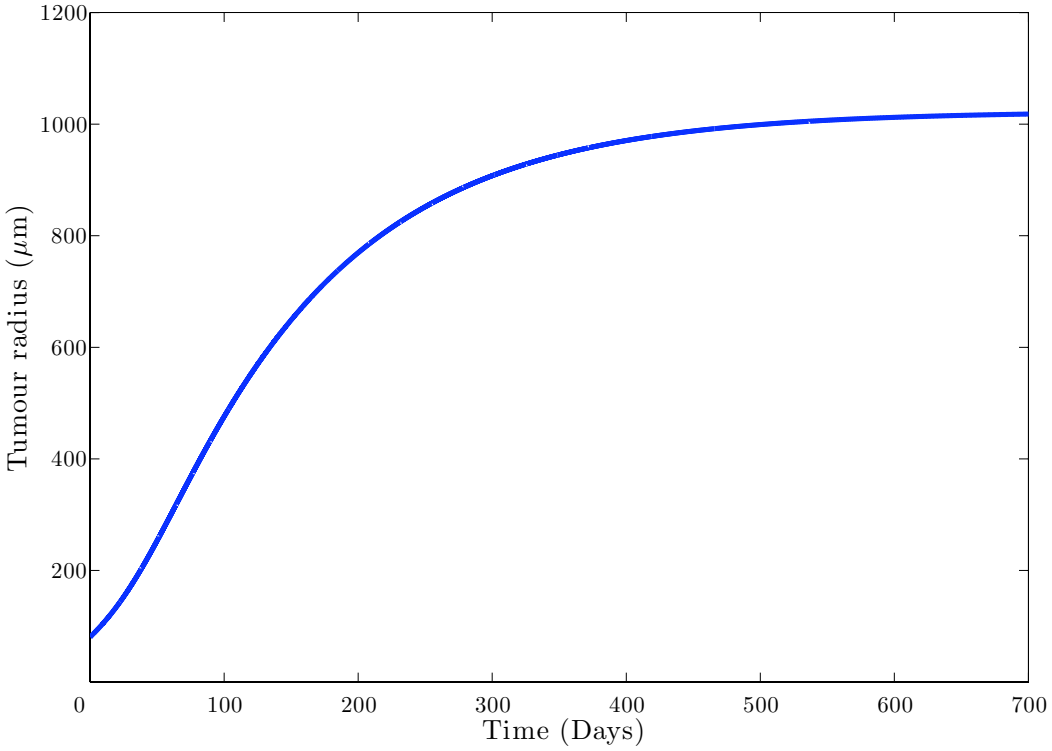

Figure 3.6: The radius of our modelled tumour as a function of time for the parameter values outlined in Table 3.2, as governed by Equations (3.16) to (3.21).

To consider the behaviour of the necrotic core we first define the necrotic core to be the region where $n \geq \frac{2}{3}$, then the radius of our simulated tumour's necrotic core as a function of the tumour radius is shown in Figure 3.7. It can be seen that the results shown in Figure 3.7 are very similar to those of Mueller-Klieser (2000) in Figure 3.5.

Finally we check whether the distance which oxygen diffuses into the tumour is realistic. The oxygen concentration in our saturated tumour as a function of the distance

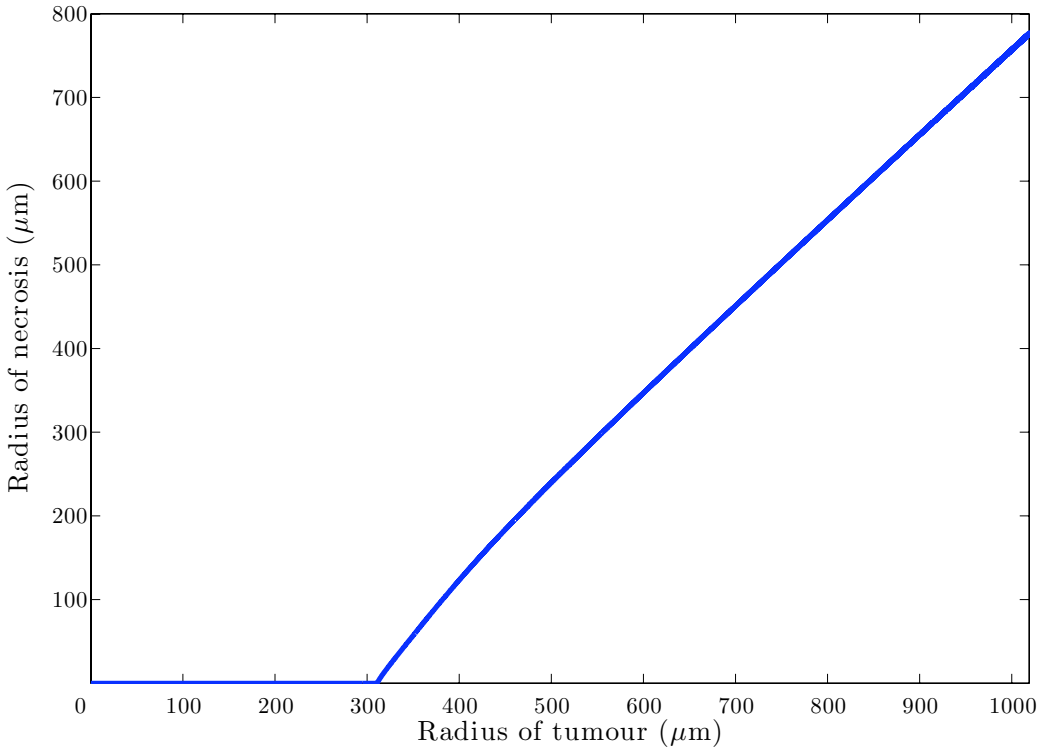

Figure 3.7: The radius of necrosis of our modelled tumour as a function of tumour radius for the parameter values outlined in Table 3.2, as governed by Equations (3.16) to (3.21).

from the centre of the tumour is shown in Figure 3.8. It can be seen that the oxygen concentration remains significant approximately 100 μm to 150 μm into the tumour, which is again consistent with observed tumour behaviour.

It should be noted that our choice of parameters is not completely unique and it is possible to alter parameters to some degree and still obtain realistic tumour growth. However, care has been taken to choose a set of parameter values so that several different aspects of tumour growth are consistent with observed tumour growth.

3.5.2 The Behaviour of the Tumour

Having chosen parameters so that the growth of our modelled tumour is realistic we now consider the behaviour of our modelled tumour and in particular we consider the evolution of the gap between the tumour and surrounding vasculature. The

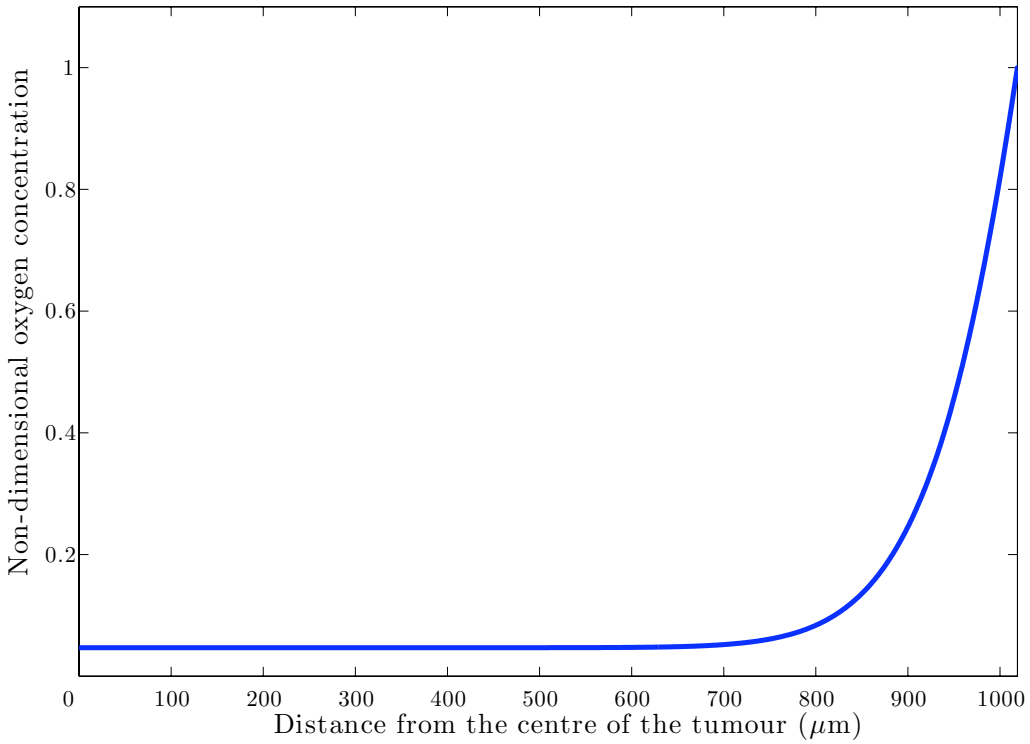

Figure 3.8: The non-dimensional oxygen concentration in our modelled tumour at saturation, as governed by Equations (3.16) to (3.21), as a function of tumour radius for the parameter values outlined in Table 3.2.

distributions of the different cell types in the tumour at saturation, as well as the distance between the tumour and vasculature as a function of tumour radius, are shown in Figure 3.9.

The properties of the saturated tumour are largely as expected. The centre of the tumour consists entirely of necrotic cells. Moving away from the centre of the tumour the necrotic core gives way to a region where the cells are quiescent and past this region of quiescent cells there is the outer rim which largely consists of proliferating cells.

The right hand axis in Figure 3.9(a) lies at the edge of the capillary spheroid and our model shows the existence of only a very thin region of healthy cells outside the tumour spheroid; so thin in fact that this region is barely visible. We consider the width of the gap between the tumour and neighbouring capillaries in more detail in Figure 3.9(f) where we plot this width as a function of tumour radius. It can be seen

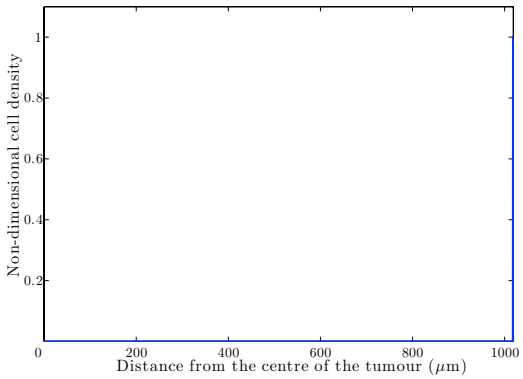

(a) The density of healthy cells.

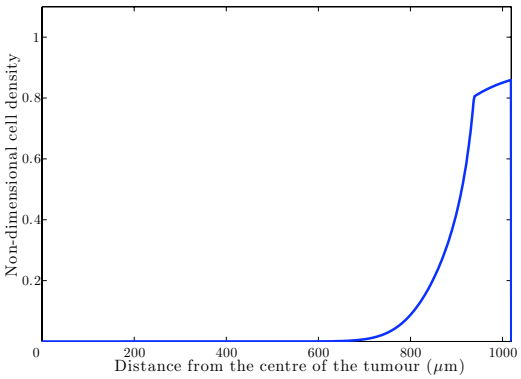

(b) The density of proliferating cells.

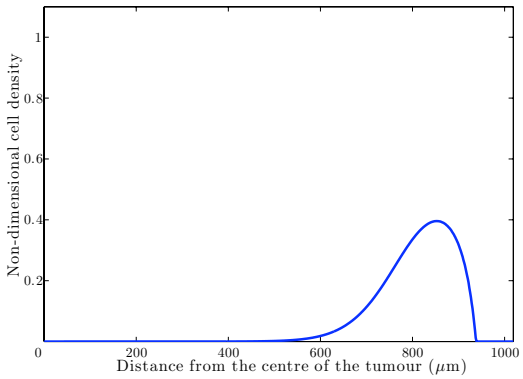

(c) The density of quiescent cells.

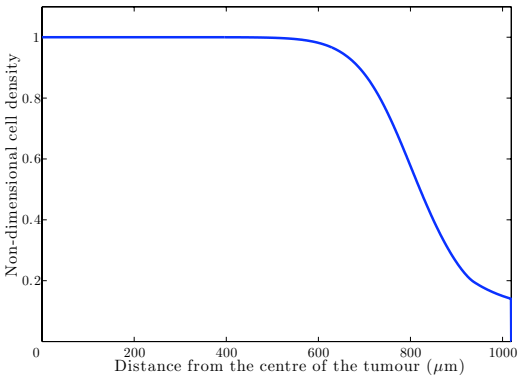

(d) The density of necrotic cells.

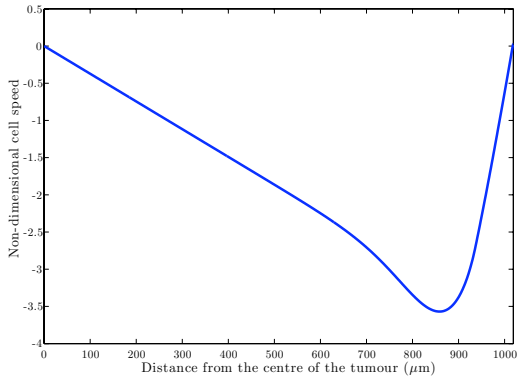

(e) The cell speed.

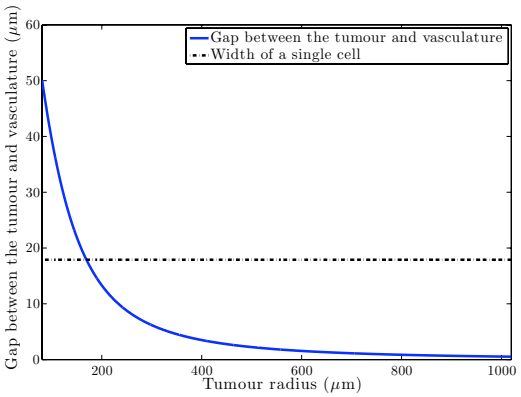

(f) The width of the gap between the tumour and vasculature.

Figure 3.9: The non-dimensional density of the different cell types in our modelled tumour at saturation as a function of the distance from the centre of the tumour, the non-dimensional cell speed at saturation as a function of the distance from the centre of the tumour, and the width of the gap between the tumour and surrounding vasculature as a function of tumour radius, all for the parameter values outlined in Table 3.2 and as governed by Equations (3.16) to (3.21).

that the gap between the tumour and surrounding vasculature rapidly decreases as the tumour grows. This decrease is so pronounced that once the tumour has grown to 200 μm or so in radius the capillaries are effectively lying on the surface of the tumour.

This result is in agreement with our earlier scaling argument, presented in Section 3.2, that as tumours begin to grow any gap between the tumour and surrounding vasculature initially closes. Furthermore, this multi-compartment model predicts that the gap between the tumour and neighbouring vasculature will continue to close even after the tumour has become established.

However, in our literature search in Section 3.1.1 we found that many mathematical models of angiogenesis assume the existence of a significant gap between the tumour and surrounding vasculature at the initiation of angiogenesis. To consider whether such a gap might be maintained by some mechanism not currently in our model we now consider whether there are other biologically reasonable cell kinetics which might lead to the existence of a significant gap between the tumour and surrounding vasculature.

3.6 The Proliferation Kinetics of Healthy Cells

We now consider four different cases for the proliferation kinetics of healthy cells to see whether we can find biologically reasonable kinetics which are capable of maintaining a significant gap between the tumour and surrounding vasculature. To isolate the effect the healthy cell kinetics have on the system the rest of our model will remain unchanged.

The work in this section generalises our previous model and much of the analysis will be exactly as before. In particular, the kinetics of the tumour cells will be unchanged and the numerical simulation of these new models will require only minor adaptations to our previous scheme. Where work is exactly as that already presented it will not be presented again.

We begin by deriving the four different kinetics for the proliferation of healthy cells.

3.6.1 Case 1: No Net Proliferation

For our first case we take the kinetics already considered. We have already noted that although healthy cells do proliferate and die, the rate of cell turnover is low and the majority of healthy cells are typically quiescent (Strain and Diehl, 1998). We also noted that in the absence of any tumour the healthy cells will exist at an approximately constant density. This suggested that the natural proliferation and death of healthy cells are approximately in balance so that to leading order it can be assumed that there is no net proliferation or death of healthy cells. Then the evolution of healthy cells is given by

$$\frac{\partial h}{\partial t} + \nabla \cdot (\underline{v} h) = 0.$$

3.6.2 Case 2: Oxygen Driven Proliferation

If the gap between the tumour and vasculature begins to thin then the average distance between the healthy cells and the surrounding capillaries will reduce. It could be conjectured that this reduction in the distance between the healthy cells and neighbouring capillaries might increase the amount of oxygen being delivered to the healthy cells, which in turn could upregulate healthy cell proliferation, which in turn again might maintain a gap between the tumour and vasculature.

For our second case we consider whether such a feedback mechanism could maintain a non-trivial gap between the tumour and vasculature. To do this we assume that the proliferation and necrosis kinetics of healthy cells depend upon the local oxygen concentration. In particular we assume that the death rate of healthy cells is equal to the corresponding death rate of tumour cells, but the proliferation rate of healthy cells is slower than the corresponding proliferation rate of cancer cells. The dimensional equation for the evolution of healthy cells is then given by

$$\frac{\partial h}{\partial t} + \nabla \cdot (\underline{v} h) = \big\{\lambda k_m(c) - k_d(c)\big\} h,$$

where $\lambda < 1$ is the relative rate of proliferation of healthy cells compared to tumour cells.

The evolution of the proliferating and quiescent tumour cells is unaffected by this change in the healthy cell kinetics and are still governed by Equations (3.9) and

(3.10) respectively, but the dimensional equation for the evolution of the necrotic cells is now given by

$$\frac{\partial n}{\partial t} + \nabla \cdot (\underline{v} n) = k_d(c)(h + p + q) - \nu n,$$

and the dimensional equation for the uptake of oxygen is given by

$$\frac{\partial c}{\partial t} + \nabla \cdot (\underline{v} c) = \nabla \cdot (D \nabla c) - \gamma k_m(c)(\lambda h + p) - k_n(c)(h + p + q).$$

The assumption that the cell volume fraction is constant is also unaffected by this change in the healthy cell kinetics and is still governed by Equation (3.12). As with the previous case, this equation for the cell volume fraction can be used to couple the equations governing the evolution of the different cell types together to obtain a first order partial differential equation which governs the local cell velocity. However, it is not desirable to do this before non-dimensionalising the system and the details of the non-dimensionalisation are not presented in detail again. Having non-dimensionalised, and dropped carets, we evaluate λ, the relative rate of proliferation of healthy cells compared to tumour cells, by noting that in the absence of any tumour the inter-capillary distance should be approximately maintained. Letting R be a sphere of healthy cells of dimensional radius $50\,\mu$m we choose λ so that the net change in volume of R is zero, i.e. we choose λ so that

$$\iiint_R \big\{\lambda k_m(c) - 0.5 k_d(c)\big\} h - \nu n \, \mathrm{d}V = 0.$$

Note that the value of λ feeds back into our system via the oxygen concentration and so this is actually an implicit equation for λ, the solution of which we find using a Newton-Raphson method. Doing this we find that taking $\lambda = 0.301$ (3 s.f.), so that healthy cells proliferate approximately 30% as quickly as equivalent tumour cells, maintains the inter-capillary distance in the absence of any tumour.

Having included oxygen driven kinetics for the evolution of healthy cells into our model, we can again transform this system into a system of characteristic equations and numerically simulate the growth of the tumour exactly as before.

3.6.3 Case 3: Forced Proliferation I

For our third case we force the healthy cells to undergo mitosis at a rate k_{h1}, which is specifically chosen so that the velocity field in the region of healthy cells is constant.

This will forcibly and artificially maintain a gap of constant width between the tumour and surrounding vasculature. Such proliferation kinetics have no biological motivation other than the maintenance of a constant gap and we consider this case to see if such proliferation is plausible.

In this case the dimensional equation for the evolution of healthy cells is given by

$$\frac{\partial h}{\partial t} + \nabla \cdot (\underline{v} h) = h k_{h1},$$

where k_{h1} is chosen so that outside the tumour, where $h = \frac{\mathcal{V}}{V_L}$, we have $\underline{v} = v_{\text{tum}} \underline{e}_r$. It is simple to show that the required form for k_{h1} is:

$$k_{h1} = \frac{2 v_{\text{tum}}}{r}.$$

The corresponding dimensional equation governing the evolution of oxygen is then

$$\frac{\partial c}{\partial t} + \nabla \cdot (\underline{v} c) = \nabla \cdot (D \nabla c) - \gamma \left(\frac{2 h v_{\text{tum}}}{r} + k_m(c) p \right) - k_n(c)(h + p + q).$$

This system can then be non-dimensionalised as before and dropping carets the non-dimensional oxygen concentration and local cell velocity are given by

$$\nabla^2 c = \gamma \left(\frac{2 h v_{\text{tum}}}{r} + k_m(c) p \right) + k_n(c)(p + q), \tag{3.31}$$

$$\nabla \cdot \underline{v} = \frac{2 h v_{\text{tum}}}{r} + k_m(c) p - 0.5 k_d(c)(p + q) - \nu n. \tag{3.32}$$

The evolution of the proliferating, quiescent, and necrotic cells is unaffected by this change in the healthy cell kinetics and are still given by Equations (3.9) to (3.11).

As before this system can be non-dimensionalised and transformed into a system of characteristic equations, which we numerically simulate similarly as before, albeit with a slight modification.

The right hand side of the Poisson equation for the oxygen concentration, Equation (3.31), now contains a v_{tum} term. To find v_{tum} we must solve Equation (3.32) but the right hand side of this equation depends upon c, the oxygen concentration. So we now have a pair of coupled, implicit differential equations.

To solve this pair of equations we make an initial estimate for the speed of the tumour front, v_{tum}, which we denote $v_{\text{tum}} = X$. We can then find the oxygen concentration, c, and local velocity, v, corresponding to this value of X. This will then give us a

new, calculated, value of the speed of the tumour front, which we denote by $g(X)$, and this will depend upon the original value of X. This process defines the function $g(X)$, where X is the assumed value of v_{tum} and $g(X)$ is the corresponding calculated value of v_{tum}. For consistency we require that $X = g(X)$ and we find this value of X using a Newton-Raphson method. Having found the value of X, we use this to approximate the speed of the tumour front, v_{tum}, and then Equations (3.31) and (3.32) can be decoupled and solved as before.

3.6.4 Case 4: Forced Proliferation II

For our fourth and final case we force the healthy cells to proliferate at a constant rate k_{h2}, which is chosen to maintain a constant gap between the tumour and surrounding vasculature. As in Case 3 a constant width gap between the tumour and surrounding vasculature is being maintained, but in Case 3 the proliferation of healthy cells was forced so that the velocity of the healthy cells was spatially constant, but the rate of healthy cell proliferation itself was not spatially constant. Here the proliferation of healthy cells is being forced so that the proliferation of healthy cells is spatially constant, but the velocity of the healthy cells is not constant.

As in Case 3 this proliferation kinetic will forcibly and artificially maintain the gap between the tumour and surrounding vasculature, but has no other biological motivation. However, it is assumed that the joint consideration of Cases 3 and 4 will consider any biologically reasonable healthy cell proliferation which might maintain a constant width gap between the tumour and healthy cells. This is because any proliferation kinetic not considered by Cases 3 and 4 must have a highly variable rate of proliferation and also a highly variable corresponding local cell velocity and such behaviour would be difficult to motivate.

In this case the dimensional equation for the evolution of healthy cells is given by

$$\frac{\partial h}{\partial t} + \nabla \cdot (\underline{v} h) = h k_{h2},$$

where k_{h2} is chosen so that $v(r_{\text{tum}}, t) = v(r_{\text{tum}} + 50\,\mu\text{m}, t) = v_{\text{tum}}$. Recalling that $h = \frac{\mathcal{V}}{V_L}$ outside the tumour this becomes a first order differential equation for v, the local cell velocity. Integrating this equation and satisfying these boundary conditions we find that the healthy cells must proliferate at the constant rate:

$$k_{h2} = \frac{3 v_{\text{tum}} (2 r_{\text{tum}} + 50\,\mu\text{m})}{3 r_{\text{tum}}^2 + 3 r_{\text{tum}} 50\,\mu\text{m} + (50\,\mu\text{m})^2}.$$

The corresponding dimensional equation for the evolution of oxygen is then:

$$\frac{\partial c}{\partial t} + \nabla \cdot (\underline{v}c) = \nabla \cdot (D\nabla c) - \gamma\{k_{h2}h + k_m(c)p\} - k_n(c)(h + p + q),$$

The evolution of the proliferating, quiescent, and necrotic cells is unaffected by this change in the healthy cell kinetics and are still given by Equations (3.9) to (3.11).

The system can then be non-dimensionalised as before and upon dropping carets the non-dimensional oxygen concentration and local cell velocity are governed by

$$\nabla^2 c = \gamma\{k_{h2}h + k_m(c)p\} + k_n(c)(p + q), \tag{3.33}$$

$$\nabla \cdot \underline{v} = k_{h2}h + k_m(c)p - 0.5k_d(c)(p + q) - \nu n. \tag{3.34}$$

As before the system can be non-dimensionalised and transformed into a system of characteristic equations which we numerically simulate. Again, Equations (3.33) and (3.34) are a pair of coupled implicit differential equations, which we de-couple by approximating the value of v_{tum} in exactly the same way as was outlined for Case 3.

3.7 Results

Having defined the healthy cell kinetics for each of our four cases, we now simulate the resultant tumour growth to see what effect the evolution of healthy cells has on the system.

Tumour Dynamics

We begin by considering what effect the healthy cell kinetics has on the growth of the tumours. The growth curves of the tumours as functions of time for each of the four cases are shown in Figure 3.10.

It can be seen that initially the growth curves for each of the cases are very similar. However as the tumour grows the tumour growth rate in Cases 3 and 4 slows relative to the tumour growth in Cases 1 and 2, and in Cases 3 and 4 the tumour saturates at a smaller radius. However, the growth curves of Cases 1 and 2 are almost identical to each other, and the growth curves of Cases 3 and 4 are almost identical to each other.

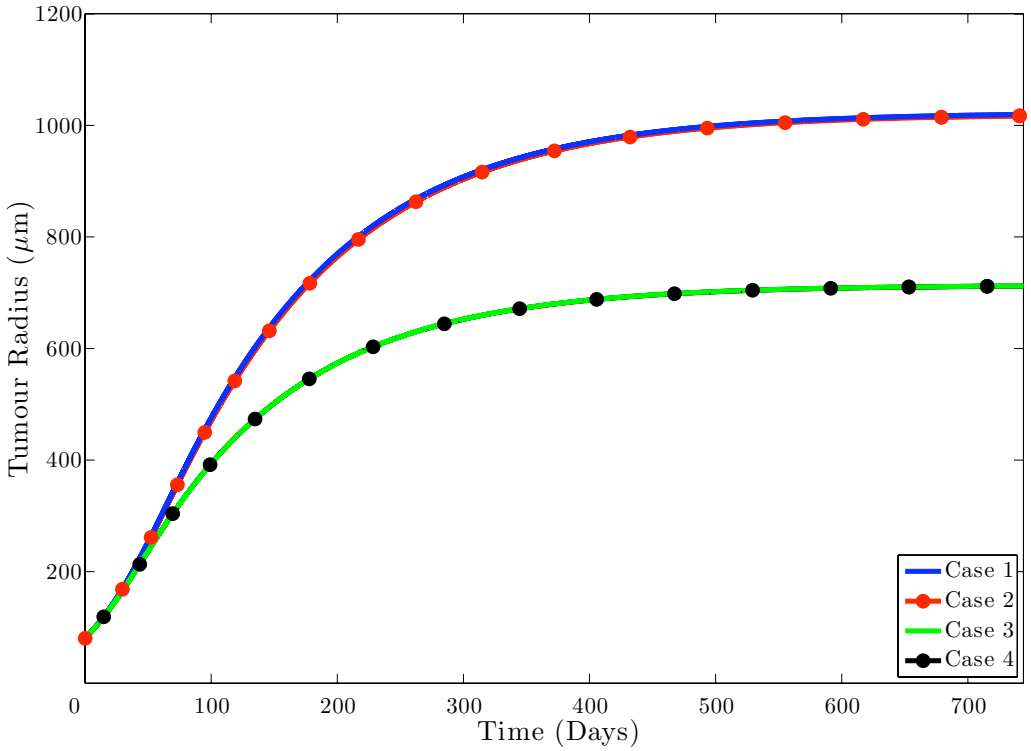

Figure 3.10: The growth curves of the tumours for the four cases of healthy cell kinetics. See text for details.

We hypothesise that this difference in the growth curves is caused by a wider gap between the tumour and vasculature in Cases 3 and 4. We consider this explicitly by plotting the width of this gap as a function of tumour radius in each of our four cases, which is shown in Figure 3.11.

In Cases 1 and 2 the width of the gap between the tumour and surrounding vasculature decreases as the tumour grows. The oxygen driven proliferation dynamics in Case 2 do marginally slow the thinning of the gap, but only by a very small amount and the capillaries still effectively reach the surface of the tumour well before the tumour growth saturates.

The results of Figure 3.11 support our hypothesis that the difference in the growth curves in Figure 3.10 is caused by the presence or not of a significant gap between the tumour and vasculature. The gap in Cases 3 and 4 is much thicker than in either Case 1 or 2 and the additional healthy cells in this gap will be consuming oxygen so that less oxygen reaches the tumour. This relative lack of oxygen will inhibit cell

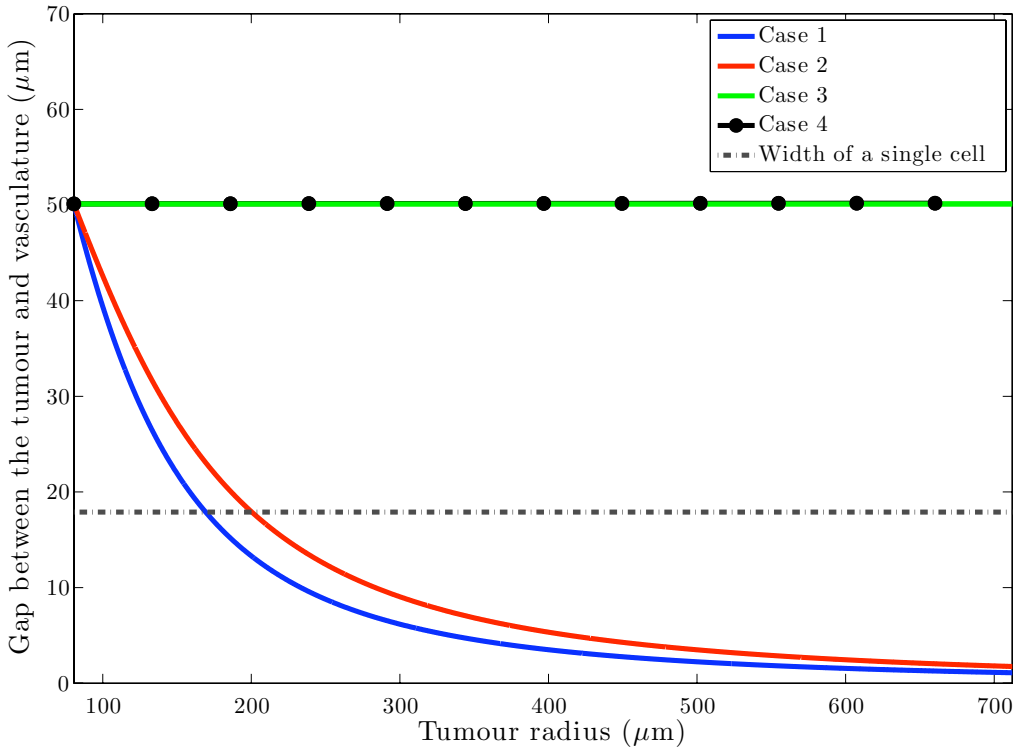

Figure 3.11: The width of the gap between the tumour and surrounding vasculature as a function of tumour radius for the four cases of healthy cell kinetics. See text for details.

proliferation and upregulate cell necrosis in the tumour and overall tumour growth will be reduced.

In Figures 3.10 and 3.11 it can be seen that the tumour growth curves and the behaviour of the distance between the tumour and vasculature are indistinguishable between Cases 3 and 4. This was to be expected because both cases have been constructed to forcibly maintain a gap of constant width between the tumour and surrounding vasculature. However the mechanism by which these two cases maintain the gap is fundamentally different, with Case 3 forcing a constant velocity field in the region of healthy cells and Case 4 forcing a constant rate of proliferation in the region of healthy cells. We now compare the results of Cases 3 and 4 in more detail to consider whether these cases are fundamentally different, or whether they are effectively equivalent.

Comparing Cases 3 and 4

To compare Cases 3 and 4 we consider the initial rate of proliferation and local cell speed within our tumour.

The cell proliferation rates in our initial tumour as a function of the distance from the centre of the tumour for Cases 3 and 4 are shown in Figure 3.12. It can be seen that the kinetics of Case 4 have successfully forced the rate of proliferation to be constant, which appears to be approximately equal to the average rate of proliferation in Case 3. The difference between the rates of healthy cell proliferation in Cases 3 and 4 is discernible.

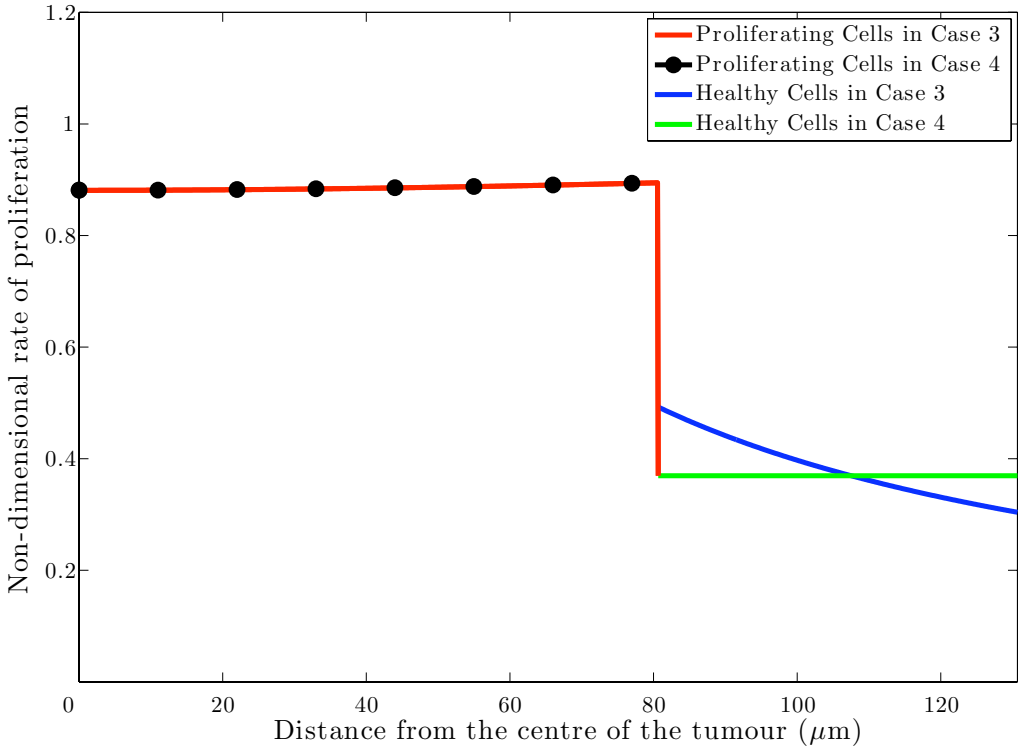

Figure 3.12: The rate of proliferation in the initial tumour as a function of the distance from the centre of the tumour for Cases 3 and 4. See text for details.

The local cell speed in our initial tumour as a function of the distance from the centre of the tumour for Cases 3 and 4 is shown in Figure 3.13. It can be seen that in Case 3 the speed of the healthy cells has been successfully forced to be constant, whereas in Case 4 the speed of the edge of the capillary spheroid has successfully been forced

to equal the speed of the tumour front. The difference between the local speeds of the healthy cells in Cases 3 and 4 is again discernible.

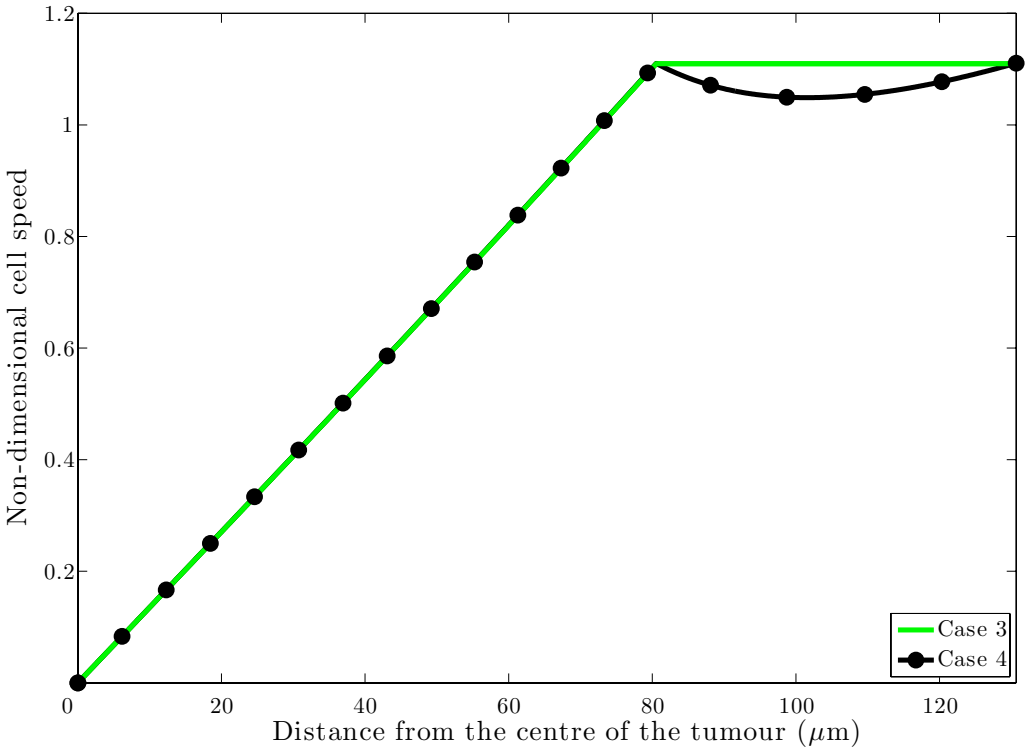

Figure 3.13: The local cell speed in the initial tumour as a function of the distance from the centre of the tumour for Cases 3 and 4. See text for details.

In Figures 3.12 and 3.13 it can be seen that the differences between Cases 3 and 4 are discernible. Given this we conclude that these two cases are not effectively equivalent and both cases should be explicitly considered in our further analysis. However, the fact that the behaviour of these two cases is quite similar suggests that any healthy cell proliferation which maintains a constant gap between the tumour and surrounding vasculature will also be similar to at least one of these cases. Hence we assume that any possible mechanism which maintains a constant width gap between the tumour and surrounding vasculature can be investigated by considering Cases 3 and 4.

The Rate of Proliferation

Recall that our initial scaling argument in Section 3.2 found that maintaining a constant width gap between the tumour and surrounding vasculature required the initial

rate of healthy cell proliferation to be unrealistically high. We now use our multi-compartment model to compare the rates of proliferation of tumour and healthy cells throughout the course of tumour growth. In particular we consider whether the rate of healthy cell proliferation required in Cases 3 and 4 to maintain a constant width gap between the tumour and vasculature is unfeasibly high. To do this we define the mean net rate of proliferation of the proliferating cells in Cases 3 and 4 to be given by

$$\frac{\int_0^{S_{\text{cap}}} \{k_m(c) - k_d(c)\} p \, \mathrm{d}V}{\int_0^{S_{\text{cap}}} p \, \mathrm{d}V},$$

and the mean net rate of proliferation of the healthy cells in Case 3 to be given by

$$\frac{\int_0^{S_{\text{cap}}} \frac{2hv_{\text{tum}}}{r} \, \mathrm{d}V}{\int_0^{S_{\text{cap}}} h \, \mathrm{d}V}.$$

Then the mean net rate of proliferation of the proliferating cells in Cases 3 and 4, the mean and maximum net rate of proliferation of the healthy cells in Case 3, and the constant net rate of proliferation of the healthy cells in Case 4, are plotted in Figure 3.14.

It can be seen that to maintain the gap of constant width between the tumour and vasculature initially requires some of the healthy cells in Case 3 to proliferate at a net rate 83% of that of the proliferating cells. Furthermore, in both Cases 3 and 4 healthy cells are on average required to proliferate at a net rate 63% of that of the proliferating cells. This initial relative net rate of proliferation of the healthy cells is higher than would be expected to be observed experimentally, except for extremely slow growing tumours or tumours growing in tissue with a particularly high turnover rate. However as the tumour grows larger the relative net rate of proliferation of healthy cells required to maintain a gap of constant width between the tumour and surrounding vasculature reduces to a more realistic level. These results agree with the findings of our simple scaling argument of Section 3.2, that the gap between the tumour and neighbouring vasculature must initially close because the healthy cells cannot proliferate fast enough to maintain the gap. Once the tumour has grown to a larger size, the re-establishement of a gap between the tumour and neighbouring vasculature would not require an unfeasibly fast rate relative rate of proliferation, but there is no obvious mechanism which would upregulate healthy cell proliferation in this way.

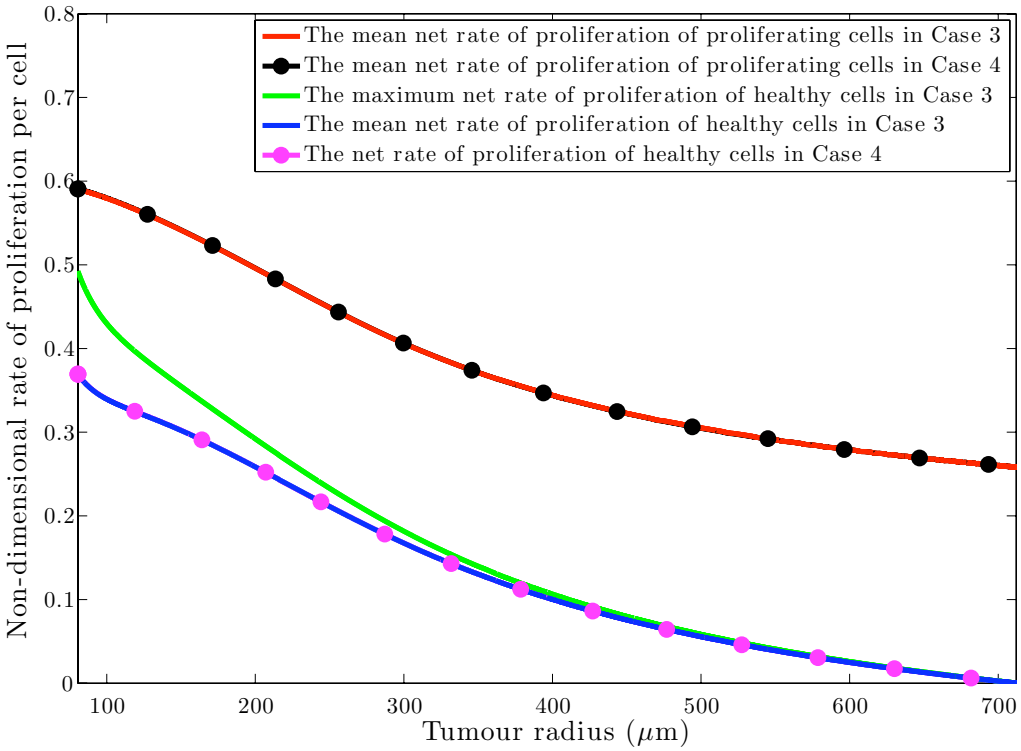

Figure 3.14: The rates of proliferation of the different cell types in Cases 3 and 4 as a function of the tumour radius, see text for details.

3.7.1 An *a Posteriori* Check of the Numerical Scheme

It can be seen in Figure 3.11 that our results for Cases 3 and 4 show a gap of constant width being maintained between the tumour and neighbouring vasculature as the tumour grows. Furthermore, it can be seen in Figure 3.12 that our results for Case 4 show the rate of healthy cell proliferation to initially be constant, and in Figure 3.13 our results for Case 3 show the local cell velocity to initially be constant throughout the region of healthy cells. Hence where terms have been deliberately chosen to force the tumour to behave in a specific way, this forced behaviour is observed in our results. The fact that our numerical simulation of the tumour growth has correctly reproduced these different forced behaviours further validates our numerical scheme.

3.8 Conclusions

In this chapter we were aiming to derive a model for the evolution of an avascular tumour spheroid and use this model to investigate whether or not a significant gap can be maintained between a growing avascular tumour and the surrounding vasculature.

We began our investigation in Section 3.2 by using a simple scaling argument to compare the rate of proliferation of tumour cells to the rate of proliferation of healthy cells in small tumours with growth fractions close to unity. For such tumours we found that the maintenance of a gap of constant width requires healthy, non-cancerous, cells to proliferate approximately half as quickly as cancerous cells. This is unrealistic for all tumours, except those with very long doubling times or those growing in tissue with a very high cell turnover rate. This suggests that for most tumours the gap between the tumour and vasculature will initially reduce in width, but our scaling argument was inconclusive at considering whether this gap could re-establish itself once the tumour exceeds the range of sizes that can be considered by this scaling argument.

In Section 3.3 we then built a model which quantified the rate at which oxygen is drawn out of the capillary network to support a variety of tumour and gap configurations. We found that the 2 mm gap between the tumour and vasculature often seen following intra-cornea implant experiments must be unique to the cornea and is an artefact of the fact that the cornea is an uniquely large region of avascular tissue. In other tissues, which are vascularised in the absence of a tumour, it was found that to support a saturated tumour with a 2 mm gap between the tumour and vasculature requires that almost 60 times as much oxygen be drawn out of the capillary network than is required to support normal tissue in the absence of a tumour. This is orders of magnitude higher that the maximum increase in oxygen supply observed experimentally and unrealistic. However, our rate of oxygen supply argument was inconclusive at considering whether a gap between the tumour and vasculature of 50 μm, which corresponds to a gap of constant width being maintained as the tumour grows, might exist.

In Section 3.4 we then considered the behaviour of the gap between the tumour and vasculature by developing a multi-compartment model for the growth of an avascular tumour. In this section we considered four different cases for the proliferation kinetics of healthy cells. In the first case we assumed that to leading order there is no net

proliferation of healthy cells and in the second case we allowed the healthy cells to proliferate and die at rates which depend upon the local oxygen concentration.

It was found that the difference between Cases 1 and 2 was minimal. This validates the assumption made in Case 1 that to leading order the natural proliferation and death of healthy cells is negligible. However, the addition of oxygen driven cell kinetics could not maintain a significant gap between the tumour and vasculature. This demonstrates that if a significant gap is to be maintained between the tumour and vasculature then more complicated cell kinetics are required.

In Cases 3 and 4 we forced the healthy cells to proliferate in a way which maintained a uniform gap between the tumour and vasculature. In Case 3 we forced the local cell velocity to be constant throughout the region of healthy, non-cancerous, cells, and in Case 4 we forced the rate of proliferation to be constant throughout the region of healthy, non-cancerous cells. Comparing the results of Cases 3 and 4 we found these two cases to exhibit discernibly, if not significantly, different tumour behaviour. The resultant behaviour of these two cases was sufficiently similar to suggest that any healthy cell proliferation kinetics which maintains a uniform gap between the tumour and surrounding vasculature can be approximated by considering these two cases. Cases 3 and 4 agreed with our initial scaling argument and again illustrated that the maintenance of a uniform gap between the tumour and surrounding vasculature initially requires unfeasibly rapid proliferation of non-cancerous cells, except possibly for tumours with very slow doubling rates or tumours growing in tissues with very high cell turnover rates.

Both our initial scaling argument and our multi-compartment model show that the rate of healthy, non-cancerous, cell proliferation initially required to maintain an uniform gap between the tumour and surrounding capillaries is unfeasibly rapid, except possibly for tumours with very slow doubling rates or tumours growing in tissues with very high turnover rates. Furthermore, even if a given tumour has a very slow doubling rate, or grows in tissue with a high cell turnover rate, or the gap between the tumour and surrounding capillaries initially closes but then later recovers, then there is no obvious mechanism which would upregulate healthy cell proliferation to the required extent, and our multi-compartment model has shown that oxygen driven healthy cell kinetics are nowhere near sufficient.

Given this, we conclude that for *in vivo* tumour spheroids, any initial gap between the tumour and surrounding vasculature quickly closes so that once the tumour grows

to be 200 μm in radius the surrounding capillaries are effectively lying on the surface of the tumour. Certainly when the tumour reaches its maximum size as given by diffusion limited control then the surrounding capillaries will effectively be lying on the surface of the tumour with no significant gap between the tumour and surrounding capillaries.

However, while applicable for micrometastases, the presence of a basal membrane near the initiation point of a carcinoma can provide a physical barrier between the tumour and surrounding vasculature. In situations where the additional, albeit thin, membraneous, biological structures exist they may limit the ultimate approach of an initiating tumour to the capillary bed.

Regardless of this, as the initial separation between tumour and capillary is of the order of the inter-capillary distance, our studies unequivocally demonstrate that sustaining a tumour with a 2 mm gap between the tumour and surrounding vasculature requires an impossibly high rate of oxygen delivery out of the vasculature. This highlights that the results of the intra-cornea implant experiment are unique to that setting. In particular, angiogenesis does not in general take place with capillaries sprouting towards and into the tumour from a significant distance away. This result is in contrast to the widespread belief of many papers in the mathematical literature. So whilst the intra-cornea implant experiment is relevant to that context, it should not be used as a starting point for general models for angiogenesis.

Chapter 4

Modelling the Evolution of a Solid Vascular Tumour

4.1 Introduction

In this chapter we derive a model for the growth of a vascular tumour. This model will be developed as a stepping stone to modelling a vascular tumour undergoing treatment by a combination of chemotherapy and/or anti-angiogenic therapy, and such therapies are included into our model in the proceeding chapters. While deriving this initial model we will remain conscious that our system must be receptive to the inclusion of these therapies. After deriving our model we will then evaluate all the parameters in it by performing a literature search and an analysis of parameters.

4.1.1 Literature Summary

Before deriving our model we conduct a review of the relevant literature.

Mathematical Literature

Early mathematical biologists hypothesised that the increased cell proliferation rate in a tumour should cause it to double at a constant rate so that tumour growth can be described by a simple exponential growth model. Collins et al. (1956) used the case study of a soldier who had observed a small "nodule" behind his left knee to highlight that tumour growth does follow the exponential model. The soldier noted the size of the nodule at various dates, but did not seek medical attention until four

years after he first noticed the tumour, by which time the tumour had grown to 15 cm in diameter. The observed growth of the soldier's tumour matched the exponential growth model.

Laird (1964) proposed that tumours actually grow by some modified exponential growth process, where successive doublings occur over increasingly longer intervals. By considering data by Patt and Blackford (1954), who inoculated mice with Krebs ascites cancer and recorded the size of the corresponding tumours at various times, Laird showed that such growth dynamics provided a good fit to their data.

Laird et al. (1965) then performed their own experiments and considered the growth of guinea pigs and recorded their weight, $W(t)$, as a function of time. It was found that $\log\left(\frac{1}{W(t)}\frac{\mathrm{d}W(t)}{\mathrm{d}t}\right)$ exhibited a very strong negative linear correlation with time. Given this relationship between animal weight and time the following non-linear first order differential equation was derived for the growth of the guinea pigs:

$$\frac{\mathrm{d}W(t)}{\mathrm{d}t} = \alpha_2 W(t) \log\left(\frac{K}{W(t)}\right), \tag{4.1}$$

where α_2 and K are positive parameters. The solution to an equation of this form is known as a Gompertzian function, and such functions inherit their name from the Gompertz law of human mortality, which was discovered whilst considering the pricing of life contingencies (Gompertz, 1825). Such functions characteristically exhibit sigmoidal curves such as the one shown in Figure 4.1.

Laird et al. (1965) considered the growth of guinea pigs to derive the Gompertz model, but the Gompertzian growth curve has also been shown to fit well with the growth of solid vascularised tumours (McCredie et al., 1965; Norton et al., 1976). However Burton (1966) noted that whilst tumours do follow Gompertzian growth for a "remarkably large range of size", they finally grow at a linear rate and the Gompertzian model fails to capture this final behaviour.

Since then the Gompertzian growth model has been widely used to describe the growth curves of various animals and organisms (Laird, 1965). Despite the motivation for Gompertzian growth being entirely empirical, and the fact that it fails to capture the final linear stage of tumour growth, the Gompertzian growth model remains a standard model for describing vascular tumour growth.

It should be noted that the Gompertzian growth model only describes the total size of a tumour. In the next chapter we will apply chemotherapy and anti-angiogeneic

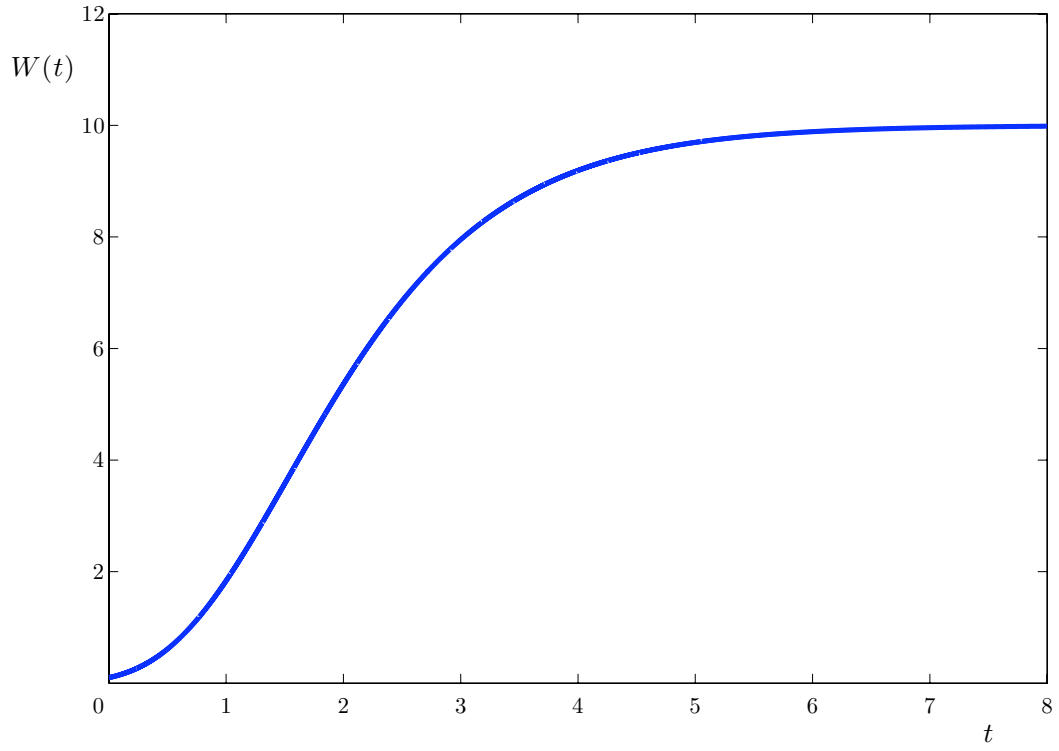

Figure 4.1: The Gompertz function, as defined by Equation (4.1), with $\alpha_2 = 1$, $\kappa = 10$, and $W(0) = 0.1$.

therapy to our modelled tumour and to consider the effect of these therapies we will explicitly model the populations of proliferating, quiescent, and necrotic cells in the tumour, as well as the level of angiogenesis which has taken place; the standard Gompertzian growth model will not be sufficient for our needs. Even so we must ensure that our model is consistent with observed tumour growth and displays sigmoidal growth curves similar to those produced by the Gompertzian growth model.

Before deriving our model we now review other multi-compartment models for vascular tumour growth and any other relevant mathematical papers.

Gyllenberg and Webb (1989) developed a two compartment model for tumour growth which considered proliferating and quiescent cells. They assumed that proliferating cells could either proliferate, become quiescent, or die, whereas quiescent cells could either become proliferative, or die. The rate of transfer from the proliferating population to the quiescent population and *vice versa* (referred to as the transfer rates) simply depended upon the size of the tumour.

Gyllenberg and Webb assumed general forms for the transfer rates between the proliferating and quiescent compartments and after imposing some biologically motivated restrictions derived a number of observed properties of tumour growth. For example, they predicted that tumour volume would be a monotonically increasing function of time and saturates at a finite size. Furthermore, upon simulating the tumour growth over time sigmoidal growth curves were observed and it was also shown analytically that terms could be specifically chosen so that the model exhibits exact Gompertzian, or logistic growth.

Whilst Gyllenberg and Webb's model does not explicitly model angiogenesis, and so is not general enough for our purposes, their work does suggest that a simple multi-compartment model can exhibit realistic, sigmoidal growth curves.

Kozusko and Bajzer (2003) align Gyllenberg and Webb's model with that of Gompertzian growth by calculating the terms required for Gyllenberg and Webb's model to exhibit exact Gompertzian growth in a more general setting. The resulting terms are complex and have no biological motivation other than recovering exact Gompertzian growth. Since exact Gompertzian growth is not required to obtain realistic growth curves, and the resulting transfer rates when Gompertzian growth is forced are overly intricate, we will build a simple multi-compartmental model where the transfer rates from one compartment to another are biologically motivated. However, we must still ensure that our model exhibits a sigmoidal growth curve.

Our model will be similar to Gyllenberg and Webb's (1989) but we make two important generalisations. Firstly Gyllenberg and Webb (1989), and Kozusko and Bajzer (2003) both ignore necrotic cells. Whilst living cells were allowed to die the progression of these necrotic cells was not considered. However, when tumours have been observed to exhibit sigmoidal growth curves it is the total volume of the tumour which is recorded and this will include the volume of any necrotic cells. So our model will also consider the evolution of necrotic cells.

Secondly, Gyllenberg and Webb, and Kozusko and Bajzer both assume that the behaviour of the tumour depends only upon the size of the tumour. We anticipate that the behaviour of the tumour will actually depend on the quality of the local vasculature. In untreated tumours it might be valid to assume that the quality of the local vasculature is a function of tumour volume, but for a tumour undergoing treatment by chemotherapy and/or anti-angiogenic therapy this will certainly not be

true. So our model will explicitly consider the dependence of the tumour growth on the quality of the local vasculature.

One paper which does model tumour treatment with anti-angiogenic therapy is that of Hahnfeldt et al. (1999) who proposed a Gompertzian based model but assumed that the carrying capacity of the tumour depends upon the vascular support provided to the tumour. The level of vasculature support could then vary depending upon the presence of angiogenesis stimulating growth factors and anti-angiogenic therapies. This simple model was able to reproduce experimental tumour growth, both in the presence and absence of anti-angiogenic therapy, which suggests that it is possible to accurately model angiogenesis and its inhibition. However, Hahnfeldt et al.'s model only considers the total volume of the tumour and as noted previously our model must be more general than this.

Motivated by the success of these previous models we now build our own multi-compartment model for vascular tumour growth. To ensure that this model is biologically realistic we first conduct a review of the relevant biological literature.

Biological Literature

Our model will consider three types of tumour cell, namely proliferating cells which are alive and actively in the cell-division cycle, quiescent cells which are alive but in the G_0 phase of the cell cycle, and necrotic cells. We will also consider the amount of vasculature support available to the tumour by considering the number of capillary endothelial cells present in the tumour. These endothelial cells are not cancerous, but if present in sufficiently large numbers will be considered to contribute to the volume of the tumour.

It is well known that cell proliferation within solid vascular tumours is heterogeneous (Tannock, 2001) and so modelling any spatial aspect of vascular tumour growth is a highly non-trivial task. This heterogeneity also makes it impossible to utilise any spatial simplifications, such as radial symmetry. So rather than model the spatial distribution of the tumour cells in each compartment we will consider the total volume of cells in each compartment.

We now review the relevant properties of the live cells preset in vascular tumour spheroids and also recall the behaviour of the cell cycle, which was described in Section 1.5.

As the tumour grows the cell cycle time of continuously proliferating cells remains essentially constant (Tubiana, 1971).

The relationship between the vasculature and cell proliferation has been considered in implanted mouse tumours (Tannock, 1968). It was observed that blood vessels had "cords" of viable tissue surrounding them and outside these viable cords large regions of necrosis were found. Furthermore, the proportion of cells which were proliferating was found to decrease with an increase in the distance away from the nearest vessel. Comparing the size of these viable cords with the diffusion distance of oxygen and considering the tumour dynamics when the mice were exposed to different background oxygen levels gave results which were consistent with the assumption that oxygen is the main driver for proliferation. However other factors, such as a lack of metabolites or an accumulation of toxic products could also be important (Tubiana, 1971). The fact that low growth fractions are found in regions of poor vasculature suggests that the presence of a poor vasculature promotes proliferating cells to become quiescent and/or inhibits quiescent cells from becoming proliferative.

It has also been observed that if a tumour is treated by a chemotherapeutic then quiescent cells begin to proliferate in greater numbers than before the treatment (Gavosto and Pileri, 1971). Chemotherapy typically reduces tumour volume to a greater extent than it reduces vasculature support and so the net effect of the treatment will actually be to improve the tumour's vasculature. The fact that large numbers of quiescent cells are recruited back into the cell cycle after the application of chemotherapy suggests that a good vasculature promotes quiescent cells to become proliferative and/or inhibits proliferating cells from becoming quiescent.

Having considered the interaction of proliferating and quiescent cells we consider one final important property of quiescent cells. Some cells can remain quiescent for many years before they regain the ability to proliferate (Tubiana, 1971). This suggests that the transfer between proliferative and quiescent states is independent of the cell's age.

We now consider the behaviour of necrotic cells. It has been observed that cell loss in tumours is considerable and this loss is primarily due to death (Gavosto and Pileri, 1971). The fact that large regions of necrosis are found away from the blood vessels suggests that a poor vasculature promotes necrosis. We also know that tumour growth saturates whilst there are still some proliferative cells present (Tubiana, 1971) and for this to occur a simple conservation of volume argument implies that there must be some breakdown of the necrotic cells.

Finally we consider the behaviour of the capillary endothelial cells in the tumour. Under normal circumstances endothelial cells are amongst the slowest to reproduce with cell turnover times of the order of hundreds of days. In contrast, during angiogenesis endothelial cells can turnover in a matter of days (Folkman and Kalluri, 2003). This increased proliferation rate is caused by the tumour releasing diffusible angiogeneic stimulators and to date more than 15 such stimulators have been found.

One of the key angiogenic stimulators is vascular endothelial growth factor (VEGF) (Oudar, 2000). Treatment with an anti-VEGF antibody has been shown to significantly impair the growth of mouse tumours, even if the antibody is applied after the tumour has become established (Kim et al., 1999). The effect of inhibiting VEGF was so significant that in one tumour line the treatment resulted in tumours growing to only 4% of the size of the untreated tumours. *In vitro* experiments have confirmed that VEGF does indeed stimulate endothelial cell growth, rather than activate some other mechanism of tumour cell division, which highlights that VEGF is an important stimulant of tumour angiogenesis.

Further evidence that VEGF is a fundamental stimulant of angiogenesis stems from the fact that VEGF controls vascular development during the growth of embryos. Inhibiting VEGF during mouse development can disrupt the embryonic vascular network and can even result in death (Carmeliet et al., 1996; Ferrara et al., 1996). Furthermore, VEGF is the only growth factor for which gene knockout during embyrogenesis is known to be lethal (Bicknell et al., 1997). This suggests that whilst other growth factors may have an effect, VEGF is the principle driver of angiogenesis.

It is well known that VEGF is produced in the presence of hypoxia (Shweiki et al., 1992, 1995) but is has also been shown that VEGF production is up-regulated by glucose deficiency and that this is independent of up-regulation by hypoxia (Shweiki et al., 1995). This suggests that VEGF production is correlated to the quality of the local vasculature, with VEGF production being up-regulated in the presence of a poor vasculature and down-regulated in the presence of a good vasculature. These observations suggest that VEGF acts as the principle mediator in a simple feedback system where a poor local vasculature promotes local endothelial cell growth and a good local vasculature inhibits local endothelial cell growth.

4.1.2 The Aims of this Chapter

In this chapter we aim to construct a model for vascular tumour growth which is receptive to the inclusion of chemotherapy and anti-angiogenic therapies. We then aim to estimate all the parameters in this model. Our model will then be ready for the inclusion of these therapies, which will be added in the next chapter.

4.2 The Model

We now derive our model and we begin by considering how to quantify the quality of the local vasculature.

4.2.1 Quantifying the Quality of the Local Vasculature

We noted in our biological review in Section 4.1.1 that cells exhibit different behaviour depending upon the local concentration of oxygen and other nutrients, and hence the quality of the local vasculature. We also noted that it is not desirable to model any spatial aspects of the tumour and so we consider the quality of the entire tumour's vasculature, which we assume correlates with the average oxygen concentration within the tumour.

To quantify the quality of the tumour's vasculature we consider the ratio of oxygen demand to oxygen supply. Oxygen will be in demand by the proliferating, quiescent, and endothelial cells in the tumour, but only supplied by the endothelial cells. As a surrogate measure of the ratio of oxygen demand to oxygen supply we consider the ratio of the total number of proliferating, quiescent, and endothelial cells to the number of endothelial cells, which we denote by X. If this ratio is order one then the tumour will be considered to be well vascularised, and if this ratio is much larger than one then the tumour will be considered to be poorly vascularised.

A Switching Function

To allow various mechanisms in our model to be up-regulated or down-regulated depending upon the quality of the local vasculature we now define a switching function, which we denote by $S_w(X, a)$, where X is our measurement of the quality of the local vasculature, a is the critical quality of the local vasculature determining when

the switching function is turned on or off, and w is the sensitivity of the switching function.

Note that our X increases as the quality of the local vasculature decreases. We choose our switching function so that it gets switched on when the quality of the local vasculature decreases, and so it must be an increasing function of X. We also choose our switching function so that it is switched completely on in the presence of an extremely poor vasculature and switched completely off in the presence of an extremely good vasculature, so it must also satisfy $\lim_{X\to\infty} S_w(X,a) = 1$ and $S_w(1,a) = 0$. Finally, we choose our switching function so that S_w switches from $S_w \sim 0$ to $S_w \sim 1$ at $X \sim a$, and so that increasing w leads to a sharper switch with $\lim_{w\to\infty} S_w(X,a) = H(x-a)$ (the Heaviside function).

There are an infinite number of candidate switching functions, but here we take

$$S_w(X,a) = \frac{\tanh(w(X-a)) + \tanh(w(a-1))}{1+\tanh(w(a-1))}. \tag{4.2}$$

A plot of this switching function for $w = 1$ and $a = 5$ is shown in Figure 4.2. With the general properties of the switching function defined we can now derive our model for the evolution of the different cell populations.

4.2.2 The Evolution of the Cell Populations

Proliferating Cells

In our review of the cell cycle in Section 1.5 we observed that proliferating cells can divide into daughter cells which are immediately either proliferating or quiescent. Here we assume that each proliferating cell divides into two daughter cells, both of which are quiescent, at a rate μ. When considering the behaviour of the quiescent cells we will assume that these quiescent daughter cells can recover the ability to proliferate. Under optimal conditions, with suitable parameter choices, these assumptions allow daughter cells to be temporarily quiescent and then quickly recover the ability to proliferate, in which case this brief period of quiescence represents the G_1 phase of the cell cycle.

We also assume that proliferating cells undergo necrosis at a rate which depends upon the quality of the local vasculature, with an increase in the quality of the vasculature downregulating necrosis and a decrease in the quality of the vasculature upregulating

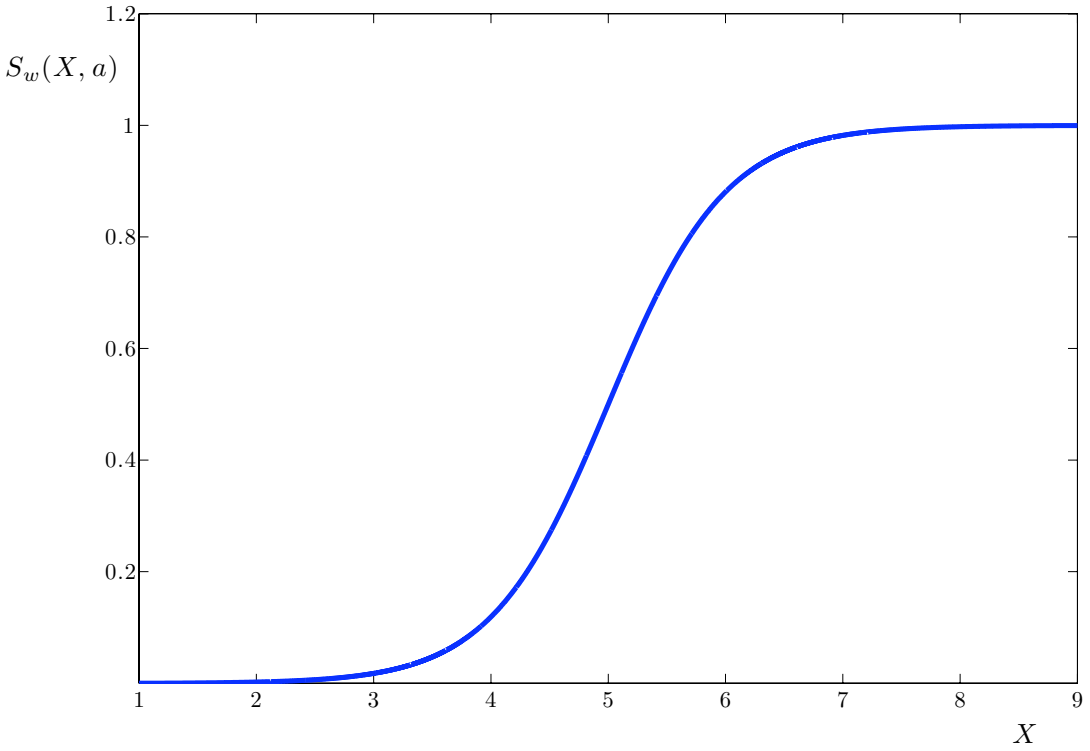

Figure 4.2: The switching function, $S_w(X, a)$, as defined by Equation (4.2), for $w = 1$ and $a = 5$.

necrosis. We also assume that the rate of necrosis is bounded by a maximum rate η, which occurs in the presence of an extremely poor vasculature.

We also assume that proliferating cells can become quiescent at a maximum rate ψ_1, but this maximum rate only occurs in the presence of an extremely poor vasculature and that quiescent cells recover the ability to proliferate at a maximum rate ψ_2, but that this maximum rate only occurs in the presence of an extremely strong vasculature.

Having made these assumptions we find that if P denotes the total volume of proliferating cells in the tumour, including any extracellular space in between the proliferating cells, then

$$\frac{\mathrm{d}P}{\mathrm{d}t} = -\Big\{\mu+\psi_1 S_{w_1}\left(\tfrac{P+Q+E}{E}, \alpha_1\right)+\eta S_{w_2}\left(\tfrac{P+Q+E}{E}, \alpha_2\right)\Big\}P+\psi_2\Big\{1-S_{w_1}\left(\tfrac{P+Q+E}{E}, \alpha_1\right)\Big\}Q, \tag{4.3}$$

where Q, and E are the total volume of quiescent, and endothelial cells respectively in the tumour, including any extracellular space in between the cells, α_1 is the critical

level of vascularisation which determines the net direction of transfer from proliferative cells to quiescent cells, α_2 is the critical level of vascularisation for cell necrosis, and the parameters w_1 and w_2 define the sharpness of the switching functions.

Quiescent Cells

As well as the previously made assumptions we assume that quiescent cells undergo necrosis at the equivalent rate as proliferating cells. Then the evolution of quiescent cells is given by

$$\frac{\mathrm{d}Q}{\mathrm{d}t} = \left\{2\mu+\psi_1 S_{w_1}\left(\tfrac{P+Q+E}{E},\alpha_1\right)\right\}P-\left\{\psi_2\left(1-S_{w_1}\left(\tfrac{P+Q+E}{E},\alpha_1\right)\right)+\eta S_{w_2}\left(\tfrac{P+Q+E}{E},\alpha_2\right)\right\}Q. \tag{4.4}$$

Note that we have assumed that during the M phase of the cell cycle one proliferating cell divides into two daughter cells which are initially quiescent. It is this division of one proliferating cell into two quiescent cells which means that whilst proliferating cells are lost due to mitosis at a rate μP, quiescent cells are gained due to mitosis at a rate $2\mu P$.

Necrotic Cells

As well as the previous assumptions we assume that necrotic cells undergo linear break up at the constant rate ν. Then if N denotes the total volume of necrotic cells in the tumour, including any extra cellularspace in between the necrotic cells, then

$$\frac{\mathrm{d}N}{\mathrm{d}t} = \eta S_{w_2}\left(\tfrac{P+Q+E}{E},\alpha_2\right)(P+Q)-\nu N. \tag{4.5}$$

Endothelial Cells

In our biological review of Section 4.1.1 we found that the principle driver of endothelial cell reproduction is the local VEGF concentration and that VEGF can be considered to act as a mediator in a simple feedback system governing the quality of the local vasculature. Rather than model the local VEGF concentration explicitly we capture this feedback system by assuming that endothelial cell proliferation is promoted by a poor quality vasculature and inhibited by a good quality vasculature.

The tumour should exhibit a sigmoidal growth curve, and culminate with the growth of the tumour saturating. Having assumed that the behaviour of the tumour cells

depends upon the quality of the tumour's vasculature this saturation must be driven by the saturation of the growth of the endothelial cells. Then the evolution of the endothelial cells is given by

$$\frac{\mathrm{d}E}{\mathrm{d}t} = \lambda \log\left(\tfrac{K}{P+Q+N+E}\right) E S_{w_3}\left(\tfrac{P+Q+E}{E}, \alpha_3\right), \tag{4.6}$$

where λ is a Gompertzian growth parameter, K is the carrying capacity of the tumour's host, w_3 measures the sharpness of the VEGF feedback loop, and α_3 is the critical level of vascularisation in the VEGF feedback loop.

This completes our simple model of vascular tumour growth and we now derive some suitable initial conditions.

4.2.3 The Initial Conditions

We are modelling the evolution of a vascular tumour, starting from a tumour undergoing the first stages of vascularisation, and finishing with a tumour at saturation. Our initial tumour should therefore be an avascular tumour which has reached its maximum size as given by diffusion limited control and is about to become vascularised.

During our analysis of parameters in Section 3.5.1 of the previous chapter we found that avascular tumours typically saturate at a radius between 0.5 mm and 2 mm (Haji-Karim and Carisson, 1978; Folkman and Hochberg, 1973) and so we take the initial radius of our tumour to be 1 mm.

For a tumour of this radius the work of Mueller-Klieser (2000) allows us to estimate that the corresponding radius volume of the necrotic population is $N(0) = 1.0\,\mathrm{mm}^3$ (2 s.f.).

In Section 3.4.2 of the previous chapter we found that the mean volume of a proliferating tumour cell is $3 \times 10^{-9}\,\mathrm{cm}^3$, that the cell volume fraction of tissue is approximately 0.66, and that the proliferating rim on the surface of an avascular tumour of radius 1 mm is typically only 2 or 3 cells thick. Given this we estimate that the initial volume of the proliferating population is $P(0) = 0.37\,\mathrm{mm}^3$ (2 s.f.).

Finally, all the cells in our initial avascular tumour will be either proliferative, quiescent or necrotic, so that $Q(0) = 2.8\,\mathrm{mm}^3$ (2 s.f.).

We also require an initial condition for the volume of the endothelial cell population. We are considering a tumour which is initially avascular, but about to undergo vascularisation. This suggests that we should take $E(0) = 0$. However, Equation (4.6), which governs the endothelial cell population, implies that if we take this initial condition then $E(t) \equiv 0$ for all time. It is simple to shown that $E = 0$ is an unstable steady state of our system and so to allow the initiation of vascularisation we take there to initially be one endothelial cell in our tumour, which corresponds to $E(0) = 1.5 \times 10^{-6}\,\mathrm{mm}^3$ (Rubin et al., 1989).

Note that our model ignores both the vasculature outside the tumour and the diffusion of any nutrients across the surface of the tumour. This is expected to be reasonable for even a moderately well vascularised tumour, but our initial tumour is effectively avascular, in which case the diffusion of nutrients across the surface of the tumour is likely to be significant. During the initial vascularisation process this assumption neglecting the diffusion of nutrients into the tumour will not be valid and we do not expect our model to accurately capture the initial onset of angiogenesis. However, we do anticipate that the endothelial cell population in our model will quickly increase and once our tumour has become vascularised our model will become valid.

4.2.4 Non-Dimensionalisation

We now non-dimensionalise our model using the following rescalings (where carets denote dimensionless variables)

$$P(t) = \frac{V_L}{\mathcal{V}}\widehat{P}\big(\widehat{t}\big), \qquad Q(t) = \frac{V_L}{\mathcal{V}}\widehat{Q}\big(\widehat{t}\big), \qquad N(t) = \frac{V_N}{\mathcal{V}}\widehat{N}\big(\widehat{t}\big),$$
$$E(t) = \frac{V_E}{\mathcal{V}}\widehat{E}\big(\widehat{t}\big), \qquad \text{and} \qquad t = \frac{\widehat{t}}{\mu},$$

where V_L is the mean volume of a living tumour cell, V_N the mean volume of a necrotic cell, V_E the mean volume of an endothelial cell, and $\mathcal{V}$ is the mean cell volume fraction. Note that under these rescalings $\widehat{P}$, $\widehat{Q}$, $\widehat{N}$, and $\widehat{E}$ are estimates of the number of proliferating, quiescent, necrotic and endothelial cells respectively in the tumour.

Upon applying these rescalings we find our system, as given by Equations (4.3) to

(4.6), non-dimensionalises to become

$$\frac{\mathrm{d}\widehat{P}}{\mathrm{d}\widehat{t}} = -\Big\{1 + \widehat{\psi}_1\mathcal{S}_1 + \widehat{\eta}\mathcal{S}_2\Big\}\widehat{P} + \widehat{\psi}_2\left(1-\mathcal{S}_1\right)\widehat{Q}, \tag{4.7}$$

$$\frac{\mathrm{d}\widehat{Q}}{\mathrm{d}\widehat{t}} = \Big\{2 + \widehat{\psi}_1\mathcal{S}_1\Big\}\widehat{P} - \Big\{\widehat{\psi}_2\left(1-\mathcal{S}_1\right) + \widehat{\eta}\mathcal{S}_2\Big\}\widehat{Q}, \tag{4.8}$$

$$\frac{\mathrm{d}\widehat{N}}{\mathrm{d}\widehat{t}} = \frac{\widehat{V}_L}{\widehat{V}_N}\widehat{\eta}\mathcal{S}_2(\widehat{P}+\widehat{Q}) - \widehat{\nu}\widehat{N}, \tag{4.9}$$

$$\frac{\mathrm{d}\widehat{E}}{\mathrm{d}\widehat{t}} = \widehat{\lambda}\log\left(\tfrac{\widehat{K}}{\widehat{V}_L(\widehat{P}+\widehat{Q})+\widehat{V}_N\widehat{N}+\widehat{E}}\right)\widehat{E}\mathcal{S}_3, \tag{4.10}$$

where $\mathcal{S}_i = S_{w_i}\left(\frac{\widehat{V}_L(\widehat{P}+\widehat{Q})+\widehat{E}}{\widehat{E}}, \alpha_i\right)$, and

$$\widehat{\psi}_1 = \frac{\psi_1}{\mu}, \qquad \widehat{\psi}_2 = \frac{\psi_2}{\mu}, \qquad \widehat{V}_L = \frac{V_L}{V_E}, \qquad \widehat{V}_N = \frac{V_N}{V_E},$$
$$\widehat{\eta} = \frac{\eta}{\mu}, \qquad \widehat{\nu} = \frac{\nu}{\mu}, \qquad \widehat{\lambda} = \frac{\lambda}{\mu}, \qquad \widehat{K} = \frac{\mathcal{V}K}{V_E}.$$

We can also non-dimensionalise the initial conditions to obtain

$$\begin{aligned} \widehat{P}(0) &= \frac{0.37\,\mathrm{mm}^3\mathcal{V}}{V_L}, & \widehat{Q}(0) &= \frac{2.8\,\mathrm{mm}^3\mathcal{V}}{V_L}, \\ \widehat{N}(0) &= \frac{1\,\mathrm{mm}^3\mathcal{V}}{V_N}, & \widehat{E}(0) &= \frac{1.5\times10^{-6}\,\mathrm{mm}^3\mathcal{V}}{V_E}. \end{aligned} \tag{4.11}$$

Having non-dimensionalised our model we now seek to evaluate the non-dimensional parameters in it. Not all the parameters can be evaluated directly from the literature, and so we will perform analysis to assist in our parameter estimation. Unfortunately, our non-dimensional system consists of a set of four coupled non-linear ordinary differential equations and an analysis on this system is not readily tractable. However, it is possible to make a temporary simplifying assumption to our system which will allow us to perform some analysis which will relate some of the parameters in our model to known biological quantities. We make this temporary simplifying assumption in the next section.

4.3 A Temporary Simplifying Assumption

It is anticipated that in the absence of any therapy the quality of the tumour's vasculature will not alter significantly as the tumour grows. More specifically, it is anticipated

that in the absence of any therapy the rate of cell necrosis, which depends upon the quality of the tumour vasculature, will not alter significantly as the tumour grows. So in the absence of any therapy we now make the temporary simplifying assumption that the non-dimensional rate of cell necrosis is constant and denoted by the parameter $\widetilde{\eta}$. This assumption is validated with an *a posteriori* validation in Section 4.6.1. Then our simplified system is given by

$$\frac{\mathrm{d}\widehat{P}}{\mathrm{d}\widehat{t}} = -\left\{1 + \widehat{\psi}_1 \mathcal{S}_1 + \widetilde{\eta}\right\}\widehat{P} + \widehat{\psi}_2 \left(1 - \mathcal{S}_1\right)\widehat{Q}, \tag{4.12}$$

$$\frac{\mathrm{d}\widehat{Q}}{\mathrm{d}\widehat{t}} = \left\{2 + \widehat{\psi}_1 \mathcal{S}_1\right\}\widehat{P} - \left\{\widehat{\psi}_2 \left(1 - \mathcal{S}_1\right) + \widetilde{\eta}\right\}\widehat{Q}, \tag{4.13}$$

$$\frac{\mathrm{d}\widehat{N}}{\mathrm{d}\widehat{t}} = \frac{\widehat{V}_L}{\widehat{V}_N}\widetilde{\eta}\left(\widehat{P} + \widehat{Q}\right) - \widehat{\nu}\widehat{N}, \tag{4.14}$$

$$\frac{\mathrm{d}\widehat{E}}{\mathrm{d}\widehat{t}} = \widehat{\lambda}\log\left(\frac{\widehat{K}}{\widehat{V}_L(\widehat{P}+\widehat{Q})+\widehat{V}_N\widehat{N}+\widehat{E}}\right)\widehat{E}\mathcal{S}_3. \tag{4.15}$$

where $\mathcal{S}_i = S_{w_i}\left(\frac{\widehat{V}_L(\widehat{P}+\widehat{Q})+\widehat{E}}{\widehat{E}}, \alpha_i\right)$.

Note that for ease of reference we will refer to the tumour modelled by this simplified system as the simplified tumour.

4.4 Parameter Estimation

Having temporarily simplified our system we now perform an asymptotic analysis to relate some of the non-dimensional parameters in our simplified model to the tumour's growth and necrotic fractions.

4.4.1 An Asymptotic Analysis

We begin our asymptotic analysis by considering the existence of a small parameter, which stems from the time scales of our system.

The Cellular and Tumoural Time Scales

We have non-dimensionalised our system with respect to the mean cumulative time for the S, G_2, and M phases of the cell cycle time which is typically of the order of a few days (Rew and Wilson, 2000). However, the mean doubling time of a tumour is

typically of the order of a few months (Perry, 2007). This suggests that there are two time scales in our system, one being the cellular time scale for the mitosis and necrosis of individual cells, and the other being the tumoural time scale for the net growth of the entire tumour. We have non-dimensionalised with respect to the cellular time scale, and we now consider when the cellular time scale will be the relevant time scale of our system, and when the tumoural time scale is the relevant time scale of our system.

In our initial conditions we took there to initially be only one endothelial cell in the tumour, which represents an extremely under-vascularised tumour. As such our tumour will initially be starved of oxygen, and other nutrients, so that the tumour cells should undergo necrosis on the cellular time scale, and angiogenesis should up-regulate endothelial cell proliferation to occur also on the cellular time scale. We therefore anticipate that our system will undergo an initial normalisation period where the tumour regresses and/or angiogenesis takes place on the cellular time scale until it becomes well vascularised. Any such normalisation will be an artefact of our initial conditions and is not expected to accurately model the onset of tumour angiogenesis.

During this initial normalisation period we anticipate that the tumour will relax to an adequately vascularised state, and following this normalisation period we anticipate that the birth and death of individual tumour cells will approximately balance so that the tumour will then evolve on the slower, tumoural time scale. Furthermore, with the tumour more adequately vascularised it is expected that angiogenesis will be less extremely up-regulated so that endothelial cells also evolve on the tumoural time scale.

We have non-dimensionalised our model with respect to the cellular time scale (for ease of parameter estimation) but it is anticipated that the tumoural time scale will be the relevant time scale of our system. So we now introduce a new non-dimensional time variable, $\widehat{\tau}$, which has been non-dimensionalised with respect to the mean tumour doubling time as defined by

$$t = T_d \widehat{\tau},$$

where T_d is the mean doubling time of the tumour. Then our non-dimensional time variables are related thus

$$\frac{1}{\mu T_d} \widehat{t} = \widehat{\tau},$$

and the fact that the mean cell cycle time of individual cells is much shorter than the mean doubling time of the tumour implies that

$$\varepsilon\widehat{t} = \widehat{\tau} \qquad \text{where} \quad \varepsilon \ll 1.$$

Approximating The Growth Fraction

To relate the non-dimensional parameters in our simplified system to the simplified tumour's growth fraction, which is the ratio of the number of proliferating cells to the total number of live tumour cells (Mendelsohn, 1960), we first add the non-dimensional equation governing the proliferating cell population, Equation (4.12), to the non-dimensional equation governing the quiescent cell population, Equation (4.13), to obtain an equation for the total live cell population in the simplified tumour

$$\frac{\mathrm{d}}{\mathrm{d}\widehat{t}}\left(\widehat{P}+\widehat{Q}\right) = \widehat{P} - \widetilde{\eta}\left(\widehat{P}+\widehat{Q}\right). \tag{4.16}$$

This can be rescaled to give the following equation governing the live tumour cell population which has been non-dimensionalised with respect to the tumoural time scale:

$$\varepsilon\frac{\mathrm{d}}{\mathrm{d}\widehat{\tau}}\left(\widetilde{P}\left(\widehat{\tau}\right)+\widetilde{Q}\left(\widehat{\tau}\right)\right) = \widetilde{P}\left(\widehat{\tau}\right) - \widetilde{\eta}\left(\widetilde{P}\left(\widehat{\tau}\right)+\widetilde{Q}\left(\widehat{\tau}\right)\right), \tag{4.17}$$

where $$\widetilde{P}\left(\widehat{\tau}\right) = \widehat{P}\left(\tfrac{\widehat{\tau}}{\varepsilon}\right), \qquad \text{and} \qquad \widetilde{Q}\left(\widehat{\tau}\right) = \widehat{Q}\left(\tfrac{\widehat{\tau}}{\varepsilon}\right).$$

So during any initial relaxation period where the system evolves on the cellular time scale, Equation (4.16) is the appropriate equation governing the evolution of live tumour cells, otherwise the system evolves on the tumoural time scale and Equation (4.17) is the appropriate governing equation for the population of live tumour cells, in which case our model contains a small parameter.

To exploit this small parameter we consider the behaviour of the total live cell population over the tumoural time scale, as governed by Equation(4.17), in more detail. Manipulating and integrating this equation gives

$$\widetilde{P}(\widehat{\tau})+\widetilde{Q}(\widehat{\tau}) = \frac{1}{\varepsilon}\int_0^{\widehat{\tau}} \widetilde{P}\left(\widehat{\tau}-s\right)e^{-\frac{\widetilde{\eta}s}{\varepsilon}}\,\mathrm{d}s + \left(\widetilde{P}(0)+\widetilde{Q}(0)\right)e^{-\frac{\widetilde{\eta}\widehat{\tau}}{\varepsilon}}. \tag{4.18}$$

We can use Watson's Lemma (Bender and Orzag, 1978) to obtain the following asymptotic expansion for the integral in this equation:

$$\int_0^{\widehat{\tau}} \widetilde{P}\left(\widehat{\tau}-s\right)e^{-\frac{\widetilde{\eta}s}{\varepsilon}}\,\mathrm{d}s \sim -\sum_{n=0}^{\infty}\left(-\frac{\varepsilon}{\widetilde{\eta}}\right)^{n+1}\frac{\mathrm{d}^n\widetilde{P}\left(\widehat{\tau}\right)}{\mathrm{d}\widehat{\tau}^n} \qquad \text{as} \qquad \varepsilon\to 0,$$

Upon substituting this asymptotic expansion into Equation (4.18) we obtain the following asymptotic expansion for the total live cell population:

$$\widetilde{P}(\widehat{\tau}) + \widetilde{Q}(\widehat{\tau}) \sim \frac{1}{\widetilde{\eta}} \sum_{n=0}^{\infty} \left(-\frac{\varepsilon}{\widetilde{\eta}} \right)^n \frac{\mathrm{d}^n \widetilde{P}(\widehat{\tau})}{\mathrm{d}\widehat{\tau}^n} + \left(\widetilde{P}(0) + \widetilde{Q}(0) \right) e^{-\frac{\widetilde{\eta}\widehat{\tau}}{\varepsilon}} \quad \text{as} \quad \varepsilon \to 0. \tag{4.19}$$

Assuming that the right hand most term in Equation (4.19) can be taken to be exponentially small we then obtain the following leading order and second order approximations for the number of live cells in the tumour.

$$\widetilde{P} + \widetilde{Q} \approx \frac{1}{\widetilde{\eta}} \widetilde{P}, \tag{4.20}$$

$$\widetilde{P} + \widetilde{Q} \approx \frac{1}{\widetilde{\eta}} \widetilde{P} - \frac{\varepsilon}{\widetilde{\eta}^2} \frac{\mathrm{d}\widetilde{P}}{\mathrm{d}\widehat{\tau}}. \tag{4.21}$$

These approximations can then be manipulated to give the corresponding leading order and second order approximations to the tumour's growth fraction, which are

$$\frac{\widetilde{P}}{\widetilde{P} + \widetilde{Q}} \approx \widetilde{\eta}, \tag{4.22}$$

$$\frac{\widetilde{P}}{\widetilde{P} + \widetilde{Q}} \approx \widetilde{\eta} + \frac{\varepsilon}{\widetilde{\eta}} \frac{\dfrac{\mathrm{d}\widetilde{P}}{\mathrm{d}\widehat{\tau}}}{\widehat{P} + \widehat{Q}}. \tag{4.23}$$

These approximations are valid when the tumour evolves over the time scale of the doubling rate of the tumour, in which case $\widehat{\tau}$ is the fundamental time scale of the problem. They can also be re-scaled and expressed in terms of $\widehat{t}$, the non-dimensional time variable of our model which has been non-dimensionalised with respect to the doubling rate of the tumour. However the approximations will still only be valid when the tumour is evolving on the tumoural time scale, even though the approximations are being expressed in terms of the cellular time scale. Doing this gives the following leading order approximation to the tumour's growth fraction:

$$\frac{\widehat{P}}{\widehat{P} + \widehat{Q}} \approx \widetilde{\eta}, \tag{4.24}$$

and the following second order approximation to the tumour's growth fraction:

$$\frac{\widehat{P}}{\widehat{P} + \widehat{Q}} \approx \widetilde{\eta} + \frac{1}{\widetilde{\eta}} \frac{\dfrac{\mathrm{d}\widehat{P}}{\mathrm{d}\widehat{t}}}{\widehat{P} + \widehat{Q}}. \tag{4.25}$$

So to leading order the growth fraction is constant and equal to the parameter $\widetilde{\eta}$, which is the non-dimensional cell necrosis rate in our simplified tumour. We have also derived the second order asymptotic expansion for the growth fraction. This second order approximation might not offer much insight beyond that afforded by the first order approximation, but we will use it in Section 4.5 to test the validity of our asymptotic expansion.

Approximating The Necrotic Fraction

We now apply a similar argument to find an asymptotic expansion for the necrotic fraction, which is the ratio of the total volume of necrotic cells in the tumour to the total volume of the tumour (Khalil et al., 1995). To do this we consider the equation for the evolution of the necrotic cell population in the simplified tumour, Equation (4.14), but rescaled to be non-dimensionalised with respect to the tumoural time scale

$$\varepsilon \frac{\mathrm{d}}{\mathrm{d}\widehat{\tau}}\left(\widetilde{N}(\widehat{\tau})\right) = \frac{\widehat{V}_L}{\widehat{V}_N}\widetilde{\eta}\left(\widetilde{P}(\widehat{\tau}) + \widetilde{Q}(\widehat{\tau})\right) - \widehat{\nu}\widetilde{N}(\widehat{\tau}),$$

where $$\widetilde{N}\left(\widehat{\tau}\right) = \widehat{N}\left(\tfrac{\widehat{\tau}}{\varepsilon}\right).$$

As before this can be manipulated and integrated to yield

$$\widetilde{N}\left(\widehat{\tau}\right) = \frac{\widehat{V}_L}{\widehat{V}_N}\frac{\widetilde{\eta}}{\varepsilon}\int_0^{\widehat{\tau}}\left(\widetilde{P}\left(\widehat{\tau}-s\right) + \widetilde{Q}\left(\widehat{\tau}-s\right)\right)e^{-\frac{\widehat{\nu}s}{\varepsilon}}\,\mathrm{d}s + \widetilde{N}(0)e^{-\frac{\widehat{\nu}\widehat{\tau}}{\varepsilon}},$$

and as before we apply Watson's Lemma to the integral in this equation to obtain the following asymptotic expansion for the necrotic cell population:

$$\widetilde{N}\big(\widehat{\tau}\,\big) \sim \frac{\widehat{V}_L}{\widehat{V}_N}\frac{\widetilde{\eta}}{\widehat{\nu}}\sum_{n=0}^{\infty}\left(-\frac{\varepsilon}{\widehat{\nu}}\right)^n\left(\frac{\mathrm{d}^n\widetilde{P}\big(\widehat{\tau}\,\big)}{\mathrm{d}\widehat{\tau}^n} + \frac{\mathrm{d}^n\widetilde{Q}\big(\widehat{\tau}\,\big)}{\mathrm{d}\widehat{\tau}^n}\right) + \widehat{N}(0)e^{-\widehat{\nu}\widehat{t}}.$$

Assuming that the right hand most term in this equation is exponentially small then as before we can obtain the leading order and second order approximations for the number of necrotic cells in the tumour (equations not presented), and as before these can be manipulated to give the following first and second order approximations to the tumour's necrotic fraction, which are

$$\frac{\widehat{V}_N\widetilde{N}}{\widehat{V}_L\left(\widetilde{P}+\widetilde{Q}\right)+\widehat{V}_N\widetilde{N}} \approx \frac{\widetilde{\eta}}{\widehat{\nu}+\widetilde{\eta}}, \tag{4.26}$$

$$\frac{\widehat{V}_N\widetilde{N}}{\widehat{V}_L\left(\widetilde{P}+\widetilde{Q}\right)+\widehat{V}_N\widetilde{N}} \approx \frac{\widetilde{\eta}}{\widehat{\nu}+\widetilde{\eta}} - \frac{\widetilde{\eta}\varepsilon}{(\widehat{\nu}+\widetilde{\eta})\widehat{\nu}}\left\{\frac{\dfrac{\mathrm{d}^n\widetilde{P}}{\mathrm{d}\widehat{\tau}^n}+\dfrac{\mathrm{d}^n\widetilde{Q}}{\mathrm{d}\widehat{\tau}^n}}{\widetilde{P}+\widetilde{Q}+\frac{\widehat{V}_N}{\widehat{V}_L}\widetilde{N}}\right\}, \tag{4.27}$$

These approximations are valid when the tumour evolves over the time scale of the doubling rate of the tumour, but as with the approximations to the tumour's growth fractions they can also expressed in terms of $\widehat{t}$. However the approximations will still only be valid when the tumour is evolving on the tumoural time scale, even though the approximations are being expressed in terms of the cellular time scale. Doing this gives the following leading order approximation to the tumour's necrotic fraction:

$$\frac{\widehat{V}_N\widehat{N}}{\widehat{V}_L\left(\widehat{P}+\widehat{Q}\right)+\widehat{V}_N\widehat{N}} \approx \frac{\widetilde{\eta}}{\widehat{\nu}+\widetilde{\eta}}, \tag{4.28}$$

$$\frac{\widehat{V}_N\widehat{N}}{\widehat{V}_L\left(\widehat{P}+\widehat{Q}\right)+\widehat{V}_N\widehat{N}} \approx \frac{\widetilde{\eta}}{\widehat{\nu}+\widetilde{\eta}} - \frac{\widetilde{\eta}}{(\widehat{\nu}+\widetilde{\eta})\widehat{\nu}}\left\{\frac{\widehat{P}-\widetilde{\eta}(\widehat{P}+\widehat{Q})}{\widehat{P}+\widehat{Q}+\frac{\widehat{V}_N}{\widehat{V}_L}\widehat{N}}\right\}, \tag{4.29}$$

where we have used Equations (4.12) and (4.13) to replace the time derivatives in the second order approximation with a function of the different cell compartments.

As with the growth fraction, to leading order the necrotic fraction is constant and determined by the parameters $\widehat{\nu}$ and $\widetilde{\eta}$. So given an estimate for the tumour's necrotic fraction, Equation (4.28) gives a leading order relationship between these two parameters. We have also derived the second order asymptotic expansion to the necrotic fraction, which might not offer much insight beyond that afforded by the first order approximation, but we will use it in Section 4.5 to test the validity of our asymptotic expansion.

4.4.2 The Steady States

We now gather some information regarding parameter values by considering the steady states of our simplified model. We are only interested in tumours which have the potential to grow to a lethal size if left untreated; for some parameter values the tumour will naturally die out and such parameter values are uninteresting for our purposes. Furthermore, we wish to consider tumours which exhibit a sigmoidal growth curve. Hence our system must exhibit at least one non-trivial stable steady state and the approach to this steady state should be monotonic.

It is simple to show that our simplified system has at most two classes of non-zero steady states. The first non-zero steady state is

$$\left(\widehat{P},\widehat{Q},\widehat{N},\widehat{E}\right) = \left(0,0,0,E^{\dagger}\right), \quad \text{for any} \quad E^{\dagger}>0,$$

which corresponds to the tissue consisting only of endothelial cells. Despite being non-zero, this steady state is trivial and will not be considered further. The non-trivial steady state is

$$\left(\widehat{P},\widehat{Q},\widehat{N},\widehat{E}\right)=\left(P^*,\left(\tfrac{1-\widetilde{\eta}}{\widetilde{\eta}}\right)P^*,\tfrac{\widehat{V}_L}{\widehat{V}_N}\tfrac{1}{\widehat{\nu}}P^*,E^*\right),$$

which exists when the simultaneous equations

$$-\left(1+\widetilde{\eta}\right)-\widehat{\psi}_1 S_{w_1}\left(\tfrac{\frac{\widehat{V}_L}{\widetilde{\eta}}P^*+E^*}{E^*},\alpha_1\right)+\widehat{\psi}_2\left(1-S_{w_1}\left(\tfrac{\frac{\widehat{V}_L}{\widetilde{\eta}}P^*+E^*}{E^*},\alpha_1\right)\right)\left(\frac{1-\widetilde{\eta}}{\widetilde{\eta}}\right)=0,$$

$$\widehat{V}_L\left(\frac{\widetilde{\eta}+\widehat{\nu}}{\widetilde{\eta}\widehat{\nu}}\right)P^*+E^*=\widehat{K},$$

have positive solutions for P^* and E^*.

It is not possible to write the solution to these simultaneous equations in simple closed form, but it can be shown that necessary, but not sufficient, conditions for this non-trivial steady state to exist are

$$1\geq\widetilde{\eta},\qquad\text{and}\qquad\widehat{\psi}_2\geq\frac{\widetilde{\eta}+\widetilde{\eta}^2}{1-\widetilde{\eta}},\tag{4.30}$$

and when the non-trivial steady state exists is it unique. These conditions imply that for a non-trivial tumour to be viable the rate of necrosis must be less than the rate of proliferation and that quiescent cells must potentially recover the ability to proliferate at a rate quicker than some critical rate determined by the rate of necrosis.

Unfortunately finding sufficient conditions for the existence of the non-trivial steady state and determining an explicit criterion for the steady state to be stable is non-trivial. So rather than having explicit bounds on the parameters which ensure that the non-trivial steady state exists and is a stable node we will only consider parameter values which satisfy Condition (4.30) and then manually verify that our tumour saturates at a non-trivial steady state and that the growth of the tumour is monotonic.

Having performed some analysis on our simplified system, which has allowed us to relate some of the non-dimensional parameters in our model to more widely known biological quantities, and derived some necessary but not sufficient conditions for the existence of a steady state we now evaluate some of the non-dimensional parameters by reviewing the literature.

4.4.3 Parameters In the Literature

We begin by recalling the cell volumes and the cell volume fraction which were previously found in Section 4.2.3. Combining these with an estimate of the volume of necrotic cells in a tumour (Landry et al., 1981, 1982) we obtain

$$V_L = 3 \times 10^{-6}\,\mathrm{mm}^3, \quad V_N = 1.5 \times 10^{-6}\,\mathrm{mm}^3, \quad V_E = 10^{-6}\,\mathrm{mm}^3, \quad \text{and} \quad \mathcal{V} = 0.66,$$

which allows us to evaluate the non-dimensionalised initial conditions, as given by Equations (4.11), to obtain

$$\widehat{P}(0) = 82,000, \qquad \widehat{Q}(0) = 620,000, \qquad \widehat{N}(0) = 440,000, \qquad \widehat{E}(0) = 1,$$

and evaluate the following non-dimensional parameters

$$\widehat{V}_L = 3, \qquad \text{and} \qquad \widehat{V}_N = 1.5.$$

We now use our asymptotic analysis of Section 4.4.1 to evaluate the non-dimensional rate of necrosis, $\widetilde{\eta}$, and the decay rate of necrotic cells, $\widehat{\nu}$. We begin by considering the tumour growth fraction. The growth fraction of a tumour can vary considerably from tumour to tumour and a growth fraction of ten percent is considered low and growth fractions of thirty to sixty percent are considered high (McKinell et al., 1998). It is conceivable that tumours with different growth fractions will respond differently to different therapy schedules and so it is desirable to be able to consider a range of growth fractions. In particular we will choose parameter values for a tumour with a low growth fraction, which we take to be 10%, a mid growth fraction, which we take to be 25%, and a high growth fraction, which we take to be 40%. Then our previous leading order asymptotic approximation of the growth fraction, Approximation (4.24), implies that we should consider three different values for the non-dimensional simplified rate of necrosis respectively, namely

$$\widetilde{\eta} = 0.1, \qquad \widetilde{\eta} = 0.25, \qquad \text{and} \qquad \widetilde{\eta} = 0.4.$$

We relate this to the non-dimensional rate of decay of the necrotic cells, $\widehat{\nu}$, using the leading order asymptotic approximation to the necrotic fraction, Approximation (4.28). Here we consider a tumour with a necrotic fraction of 25%, which is typical for an *in vivo* tumour (Khalil et al., 1995), so that

$$\frac{\widetilde{\eta}}{\widehat{\nu} + \widetilde{\eta}} = 0.25, \qquad \Longrightarrow \qquad \widehat{\nu} = 3\widetilde{\eta}.$$

So having taken $\widetilde{\eta} = 0.1$, $\widetilde{\eta} = 0.25$, and $\widetilde{\eta} = 0.4$, we must also take $\widehat{\nu} = 0.3$, $\widehat{\nu} = 0.75$, and $\widehat{\nu} = 1.2$ accordingly.

We now recall the necessary condition for the existence of the non-trivial steady state, given by Condition (4.30). This criterion gives a bound for the non-dimensional maximum rate at which quiescent cells become proliferative, $\widehat{\psi}_2$, for each value of the non-dimensional necrosis rate, $\widetilde{\eta}$, and we find that for

$$\widetilde{\eta} = 0.1, \qquad \widetilde{\eta} = 0.25, \qquad \text{and} \qquad \widetilde{\eta} = 0.4,$$

the respective bounds on $\widehat{\psi}_2$ (to 3 s.f.) are

$$\widehat{\psi}_2 \geq 0.122, \qquad \widehat{\psi}_2 \geq 0.417, \qquad \text{and} \qquad \widehat{\psi}_2 \geq 0.933. \tag{4.31}$$

We can redimensionalise these bounds on $\widehat{\psi}_2$ to obtain bounds for the corresponding dimensional cell cycle time, but first we must estimate the value of the dimensional cell proliferation rate μ.

Consider our dimensional model applied to a tumour dividing optimally in the presence of an extremely good vasculature. Under these conditions the $S_{w_1}\left(\frac{P+Q+E}{E}, \alpha_1\right)$ switching function will be small and can be neglected. In this situation a proliferating cell gives birth to two quiescent cells in a mean time T_1 and these quiescent cells become proliferative in a mean time T_2, where T_1 and T_2 can be related to the dimensional cell proliferation rate, μ, and the dimensional maximum rate at which quiescent cells become proliferative, ψ_2, as follows

$$\mu = \frac{\log 2}{T_1}, \qquad \text{and} \qquad \psi_2 = \frac{\log 2}{T_2}.$$

T_1 corresponds to the mean cumulative time for the S, G_2 and M phase of the cell cycle. The duration of each of these phases of the cell cycle has been recorded, are roughly invariant, and cumulatively take approximately 11 hours (Murray and Hunt, 1994; Andreef et al., 2000). From this we find that $\mu = 0.0630$ hour^{-1} (3 s.f.) and that we have non-dimensionalised time with respect to $T = \frac{1}{\mu} = 15.9$ hours (3 s.f.).

With the cellular time scale of our system evaluated we can re-dimensionalise the bounds on the maximum rate at which quiescent cells become proliferative, as given by Condition (4.31), to find that these bounds correspond to the total cell cycle time being less than 101 hours, 37 hours, and 23 hours respectively to the nearest hour. The total cell cycle time is typically of the order of a couple of days with the cell cycles as short as 18 hours observed (Rew and Wilson, 2000). Hence the cell cycle

times required to satisfy Condition (4.31) are all consistent with observed cell cycle times.

We now estimate the non-dimensional carrying capacity of our tumour's host, $\widehat{K}$. Previous applications of Gompertzian models have estimated the carrying capacity and estimates of the order of 3×10^{12} cells are typical (Norton, 1988; Yorke et al., 1993). However these models were single compartment models and did not consider the fact that vascular tumours consist of a mix of cell types and that these different cell types can have different mean volumes. If we assume that the proliferative cells, quiescent cells, and necrotic cells form the bulk of the tumour volume then for our tumour with a necrotic fraction of 25% we can estimate that $\widehat{K} = 7.2 \times 10^{12}$, as outlined in Appendix B.2.

We now use the cell cycle times of endothelial cells to estimate the magnitude of the Gompertzian growth parameter $\widehat{\lambda}$. Ishiwata et al. (1990) studied the doubling rates of endothelial cells for different concentrations of tumour angiogenesis factor (TAF) and found that for high concentrations of TAF the doubling time of the endothelial cells was approximately 60 hours, which corresponds to an exponential growth rate of $\frac{\log 2}{60}$ hours^{-1} and a non-dimensional exponential growth rate of 0.184 (3 s.f.). We relate this experimental exponential growth rate to the parameters in our model by calculating the exponential growth rate of our modelled endothelial cells in the presence of high TAF concentrations.

The evolution of endothelial cells in our simplified model is governed by Equation (4.15). In the presence of high concentrations of TAF, which corresponds to a situation where the tumour is heavily under-vascularised, the switching function in Equation (4.15) will be close to unity and the endothelial cell population will be approximately governed by

$$\frac{\mathrm{d}\widehat{E}}{\mathrm{d}\widehat{t}} = \widehat{\lambda} \log\left(\frac{\widehat{K}}{\widehat{V}_L(\widehat{P}+\widehat{Q})+\widehat{V}_N\widehat{N}+\widehat{E}}\right)\widehat{E}.$$

In this case the endothelial cells in our model will undergo an initial period of approximately exponential growth at the non-dimensional exponential growth rate

$$\widehat{\lambda} \log\left(\frac{\widehat{K}}{\widehat{V}_L(\widehat{P}(0)+\widehat{Q}(0))+\widehat{V}_N\widehat{N}(0)+\widehat{E}(0)}\right).$$

Comparing this to the doubling time observed by Ishiwata et al. (1990) we can esti-

mate the value of $\widehat{\lambda}$ to be

$$\begin{aligned}\widehat{\lambda} &\approx \frac{0.184}{\log\left(\frac{\widehat{K}}{\widehat{V}_L(\widehat{P}(0)+\widehat{Q}(0))+\widehat{V}_N\widehat{N}(0)+\widehat{E}(0)}\right)}, \\ &= 0.0124 \quad (3 \text{ s.f.}).\end{aligned} \tag{4.32}$$

However we have had to make some assumptions in deriving this expression for the Gompertzian growth parameter $\widehat{\lambda}$. In particular, if the switching function in Equation (4.15) is slightly less than one then we will have underestimated the value of $\widehat{\lambda}$. Hence we expect that the Estimate (4.32) will give the likely magnitude of $\widehat{\lambda}$, but that the appropriate value may actually be slightly larger than this estimate.

Having evaluated all the non-dimensional parameters we can from the literature, we will now perform an analysis of parameters to estimate the values of the yet undetermined parameters in our simplified system, namely

$$\psi_1, \quad \psi_2, \quad \alpha_1, \quad \alpha_3, \quad \lambda, \quad w_1, \quad w_3.$$

4.4.4 Analysis of Parameters

To perform our analysis of parameters we make an initial estimate of the remaining parameters, and then varying each parameter in turn to investigate to which parameters the tumour is most sensitive and which aspect of tumour growth is affected by each parameter. We will then refine our estimation of parameters by a sequence of trial and improvement until our modelled tumour growth is consistent with observed tumour growth. However, there are no recorded growth curves for untreated *in vivo* human tumours from vascularisation to saturation and it is expected that the growth curves of animal tumours and *in vitro* tumours will only give us qualitative, but not quantitative, information about the desired behaviour of our simplified model. Hence we can only chose parameters to ensure that our simplified tumour exhibits a sigmoidal growth curve and that the tumour growth takes several years to saturate (Yorke et al., 1993).

To perform this analysis of parameters we must first be able to simulate the evolution of the tumour for a given set of parameter values. We now recap the non-dimensional simplified model and consider how to simulate its evolution.

The Non-Dimensional Simplified Model

We now drop carets in our non-dimensional simplified model to obtain

$$\frac{\mathrm{d}P}{\mathrm{d}t} = -\left\{1 + \psi_1 \mathcal{S}_1 + \widetilde{\eta}\right\} P + \psi_2 \left(1 - \mathcal{S}_1\right), \tag{4.33}$$

$$\frac{\mathrm{d}Q}{\mathrm{d}t} = \left\{2 + \psi_1 \mathcal{S}_1\right\} P - \left\{\psi_2 \left(1 - \mathcal{S}_1\right) + \widetilde{\eta}\right\} Q, \tag{4.34}$$

$$\frac{\mathrm{d}N}{\mathrm{d}t} = 2\widetilde{\eta}(P + Q) - \nu N, \tag{4.35}$$

$$\frac{\mathrm{d}E}{\mathrm{d}t} = \lambda \log\left(\tfrac{K}{3(P+Q)+1.5N+E}\right) E\mathcal{S}_3, \tag{4.36}$$

where $\mathcal{S}_i = S_{w_i}\left(\frac{3(P+Q)+E}{E}, \alpha_i\right)$, with the initial conditions

$$P(0) = 82,000, \qquad Q(0) = 620,000, \qquad N(0) = 440,000, \qquad E(0) = 1. \tag{4.37}$$

Simulating the Tumour Growth

To simulate the evolution of our simplified tumour we must first recall that our switching function is given by Equation (4.2), it is then simple to simulate the evolution of Equations (4.33) to (4.36) using a standard quadrature method. Recalling that in Section 4.4.1 we asserted that our system should exhibit two distinct time scales, the cellular time scale and the tumoural time scale, we simulate our system using an adaptive linear multistep method where the adaptive time stepping has been optimised for stiff systems.

The Analysis

We now perform our analysis of parameters whereby we vary each yet unchosen parameter in turn to determine to which parameters the tumour is most sensitive, and which aspects of tumour growth each parameter affects.

Doing this we find that w_3, which controls the sensitivity of the angiogenic switch, has a particularly significant effect on the tumour. If w_3 is taken to be too small then the growth of the tumour is not monotonic and instead the tumour volume overshoots its maximum size and then oscillates around the carrying capacity of the tumour. However, if w_3 is taken to be too large then the tumour cannot grow to a significant

size and instead dies out. As a compromise between these effects we find that we should take $w_3 = 1$ for each of the tumours of different growth fraction.

We also find that w_1, which controls the sensitivity of the switch in the transfer rate between the proliferating and quiescent compartments, has only a slight effect on the tumour. In particular it has only a slight effect on the time it takes the tumour to reach saturation. We expect that the transfer of cells between the proliferating and quiescent compartments and the angiogenic switch will both be significant, so we choose w_1 to be of a similar magnitude to w_3, but this choice is not unique.

The critical levels of vasculature for the transfer between proliferating and quiescent states, α_1, and angiogenesis, α_3, both have a significant effect on the tumour. Taking either of these parameters to be too small we find that the tumour does not grow and instead dies out and taking either of these parameters to be too large causes the tumour to grow unrealistically quickly and be prone to oscillations rather than monotonic growth. We also assume that the transfer between proliferating and quiescent states and angiogenesis will both be significant so that α_1 and α_3 should be of a similar magnitude. As a compromise between all these affects we take $\alpha_1 = \alpha_3 = 10$ for each tumour of different growth fraction.

Note that we have taken the same values of α_1, α_3, w_1, and w_3 for each tumour of different growth fraction, whereas we alter the values of ψ_1, ψ_2 and λ for each tumour of different growth fraction.

To estimate ψ_2, which is the rate at which quiescent cells can become proliferative, we recall Condition (4.30), which is a necessary condition for a non-trivial steady state to exist. If ψ_2 is close to the lower bound in this condition then the tumour dies out rather than becoming established. However, if ψ_2 is taken to be too large then the corresponding dimensional cell cycle time becomes unrealistically short. So for each different growth fraction we choose ψ_2 as a compromise between these effects.

Finally we must choose the parameters ψ_1, which is the rate at which proliferating cells become quiescent, and λ, which is a Gompertzian growth parameter. These parameters both affect the time it takes the tumour growth to saturate. In Section 4.4.3 we estimated the expected magnitude of λ and we anticipate that the transfer of proliferating cells to a quiescent state and the transfer of quiescent cells to a proliferating state will both be significant, so that ψ_1 and ψ_2 will be of similar magnitudes. We therefore choose λ and ψ_2 as a balance between these effects and so that the resulting tumour also exhibits a realistic time to saturation.

Our analysis of parameters then leads us to the parameter values given in Table 4.1. For these parameter values the growth curves of the different growth fraction tumours are shown in Figure 4.3 and the evolution of each of the cell compartments for the different growth fraction tumours are shown in Figure 4.4. In Figure 4.3 it can be seen that as required the growth curve for each tumour is sigmoidal, with saturation occurring just under three years after vascularisation. In Figure 4.4 it can be seen that each of the cell compartments in the tumours also follows a sigmoidal growth curve with the same time to saturation as the entire tumour.

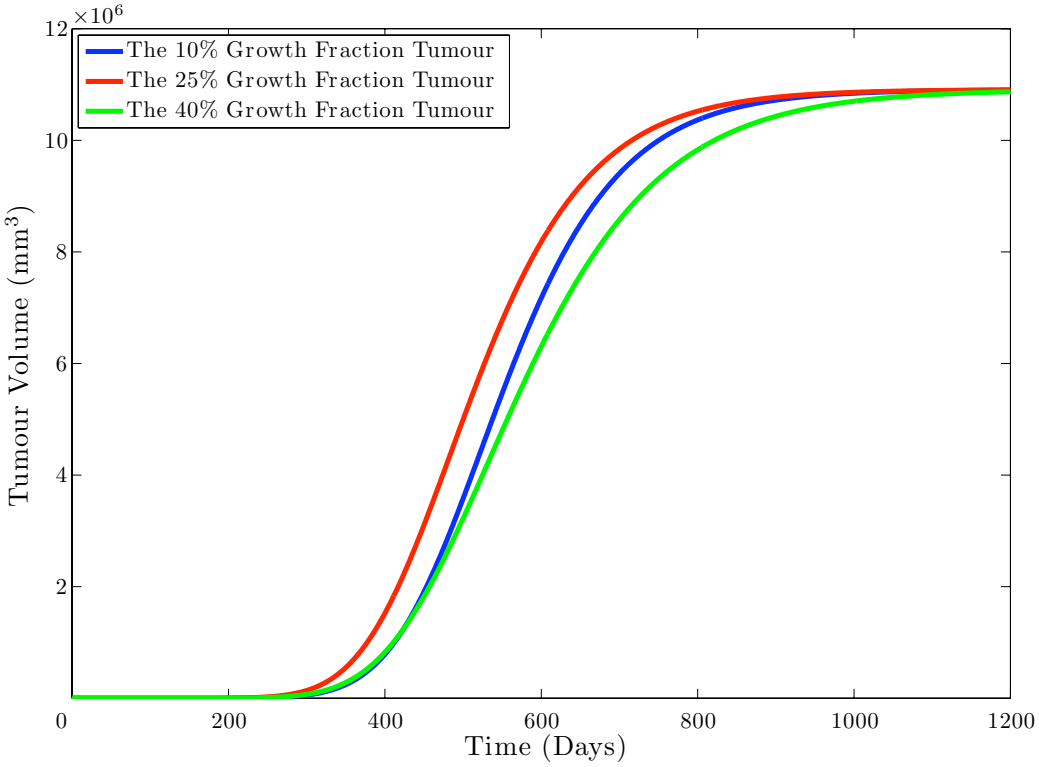

Figure 4.3: The growth curves of our simplified tumours for the parameter values outlined in Table 4.1, as governed by Equations (4.33) to (4.36).

During the analysis of parameters we also simulated the growth of the tumour with different initial conditions but the same parameter values (results not shown). This allowed us to investigate how sensitive our model is to changes in the initial conditions. It was found that the system is very robust to changes in the initial conditions. So whilst our initial conditions derived in Section 4.2.3, and the ensuing initial vascularisation of our model, are unlikely to represent actual tumour growth, the long time dynamics of our tumour are largely independent of the initial conditions. So

Parameter	Description	Value			Reference
		10% G.F.	25% G.F.	40% G.F.	
w_1	The sensitivity of the switch between P and Q	1	1	1	Analysis of parameters
w_3	The sensitivity of the angiogenic switch	1	1	1	Analysis of parameters
α_1	Critical level of vasculature for the switch between P and Q	10	10	10	Analysis of parameters
α_3	Critical level of vasculature for the angiogenic switch	10	10	10	Analysis of parameters
$\widetilde{\eta}$	Rate of necrosis of live cells	0.1	0.25	0.4	See text
ν	Necrotic cell decay rate	0.3	0.75	1.2	See text
ψ_1	The maximum rate of transfer from P to Q	0.2	0.6	1.35	Analysis of parameters
ψ_2	The maximum rate of transfer from Q to P	0.2	0.6	1.35	See text
K	Tumour carrying capacity	7.2×10^{12}	7.2×10^{12}	7.2×10^{12}	See text
λ	Gompertzian parameter of endothelial cell growth	0.02	0.03	0.03	See text

Table 4.1: The non-dimensional parameters taken in our simplified model, as governed by Equations (4.33) to (4.36), for each tumour of different growth fraction.

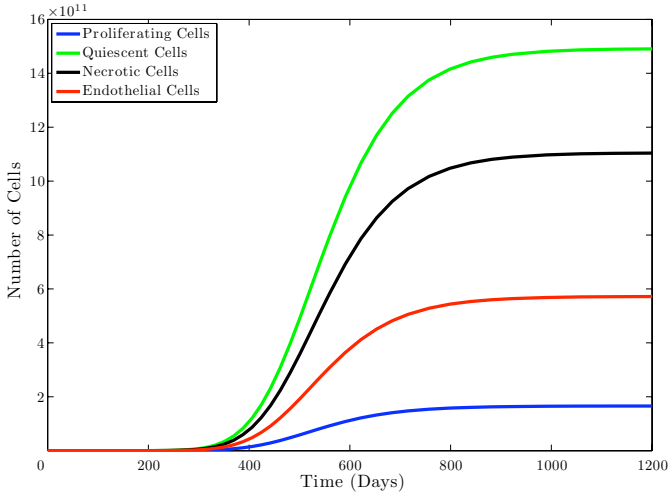

(a) The 10% growth fraction tumour.

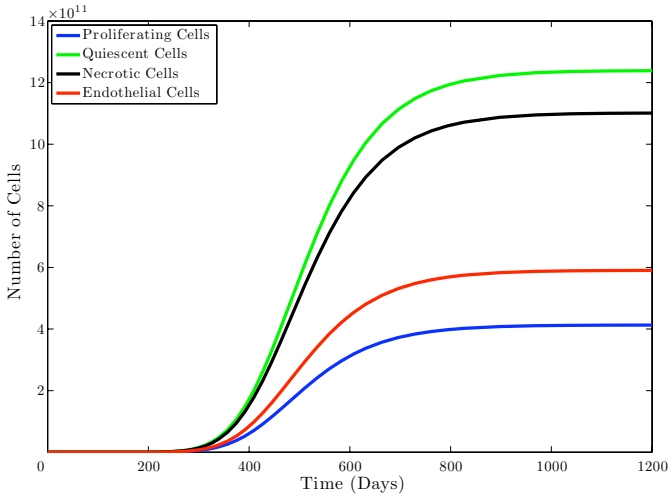

(b) The 25% growth fraction tumour.

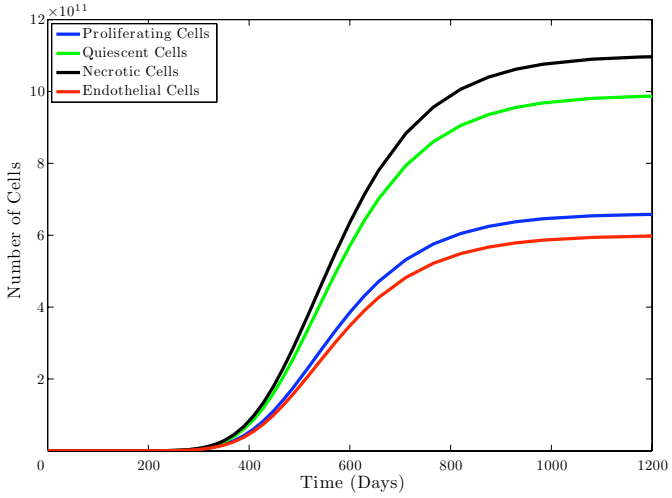

(c) The 40% growth fraction tumour.

Figure 4.4: The growth curves of each cell type in our simplified tumours of different growth fractions for the parameter values outlined in Table 4.1, as governed by Equations (4.33) to (4.36).

our choice of initial conditions is sufficient for closing the model and yielding realistic long time tumour dynamics.

4.5 Validating the Asymptotic Analysis

Having evaluated all the parameters in our simplified system we now test the validity of the asymptotic analysis which was performed in Section 4.4.1.

We begin by considering the simplified tumour's growth fraction, which can readily be calculated from the simulations of the evolution of the tumour, and the asymptotic approximations to it as given by Equations (4.24) and (4.25). These quantities for the 25% growth fraction simplified tumour are shown in Figure 4.5. It can be seen that except for the very early behaviour our leading order approximation suffers from an error of less than 15% and our second order approximation suffers from an error of less than 2%. In Figure 4.5(b) it can be seen that initially the approximations are not valid, but after a period of approximately 12 days they become reasonable. We anticipate this is due to the tumour initially undergoing a relaxation on the cellular time scale, during which our Watson's lemma based asymptotic analysis does not apply. To consider this in detail we consider the initial behaviour of the tumour in Figure 4.6. It can be seen that as anticipated the tumour initially regresses on the cellular time scale until the tumour is relatively well vascularised, at which point it then starts growing on the slower tumoural time scale. The presence of this initial relaxation is an artefact of our initial conditions and during this relaxation our Watson's lemma based analysis does not apply and so it is to be expected that our asymptotic analysis breaks down here. Furthermore the time frame for which our approximations are initially not valid, 12 days or so, is consistent with them not being initially valid over the short time scale, of a few days, but being valid over the long time scale, of a few months. This is also as expected given the assumptions of our Watson's lemma based analysis.

Figure 4.7 show the necrotic fraction of our simplified tumour and the first two approximations to it. This behaves similarly to the growth fraction whereby the approximations are initially not valid, but do become valid once the initial relaxation has taken place. Once valid the leading order approximation suffers from an error of less than 4% and the second order approximation suffers from an error of less than 0.02%.

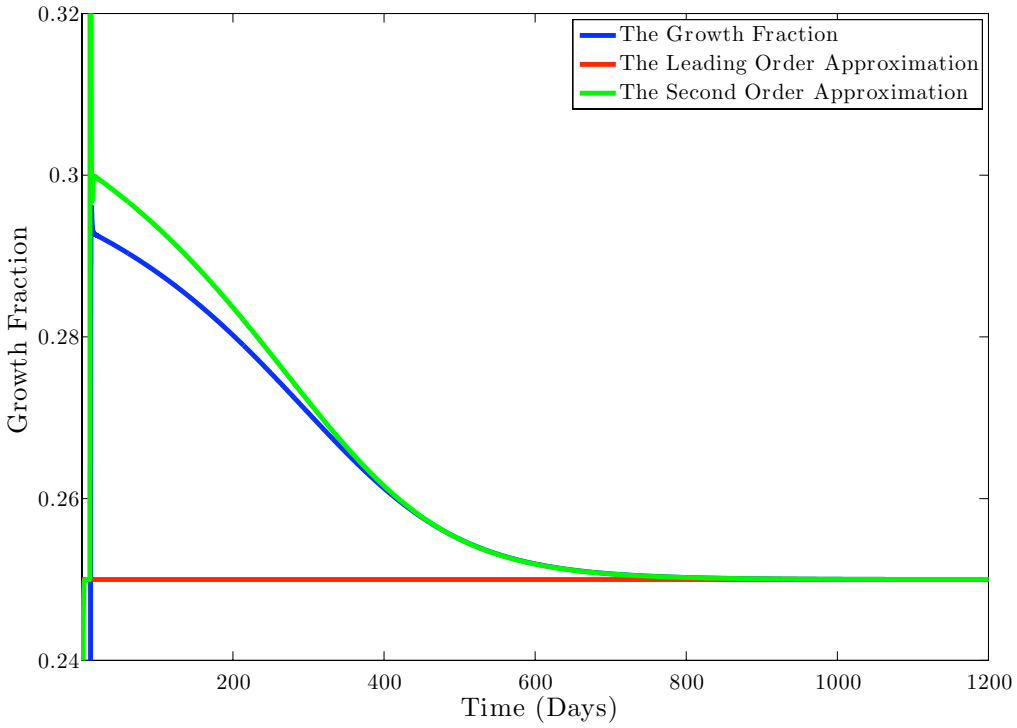

(a) The long time behaviour.

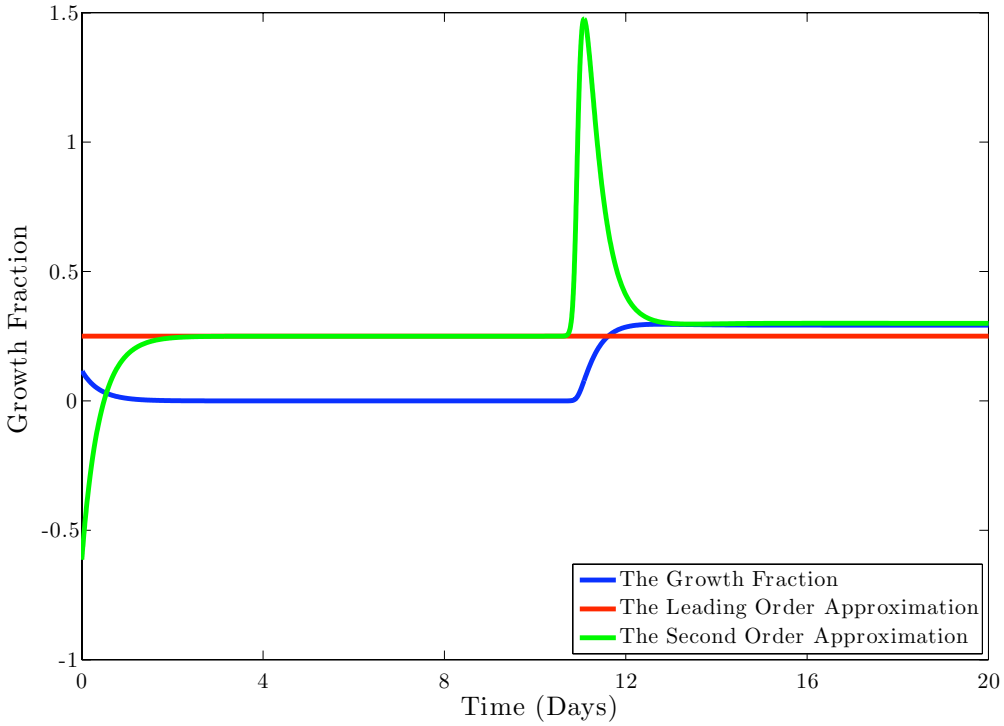

(b) The initial behaviour.

Figure 4.5: The growth fraction and the first two approximations to the growth fraction, for our simplified tumour with a growth fraction of 25%, for the parameter values outlined in Table 4.1, as governed by Equations (4.33) to (4.36).

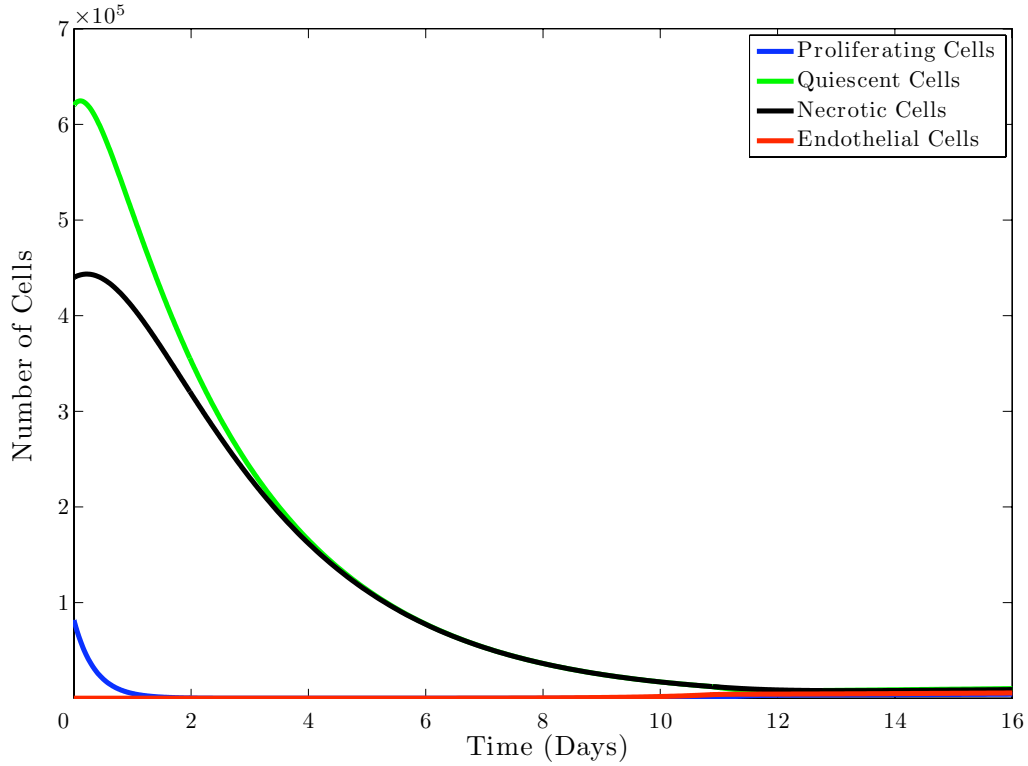

Figure 4.6: The initial behaviour of each cell type in our simplified tumour with a growth fraction of 25% for the parameter values outline in Table 4.1, as governed by Equations (4.33) to (4.36).

The evolution of the simplified tumour has shown the predictions of Section 4.4.1 to be correct. As predicted there are two time scales in our system. Initially the tumour regresses on the cellular time scale, but once adequately vascularised the tumour evolves more slowly on the tumoural time scale. When the system evolves on the slower, tumoural, time scale our leading order asymptotic approximations to the tumour's growth and necrotic fraction are sufficiently accurate to validate their use in estimating parameters in our simplified model. Furthermore, our second order approximations to the growth and necrotic fraction are an order of magnitude more accurate than the first approximations, which validates our asymptotic analysis.

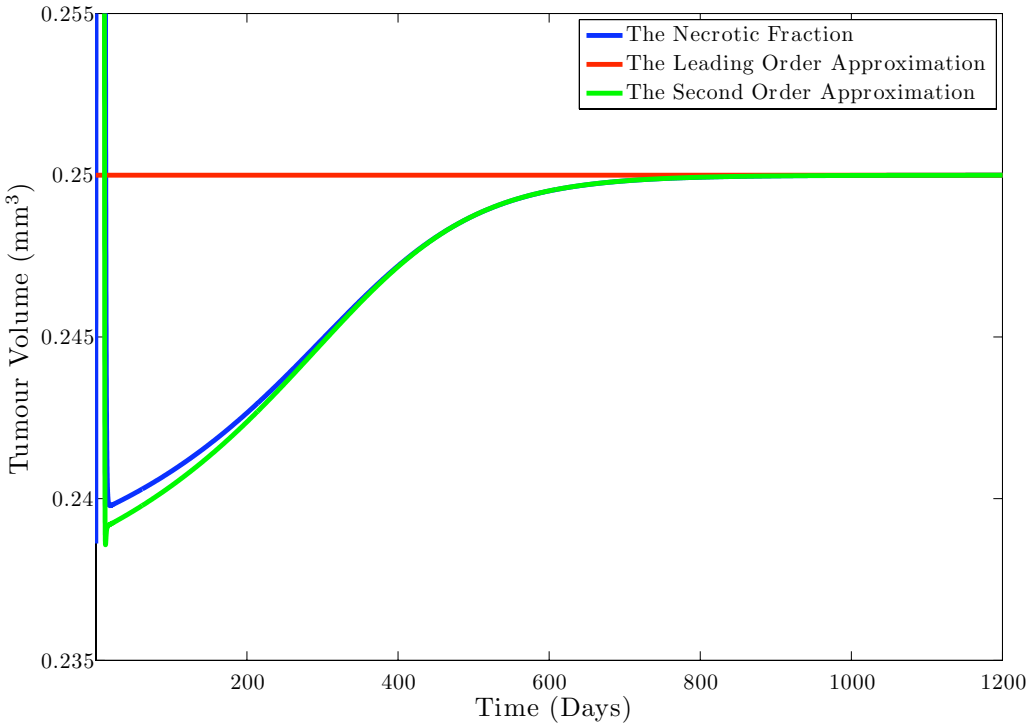

(a) The long time behaviour.

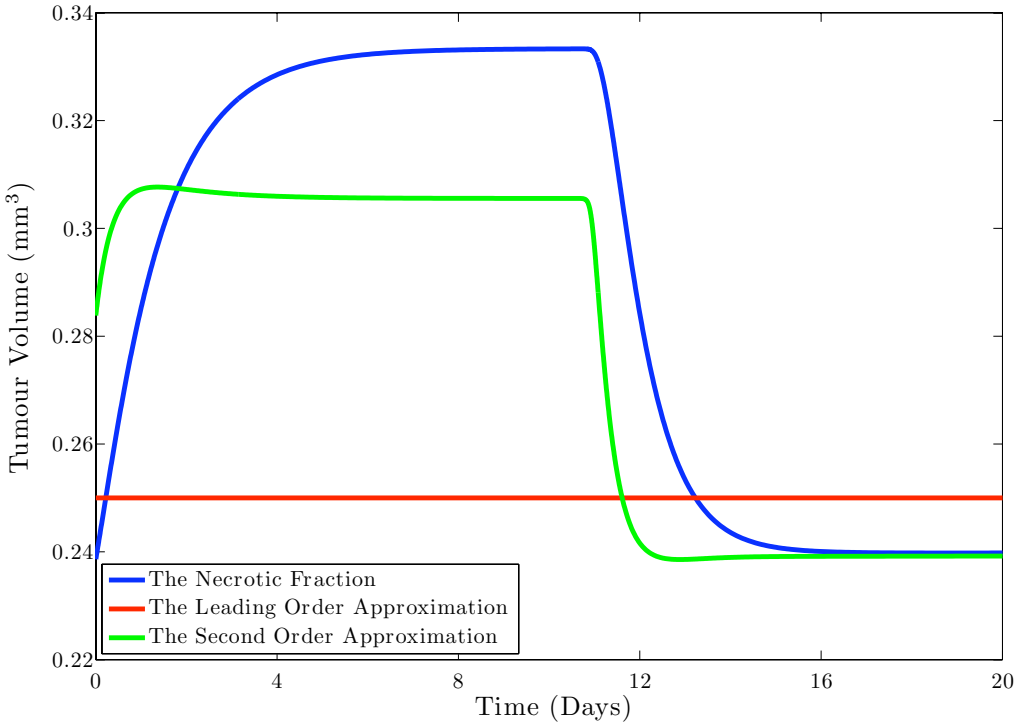

(b) The initial behaviour.

Figure 4.7: The necrotic fraction and the first two approximations to the necrotic fraction, for our simplified tumour with a growth fraction of 25%, for the parameter values outlined in Table 4.1, as governed by Equations (4.33) to (4.36).

4.6 Re-Generalising the Model

In Section 4.3 we temporarily simplified our model by assuming that the rate of necrosis was constant, rather than depending upon the local oxygen concentration. This simplification allowed us to perform an asymptotic analysis to assist with our parameter estimation. It was anticipated that this simplification would be valid for a tumour growing in the absence of any therapy, but not for a tumour undergoing treatment. We now relax this temporary simplification and use the parameter values summarised in Table 4.1 for our simplified model to find parameter values which provide realistic growth dynamics for the re-generalised system. Upon re-generalising we obtain the following non-dimensional system

$$\frac{\mathrm{d}P}{\mathrm{d}t} = -\Big\{1 + \psi_1 \mathcal{S}_1 + \eta \mathcal{S}_2\Big\} P + \psi_2 \left(1 - \mathcal{S}_1\right) Q, \tag{4.38}$$

$$\frac{\mathrm{d}Q}{\mathrm{d}t} = \Big\{2 + \psi_1 \mathcal{S}_1\Big\} P - \Big\{\psi_2 \left(1 - \mathcal{S}_1\right) + \eta \mathcal{S}_2\Big\} Q, \tag{4.39}$$

$$\frac{\mathrm{d}N}{\mathrm{d}t} = 2\eta \mathcal{S}_2 (P + Q) - \nu N, \tag{4.40}$$

$$\frac{\mathrm{d}E}{\mathrm{d}t} = \lambda \log\left(\tfrac{K}{3(P+Q)+1.5N+E}\right) E \mathcal{S}_3, \tag{4.41}$$

where $\mathcal{S}_i = S_{w_i}\left(\frac{3(P+Q)+E}{E}, \alpha_i\right)$, with the initial conditions

$$P(0) = 82,000, \qquad Q(0) = 620,000, \qquad N(0) = 440,000, \qquad E(0) = 1. \tag{4.42}$$

Where parameters in this generalised system have exact parallels to parameters in the simplified system we will use the parameter value presented in Table 4.1. However the parameters relating to cell necrosis, η, w_2, and α_2, do not have exact parallels with the previous system.

It is expected that cell necrosis will not dominate cell proliferation or tumour angiogenesis and *vice versa*, and instead we anticipate that all of these processes will be significantly up and down-regulated across the range of conditions observed in an *in vivo* tumour. To allow the necrosis switching function to switch on and off over the same range of conditions as the other switching functions we take $\alpha_2 = 10$ and $w_2 = 1$.

We now estimate the maximum rate at which cells can undergo necrosis, η. We do this by ensuring that the rate of necrosis in the general model is comparable to the

rate of necrosis in the simplified model by choosing parameters in our general model so that

$$\eta S_{w_2}\left(\tfrac{3(P+Q)+E}{E}, \alpha_2\right) \approx \widetilde{\eta}.$$

However to evaluate the switching function in this approximation we must simulate the evolution of the generalised tumour, but we cannot do this until we evaluate the parameter η. Instead we estimate the value of the switching function in this approximation by comparing it to the equivalent switching function in the simplified model.

For our 10% growth fraction simplified tumour at saturation the switching function, as given by Equation (4.2), takes the value $S_{w_2}\left(\tfrac{3(P+Q)+E}{E}, \alpha_2\right) = 0.350$ (3 s.f.) when $\alpha_2 = 10$ and $w_2 = 1$. Assuming that the quality of the vasculature at saturation in our simplified model will serve as a good estimate for the quality of the vasculature at saturation in our generalised model, and recalling that in our simplified model we took $\widetilde{\eta} = 0.1$, we now take $\eta = \frac{0.1}{0.350} = 0.286$ (3 s.f.) in our generalised model.

By a similar argument we take $\eta = 1.09$ (3 s.f.) for the 25% growth fraction tumour and $\eta = 2.16$ (3 s.f.) for the 40% growth fraction tumour.

Thus, for our generalised model we take the parameter values presented in Table 4.2. This parameter estimation is reliant upon the simplified and re-generalised models behaving similarly in the absence of any therapy, and we now check this.

4.6.1 Comparing the Simplified and Generalised Models

Having re-generalised our model we now compare the behaviour of the simplified and generalised models to ensure that the generalised model also exhibits realistic tumour growth. In Figure 4.8 we plot the growth curves of the simplified and generalised models for the parameter values corresponding to the 25% growth fraction tumour.

It can be seen that the growth curves for both the simplified and generalised models are sigmoidal. However, the generalised tumour grows more quickly than the simplified tumour. The reason for this can be seen in Figure 4.9, where we plot the constant rate of cell necrosis used in the simplified model, $\widetilde{\eta}$, and the rate of cell necrosis which depends upon the quality of the vasculature used in the general model, $\eta S_{w_2}\left(\tfrac{3(P+Q)+E}{E}, \alpha_2\right)$. It can be seen that following the initial normalisation the rate of cell necrosis is lower in the general model than in the simplified model. The reason

Parameter	Description	Value			Reference
		10% G.F.	25% G.F.	40% G.F.	
w_1	The sensitivity of the switch between P and Q	1	1	1	Analysis of parameters
w_2	The sensitivity of the necrotic switch	1	1	1	Analysis of parameters
w_3	The sensitivity of the angiogenic switch	1	1	1	Analysis of parameters
α_1	Critical level of vasculature for the switch between P and Q	10	10	10	Analysis of parameters
α_3	Critical level of vasculature for the angiogenic switch	10	10	10	Analysis of parameters
η	The maximum rate of necrosis of live cells	0.286	1.09	2.16	See text
ν	Necrotic cell decay rate	0.3	0.75	1.2	See text
ψ_1	The maximum rate of transfer from P to Q	0.2	0.6	1.35	Analysis of parameters
ψ_2	The maximum rate of transfer from Q to P	0.2	0.6	1.35	See text
K	Tumour carrying capacity	7.2×10^{12}	7.2×10^{12}	7.2×10^{12}	See text
λ	Gompertzian parameter for endothelial cell growth	0.02	0.03	0.03	See text

Table 4.2: The non-dimensional parameters used in our general model, as governed by Equations (4.38) to (4.41), for each tumour of different growth fraction.

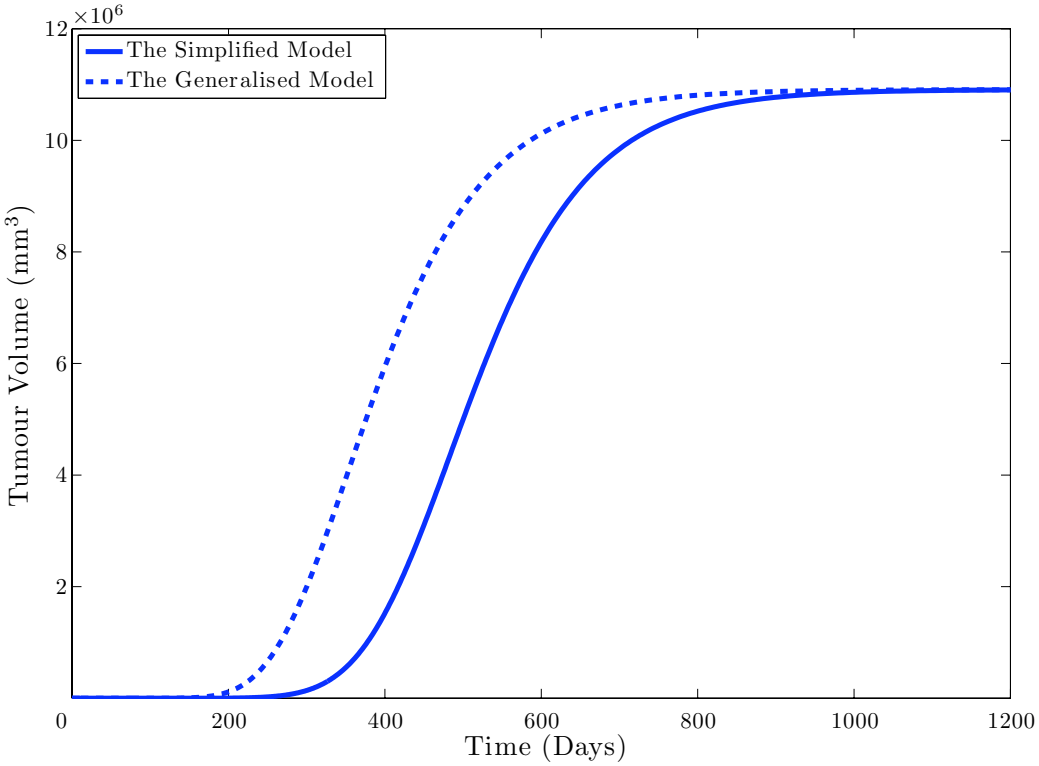

Figure 4.8: The growth curves of our simplified model, as governed by Equations (4.33) to (4.36), and our generalised model, as governed by Equations (4.38) to (4.41), for the parameter values corresponding to a 25% growth fraction tumour as outlined in Tables 4.1 and 4.2.

for this is that following the initial normalisation the quality of the tumour vasculature in both models is comparatively good, but decreases as the tumour grows (results not shown). Hence allowing the rate of necrosis to depend upon the quality of the tumour vasculature causes the rate of cell necrosis to be relatively low following the initial normalisation, but it then increases as the tumour grows. However, the overall effect of this is only to slow the growth of the tumour, though orders of magnitude are not changed. This validates our temporary simplifying assumption that the rate of necrosis in the absence of any therapy can be assumed to be constant for the purpose of parameter fitting, which was made in Section 4.3.

In Figure 4.8 we only plotted the total volume of the tumour. To ensure that each cell compartment in the general tumour behaves suitably similarly to the corresponding cell compartment in the simplified tumour we consider the evolution of each of the different cell compartments, which we plot in Figure 4.10. Again it can be seen that

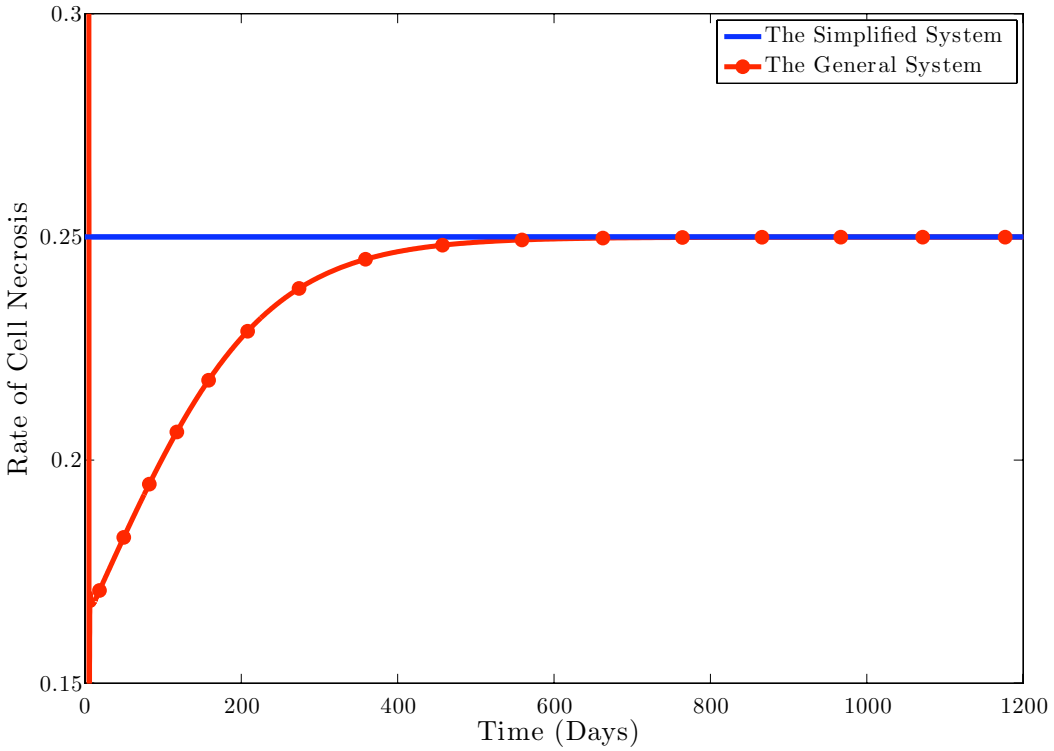

Figure 4.9: The rate of cell necrosis in the simplified model, $\widetilde{\eta}$, for the 25% growth fraction tumour for the parameter values outlined in Table 4.1, as governed by Equations (4.33) to (4.36) and the rate of cell necrosis in the general model, $\eta S_{w_2}\left(\frac{3(P+Q)+E}{E}, \alpha_2\right)$, for the 25% growth fraction tumour for the parameter values outlined in Table 4.2, as governed by Equations (4.38) to (4.41).

each of the different cell compartments in the generalised model behaves similarly to the corresponding compartment in the simplified model, albeit with the generalised model growing more quickly. Despite growing slightly quicker than the simplified model, the time to saturation of our generalised model is still biologically realistic and so the evolution of the generalised model is as realistic as the simplified model.

The asymptotic analysis performed in Section 4.4.1 which assisted in evaluating parameters is not valid in our generalised tumour, however the simplified and generalised systems may behave suitably similarly that the resulting approximations to the growth and necrotic fractions may still be valid in the generalised model. To consider this we compare the growth and necrotic fractions of the simplified and generalised tumour and we plot these fractions of the two modelled tumours in Figure 4.11. It can be seen that whilst there is some variation in the growth fraction and necrotic fraction

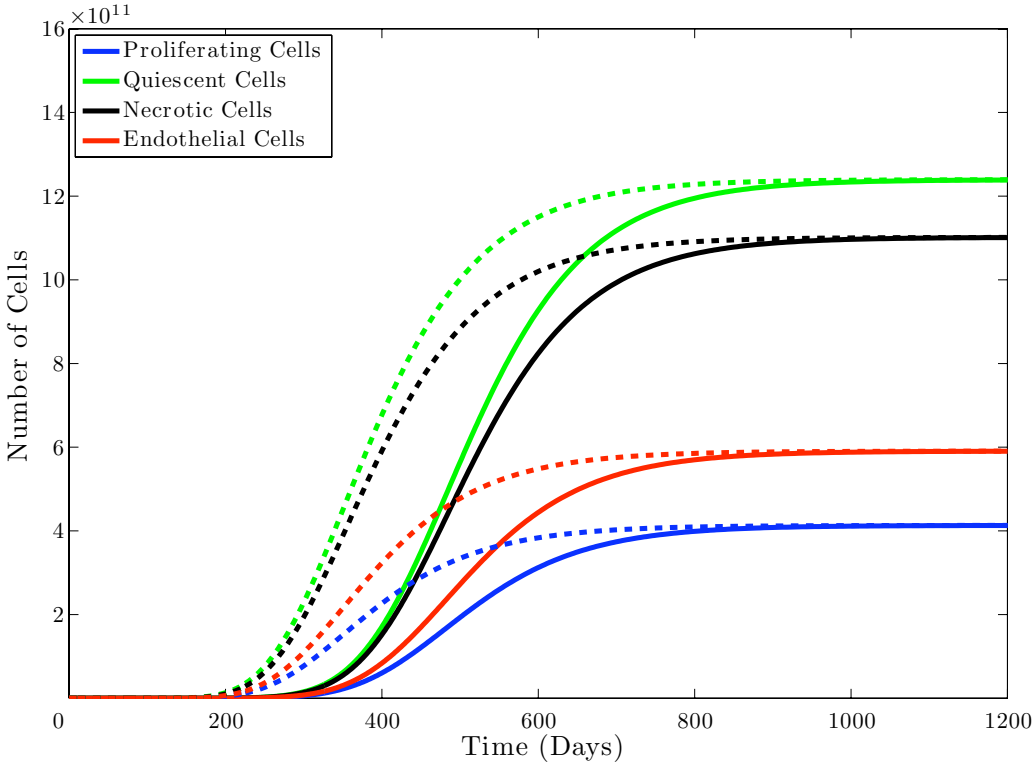

Figure 4.10: The evolution of the different cell compartments in our simplified model (plotted with solid lines), as governed by Equations (4.33) to (4.36), and our generalised model (plotted with dashed lines), as governed by Equations (4.38) to (4.41), for the parameter values corresponding to a 25% growth fraction tumour, as shown in Tables 4.1 and 4.2.

in each case, the trends remain the same and the fractions of the two models converge at saturation. We primarily used our asymptotic analysis to estimate parameter values in our simplified model pertaining to the growth and necrotic fractions. The fact that the growth and necrotic fractions in the simplified and generalised models behave similarly validates the use of this asymptotic analysis in our parameter estimation.

4.7 Discussion

In this chapter we were aiming to construct a model for the growth of a vascular tumour which would be receptive to the inclusion of chemotherapy and anti-angiogenic therapies. In particular we wanted to construct a model which exhibited realistic growth dynamics and which also considered the evolution of different cell compart-

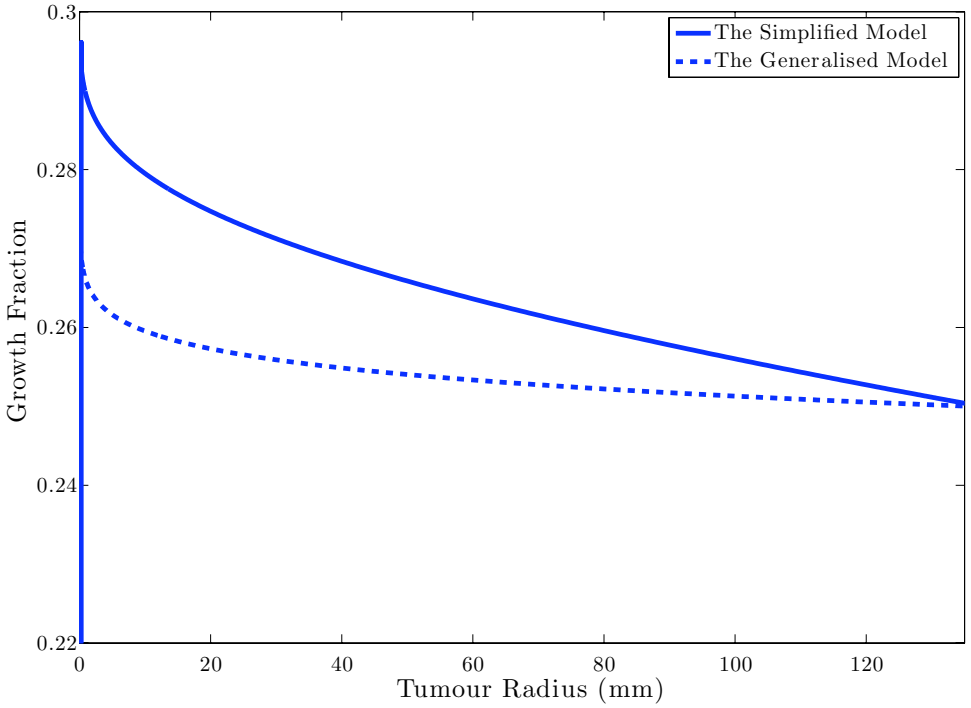

(a) The growth fraction.

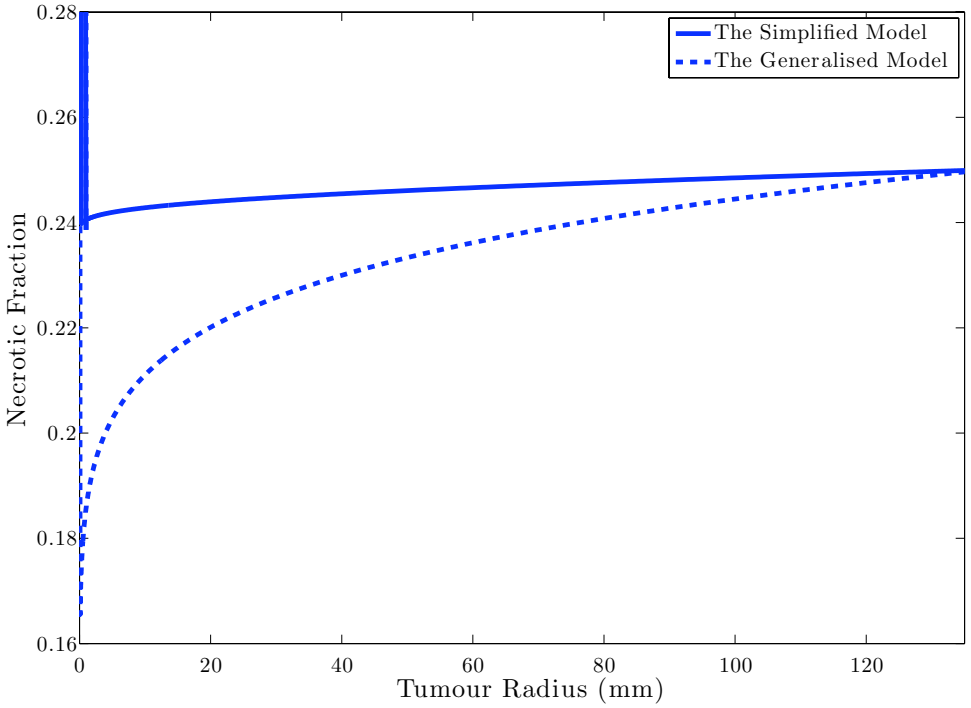

(b) The necrotic fraction.

Figure 4.11: A comparison of the growth and necrotic fractions of our simplified model, as governed by Equations (4.33) to (4.36), and our generalised model, as governed by Equations (4.38) to (4.41), for the parameter values corresponding to a 25% growth fraction tumour outlined in Tables 4.1 and 4.2.

ments in the tumours and explicitly depended upon the quality of the tumour vasculature.

Having reviewed the biological literature we derived a set of coupled ordinary differential equations for the evolution of each cell compartment within the tumour. We closed this model by deriving the corresponding initial conditions for an avascular tumour at saturation which has just begun to undergo angiogenesis.

Upon non-dimensionalising the model we evaluated some, but not all, of the non-dimensional parameters in the model by performing a literature search. We then performed analysis which related some of the unknown parameters to biologically known quantities. In particular, we temporarily simplified the model by assuming that the death rate of tumour cells was constant, rather than depending upon the quality of the local vasculature, and introduced a small parameter by comparing the cellular and tumoural time scales. This small parameter allowed us to perform an asymptotic analysis which showed that the leading order growth and necrotic fractions of the simplified tumour are given by the tumour cell death rate and the necrotic cell decay rate, which allowed the estimation of these parameters. We also used the criterion that we are only interested in tumours with a stable non-trivial steady state to obtain bounds on some of the remaining unknown parameters.

We finalised our parameter estimation by performing an analysis of parameters, whereby we ensured that the evolution of our simulated tumour was suitably realistic. In particular we ensured that our simulated tumour exhibited a realistic monotonic Gompertzian style growth curve.

With a complete set of parameter values chosen for our simplified model, we then re-generalised our model and converted these parameter values into an estimation of the parameter values in our general system. By comparing the behaviour of our simplified and general systems we found that they behave similarly, although the general tumour grows quicker than the corresponding simplified tumour, but not extensively so. We also found that both models undergo an initial relaxation where the tumour regresses and the endothelial cells proliferate on the cellular time scale. This is not expected to suitably model the initial vascularisation process; however the behaviour of our model after the normalisation relaxation is very robust to the behaviour of this initial relaxation. Hence the details of the initial conditions and the associated transient dynamics are not significant for tumour dynamics on longer timescales.

Hence our general model is a empirically motivated model for vascular tumour growth with sets of parameter values which provide realistic growth dynamics for a range of growth fractions. Furthermore, the fact that our model distinguishes between the different tumour cell types makes it receptive to the inclusion of a chemotherapeutic, and the fact that our model explicitly depends upon the quality of the tumour's vascular makes it receptive to the inclusion of any therapy which provides an anti-angiogenic effect. We include such therapies in our model in the next chapter.

Chapter 5

Incorporating Therapy

5.1 Introduction

In this chapter we incorporate therapy into our previous model for the evolution of a vascularised tumour. The resulting model for the evolution of a vascular tumour undergoing treatment is then used to consider some key clinical questions regarding tumour treatment. Before doing this we will consider what relevant mathematical modelling has already been done, and how well the relevant biology is understood, by conducting a review of the relevant mathematical and biological literature.

5.1.1 Literature Summary

Mathematical Literature

One of the first, and most influential, mathematical papers concerning chemotherapy was that by Skipper et al. (1964). Amongst other results, Skipper et al. used a law of mass action type argument to show that chemotherapy follows a log-kill rule, where each application of therapy kills a constant fraction of the tumour, rather than killing a constant number of cells.

This log-kill rule was later generalised by Norton and Simon (1977a) who proposed that tumour regression in response to radiotherapy is actually proportional to the growth rate of the unperturbed tumour, rather than simply being proportional to the size of the tumour, and they validated this assertion by using a model to reproduce the observed *in vivo* response of rat tumours to radiotherapy. Norton and Simon (1977b) then showed that this result also applied to chemotherapy and assuming

chemotherapy induces tumour regression at a rate proportional to the growth rate of the unperturbed tumour gave greater agreement between the modelling and *in vivo* results than using either a constant cell kill or a log-kill model. The assumption that chemotherapy induces tumour regression at a rate proportional to the growth rate of the unperturbed tumour has since been dubbed the Norton-Simon model and remains a standard model for tumour response to chemotherapy.

Norton and Simon (1977b) also used this model to consider tumour response to different treatment regimes and concluded that brief periods of high doses of chemotherapy are more effective at treating a tumour than prolonged periods of low doses of chemotherapy. This assertion, that dose dense therapies are more effective than dose sparse therapies, has become known as the Norton-Simon hypothesis. However, the work of Norton and Simon (1977b) neglects the important effect of therapy resistance.

Since these general results were derived much work has been carried out which considers more specific questions concerning the treatment of vascular tumours with chemotherapy. It is unfeasible to review all this work here, however the aforementioned papers are the most general, and influential, concerning the mathematical modelling of chemotherapy scheduling.

Biological Literature

The term chemotherapy refers to any drug which has a toxic effect on cells. The term is typically applied to drugs which are used in the treatment of malignant tumours and we will only use it in that context here. Also, whilst chemotherapy can refer to any drug which kills tumour cells, it typically only refers to therapies which are more toxic to malignant cells than healthy cells, and again we will use it in that context here.

Many chemotherapies interfere with proliferating cells as they are going through the cell cycle in some way which causes the them to undergo a form of cell suicide known as apoptosis (Goldie, 2008). Such drugs can only affect cells which are actively going through the cell cycle and are known as cell cycle specific drugs. Cell cycle non-specific chemotherapies which target all living cells independently of whether or not they are actively in the cell cycle also exist, but in this investigation we limit ourselves to considering cell cycle specific therapies.

During treatment, chemotherapy is often delivered intravenously, but can also be given orally (Freter and Perry, 2008) and at clinically relevant doses chemotherapy

uptake by the cells often increases linearly with therapy dose (Mistry et al., 1992; Hromas et al., 1987; Johnson et al., 1996).

As well as targeting tumour cells, chemotherapy has also been found to be able to provide an effective anti-angiogenic effect by killing endothelial cells; however a small proportion of chemotherapeutics possess no significant anti-angiogenic efficacy (Browder et al., 2000). In fact, traditional chemotherapies have been shown to work as effective anti-angiogenic agents in resistant *in vivo* mouse tumours and it has been suggested that chemotherapy might be scheduled to provide a predominately anti-angiogenic effect. One of the key benefits of such a therapy is that the population of endothelial cells within a vascular tumour would not be expected to acquire resistance to the therapy (Browder et al., 2000).

5.1.2 The Aims of this Chapter

In this chapter we aim to build a model for the evolution of a vascular tumour being treated by chemotherapy and use this model to consider some of the key clinical questions regarding tumour treatment. In particular we aim to build a model which explicitly considers the role of angiogenesis and the possibility of scheduling chemotherapy to provide an anti-angiogenic affect.

5.2 Modelling the Inclusion of Chemotherapy

We now take our previous model for the growth of an untreated vascular tumour, which was derived in Section 4.2 of the previous chapter, and include chemotherapy into this model. We begin by considering how chemotherapy is delivered to our tumour.

5.2.1 The Delivery of Chemotherapy

We assume that chemotherapy is delivered to the patient intravenously so that the intravenous chemotherapy concentration is prescribed and given by $L(t)$, which is a function of time. Then the amount of chemotherapy delivered to the tumour will depend upon the quality of the tumour's vasculature, with a well vascularised tumour

receiving a higher dose of therapy than an equivalent poorly vascularised tumour. Hence we take the mean chemotherapy concentration within the tumour, $C(t)$, to be

$$C(t) = \left(1 - S_{w_4}\left(\tfrac{P+Q+E}{E}, \alpha_4\right)\right) L(t),$$

where $S_w(X, a)$ is the switching function discussed in Section 4.2.1 of the previous chapter, α_4 is the critical vasculature for the delivery of chemotherapy, w_4 is the sensitivity of the chemotherapy delivery switch and P, Q, and E are the total volumes of proliferating, quiescent and endothelial cells, respectively, in the tumour.

Note that this simple model implicitly assumes that the half-life of the chemotherapeutic is sufficiently fast for the chemotherapeutic concentration to quickly decay to zero upon completion of the therapy. This will be valid for a chemotherapy such as Fluorouracil (5-FU) which has a half-life of 10-15 minutes (White, 2001).

We now consider what effect this chemotherapy should have upon the tumour.

5.2.2 The Effect of the Chemotherapy

We are limiting our model to the action of cell cycle specific drugs which only affect the actively proliferating cells and we also assume that at clinically relevant concentrations the rate of cell kill increases linearly with chemotherapy concentration. Then the proliferating tumour cells undergo chemotherapy induced apoptosis at a rate $\kappa_1 CP$, where κ_1 is the linear kill rate of proliferating cells exposed to the chemotherapy.

The findings of Browder et al. (2000) highlight that the endothelial cells will also be susceptible to the therapy and we model this by applying the Norton-Simon model and assuming that endothelial cells undergoing therapy undergo net regression at a rate proportional to the growth rate of an equivalent untreated endothelial cell population. Then the endothelial cells undergo chemotherapy induced apoptosis at a rate $\kappa_2 C \frac{\mathrm{d}E}{\mathrm{d}t}_{\mathrm{un}}$, where κ_2 is the linear relative kill rate of endothelial cells exposed to the chemotherapy and $\frac{\mathrm{d}E}{\mathrm{d}t}_{\mathrm{un}}$ is the growth rate of an equivalent untreated population of endothelial cells.

In this model we combine the populations of apoptotic cells and necrotic cells and model them as a single compartment of dead cells. This compartment of dead cells will behave equivalently to the necrotic cell compartment in the previous chapter. It is possible that apoptotic cells and necrotic cells will actually exhibit slightly different dynamics, however any slight difference between these cell types is not expected to

have a significant feedback into the system and so this approach is considered more desirable than modelling the apoptotic cells separately and introducing additional unknown parameters into our model.

5.2.3 The Non-Dimensional Model

We now include chemotherapy into our model. Due to the similarity between our previous model without chemotherapy, presented in Section 4.2 of the previous chapter, and our current model including chemotherapy we do not present the current dimensional model explicitly, and instead we immediately present the model which has been non-dimensionalised using the rescalings of Section 4.2.4 of the previous chapter, as well as the additional rescalings

$$L(t) = \mathcal{L}\widehat{L}\big(\widehat{t}\big), \qquad \text{where} \qquad \mathcal{L} = \max_t L(t), \tag{5.1}$$

where caret denotes non-dimensional variables. Defining the following non-dimensional quantities

$$\widehat{C}\big(\widehat{t}\big) = \frac{C(t)}{\mathcal{L}}, \qquad \widehat{\kappa}_1 = \frac{\kappa_1 \mathcal{L}}{\mu}, \qquad \text{and} \qquad \widehat{\kappa}_2 = \kappa_2 \mathcal{L},$$

we find that upon introducing chemotherapy to our previous model and dropping carets we obtain the following non-dimensional system

$$\frac{\mathrm{d}P}{\mathrm{d}t} = -\Big\{1 + \psi_1 \mathcal{S}_1 + \eta \mathcal{S}_2 + \kappa_1 C\Big\} P + \psi_2 \left(1 - \mathcal{S}_1\right) Q, \tag{5.2}$$

$$\frac{\mathrm{d}Q}{\mathrm{d}t} = \Big\{2 + \psi_1 \mathcal{S}_1\Big\} P - \Big\{\psi_2 \left(1 - \mathcal{S}_1\right) + \eta \mathcal{S}_2\Big\} Q, \tag{5.3}$$

$$\frac{\mathrm{d}N}{\mathrm{d}t} = 2\eta \mathcal{S}_2 (P + Q) + 2\kappa_1 C P + \tfrac{2}{3} \kappa_2 C \lambda \log\left(\tfrac{K}{3(P+Q)+1.5N+E}\right) E \mathcal{S}_3 - \nu N, \tag{5.4}$$

$$\frac{\mathrm{d}E}{\mathrm{d}t} = (1 - \kappa_2 C) \lambda \log\left(\tfrac{K}{3(P+Q)+1.5N+E}\right) E \mathcal{S}_3, \tag{5.5}$$

$$C(t) = \left(1 - \mathcal{S}_4\right) L(t). \tag{5.6}$$

where $\mathcal{S}_i = S_{w_i}\left(\frac{3(P+Q)+E}{E}, \alpha_i\right)$, and $\max_t L(t) = 1$.

Note that our non-dimensional parameters defining the potency of the chemotherapy, κ_1 and κ_2, quantify the potency of the therapy in different ways. κ_1 is the rate at which proliferating cells undergo apoptosis per unit of chemotherapy, whereas κ_2 is the relative rate at which endothelial cells undergo apoptosis per unit of chemotherapy compared to the growth rate of untreated endothelial cells. Hence setting $\kappa_1 = \kappa_2$ would not correspond to the proliferating cells and endothelial cells being equally susceptible to the therapy.

5.2.4 Parameter Estimation

We now attempt to evaluate the non-dimensional parameters which are present in this model but absent from the previous model outlined in Section 4.2.4. We begin by estimating the value of κ_2, which is the non-dimensional rate of chemotherapy induced apoptosis of the endothelial cells. To do this we use the work of Browder et al. (2000) who considered the potential of using traditional chemotherapies as anti-angiogenic agents in drug-resistant tumours. It was found that chemotherapy successfully recessed the endothelial cell population in the drug-resistant tumour. To reproduce this result in our model would require that

$$\begin{aligned} 1 - \kappa_2 C &< 0 \\ \implies \kappa_2 &> \frac{1}{C} \geq 1. \end{aligned}$$

Hence for the endothelial cell population to be a viable target of the chemotherapy require that κ_2 be at least O(1).

We now use this result to estimate the magnitude of κ_1, which is the non-dimensional rate of chemotherapy induced apoptosis of the proliferating cells, by supposing that tumour cells and endothelial cells are as equally sensitive. The Norton-Simon model states that the endothelial cell population will undergo chemotherapy induced apoptosis at the rate

$$\kappa_2 C \left(\frac{\mathrm{d}E}{\mathrm{d}t}\right)_{\text{un}}. \tag{5.7}$$

However, if we let the fraction of endothelial cells which are instantaneously proliferating be denoted by ϕ and assume that endothelial cells and tumour cells are equally sensitive to the therapy, then the endothelial population will undergo chemotherapy induced apoptosis at the rate

$$\kappa_1 C \phi E. \tag{5.8}$$

To use Expressions (5.7) and (5.8) to relate κ_1 and κ_2 together we must find an expression for ϕ, the fraction of endothelial cells which are actively proliferating. To do this we compare the potential doubling time of the endothelial cell population to the actual doubling time of the endothelial cell population. In Section 4.4.3 of the previous chapter we found that the cell cycle time of endothelial cells is 60 hours. This corresponds to a non-dimensional cell cycle time of $\frac{60}{15.9}$ and a non-dimensional exponential growth rate of $\frac{15.9\log(2)}{60}$. However the endothelial cell population does

not grow at this potential rate, instead only a fraction ϕ of the endothelial cells are proliferating, so that

$$\left(\frac{\mathrm{d}E}{\mathrm{d}t}\right)_{\mathrm{un}} = \frac{15.9\log(2)}{60}\phi E. \tag{5.9}$$

Substituting this expression into Expression (5.7) and equating it to Expression (5.8) we find that

$$\begin{aligned}\kappa_1 &= \frac{15.9\log(2)}{60}\kappa_2,\\ &\approx 0.184\kappa_2.\end{aligned}$$

Therefore, assuming that the tumour cells and endothelial cells are equally sensitive to the therapy implies that κ_1 should be approximately one fifth of the value of κ_2.

Note also that we can use this analysis to obtain an estimate of the fraction of endothelial cells which are proliferating. Re-arranging Equation (5.9) we find that

$$\phi = \frac{60}{15.9\log(2)}\frac{1}{E}\left(\frac{\mathrm{d}E}{\mathrm{d}t}\right)_{\mathrm{un}}.$$

Given this expression we can use our previous model for vascular tumour growth in the absence of any therapy, which was presented in Chapter 4, to estimate the fraction of endothelial cells which are actively proliferating in an untreated tumour. We find that immediately after the initial relaxation the fraction of endothelial cells actively proliferating in our untreated 10%, 25%, and 40% growth fraction tumours are 39%, 56%, and 57% (2 s.f.) respectively.

Initial Conditions

In this chapter we will be considering a tumour which is undergoing treatment with a chemotherapeutic and as such our initial conditions should correspond to a tumour which has grown to a clinically detectable size. We therefore take initial conditions which correspond to an untreated tumour which has grown to half the maximum size allowed by Gompertzian saturation. We can then extract the corresponding size of each cell compartment from our model for tumour growth in the absence of any therapy, as defined by Equations (4.3) to (4.6) in the previous chapter, to obtain the initial conditions given in Table 5.1.

Tumour Growth Fraction	Initial P	Initial Q	Initial N	Initial E
10%	8.23×10^{10}	6.97×10^{11}	5.10×10^{11}	3.27×10^{11}
25%	2.15×10^{11}	6.33×10^{11}	5.63×10^{11}	3.90×10^{11}
40%	3.09×10^{11}	4.52×10^{11}	5.05×10^{11}	3.52×10^{11}

Table 5.1: The initial conditions (to 3 significant figures) relevant to the current model, as defined by Equations (5.2) to (5.5), which corresponds to an untreated tumour which has grown to half the maximum size as given by Gompertzian growth.

5.2.5 Treatment Schedule

We will begin by applying a very simple treatment schedule to our modelled tumour to gain an insight into how our model behaves; we will consider more complicated schedules later when posing more specific questions of our model. This initial treatment schedule will consist of applying therapy continuously for one day, and then following this therapy application by a rest period, the length of which is a free parameter. This sequence of therapy application will be repeated a number of times.

5.2.6 Numerically Simulating the Treatment of the Tumour

As in Section 4.4.4 of the previous chapter we simulate the evolution of our model using an adaptive linear multistep method. Our current initial conditions have been extracted from our previous model and correspond to a tumour which has grown to half the maximum size as given by Gompertzian saturation. As such we would not expect this system to undergo any initial relaxation, such as that observed in Section 4.5 of the previous chapter. However our model may still be stiff with the time scale for tumour recession during treatment potentially being much quicker than the time scale of tumour growth during the rest phase. So as before we optimise our adaptive time stepping for stiff systems. Furthermore, we will prescribe a maximum step size in our quadrature method to ensure that each therapy application is always resolved.

5.2.7 Analysis of Parameters

We now use the findings of our parameter estimation in Section 5.2.4 to make an initial estimate of the new parameters which are present in this model but absent from the

previous one. We will then vary each parameter in turn and see how this affects the resulting behaviour of our model (results not shown). This analysis of parameters will allow us to identify the crucial parameters which determine how our tumour responds to chemotherapy, and how the tumour depends upon these parameters. It will also allow us to assign clinically relevant, and interesting, values to the new parameters.

We begin our analysis of parameters by making an initial estimate of the new parameters in our model. We choose the parameters concerning the switching function for chemotherapy delivery so that it exhibits similar behaviour to the switching functions for nutrient delivery, and we initially consider a treatment schedule where treatment is applied once a fortnight.

In our parameter estimation of Section 5.2.4 we found that if a continuous application of chemotherapy is to be effective at targeting endothelial cells, then we require $\kappa_2 > 1$. Given this we anticipate that for a therapy being applied once a fortnight to be effective at targeting endothelial cells we will require that $\kappa_2 \gg 1$. In Section 5.2.4 we also found that κ_1 should be approximately one fifth of the size of κ_2. Guided by this we make the initial estimate of the new parameter values outlined in Table 5.2.

Parameter	Description	Value
κ_1	Sensitivity of proliferating cells to chemotherapy	5
κ_2	Sensitivity of endothelial cells to chemotherapy	25
The rest period	The rest period between therapies	13 days
α_4	Critical level of vasculature for chemotherapy	10
w_4	Sensitivity of chemotherapy delivery to vasculature	1

Table 5.2: The initial values of the non-dimensional parameters pertaining to chemotherapy used in our analysis of parameters.

Altering κ_1

We begin by altering κ_1, which denotes the sensitivity of proliferating cells to chemotherapy, and in particular we consider the values $\kappa_1 = 0$, 1, 5, 25, and 100 and investigate the long time behaviour of our model. We then consider the evolution of our 25% growth fraction tumour with the parameter values given in Table 4.2 for these values of κ_1 and the values of the other parameters given in Table 5.2.

Taking $\kappa_1 = 5$ did not significantly impair the growth of the tumour. Upon each application of the therapy the tumour volume decreased, but recovered to the pre-application volumes during the rest phase. It was also found that each application of therapy had only a minimal effect on the endothelial cell population. So during each application of the therapy the population of proliferating cells was significantly reduced, but with a functional vasculature still present the remaining quiescent cells quickly recovered the ability to proliferate and the tumour recovered and continued to grow during the rest phase.

Increasing the value of κ_1, so that the therapy becomes more potent at targeting the proliferating cells, increased the magnitude of the recession the tumour underwent upon each application of the therapy, to a point, but the tumour could still fully recover during the rest phase and tumour cure, or even maintenance, was not achieved even when $\kappa_1 = 100$.

However, taking $\kappa_1 = 0$, so that the proliferating cells were unaffected by the chemotherapy, led to significant tumour regression and this was driven by regression of the endothelial cells. In particular the endothelial cell population underwent significant regression when $\kappa_1 = 0$, but no significant endothelial cell regression was observed when $\kappa_1 \geq 10$. This is highly counterintuitive and we will consider the reasons for this is more detail in Section 5.2.8.

Altering κ_2

We now alter κ_2, which denotes the sensitivity of endothelial cells to chemotherapy. Recalling that we found in Section 5.2.4 that κ_2 should be approximately fives times larger than κ_1 and also recalling the range of values of κ_1 just used we consider the values $\kappa_2 = 0$, 10, 25, 50, and 250 with our 25% growth fraction tumour and the values of the other parameters as given in Table 5.2. It is found that altering κ_2 across these values had only a slight effect on the tumour. In particular the only discernible effect occurred when $\kappa_2 = 250$, where tumour recession was observed and this was driven by a recession of the endothelial cells. Hence when $\kappa_1 = 5$, κ_2 must be taken very large ($\kappa_2 = 250$) for endothelial driven tumour recession to occur, but when $\kappa_1 = 0$, κ_2 could be taken much smaller ($\kappa_2 = 25$) for endothelial driven tumour recession to occur. Again, this is highly counterintuitive and we will consider the reasons for this in Section 5.2.8.

Altering α_4

We now alter α_4, which is the critical level of vasculature in the chemotherapy delivery switch. Recalling that in Section 4.4.4 of the previous chapter we took the critical levels of vasculature in the switching functions for tumour growth to be $\alpha_1 = \alpha_3 = 10$ we anticipate that α_4 should be of a comparable magnitude and consider a range of values of similar order, namely $\alpha_4 = 1$, 5, 10, 20, and 50. Then for these values of α_4, and the other parameter values as given in Table 5.2 for our 25% growth fraction tumour we find that altering α_4 had a significant effect on the tumour, with larger values of α_4 leading to more tumour regression during each therapy application. By extracting measures of the quality of the vasculature and the corresponding values of the switching functions from our results we find that altering α_4 does not significantly alter the quality of the local vasculature and instead it merely alters the value of the chemotherapy delivery switching function so that more or less therapy reaches the tumour.

Altering w_4

Considering the values $w_4 = 0.1$, 0.3, 1, 3, and 10, where w_4 denotes the sensitivity of the chemotherapy delivery switch, and other parameter values as given in Table 5.2 for our 25% growth fraction tumour we find that altering the value of w_4 had a negligible effect on the tumour.

Altering the Duration of the Rest Phase

To alter the duration of the rest phase between therapies we considered applying the therapy continuously with no rest phase, applying the therapy once a week, once a fortnight, once a month, and once every six months, with the other parameter values as given in Table 5.2 for our 25% growth fraction tumour. We found that decreasing the rest phase of the therapy increased its effectiveness; however this was to be expected because in a fixed time period more therapy is applied. Tumour cure was only possible with a continuous therapy, and when tumour cure was not observed a shorter rest period slowed the tumour growth to a greater extent than a longer rest period.

Altering the Tumour Growth Fraction

Considering the parameter values corresponding to the 10%, 25%, and 40% growth fraction tumours as given in Table 4.2 of the previous chapter and other parameter values as given by Table 5.2 it was found that increasing the tumour growth fraction caused the tumour to undergo greater regression upon each application of the therapy. This is because each application of the therapy can target a higher proportion of the tumour in higher growth fraction tumours. However for all the tumours of different growth fractions the tumour completely recovered during the rest phase and whether or not tumour cure could be achieved did not depend significantly upon the growth fraction of the tumour.

Conclusions

Our analysis of parameters has found that the value of α_4, which denotes the critical level of vasculature in the chemotherapy delivery switch, is important, but it is assumed that chemotherapy delivery should saturate at the same quality of vasculature as oxygen and nutrient delivery. We also found that the value of w_4, which denotes the sensitivity of the chemotherapy delivery switch, does not appear to be significant, although again we would expect that chemotherapy delivery should behave similarly to oxygen and nutrient delivery.

We have also found that the tumour depends strongly upon the duration of the rest phase between therapies, with shorter rest phases leading to a more successful therapy. However, in a constant time period therapies with shorter rest periods will deliver more drug than therapies with longer rest periods, and would therefore be expected to be more toxic. Hence when altering the duration of the rest phase care should be taken to ensure that comparably toxic therapies are investigated. We will consider this in more detail in Section 5.3 where we consider the Norton-Simon hypothesis.

We have also found that our tumour depends strongly upon both the chemotherapy kill rates, κ_1 and κ_2. Furthermore, we have found that for some values of κ_1 and κ_2 tumour treatment is driven by endothelial cell recession and for other parameter values it is driven by proliferating cell recession. This suggests that there are at least two distinct mechanisms of tumour treatment and that which of these mechanisms takes effect strongly depends upon the relative strength of the therapy at targeting the proliferating and endothelial cells. We consider this in more detail in the next section.

5.2.8 Jointly Altering the Chemotherapy Kill Rates

To consider the joint sensitivity of our tumour to the chemotherapy kill rates, κ_1 and κ_2, we now consider the final dimensional volume of tumour cells within the tumour, as defined by $\frac{\{3(P+Q)+1.5N\}}{0.66}10^{-6}\,\text{mm}^3$, upon completion of the tenth application of the therapy, where the therapy is applied once a week, for the range of parameters $0 \leq \kappa_1 \leq 10$ and $0 \leq \kappa_2 \leq 50$, and the other parameter values as given in Table 5.2. The results of which are shown in Figure 5.1.

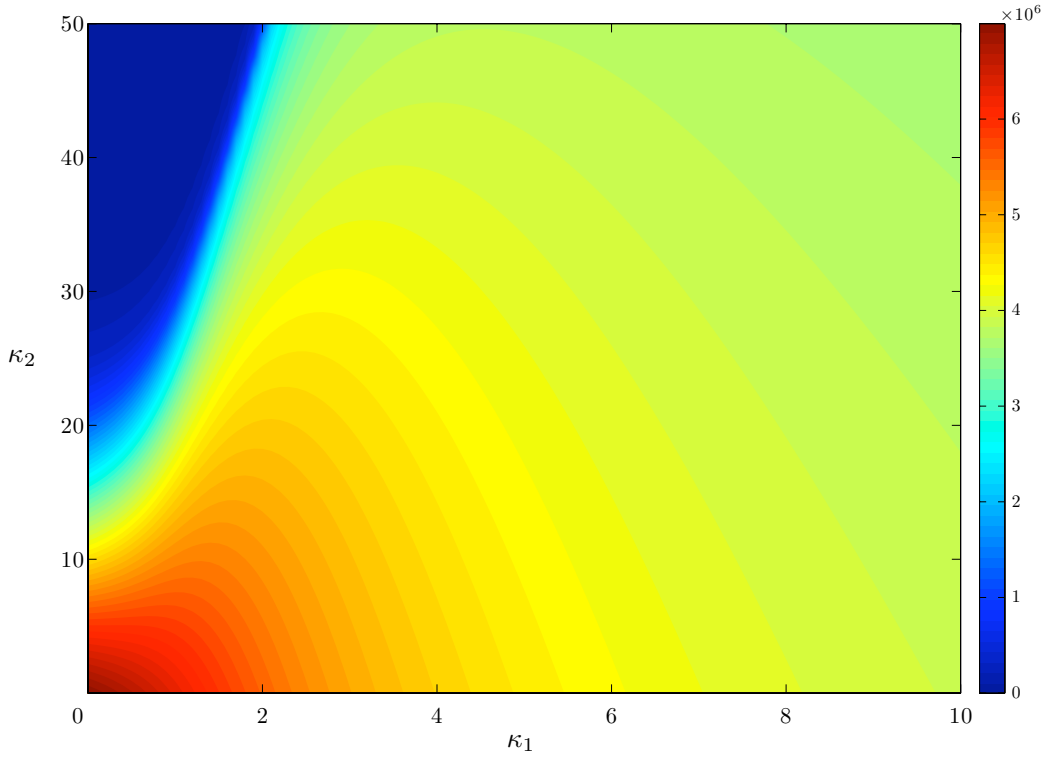

Figure 5.1: The volume of our modelled 25% growth fraction tumour (in mm^3) upon completion of the tenth application of chemotherapy, as a function of the chemotherapy kill rates κ_1 and κ_2 for the parameter values given in Table 5.2, as governed by Equations (5.2) to (5.6).

It can be seen that tumour cure is possible when κ_1 is very small and κ_2 is large, even though for such parameter values the therapy is very poor at targeting the tumour cells. Therapy failure is observed when κ_1 and κ_2 are both very small so that the chemotherapy is poor at targeting either cell population, as would be expected, and tumour inhibition and possibly maintenance is observed when κ_1 and κ_2 are both

large, so that the chemotherapy is good at targeting both cell populations. Whatever the value of κ_1 increasing κ_2 provides a more effective therapy. However, for low values of κ_1, increasing κ_1 can make the therapy less effective and can even lead to therapy failure; whereas for high values of κ_1, increasing κ_1 makes the therapy more effective. This mutual dependency of the model upon the parameters κ_1 and κ_2 suggests that there are at least two distinct mechanisms by which the therapy can treat the tumour, and we now identify these mechanisms.

Using the Therapy as a Traditional Chemotherapeutic

We begin by considering the model when both κ_1 and κ_2 are large and the therapy appears to be providing some maintenance effect, but not curing the tumour. The growth curves of the cell populations until the end of the fifth application of therapy for $\kappa_1 = 10$, $\kappa_2 = 30$, and the other parameter values as given by Table 5.2, are shown in Figure 5.2. It can be seen that each application of the therapy heavily reduces the population of live tumour cells, but the endothelial cell population does not reduce in volume. At the end of each application of the therapy, the functional remaining vasculature allows the tumour to regrow and do so quickly.

For these parameter values the therapy is targeting the live tumour cells and the endothelial cells are not successfully targeted; hence the therapy acts like a traditional chemotherapeutic.

The perceived success of the therapies with high values of κ_1 and κ_2 in Figure 5.1 is due to sampling the tumour at the end of an application of therapy. If the success of the therapy was instead measured by considering the tumour volume at the end of the rest phase, then this therapy would be considered to be failing.

Using the Therapy to Exploit an Angiogenesis-Therapy Feedback Loop

We now consider the behaviour of the tumour when κ_1 is small and κ_2 is large, so that the therapy is relatively poor at targeting the tumour cells but relatively good at targeting the endothelial cells, and tumour cure is observed. The corresponding growth curves of the cell populations until the end of the tenth application of therapy for $\kappa_1 = 1$ and $\kappa_2 = 30$ and the other parameter values as given in Table 5.2 are shown in Figure 5.3. It can be seen that each application of the therapy provides a more modest reduction in each of the tumour cell compartments than when the

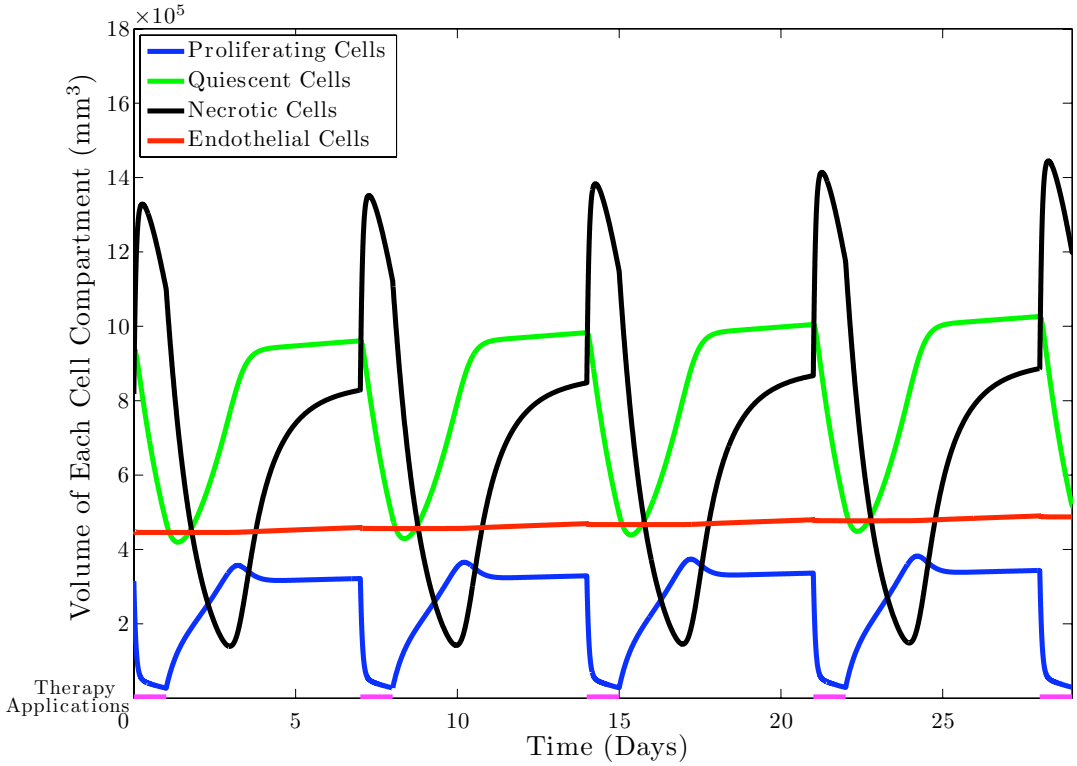

Figure 5.2: The evolution of our modelled 25% growth fraction tumour when the chemotherapy kill rates are $\kappa_1 = 10$ and $\kappa_2 = 30$, and the other parameter values are as given in Table 5.2, as governed by Equations (5.2) to (5.6). The times during which the therapy is being applied are highlighted in purple along the time axis.

therapy was acting as a traditional chemotherapeutic, but for these parameter values the endothelial cell compartment is successfully being targeted by each application of the therapy. This is despite the strength of the therapy as an anti-angiogenic therapy, κ_2, being the same as when the therapy acted as a traditional chemotherapeutic in Figure 5.2.

This therapy can provide a successful anti-angiogenic effect where the previous one could not, and this is despite both therapies having the same value of κ_2, which is the sensitivity of the endothelial cells to chemotherapy. This happens because this therapy is less effective at targeting the tumour cells than the endothelial cells and so the first application of therapy eradicates a greater proportion of the endothelial cells than the tumour cells. This serves to undervascularise the tumour and then the tumour responds by upregulating angiogenesis which causes the endothelial cells to proliferate more quickly than before. With more endothelial cells proliferating the

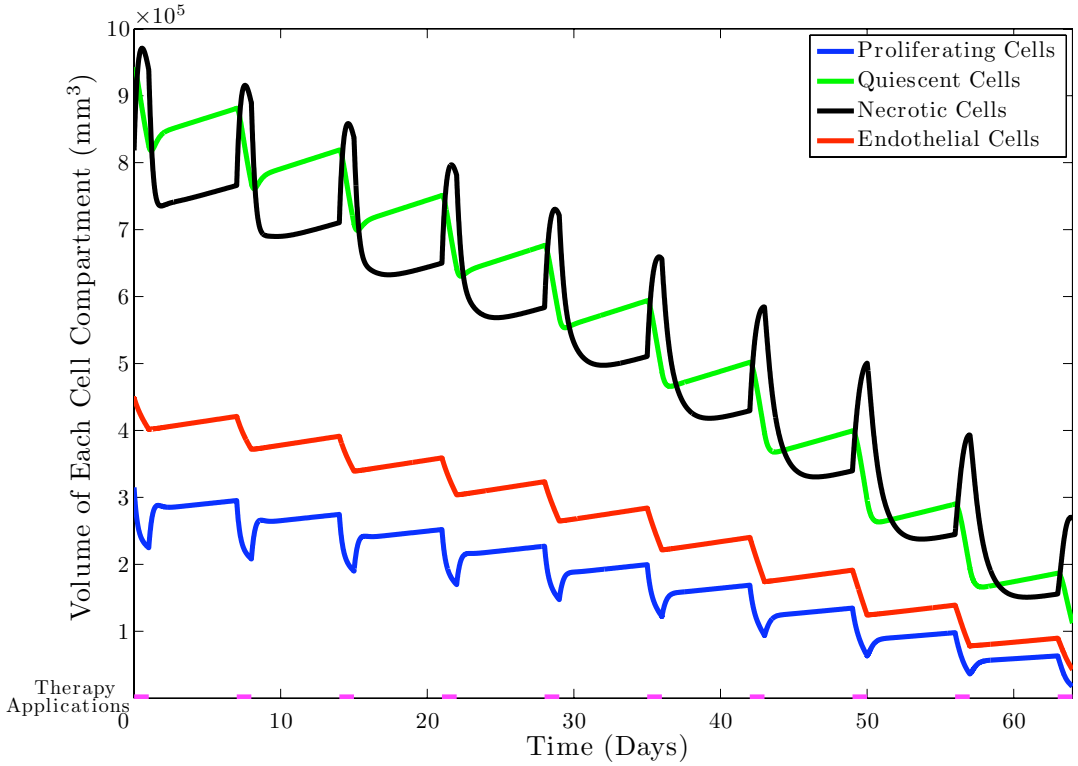

Figure 5.3: The evolution of our modelled 25% growth fraction tumour when the chemotherapy kill rates are $\kappa_1 = 1$ and $\kappa_2 = 30$, and the other parameter values are as given in Table 5.2, as governed by Equations (5.2) to (5.6). The times during which the therapy is being applied are highlighted in purple along the time axis.

Norton-Simon hypothesis implies that the second application of therapy will be even more effective at targeting the endothelial cells than the first, which then further undervascularises the tumour. Angiogenesis will then continue to be upregulated so that the third application of therapy will also be more effective at targeting the endothelial cells. Hence this therapy is exploiting an angiogenesis-therapy feedback loop where the therapy is more effective at targeting the endothelial cells than the tumour cells because each application of this therapy undervascularises the tumour, which then upregulates angiogenesis, which then primes the tumour for the next application of endothelial cell targeting therapy. This is why each application of the therapy in Figure 5.3 can be seen to provide a slightly increased endothelial cell kill than the previous therapy. Even though this therapy exploits the angiogenesis-therapy feedback loop and does not target the tumour cells directly, a reduction in the tumour population is still observed because the lack of endothelial cells starves

the tumour of nutrients and oxygen and the tumour reduces in size.

The fact that this therapy provides an effective anti-angiogenic effect, even though its strength as an anti-angiogenic, κ_2, is the same as the therapy which acted as a traditional chemotherapeutic highlights that the critical factor is not the anti-angiogenic strength of the therapy, but the relative strength of the therapy at targeting the endothelial cells compared to the tumour cells.

Comparing Figure 5.2 to Figure 5.3 we see that when the therapy exploits the angiogenesis-therapy feedback loop the tumour recovers more slowly during the rest phase than when the therapy acted as a traditional chemotherapeutic. When the therapy exploits the angiogenesis-therapy feedback loop it is targeting the tumour's vasculature, which results in the tumour being relatively undervascularised at the end of each application. Hence when the tumour regrows during the rest phase it does so at the rate of angiogenesis. When the therapy previously acted as a traditional chemotherapeutic the tumour was overvascularised at the end of each therapy application. So when the tumour regrew during the rest phase it did so at a rate approaching the potential doubling rate of the tumour, which is quicker than the rate of angiogenesis. For our rest period of six days the tumour almost completely regrew when the therapy acted as a traditional chemotherapeutic, but does not completely regrow when the therapy exploited the angiogenesis-therapy feedback loop.

5.2.9 Conclusions

So far we have successfully added chemotherapy into our previous model for vascular tumour growth and performed an analysis of parameters. Our analysis of parameters has found that there are two distinct mechanisms by which the therapy can treat the tumour. The therapy can either act as a traditional chemotherapy whereby the tumour cells are targeted, or it can exploit the angiogenesis-therapy feedback loop whereby the endothelial cells are targeted. The analysis of parameters also highlighted the potential of using chemotherapy to exploit the angiogenesis-therapy feedback loop. When varying the chemotherapy kill rates, κ_1 and κ_2, the therapy was most effective when targeting the endothelial cells. This was primarily because when the therapy exploits the angiogenesis-therapy feedback loop there is a compounding effect whereby each application of the therapy treats the tumour, but also primes the tumour for the next application of therapy. Furthermore, the tumour recovers more slowly following

a therapy which exploits the angiogenesis-therapy feedback loop than a traditional chemotherapeutic, which also contributes to such therapies being more effective.

Note that although our therapy is nominally referred to as a chemotherapy, and we have demonstrated the potential of using chemotherapy to provide an anti-angiogenic effect, parameters could equally be chosen so that the therapy is specifically an anti-angiogenic therapy, rather than a chemotherapy which can provide an anti-angiogenic therapy.

Regarding parameter values, we now find parameters for which the therapy acts as a traditional chemotherapeutic, and for which the therapy exploits the angiogenesis-therapy feedback loop. We have found that the value of α_4, which denotes the critical level of vasculature in the chemotherapy delivery switch, is important, but it is expected that chemotherapy delivery should saturate at the same level of vasculature as oxygen and nutrient delivery. We also found that the value of w_4, which denotes the sensitivity of the chemotherapy delivery switch, does not appear to be significant, although again we expect chemotherapy delivery to behave similarly to oxygen and nutrient delivery. The results of Figure 5.1 allow us to identify parameter values where the therapy acts as a traditional chemotherapy, presented in Table 5.3, and parameter values where the therapy exploits the angiogenesis-therapy feedback loop, presented in Table 5.4.

Parameter	Description	Value
κ_1	Sensitivity of proliferating cells to chemotherapy	10
κ_2	Sensitivity of endothelial cells to chemotherapy	30
The rest period	The rest period between therapies	13 days
α_4	Critical level of vasculature for chemotherapy	10
w_4	Sensitivity of chemotherapy delivery to vasculature	1

Table 5.3: Non-dimensional parameter values for which the therapy acts as a traditional chemotherapeutic when treating the 25% growth fraction tumour.

Finally, we also found that reducing the rest phase between the applications gives a more effective therapy, which appears to be consistent with the Norton-Simon hypothesis. We consider this in more detail in the next section.

Parameter	Description	Value
κ_1	Sensitivity of proliferating cells to chemotherapy	1
κ_2	Sensitivity of endothelial cells to chemotherapy	30
The rest period	The rest period between therapies	13 days
α_4	Critical level of vasculature for chemotherapy	10
w_4	Sensitivity of chemotherapy delivery to vasculature	1

Table 5.4: Non-dimensional parameter values for which the therapy exploits the angiogenesis-therapy feedback loop when treating the 25% growth fraction tumour.

5.3 The Norton-Simon Hypothesis

We now consider whether our model provides a framework which agrees or disagrees with the Norton-Simon hypothesis, which states that dose dense therapy schedules provide more effective cell kill than dose sparse therapies. In particular we will investigate this for a therapy which acts as a traditional chemotherapeutic, and also for a therapy which exploits the angiogenesis-therapy feedback loop, and we will also study it for discrete applications of therapy with a varying rest phase, and a continuous application of therapy of varying length.

5.3.1 The Norton-Simon Hypothesis for a Discrete Therapy

We begin by considering the case where discrete applications of therapy are applied and in particular we begin by considering a therapy which acts as a traditional chemotherapeutic.

A Therapy which Acts as a Traditional Chemotherapeutic

To consider the Norton-Simon hypothesis for a discrete therapy which acts as a traditional chemotherapeutic we take parameters pertaining to our 25% growth fraction tumour, as given in Table 4.2, and the therapy parameter values given in Table 5.3, except for the duration of the rest phase which is being varied. To quantify the effectiveness of the therapy we consider the total volume of the tumour cells, as defined by $\frac{\{3(P+Q)+1.5N\}}{0.66}10^{-6}\,\mathrm{mm}^3$, upon completion of the tenth application of therapy. The

final size of the tumour as a function of the rest phase for the 25% growth fraction tumour when the therapy acts as a traditional chemotherapeutic is shown in Figure 5.4.

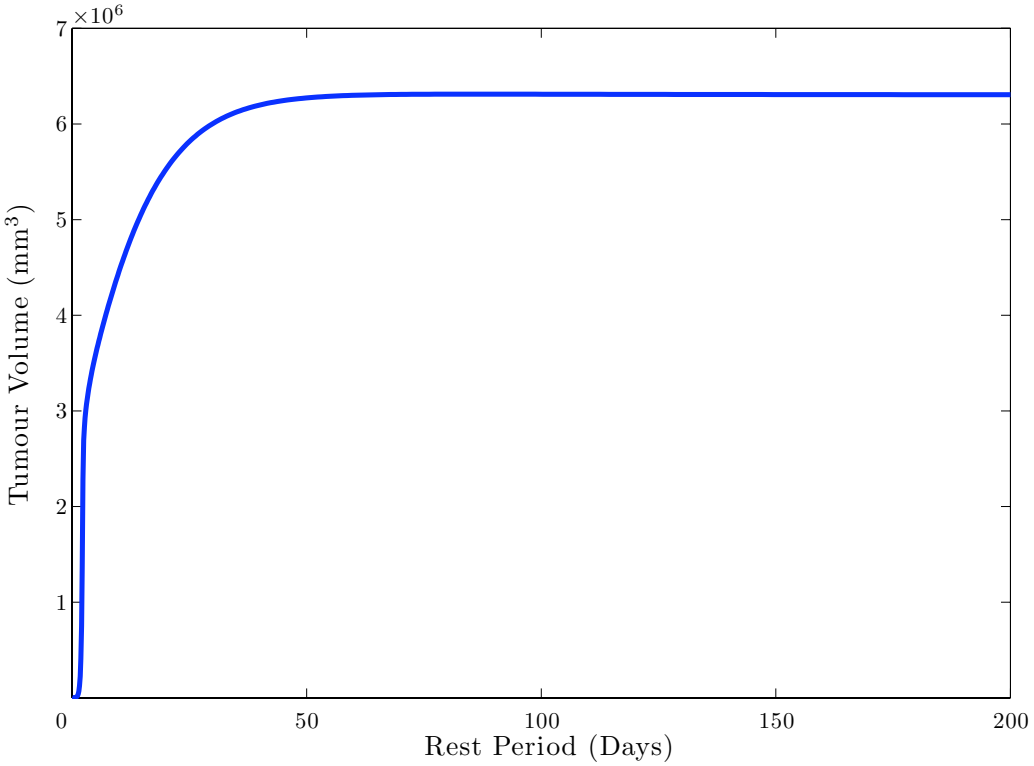

Figure 5.4: The volume of our modelled 25% growth fraction tumour upon completion of the tenth discrete application of chemotherapy, as a function of the rest period between therapy applications for the other parameter values given in Table 5.3, as governed by Equations (5.2) to (5.6). Plot generated for a large number of discrete values of the rest period and then linearly interpolated.

It can be seen in Figure 5.4 that dose dense therapies lead to smaller tumours than dose sparse therapies and by examining the growth curves of the tumour and endothelial cell populations, such as those shown in Figure 5.5 where the rest period is one day, we see that the chemotherapy acts as a traditional chemotherapeutic and targets the proliferating cells, rather than having any anti-angiogenic effect. Upon examining the tumour growth curves we find that the tumour undergoes significant cell kill during each application of the therapy, but then regrows during the rest phase. By shortening the rest phase between applications of therapy the amount the tumour regrows during the rest phase is reduced and overall a smaller tumour is observed.

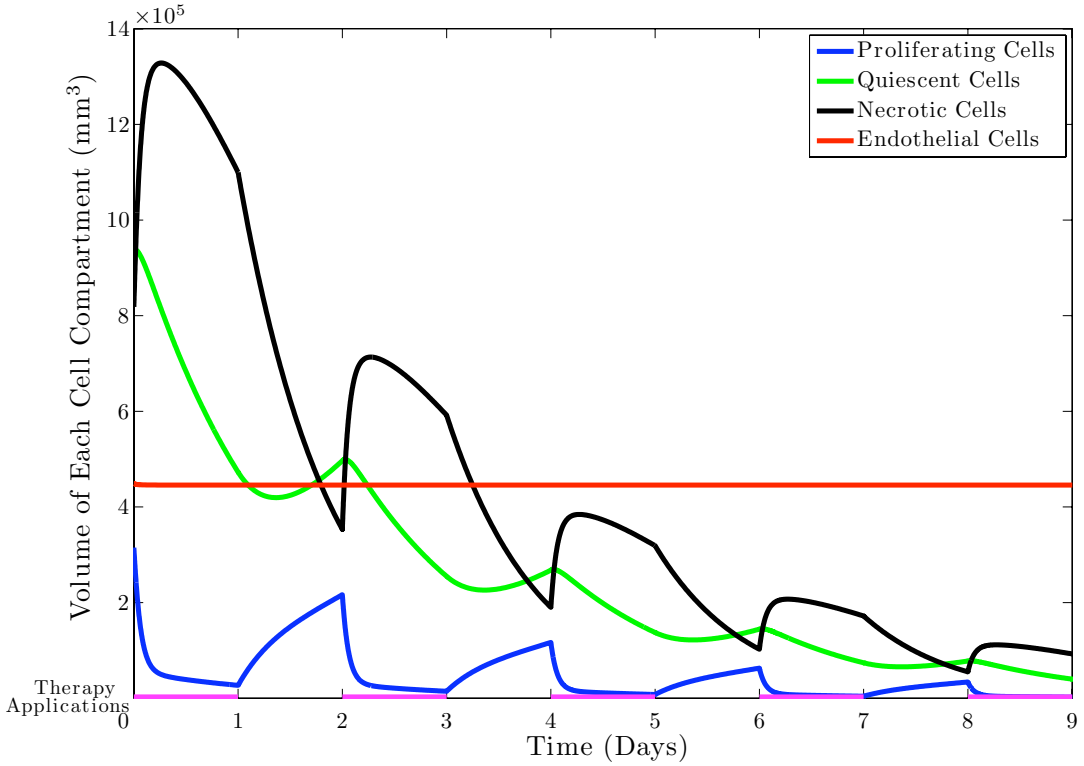

Figure 5.5: The evolution of our modelled 25% growth fraction tumour when the rest period between applications of the therapy is one day for the other parameter values given in Table 5.3, as governed by Equations (5.2) to (5.6). The times during which the therapy is being applied are highlighted in purple along the time axis.

Furthermore, it can also be seen in Figure 5.4 that therapies with rest periods of less than two days are dramatically more effective than therapies with slightly longer rest periods. The reason for this can be understood by considering the evolution of the tumour for a rest period of one day, which is shown in Figure 5.5, where it can be seen that whilst each application of the therapy provides near eradication of the proliferating cells, the quiescent cells are less affected by the therapy. Each application of therapy lasts one day, which is only slightly longer than the cell cycle time of our tumour cells, and so a single dose of the therapy can target the proliferating cells within the tumour, but is not applied for long enough for a significant proportion of the quiescent cells to be recruited into a proliferative state and then targeted by the therapy.

At the end of the therapy application there remains a large bank of quiescent cells in the tumour, some of which are immediately recruited back into the cell cycle. If

another application of therapy is applied when some of the quiescent cells have been recruited back into the cell cycle, but significant cell proliferation has not yet occurred, then some of the quiescent cells remaining in the tumour after the first therapy can be targeted by the second therapy without the tumour recovering significantly and a more effective therapy is obtained.

Having considered the Norton-Simon hypothesis for a discrete therapy when the therapy acts as a traditional chemotherapeutic, we now consider the case where the therapy exploits the angiogenesis-therapy feedback loop.

A Therapy which Exploits the Angiogenesis-Therapy Feedback Loop

To consider the Norton-Simon hypothesis for a discrete therapy which exploits the angiogenesis-therapy feedback loop we take parameters pertaining to our 25% growth fraction tumour, as given in Table 4.2, and the therapy parameter values as given in Table 5.4, except for the duration of the rest phase which is being varied. Since this therapy exploits the angiogenesis-therapy feedback loop to provide an anti-angiogenic effect we will measure the effectiveness of this therapy by considering the evolution of both the tumour volume and the volume of endothelial cells in the tumour. The final size of the tumour, as defined by $\frac{\{3(P+Q)+1.5N\}}{0.66}10^{-6}\,\text{mm}^3$, and the final size of the endothelial cell population in the tumour as functions of the rest phase for the 25% growth fraction tumour when the therapy exploits the angiogenesis-therapy feedback loop are shown in Figure 5.6.

In Figure 5.6 it can be seen that again dose dense therapies lead to smaller tumours than dose sparse therapies and by examining the growth curves of the tumour and endothelial cell population in detail (results not shown) it can be confirmed that the therapy is exploiting the angiogenesis-therapy feedback loop. The growth curves also show that during each application of therapy the endothelial cells undergo significant regression and that this causes a corresponding regression of the tumour cells. Both cell populations then regrow during the rest phase. By shortening the rest phase between therapies the amount of tumour regrowth before the next application of therapy is reduced and overall a smaller tumour is observed. However, extremely intense therapy schedules with rest periods of less than a day are observed to perform worse than therapy schedules with a slightly longer rest period and investigating the growth curves of the tumour and endothelial cell populations in detail (results not shown) it is found that such intense therapies begin to become more potent

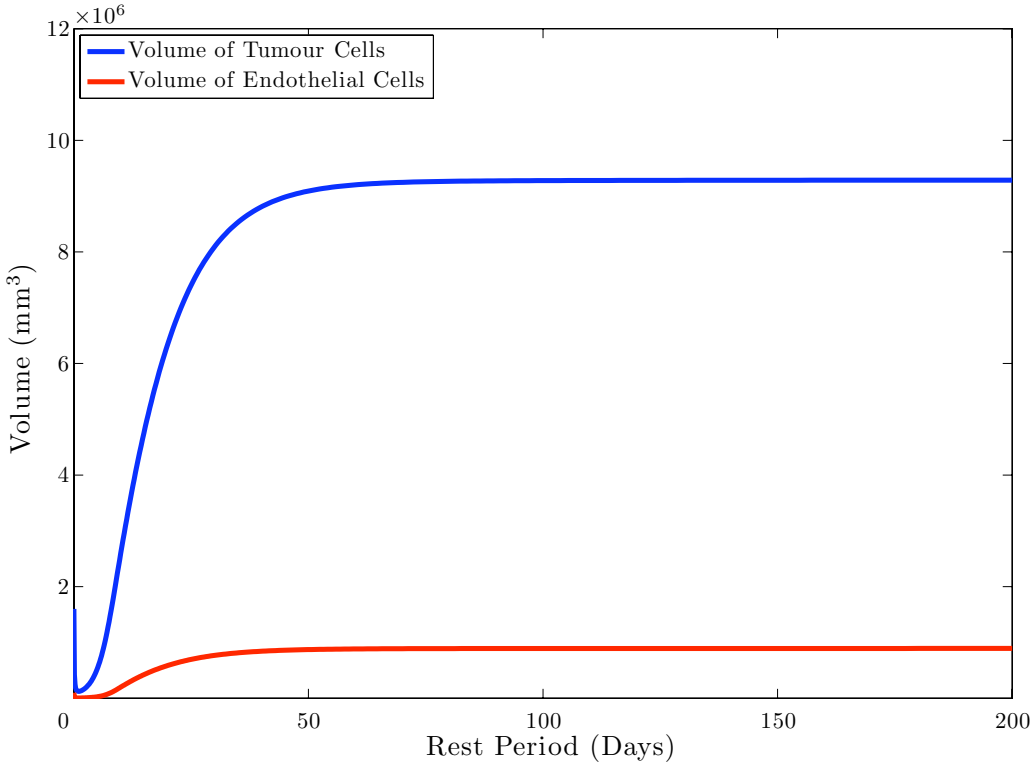

Figure 5.6: The volume of our modelled 25% growth fraction tumour and the corresponding endothelial cell population, upon completion of the tenth application of discrete chemotherapy, as a function of the rest period between therapy applications, for the other parameter values given in Table 5.4, as governed by Equations (5.2) to (5.6). Plot generated for a large number of discrete values of the rest period and then linearly interpolated.

as traditional chemotherapeutics, which actually limits their ability to successfully exploit the angiogenesis-therapy feedback loop.

Comparing Figure 5.4 to Figure 5.6 it can be seen that the therapy which exploits the angiogenesis-therapy feedback loop is effective over a wider range of rest phases than the therapy which acts as a traditional chemotherapeutic, however when the therapies are ineffective the traditional chemotherapeutic results in a smaller tumour that the therapy which exploits the angiogenesis-therapy feedback loop.

The reason that the therapy which exploits the angiogenesis-therapy feedback loop is effective over a wider range of rest phases is that during an application of such a therapy the tumour cells are more intensively targeted than the endothelial cells so that at the end of the therapy the tumour is relatively overvascularised. The tumour then

recovers by undergoing cell proliferation and since the tumour is relatively overvascularised this happens on a time scale approaching the potential doubling rate of the tumour. During an application of the therapy which exploits the angiogenesis-therapy feedback loop the vasculature is targeted directly. This then starves the tumour and leads to tumour regression so that at the end of the therapy the tumour is averagely well vascularised. The tumour then recovers on the time scale of normal vascular tumour growth, which is slower than the time scale of recovery following a therapy which acts as a traditional chemotherapeutic. Since the tumour recovers more slowly following the therapy which exploits the angiogenesis-therapy feedback loop a longer rest phase can be taken between therapies.

We now consider the reason that when both therapies are ineffective the traditional chemotherapeutic results in a smaller tumour than the therapy which exploits the angiogenesis-therapy feedback loop. Even when both therapies are ineffective at treating the tumour there is still some pruning of the tumour during the application of therapy. The traditional chemotherapeutic prunes the live cells in the tumour, whereas the angiogenesis-therapy feedback loop targeting therapy prunes the endothelial cells in the tumour. Hence the traditional chemotherapeutic can prune a greater proportion of the tumour and immediately following an application of the therapy the traditional chemotherapy results in a smaller tumour than the angiogenesis-therapy feedback loop exploiting therapy. Since Figures 5.4 and 5.6 sample the tumour at the end of an application of therapy, the tumour which results from an ineffective traditional chemotherapeutic appears to be smaller than the tumour which results from an ineffective angiogenesis-therapy feedback loop targetting therapy. This is for the reasons outlined above and if these results are re-considered at the end of a rest phase, after the tumour has recovered from any temporary pruning, the two therapies result in exactly the same size tumour when ineffective (results not shown).

For both therapy mechanisms we have found the length of the rest phase to be fundamental to the success of the therapy and therapies which are dense enough to have a compounding affect whereby the next application of therapy is applied before the tumour had completely recovered from the previous application are particularly successful. Since we have found dense therapies to be most successful, we now consider the effectiveness of a longer single application of therapy and consider the Norton-Simon hypothesis for a continuous therapy.

5.3.2 The Norton-Simon Hypothesis for a Continuous Therapy

We now consider the optimal duration for a therapy by investigating the Norton-Simon hypothesis for continuous therapies. In this investigation we consider a continuous therapy of length T^* days and of non-dimensional concentration $\frac{10 \text{ days}}{T^* \text{ days}}$. Then the total amount of therapy applied is constant and the continuous therapy lasting ten days will be equivalent to the application with no rest phase in the previous discrete case. Note that for extremely dose dense therapy schedules, with short delivery times and high chemotherapy concentrations, the effect of the chemotherapy would eventually be expected to saturate which invalidates our assumption that the rate of cell kill increases linearly with therapy concentration. So for extremely dose dense therapies we would expect a clinical tumour to respond more poorly than our modelled tumour.

A Therapy which Acts as a Traditional Chemotherapeutic

To consider a continuous therapy which acts as a traditional chemotherapeutic we take parameter values pertaining to our 25% growth fraction tumour, as given in Table 4.2, and the therapy parameter values as given in Table 5.3, except for the duration of the rest phase which is set to zero. Again we use tumour size, as defined by $\frac{\{3(P+Q)+1.5N\}}{0.66} 10^{-6} \text{ mm}^3$, upon completion of the therapy as a measure of the effectiveness of the therapy. Doing this the relationship found between the therapy duration and tumour size at completion of the therapy is shown in Figure 5.7.

In Figure 5.7 it can be seen that for a large range of therapy durations, from approximately 10 days to 50 days, the therapy provides effective tumour cure. However if the therapy is denser than this, with a duration of less than 10 days or so, then the therapy becomes dramatically less effective. The reason for this can be understood by considering the evolution of the cell populations when the total therapy duration is shorter than ten days (results not shown) and it is found that if the therapy is applied for too short a duration then there is not sufficient time for all the live cells in the tumour to be recruited into the cell cycle and then be targeted. Hence the therapy can first provide cure when the therapy is applied for long enough for all the live cells to be recruited into an actively proliferating state and then targeted by the drug.

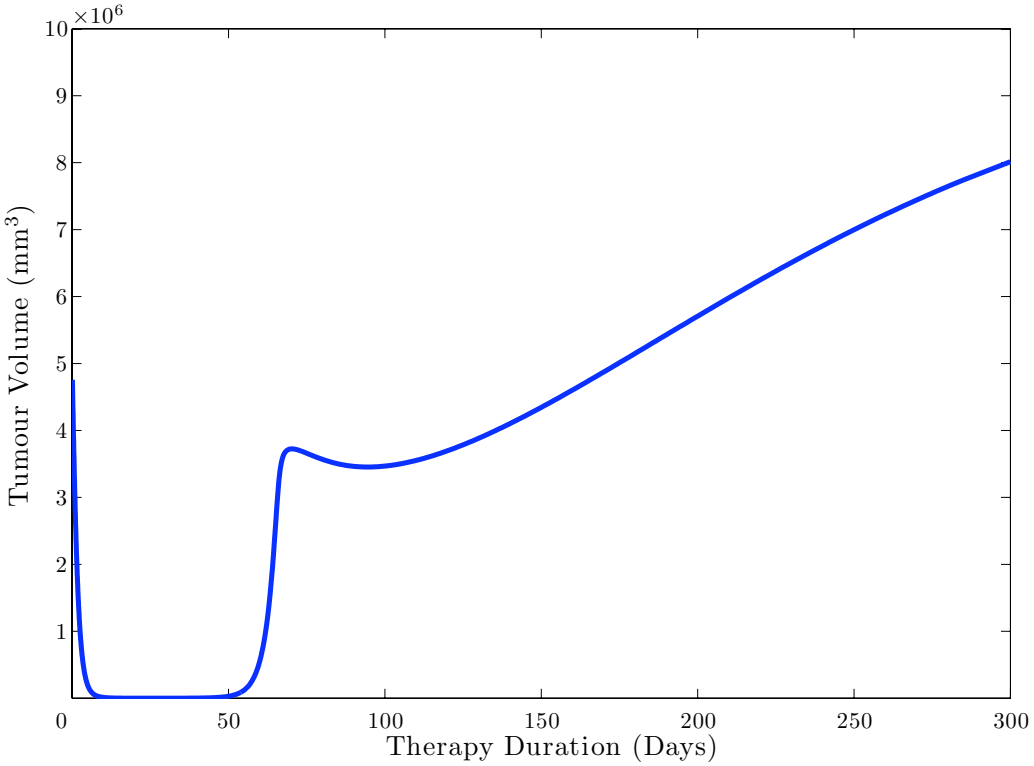

Figure 5.7: The volume of our modelled 25% growth fraction tumour upon completion of a continuous chemotherapy as a function of therapy duration, for the other parameter values given in Table 5.3, as governed by Equations (5.2) to (5.6). Plot generated for a large number of discrete values of therapy duration and then linearly interpolated.

If the therapy is applied for a duration of approximately 50 days or so, then increasing the duration of the therapy results in the therapy becoming significantly less effective. The reason for this is that the therapy concentration becomes too low and cell apoptosis is not upregulated significantly enough to cause tumour regression and instead growth is merely inhibited.

There is then a locally worst therapy duration of approximately 70 days before the therapy improves slightly with a locally best therapy duration at approximately 95 days. Increasing the therapy duration past this local optimum leads to a less successful therapy. The reason there is such a local best therapy duration is that this is the precise therapy duration at which the therapy can slightly exploit the angiogenesis-feedback loop and provide some growth inhibition. If the therapy exhibits absolutely no anti-angiogenic affect, so that $\kappa_2 = 0$, then the tumour volume at completion of

therapy as a function of the tumour duration exhibits no turning points outside the window where the therapy provides effective cure, as can be seen in Figure 5.8.

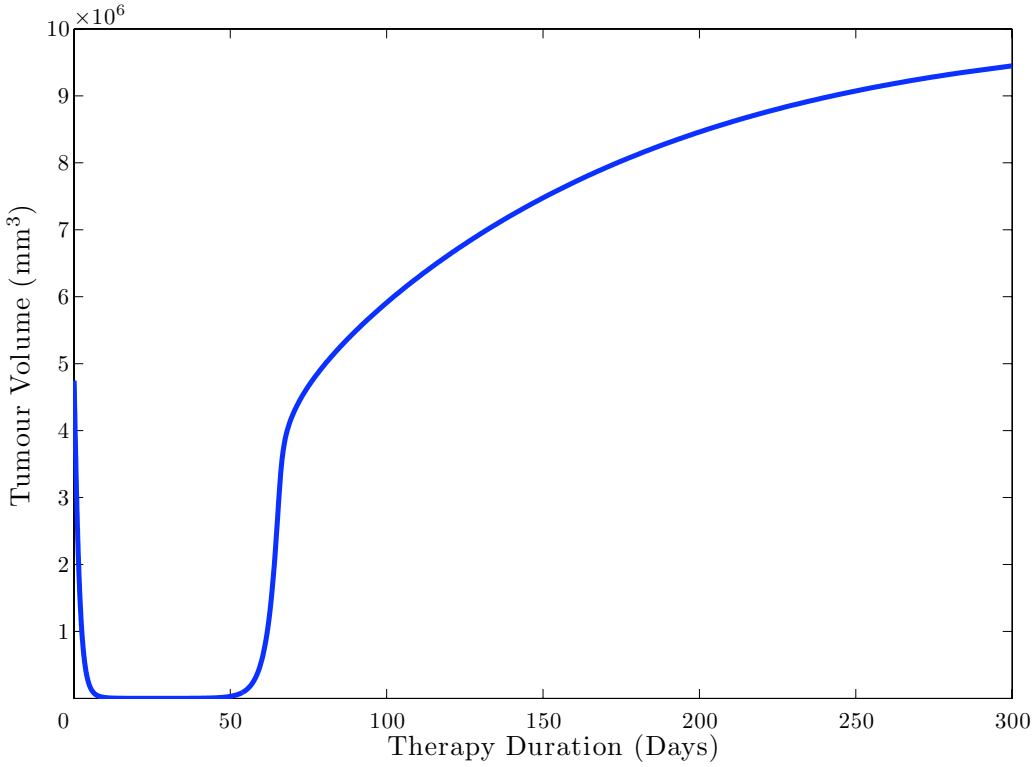

Figure 5.8: The volume of our modelled 25% growth fraction tumour upon completion of a continuous chemotherapy as a function of the therapy duration, for $\kappa_2 = 0$ and the other parameter values given in Table 5.3, as governed by Equations (5.2) to (5.6). Plot generated for a large number of discrete values of the therapy duration and then linearly interpolated.

A Therapy which Exploits the Angiogenesis-Therapy Feedback Loop

We now consider the Norton-Simon hypothesis for a continuous therapy which exploits the angiogenesis-therapy feedback loop by taking parameter values pertaining to our 25% growth fraction tumour, as given in Table 4.2, and the therapy parameters as given in Table 5.4, except for the duration of the rest phase which is set to zero. Doing this the relationship between the therapy duration and tumour volume, as defined by $\frac{\{3(P+Q)+1.5N\}}{0.66} 10^{-6}\,\mathrm{mm}^3$, and the volume of endothelial cells in the tumour upon completion of the therapy is shown in Figure 5.9.

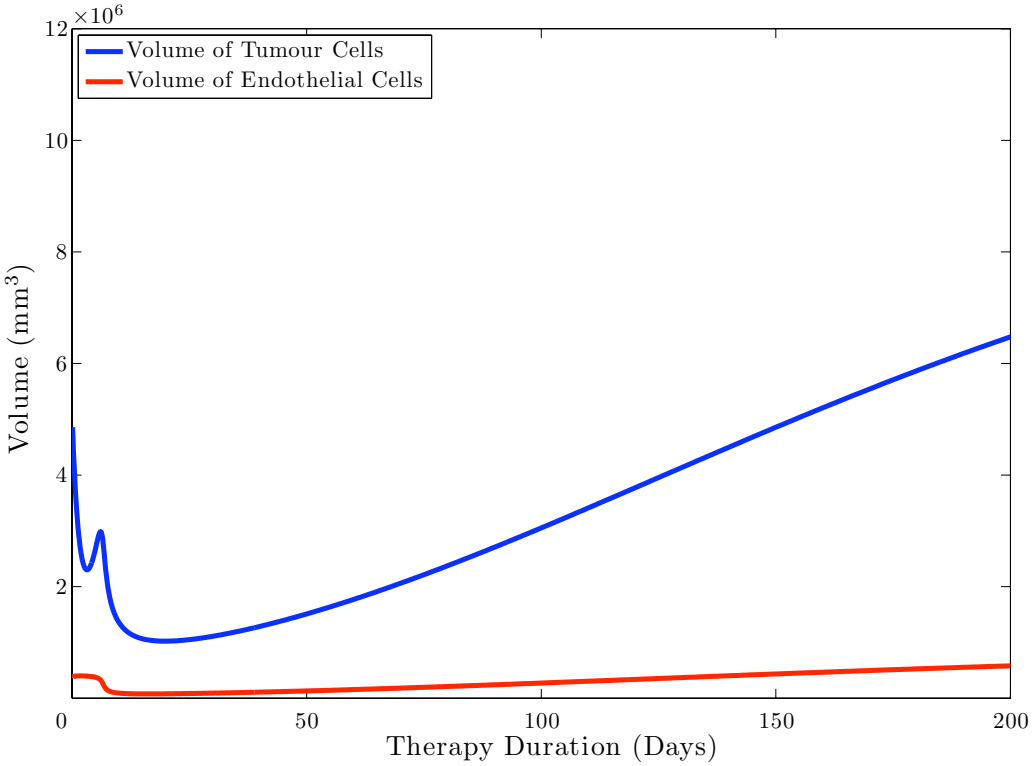

Figure 5.9: The volume of our modelled 25% growth fraction tumour and the corresponding endothelial cell population upon completion of the continuous chemotherapy as a function of the therapy duration for the other parameter values given by Table 5.4, as governed by Equations (5.2) to (5.6). Plot generated for a large number of discrete values of the therapy duration and then linearly interpolated.

Figure 5.9 exhibits some similarities to Figure 5.7. There is a local optimal therapy duration at approximately two days, and this is the duration for which the therapy actually inhibits tumour growth by acting as a traditional chemotherapeutic. If the behaviour between the final size and therapy duration is reconsidered when the therapy provides no cell kill of the tumour cells, so that $\kappa_1 = 0$, then this local optimal therapy duration is no longer present (result not shown). There is then a local worst therapy duration of length approximately 6 days, which is present because the therapy must fail as a traditional chemotherapeutic before it can exploit the angiogenesis-therapy feedback loop. The optimal therapy duration is approximately 20 days, which occurs when the therapy is at exploiting the angiogenesis-therapy feedback loop.

5.3.3 Conclusions

Our investigation largely validates the Norton-Simon hypothesis. For discrete therapy with a rest period inbetween applications of therapy, a dose dense therapy was generally more effective. This is true of both kill mechanisms and this is because a shorter rest phase allowed less regrowth between the applications of the therapy. However, really dense therapies with a rest phase of a few days or less were found to be significantly more effective.

For continuous therapies dose densing was again generally found to be more effective, except for therapies which were extremely dose dense and administered for a total duration of less than a few days. This is despite our modelled tumour being expected to respond better to extremely dense therapy schedules than a clinical tumour would because of saturation effects. The reason that very short duration therapies were ineffective was that to eradicate the tumour all the proliferating cells must be targeted and then all the remaining quiescent cells must gain the ability to proliferate and then be targeted. For this to have time to occur the therapy must be active for at least a couple of cell cycle times. Therapies with shorter durations than this are therefore ineffective.

This result explains the success of extremely dose dense discrete therapies. Each individual application of therapy is applied for too short a duration to recruit and then target the quiescent cells, but if the discrete therapy is significantly dense then the quiescent cells can be recruited and targeted by the next application of therapy and the discrete applications of therapy can effectively act like a longer continuous therapy.

Hence dose dense therapies are generally more effective, but it is critical that for a cell cycle specific therapy each application of the therapy must be effective for at least a couple of cell cycle times.

We also found that by altering the therapy duration, and hence concentration, with fixed total dose the therapy which nominally was a traditional chemotherapeutic could exploit the angiogenesis-therapy feedback loop and similarly the therapy which nominally exploits the angiogenesis-therapy feedback loop could act as a traditional chemotherapeutic. This highlights how non-trivial the relationship between the therapy acting as a traditional chemotherapeutic and exploiting the angiogenesis-therapy

feedback loop is. The fact that more intense therapies tended to act as a traditional chemotherapeutic, and less intense therapies tended to exploit the angiogenesis-therapy feedback loop highlights that to exploit the angiogenesis-therapy feedback loop it is not sufficient for the therapy to be better at targeting the endothelial cells than the tumour cells, it is actually necessary for the therapy to be sufficiently poor at targeting the tumour cells that it fails to significantly kill them, while retaining a significant anti-angiogenic activity.

Having shown that theoretically chemotherapy can treat the tumour by exploiting the angiogenesis-therapy feedback loop, we now attempt to recreate the results of an experimental paper exploring the anti-angiogenic influences of therapy.

5.4 Using Chemotherapy as an Angiogenesis Inhibitor

5.4.1 Introduction

In the previous section we found that chemotherapy can successfully treat a tumour by exploiting the angiogenesis-therapy feedback loop. One paper which considered the use of chemotherapy as an anti-angiogen is that of Browder et al. (2000), who showed that chemotherapy can significantly impair mice tumour growth, even if the tumour cells are resistant to therapy. Furthermore, a schedule of 170 mg/kg of chemotherapy every six days (which Browder et al. refer to as an anti-angiogenic schedule) was found to be more effective at treating both drug-sensitive and drug-resistant tumours compared to three doses of 150 mg/kg of chemotherapy every other day every twenty-one days (which Browder et al. refer to as a conventional schedule). We now attempt to reproduce these results with our model and consider what mechanisms cause the anti-angiogenic schedule to be more effective than the conventional schedule.

5.4.2 Modelling the Experiments of Browder et al.

We now take our model, as given by Equations (5.2) to (5.6) and attempt to choose parameters to reproduce the results of Browder et al.. As explained in our analysis of parameters in Section 5.2.7 we will take the switching parameters for chemotherapy delivery to be the same as for nutrient delivery, so that $w_4 = 1$ and $\alpha_4 = 10$. To be consistent with the anti-angiogenic schedule of Browder et al. we apply therapy of

non-dimensional concentration 1, where a dose of therapy is delivered for one day and a dose is delivered every six days and to be consistent with the conventional schedule of Browder et al. we deliver therapy of non-dimensional concentration $\frac{15}{17}$, where a dose of therapy is applied for one day and a dose is delivered every other day for three doses, every twenty-one days.

Browder et al.'s experiments considered a tumour with an initial volume of $100\,\text{mm}^3$. To model a tumour of this initial volume we consider our previous model of untreated tumour growth, as governed by Equations (4.3) to (4.6), and extract the cell populations shown in Table 5.5.

Tumour Growth Fraction	Initial P	Initial Q	Initial N	Initial E
10%	2.01×10^6	1.51×10^7	6.26×10^6	6.13×10^6
25%	4.22×10^6	1.18×10^7	7.84×10^6	5.83×10^6
40%	6.44×10^6	9.29×10^6	8.82×10^6	5.77×10^6

Table 5.5: The initial conditions taken when modelling the work of Browder et al. (2000), which corresponds to a tumour of volume $100\,\text{mm}^3$, all to three significant figures.

We now attempt to choose our remaining free parameters, which are the chemotherapy kill rates, to reproduce the experimental results of Browder et al., which are shown in Figure 5.10. Note that Browder et al. considered *in vivo* tumours in mice, whereas we are modelling a human tumour. Hence we would only expect to be able to achieve qualitative, rather than quantitative, agreement with their results.

Results

We begin by considering the results of Figure 5.10(a) for a drug-resistant tumour, and so we take $\kappa_1 = 0$. In Figure 5.10(a) it can be seen that in Browder et al.'s experiments the anti-angiogenic schedule gave a significantly more effective therapy than the conventional schedule. However for all values of κ_2, the strength of the therapy as an anti-angiogenic, the anti-angiogenic schedule applied to our modelled tumour gave only a slight improvement over the conventional schedule. For example, taking $\kappa_2 = 2$ gives the results shown in Figure 5.11, where the anti-angiogenic schedule can be seen to perform only slightly better than the conventional schedule. In particular

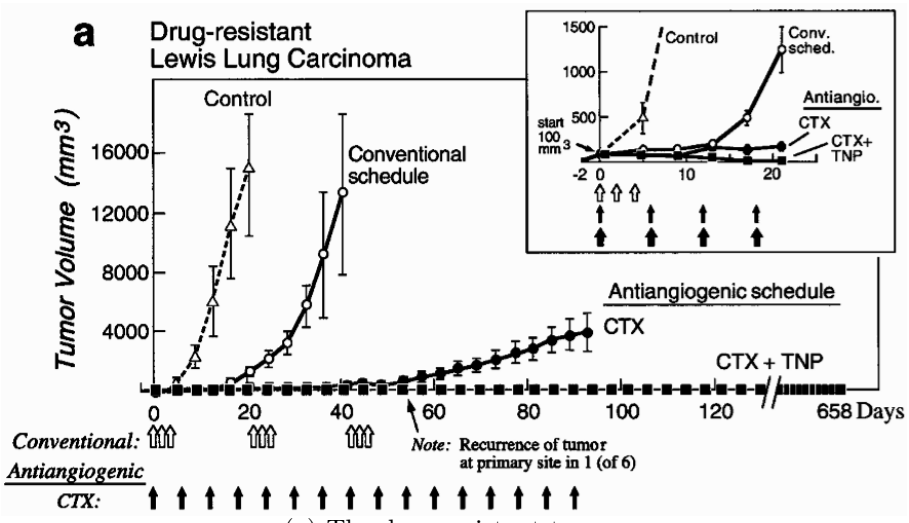

(a) The drug-resistant tumour

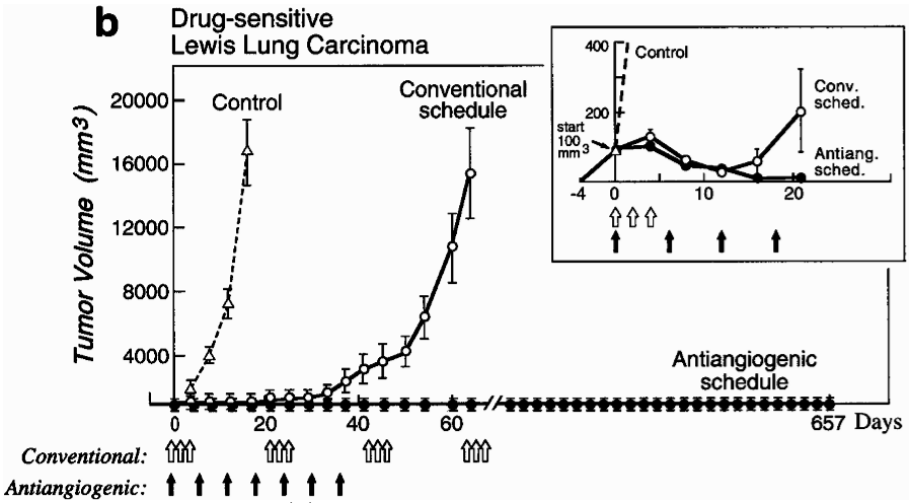

(b) The drug-sensitive tumour

Figure 5.10: The observed *in vivo* growth curves of a drug-resistant and drug-sensitive tumour being treated by the conventional therapy schedule and the anti-angiogenic therapy schedule (reproduced with permission from Browder et al., 2000).

after 70 days, which corresponds to just after the fourth application of chemotherapy in the conventional therapy, the tumour undergoing the anti-angiogenic schedule is 83% (2 s.f.) of the size of the tumour undergoing the conventional schedule.

Similarly, in Figure 5.10(b) it is seen that for drug-sensitive tumours the conventional scheduling only impaired the growth of the tumour, whereas the anti-angiogenic scheduling provided complete tumour cure. However, our modelled drug-sensitive tumour was found to exhibit only a slight difference between the different therapy schedules, such as that seen in Figure 5.12 where the two schedules are shown for

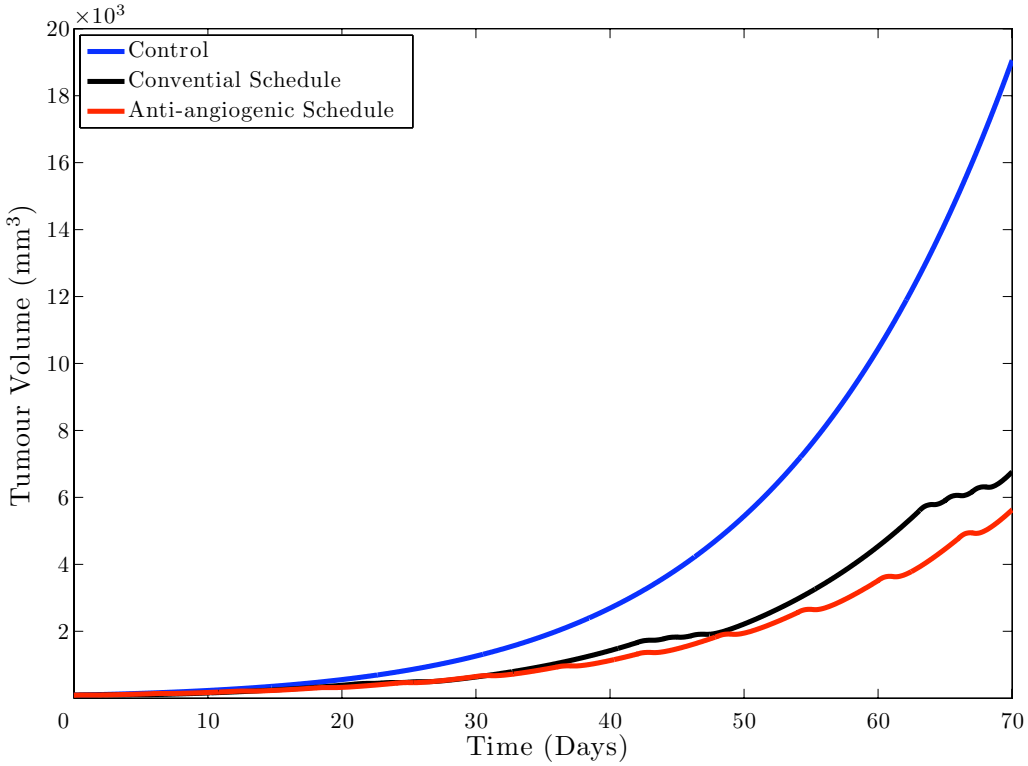

Figure 5.11: The volume of the tumour cells as a function of time for the conventional and anti-angiogenic therapy schedules for our modelled drug-resistant tumour with $\kappa_1 = 0$ and $\kappa_2 = 2$, and the other parameters as outlined in the text, as governed by Equations (5.2) to (5.6).

$\kappa_1 = 0.4$ and $\kappa_2 = 2$. In particular, after 70 days, which corresponds to just after the fourth application of chemotherapy in the conventional therapy, the tumour undergoing the anti-angiogenic schedule is 86% (2 s.f.) of the size of the tumour undergoing the conventional schedule.

Hence our model disagrees with the experimental results of Browder et al.. In particular, they found the anti-angiogenic schedule to be significantly more effective than the conventional schedule, whereas our model has found the anti-angiogenic schedule to only be slightly more effective than the conventional schedule. To investigate why this discrepancy exists between their results and our model we consider the observed apoptotic rates of the tumour and endothelial cells in their experiments.

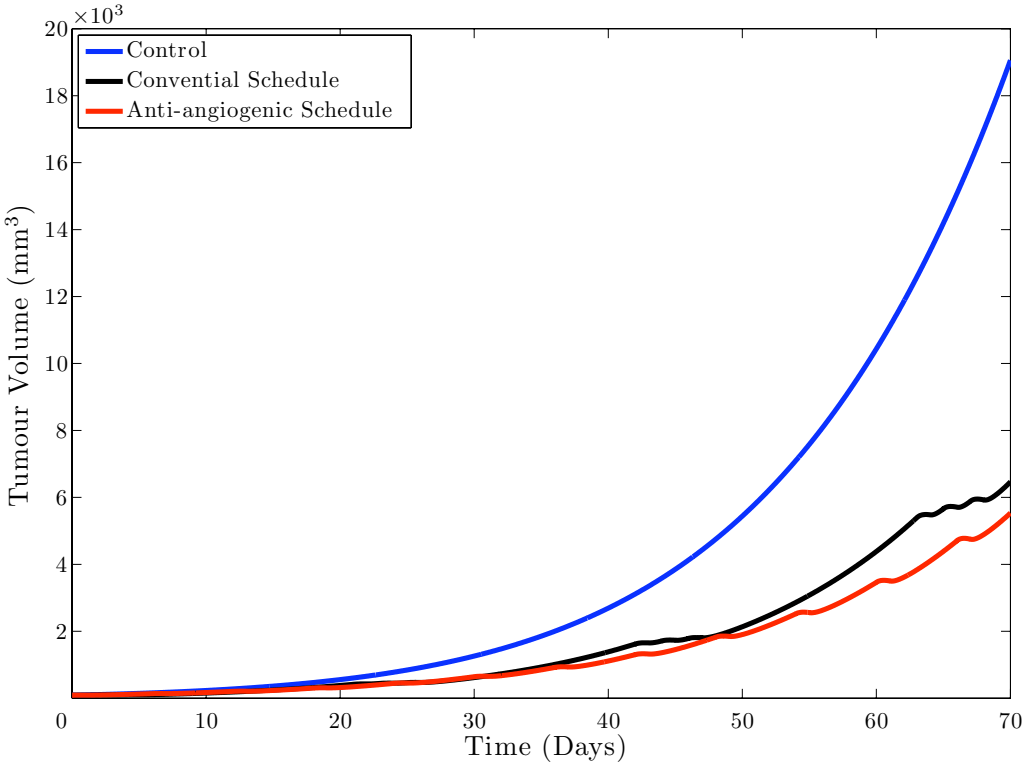

Figure 5.12: The volume of the tumour cells as a function of time for the conventional and anti-angiogenic therapy schedule for our modelled drug-sensitive tumour with $\kappa_1 = 0.4$ and $\kappa_2 = 2$, and the other parameters as outlined in the text, as governed by Equations (5.2) to (5.6).

5.4.3 Prescribing the Apoptotic Rates

We now attempt to reproduce the drug-resistant tumour growth curves of Browder et al. (2000) by prescribing the endothelial cell apoptotic rates observed during the conventional and anti-angiogenic therapies. Browder et al. (2000) recorded the proportion of both tumour and endothelial cells that are apoptotic in their drug-resistant tumour and they are shown in Figure 5.13. However their tumour is drug resistant and so chemotherapy will primarily be inducing apoptosis in the endothelial cells, and any death of the tumour cells will be a reaction to the apoptosis of the endothelial cells.

To approximate this we take the proportion of endothelial cells undergoing apoptosis

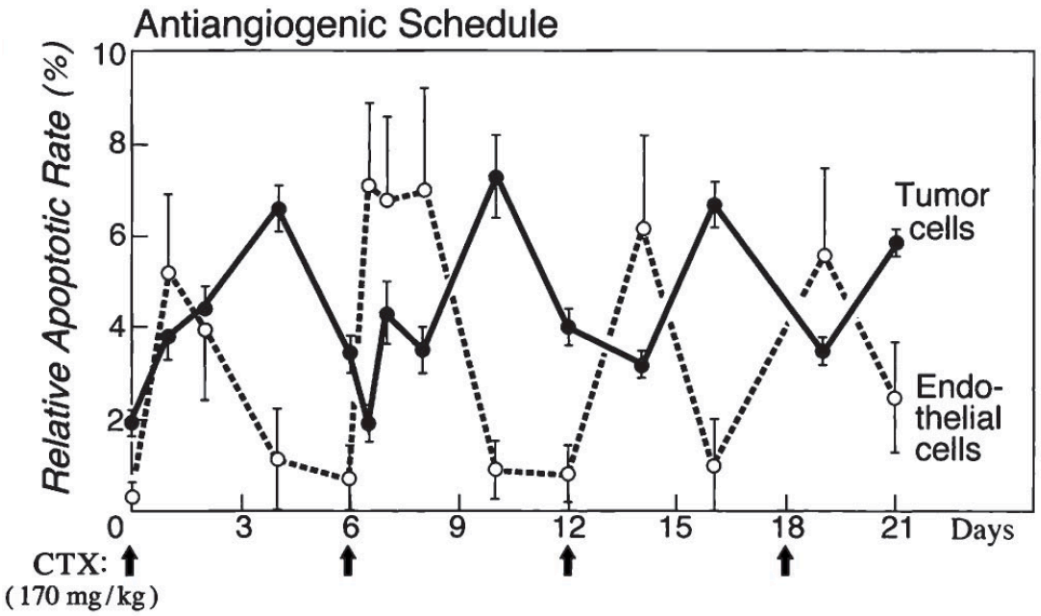

(a) The anti-angiogenic schedule

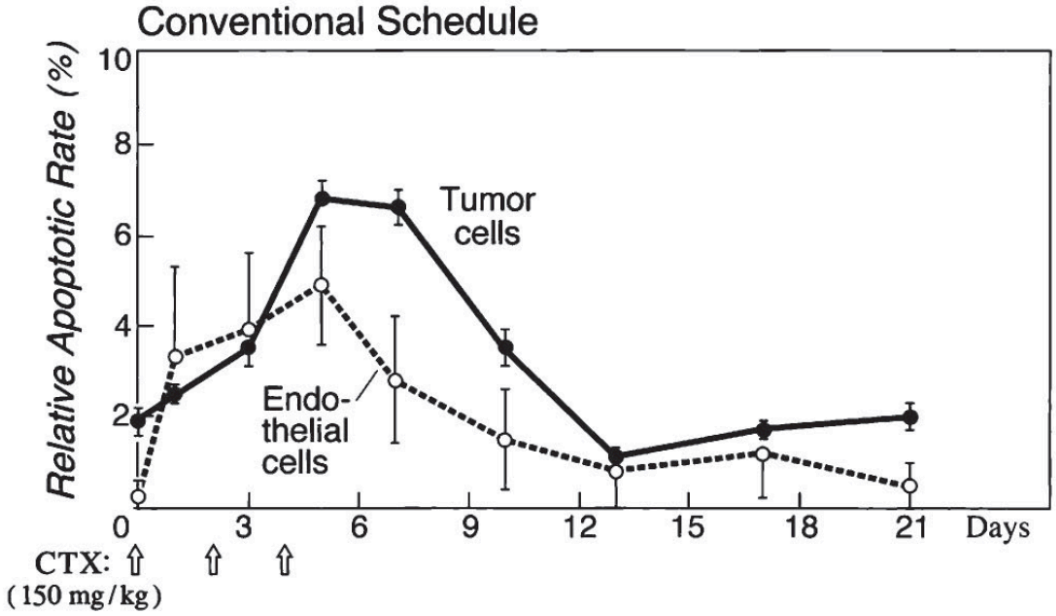

(b) The conventional schedule

Figure 5.13: The *in vivo* proportion of tumour and endothelial cells which are apoptotic in a drug-resistant tumour for the anti-angiogenic and conventional therapy schedules (reproduced with permission from Browder et al., 2000).

in the anti-angiogenic schedule to be

$$A_{\text{angio}}(t) = \frac{2.5 \sin\left(\frac{\pi t}{31 \text{ days}} - \frac{\pi}{2}\right) + 3.5}{100}, \tag{5.10}$$

and the proportion of endothelial cells undergoing apoptosis in the conventional schedule to be

$$A_{\text{conv}}(t) = \begin{cases} \frac{5}{100} \sin\left(\frac{\pi\tau}{12}\right) & \text{if } \tau < 12 \\ 0 & \text{if } \tau \geq 12 \end{cases} \quad \text{where} \quad \tau = \frac{t}{1 \text{ day}} \bmod 21. \tag{5.11}$$

These approximated proportions of endothelial cells which are undergoing apoptosis are shown in Figure 5.14.

Note that although the fraction of endothelial cells undergoing apoptosis is being prescribed, we do not know the exponential decay rate of a group of cells undergoing apoptosis, so the rate at which endothelial cells undergo apoptosis is still unknown. Defining λ_a to be the non-dimensional exponential decay rate of endothelial cells undergoing apoptosis we find that forcing endothelial cell apoptosis upon our previous model, as defined by Equations (5.2) to (5.6), yields the non-dimensional system

$$\frac{\mathrm{d}P}{\mathrm{d}t} = -\Big\{1 + \psi_1 \mathcal{S}_1 + \eta \mathcal{S}_2\Big\} P + \psi_2 \left(1 - \mathcal{S}_1\right) Q, \tag{5.12}$$

$$\frac{\mathrm{d}Q}{\mathrm{d}t} = \Big\{2 + \psi_1 \mathcal{S}_1\Big\} P - \Big\{\psi_2 \left(1 - \mathcal{S}_1\right) + \eta \mathcal{S}_2\Big\} Q, \tag{5.13}$$

$$\frac{\mathrm{d}N}{\mathrm{d}t} = 2\eta \mathcal{S}_2 (P + Q) + \tfrac{2}{3} \lambda_a A_i E - \nu N, \tag{5.14}$$

$$\frac{\mathrm{d}E}{\mathrm{d}t} = \lambda \log\left(\frac{K}{3(P+Q)+1.5N+E}\right) E \mathcal{S}_3 - \lambda_a A_i E, \tag{5.15}$$

where $\mathcal{S}_j = S_{w_j}\left(\frac{3(P+Q)+E}{E}, \alpha_j\right)$, for $i \in \{\text{conv, angio}\}$.

As in Section 5.2.6 we simulate the evolution of this model using an adaptive linear multistep method and it is found that for all values of λ_a the anti-angiogenic schedule performs an order of magnitude better than the conventional schedule. For example, the tumour growth curves when $\lambda_a = 0.7$, with the other parameter values as given in Table 4.2 for the 25% growth fraction tumour, are shown in Figure 5.15 and it is found that after 70 days, which corresponds to being just after the fourth application of chemotherapy in the conventional schedule, the tumour undergoing the anti-angiogenic schedule is only 47% (2 s.f.) of the size of the tumour undergoing the conventional schedule, which is much more consistent with the experimental results

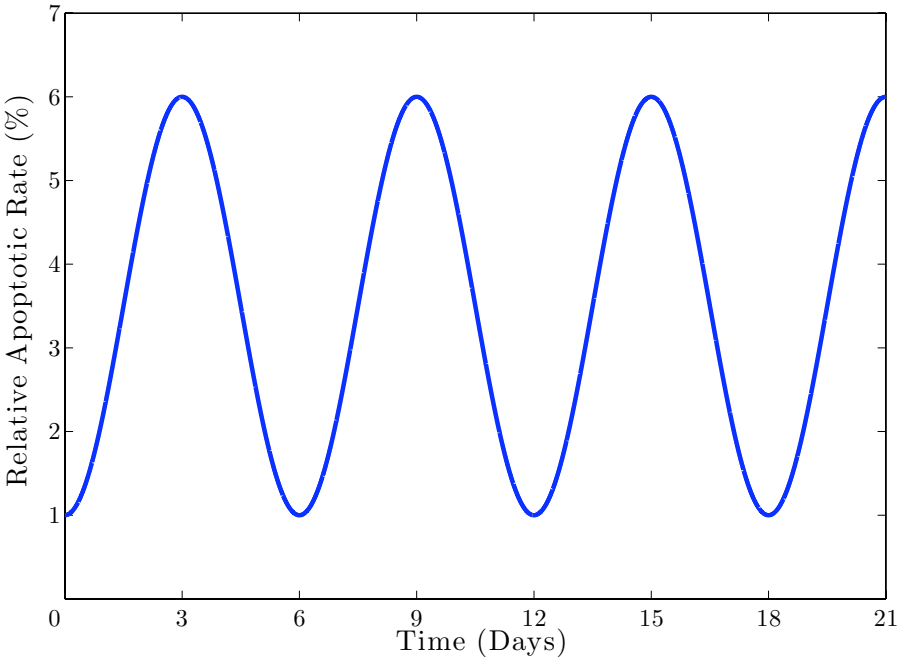

(a) The anti-angiogenic schedule

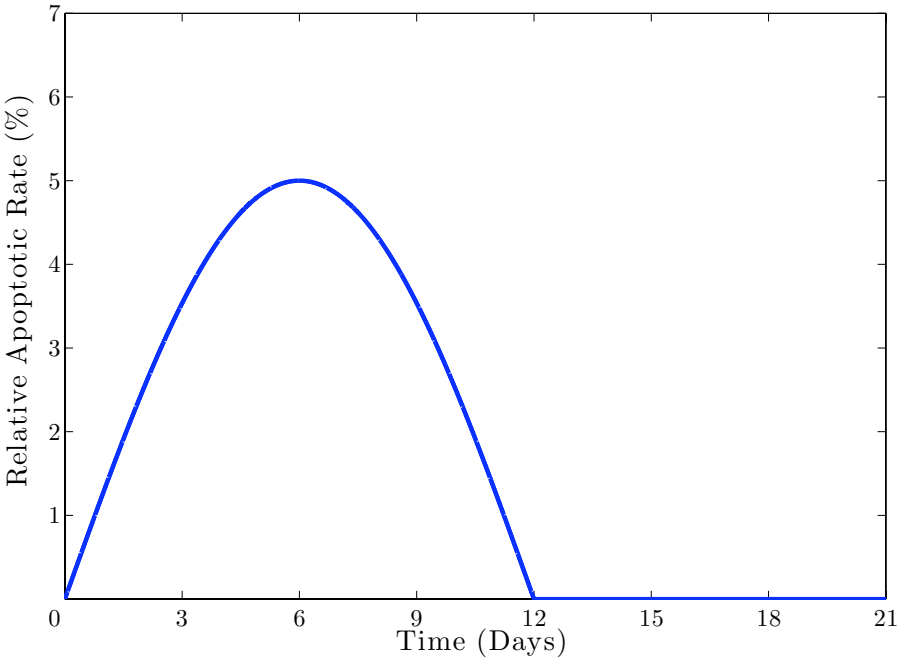

(b) The conventional schedule

Figure 5.14: The modelled proportion of endothelial cells undergoing apoptosis for the anti-angiogenic and conventional therapy schedules as defined by Equations (5.10) and (5.11).

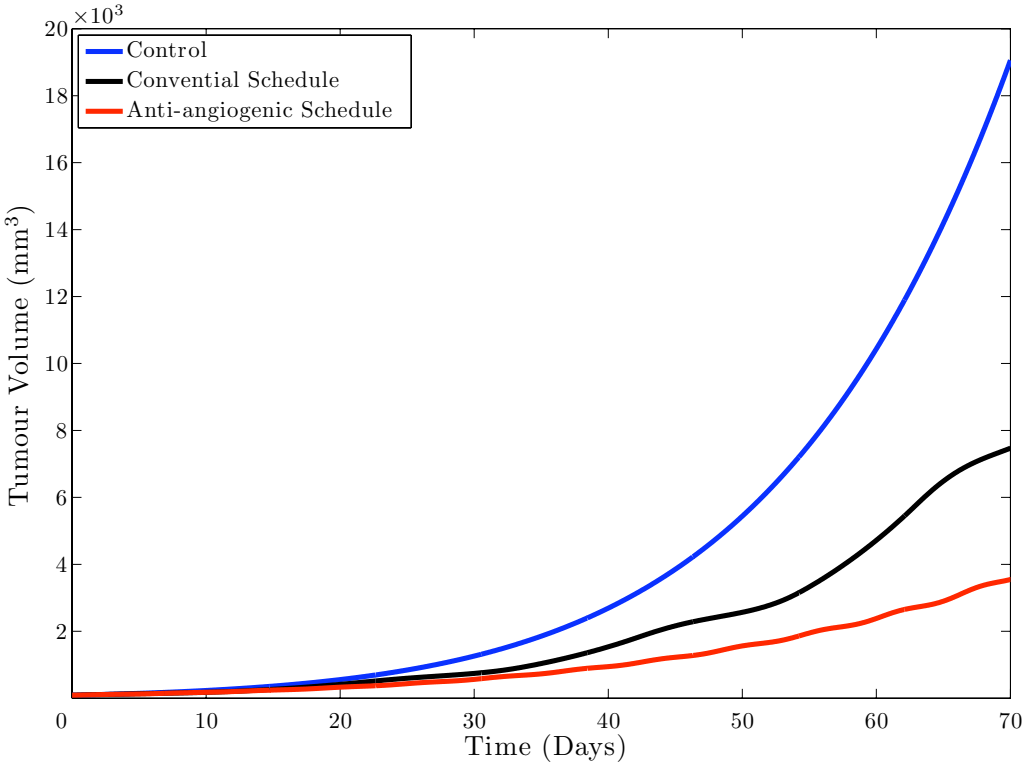

Figure 5.15: The volume of tumour cells as a function of time for the conventional and anti-angiogenic therapy schedules for our modelled drug-resistant tumour where $\lambda_a = 0.7$ and the other parameter values are as in Table 4.2, as governed by Equations (5.10) to (5.15).

of Browder et al. than the work of Section 5.4.2 where the therapy schedule was prescribed.

We have found that prescribing the treatment schedule is less successful at reproducing the experimental results of Browder et al. (2000) than prescribing the apoptotic rates. This suggests that the model presented in Section 5.2 is failing to accurately capture the induced rate of cell apoptosis in Browder et al.'s experiments following an application of therapy. We consider this in more detail in the next section.

5.5 The Saturation of Chemotherapy

5.5.1 Introduction

We now consider the apoptotic rates observed by Browder et al. in more detail. In Figure 5.13(a), which shows the apoptotic rates observed during the anti-angiogenic schedule, it can be seen that after each application of the therapy the apoptotic rate is raised for a period of 5-6 days. This suggests that the chemotherapeutic remains active within the tumour after the application of the therapy and decays with a half-life of the order of a few days.

Given this, we would expect that when the therapy is applied every other day in the conventional schedule the different applications of therapy would interact so that a higher concentration of chemotherapy is present after the second and third applications than after the first. Whilst it can be seen in Figure 5.13(b) that during the conventional schedule the apoptotic rate is raised for longer following the third application of therapy than following after a single application of therapy, which is consistent with a higher chemotherapy concentration being present, a corresponding increase in the relative apoptotic rate is not observed. This suggests that in this experiment the effect of the chemotherapy is saturating, and so we now model the saturation of chemotherapy to see if this gives better agreement with the results of Browder et al. (2000).

5.5.2 Modelling Chemotherapy Saturation

We now consider the evolution of the tumour where we allow the action of the chemotherapy on the tumour to saturate. To do this we take the rates of chemotherapy induced apoptosis to be saturating functions of the chemotherapy concentration, and in particular we take them to be given by Michaelis-Menten kinetics. Such kinetics are often used to model saturating nutrient uptake and have been validated experimentally for oxygen uptake (Lin, 1976; Hlatky and Alpen, 1985). We also note that in the experiments of Browder et al. (2000) the chemotherapy is given to the mouse by subcutaneous injection and to model this we assume that the chemotherapy concentration within the tumour undergoes a discontinuous jump after each injection and that the magnitude of each jump depends upon how well vascularised the tumour is, with more chemotherapy being delivered to a well vascularised tumour than

an equivalent poorly vascularised tumour. In between injections we assume that the chemotherapy concentration undergoes exponential decay at the non-dimensional decay rate λ_c. Incorporating these assumptions into our previous non-dimensional model, derived in Section 5.2, we obtain the non-dimensional system of equations

$$\frac{\mathrm{d}P}{\mathrm{d}t} = -\left\{1 + \psi_1\mathcal{S}_1 + \eta\mathcal{S}_2 + \frac{\kappa_1 C}{C^* + C}\right\} P + \psi_2\left(1 - \mathcal{S}_1\right) Q, \tag{5.16}$$

$$\frac{\mathrm{d}Q}{\mathrm{d}t} = \Big\{2\mu + \psi_1\mathcal{S}_1\Big\}P - \Big\{\psi_2\left(1 - \mathcal{S}_1\right) + \eta\mathcal{S}_2\Big\}Q, \tag{5.17}$$

$$\frac{\mathrm{d}N}{\mathrm{d}t} = 2\eta\mathcal{S}_2(P + Q) + \frac{2\kappa_1 CP}{C^* + C} + \frac{2\kappa_2 C}{3(C^* + C)}\lambda\log\left(\tfrac{K}{3(P+Q)+1.5N+E}\right) E\mathcal{S}_3 - \nu N, \tag{5.18}$$

$$\frac{\mathrm{d}E}{\mathrm{d}t} = \left(1 - \frac{\kappa_2 C}{C^* + C}\right)\lambda\log\left(\tfrac{K}{3(P+Q)+1.5N+E}\right) E\mathcal{S}_3, \tag{5.19}$$

$$\frac{\mathrm{d}C}{\mathrm{d}t} = \sum_{i\in I}\left(1 - \mathcal{S}_4\right) L(t_i)\delta(t - t_i) - \lambda_c C, \tag{5.20}$$

where $\mathcal{S}_i = S_{w_i}\left(\frac{3(P+Q)+E}{E}, \alpha_i\right)$, $\left\{t_i | i \in I\right\}$ are the non-dimensional times of the therapy application, $L(t_i)$ are the non-dimensional strengths of the therapy applications, and C^* is the non-dimensional critical chemotherapy concentration in the Michaelis-Menten kinetics. We close this model by taking the initial conditions outlined in Table 5.5, which correspond to a tumour $100\,\mathrm{mm}^3$ in volume, and the additional initial condition that $C(0) = 0$.

5.5.3 Numerical Methods for Simulating the Treatment of the Tumour

As before we simulate the evolution of our model using an adaptive linear multistep method. However, we note that it is simple to integrate Equation (5.20) to obtain

$$C(t) = \begin{cases} 0 & \text{if} \quad t \leq \min\limits_i(t_i), \\ \displaystyle\sum_i \left(1 - S_{w_4}\left(\tfrac{3(P(t_i)+Q(t_i))+E(t_i)}{E(t_i)}, \alpha_4\right)\right) L(t_i) e^{\lambda_c(t-t_i)} & \forall\, i \text{ s.t. } t_i < t. \end{cases}$$

This explicit expression for the nutrient concentration can simply be included into the numerical scheme.

5.5.4 Choosing Parameter Values to Reproduce the Results of Browder et al. (2000)

We now attempt to choose the values of the parameters which are present in this model but absent from the model outlined in Section 5.2 to reproduce the experimental results of Browder et al. (2000). In particular we seek parameter values so that the anti-angiogenic therapy schedule is an order of magnitude more effective than the conventional therapy schedule. For this to occur we require the chemotherapy concentration to decay significantly over a rest period of 16 days, but not over a rest period of 6 days. This implies that the chemotherapeutic should have a half-life of approximately 6 days, so that $\lambda_c \approx \frac{\log 2}{9} = 0.077$ (2 s.f.). Furthermore, for the effect of saturation to be significant with our chemotherapy concentration we would expect that $C^* \ll 1$.

5.5.5 Results

Guided by this initial consideration of the parameter values we find that taking the parameter values in Table 5.6, along with the other parameters listed in Tables 4.2 and 5.2 for a 25% growth fraction tumour, gives the results shown in Figure 5.16.

Parameter	Description	Value
λ_c	The decay rate of the chemotherapy	0.2
κ_1	Sensitivity of proliferating cells to chemotherapy	0
κ_2	Sensitivity of endothelial cells to chemotherapy	0.5
C^*	Critical chemotherapy concentration in the Michaelis-Menten kinetics	0.1
w_4	Sensitivity of chemotherapy delivery to vasculature	1

Table 5.6: The non-dimensional parameter values used in our drug-resistant model of chemotherapy saturation, as governed by Equations (5.16) to (5.20).

It can be seen that although these results are not as conclusive as the experimental results of Browder et al. (2000), saturation has allowed the anti-angiogenic schedule to perform better compared to the conventional schedule than was observed in our model ignoring saturation (the results of which were shown in Figure 5.11). In particular after 70 days, which corresponds to just after the fourth application of chemotherapy in the conventional therapy, the tumour undergoing the anti-angiogenic schedule is

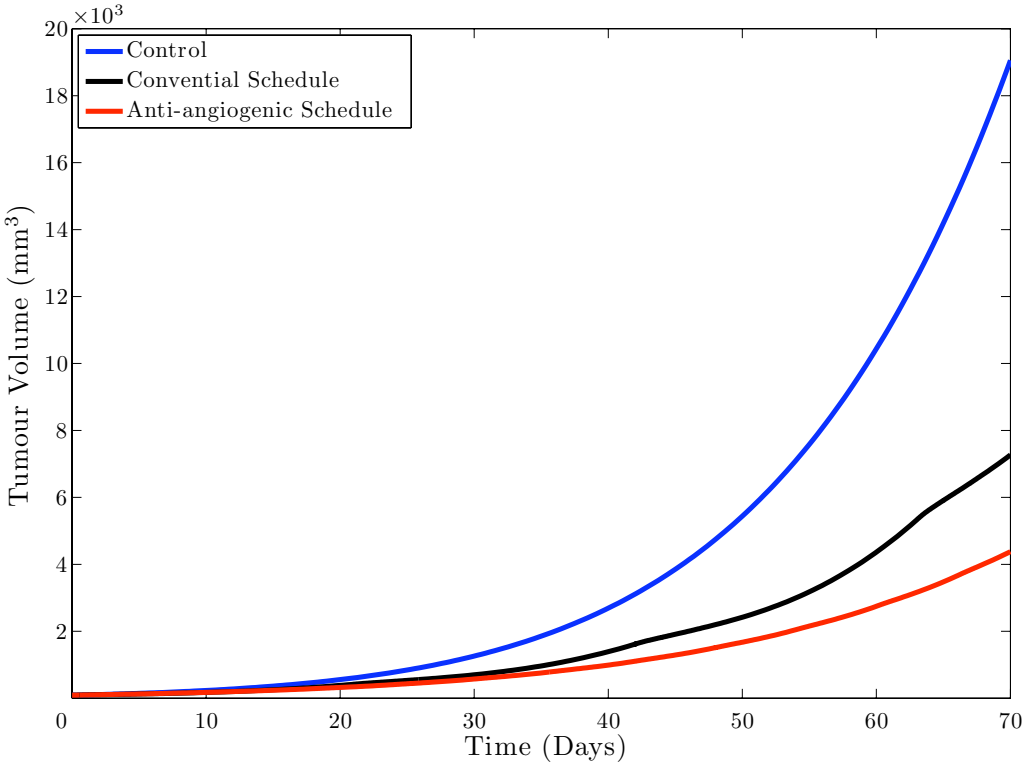

Figure 5.16: The volume of the tumour cells as a function of time for the conventional and anti-angiogenic therapy schedules for our modelled drug-resistant tumour with the parameter values given in Table 5.6 and the other parameter values outlined in the text, as governed by Equations (5.16) to (5.20).

60% (2 s.f.) of the size of the tumour undergoing the conventional therapy. This is not as low as the 47% (2 s.f.) relative size which was observed in Section 5.4.3 when the apoptotic rates of the endothelial cells were prescribed, but it is still significantly lower than the 83% (2 s.f.) relative size observed in the absence of any saturation in Section 5.4.2. Furthermore, a more significant difference between the conventional and anti-angiogenic schedules can be created by taking more extreme values of the saturation parameters.

We now consider a drug-sensitive tumour by taking $\kappa_1 = 0.1$ and using the other parameter values as given by Tables 4.2, 5.2, and 5.6, which gives the results shown in Figure 5.17. It can be seen that, as with the drug-resistant tumour, saturation has allowed a significant difference between the conventional and anti-angiogenic schedules. In particular after 70 days, which corresponds to just after the fourth application of chemotherapy in the conventional therapy, the tumour undergoing the anti-angiogenic

schedule is 55% (2 s.f.) of the size of the tumour undergoing the conventional schedule.

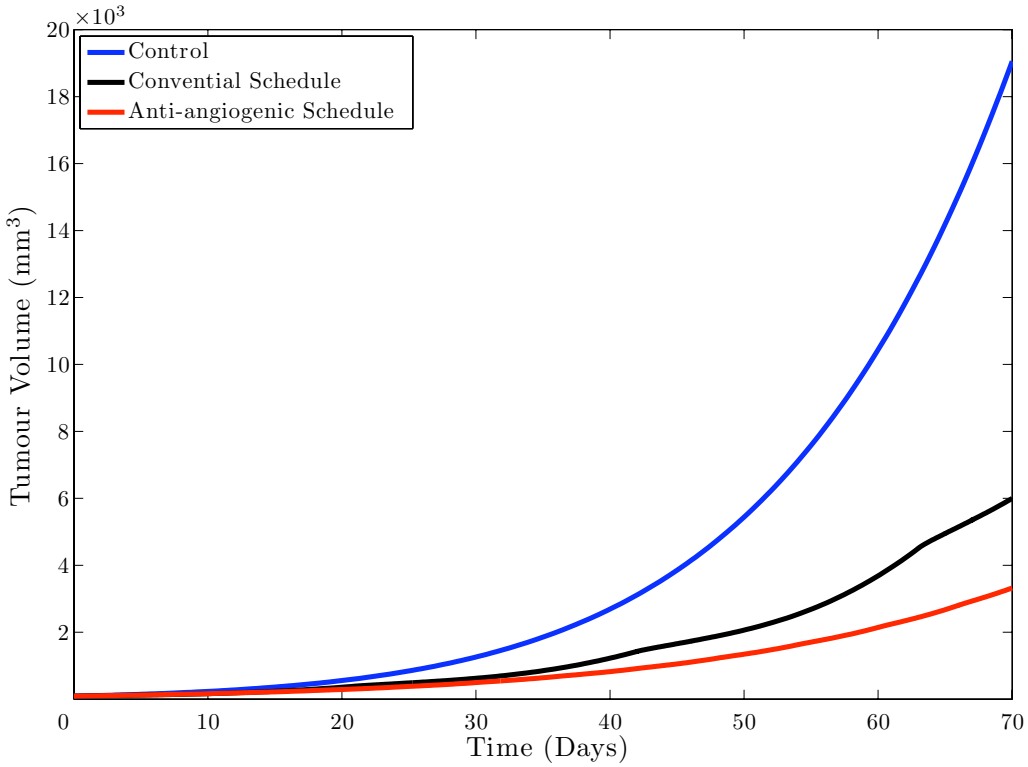

Figure 5.17: The volume of tumour cells as a function of time for the conventional and anti-angiogenic therapy schedules for our modelled tumour with $\kappa_1 = 0.1$ and the other parameter values given in Table 5.6 and outlined in the text, as governed by Equations (5.16) to (5.20).

To further consider whether our model including chemotherapy saturation gives qualitative agreement with the results of Browder et al. (2000) we compare the observed experimental apoptotic rates of the endothelial cells shown in Figure 5.13 to the corresponding Michaelis-Menten kinetics of our modelled tumour which are shown in Figure 5.18. Note that Figure 5.18 is showing the non-dimensional value of the Michaelis-Menten endothelial cell apoptosis kinetics, whereas Figure 5.13 shows the proportion of endothelial cells which are observed to be undergoing apoptosis. Hence we would only expect there to be qualitative but not quantitative agreement between these figures and in particular we would expect Figure 5.13 to be smoother than Figure 5.18.

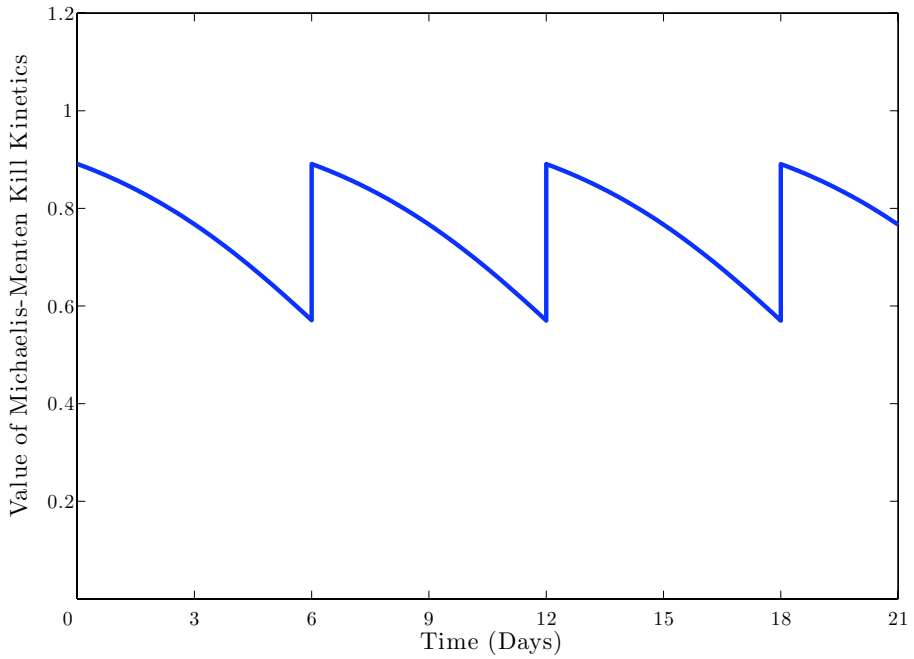

(a) The anti-angiogenic schedule

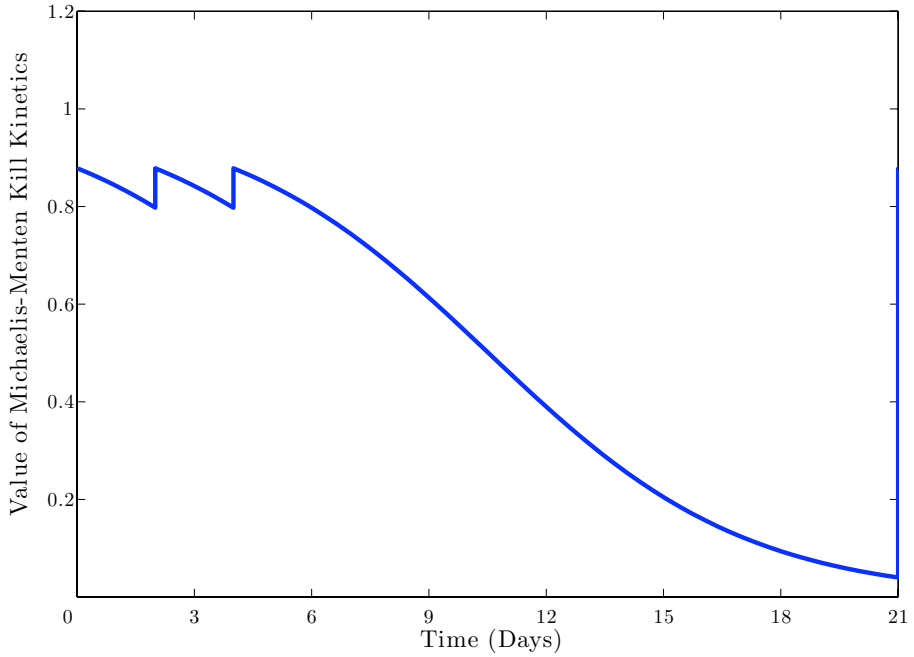

(b) The conventional schedule

Figure 5.18: The non-dimensional value of the Michaelis-Menten endothelial cell apoptosis kinetics as a function of time in our simulated modelled tumour, as governed by Equations (5.16) to (5.20).

Comparing Figure 5.13(a) to Figure 5.18(a) we find that in both figures the apoptotic rate of endothelial cells during the anti-angiogenic schedule oscillates regularly with a period of 6 days. Also, comparing Figure 5.13(b) to Figure 5.18(b) we find that in both figures the apoptotic rate during the conventional schedule is raised for approximately 12 to 15 days, but the maximum observed apoptotic rate is no higher than in the anti-angiogenic rate. Hence we have qualitative agreement between our saturation model and the apoptotic rates observed experimentally by Browder et al. (2000).

5.5.6 Conclusions

In this section we investigated whether chemotherapy saturation could explain the results of Browder et al. (2000), who found that their anti-angiogenic schedule therapy was considerably more effective at treating mice tumours than their conventional schedule therapy.

We have found that modelling saturation did get closer to reproducing the results of Browder et al. (2000) than our original model presented in Section 5.2. In particular, after 70 days the tumour undergoing the anti-angiogenic schedule in our initial model, as given by Equations (5.16) to (5.19), was 83% (2 s.f.) of the size of the tumour undergoing the conventional schedule, but after 70 days the tumour undergoing the anti-angiogenic schedule in the model including saturation, as given by Equations (5.2) to (5.5), was 60% (2 s.f.) of the size of the tumour undergoing the conventional schedule. Whilst this result is not as pronounced as those in Section 5.4.3 where the apoptotic rate of the endothelial cells was prescribed, where after 70 days the tumour undergoing the anti-angiogenic schedule was just 47% (2 s.f.) of the size of the tumour undergoing the conventional schedule, it does highlight how saturation allows the anti-angiogenic schedule to perform better than the conventional schedule. Furthermore, more extreme saturation kinetics could be taken which would show a more pronounced difference between the anti-angiogenic and conventional schedules, but such kinetics would be harder to justify.

Furthermore, choosing parameter values to maximise the amount by which the anti-angiogenic schedule performs better than the conventional schedule yielded Michaelis-Menten kinetics which were consistent with the observed apoptotic rates. This again highlights the fact that the experimental results of Browder et al. (2000) can be explained by chemotherapy saturation.

Browder et al. (2000) conclude that chemotherapy has the potential to provide an effective anti-angiogenic effect by targeting the endothelial cells. They also note that the anti-angiogenic schedule "provided more sustained apoptosis of vascular endothelial cells within the tumour bed" than the conventional schedule. Following our model we conclude that this is because the effect of their applied chemotherapy saturates. In particular, in the conventional therapy the three dose dense applications of therapy do not lead to an increased rate of endothelial cell apoptosis because this rate has already saturated, but the longer rest phase of the conventional schedule allows the apoptotic rate to decrease significantly in between applications. In the anti-angiogenic schedule, the therapy is applied at regular intervals which match the decay rate of the therapy to constantly top up the chemotherapy concentration. Hence significant cell kill is always present and the mean rate of apoptosis in the anti-angiogenic schedule is greater than in the conventional schedule.

5.6 Conclusions

In this chapter we were aiming to build a model for the treatment of a vascularised tumour by chemotherapy and consider the possibility of scheduling chemotherapy to provide an anti-angiogenic affect. We have successfully done this.

During our analysis of parameters of Section 5.2.7 we found that altering the sensitivity of the proliferating and endothelial cells to the therapy, by altering the parameters κ_1 and κ_2, allowed the therapy to either act as a traditional chemotherapeutic or exploit the angiogenesis-therapy feedback loop. In the later case each application of therapy was more effective at targeting the endothelial cells than the tumour cells. This meant that each application of therapy undervascularised the tumour, which in turn upregulated angiogenesis, which primed the endothelial cells for the next application of endothelial cell targeting therapy.

We also found that for the range of parameter values considered the most effective therapy exploited the angiogenesis-therapy feedback loop. The main reason for this is that when the therapy acts as a traditional chemotherapeutic the tumour is relatively over-vascularised upon cessation of the therapy, so that the tumour recovers at the time scale of the potential doubling rate of the tumour. However, when the therapy exploits the angiogenesis-therapy feedback loop the tumour is relatively undervascularised upon cessation of the therapy and the tumour recovers on the time scale

of angiogenesis, which is slower than the potential doubling rate of the tumour. Hence the tumour recovers more slowly following treatment by an angiogenesis-therapy feedback loop exploiting therapy than a traditional chemotherapeutic. The therapy which exploits the angiogenesis-therapy feedback loop also exhibits a compounding effect where each application of the therapy primes the endothelial cells for the next application of therapy, which also helps make the angiogenesis-therapy feedback loop exploiting therapies effective.

We also found that there are cases where making the proliferative cells less susceptible to the chemotherapy made the treatment more effective by improving the ability of the therapy to exploit the angiogenesis-therapy feedback loop. This highlights that the optimal joint treatment of a tumour with a combination of chemotherapy and angiogenesis inhibitors is highly non-trivial because these two types of therapy have the potential to be mutually inhibitory.

Next we considered the Norton-Simon hypothesis, which states that dose dense schedules of chemotherapy provide more effective cell kill than dose sparse schedules. By considering the Norton-Simon hypothesis applied to both continuous and discrete applications of therapy when the therapy acted as both a traditional chemotherapeutic and exploited the angiogenesis-therapy feedback loop we found that the total duration of the therapy is important.

For cell cycle specific chemotherapies which act as a traditional chemotherapeutic it is vital that chemotherapy is applied for long enough for all the quiescent cells to recover the ability to proliferate and then be targeted, which corresponds to applying the chemotherapy for at least a few cell cycles, or equivalently a few days. This result is consistent with the observation of Norton (2005) who noted that doses of chemotherapy can be made more effective by delivering the doses: “more often, although not so often that we are trying to ‘to kill cells that are already dead.’ ”

For both therapies which act as a traditional chemotherapeutic and therapies which exploit the angiogenesis-therapy feedback loop it was found that as long as the therapy is active for at least a few cell cycle times then the Norton-Simon hypothesis holds and dose dense therapies are more effective at providing cell kill than dose sparse therapies. For continuous applications of therapy this is primarily because dose dense therapies allow greater concentrations of chemotherapy to be delivered which provide greater cell kill, assuming there are no saturation effects, and for discrete applications

of therapy this is primarily because dose dense therapies allow less tumour recovery during the shorter rest periods.

We also found that for continuous therapies with constant chemotherapy kill rates, κ_1 and κ_2, and a constant total application of chemotherapy, dose dense therapies tended to act as a traditional chemotherapeutic and dose sparse therapies tended to exploit the angiogenesis-therapy feedback loop. Hence therapies with fixed chemotherapy kill rates and a fixed total application of chemotherapy can either act as a traditional chemotherapeutic or exploit the angiogenesis-therapy feedback loop depending upon the concentration of the therapy. This highlights how non-trivial the interaction between the therapy acting as a traditional chemotherapeutic and exploiting the angiogenesis-therapy feedback loop is.

We then attempted to reproduce the results of Browder et al. (2000), who considered the use of chemotherapy as an anti-angiogenic agent in mouse tumours, and found that their "anti-angiogenic" schedule was considerably more effective at treating the tumours than their "conventional schedule". Our initial model would not reproduce this trend, but prescribing the apoptotic rates observed by Browder et al. into our model could. We used this to suggest that the action of the chemotherapy in the experiments might be saturating and modelling saturation allowed us to demonstrate that the "anti-angiogenic" schedule can be significantly more effective than the "conventional" schedule whilst also yielding relative apoptotic rates consistent with those observed experimentally. This suggests that the reason the "anti-angiogenic" schedule is more effective than the "conventional" schedule is due to saturation. Hence, rather than being a comparison of anti-angiogenic and conventional schedules, we can use the results of Browder et al. to reach a more general conclusion concerning the scheduling of therapies which saturate. We conclude that when the effect of the drug saturates the therapy should be applied with a rest phase similar to the therapy's half-life, and not denser than this. This then tops up the therapy as it decays, rather than delivering excessive therapy which does not result in greater cell kill due to saturation.

Hence in this chapter we find that the Norton-Simon hypothesis is generally true but we should add some caveats to it, namely that dose dense schedules do provide more effective cell kill than dose sparse therapies, when the action of the therapy does not saturate, but to be effective a cell-cycle specific therapy must be active for at least a few cell cycle times. When the therapy does saturate, it should be applied with a rest phase similar to the therapy's half-life.

Chapter 6

Incorporating Resistance

6.1 Introduction

Chemotherapy often fails because the tumour undergoing treatment develops resistance to the therapy (Persidis, 1999). This makes the relationship between therapy application and the development of resistance crucial to the long term prognosis of the patient. In this chapter we will add resistance to our previous model for vascular tumour growth undergoing chemotherapy, which was presented in Chapters 4 and 5, and consider some key clinical questions concerning resistance. To guide our model we first review the relevant biological and mathematical literature.

6.1.1 Literature Summary

Biological Literature

Luria and Delbrück (1943) demonstrated in their Nobel prize winning work that bacteria develop resistance to viruses via random spontaneous mutations which occur independently of the action of the virus. Law (1952) then demonstrated that *in vivo* L1210 leukaemia cells also develop drug resistance through random spontaneous mutations. Furthermore Summers and Handschumacher (1973) and Jaffrézou et al. (1994) both demonstrated that drug resistance in *in vitro* cancer cell systems is acquired at random. It is now widely, but not universally, accepted that drug resistance is typically acquired due to random cell mutations (Goldie, 2008).

There are a number of different mechanisms by which a cell can exhibit resistance to a particular chemotherapy. One of the most prominent mechanisms of resistance

is altered membrane transport, where resistant cells extrude chemotherapy molecules quickly enough to keep the intra-cellular concentration below some fatal threshold, but other mechanisms can also cause resistance, including but not limited to: enhanced DNA repair, alterations in target molecules, and enhanced drug metabolism (Luqmani, 2005). These mechanisms make the resistant cells more resilient to the action of the drugs, but not completely unaffected by it (Scappini et al., 2004). Hence resistant cells are only partially resistant, so that they are less susceptible but not completely insusceptible, to the therapy.

These resistance mechanisms use up energy which would otherwise be available for proliferation and/or invasion. This additional metabolic cost of being resistant actually reduced the fitness so that there is a proliferative cost of being resistant (Gatenby, 2009). In the absence of any therapy this cost of being resistant gives the sensitive cells a competitive advantage over the resistant cells and resistant tumours have been observed to lose resistance if the therapy is ceased for a sufficiently long period of time (Scappini et al., 2004).

Endothelial cells are typically more genetically stable than tumour cells and therefore mutate less often. Hence endothelial cells typically do not become resistant to chemotherapy (Boehm et al., 1997).

Mathematical Literature

Given that resistance to therapy is randomly acquired, Goldie and Coldman (1979) calculated the probability of a tumour of a given size containing no cells which are resistant to a given therapy. Their result depends upon the mutation rate of the tumour cells, but for one estimate of the mutation rate it was found that for a tumour consisting of 10^5 cells, which corresponds to a volume of at most $0.3\,\mathrm{mm}^3$, there is a probability of 99% (2 s.f.) that none of the tumour cells are resistant to the therapy, whereas for a tumour consisting of 10^8 cells, which corresponds to a volume of at most $30\,\mathrm{mm}^3$, there is a probability of 0.005% (1 s.f.) that none of the tumour cells are resistant to the therapy. This highlights that in clinically diagnosable primary tumours there can be expected to be at least one cell which is resistant to any given therapy.

Goldie et al. (1982) considered chemotherapy scheduling and its affect on drug resistance. In particular they assumed that resistance was acquired due to random cell mutation and then considered the probability of a doubly resistant cell existing when

two non-cross-resistant chemotherapies are applied. They found that for therapies of equal potency alternating the therapies as quickly as possible minimised the probability of a doubly resistance population becoming established compared to applying several hits of one therapy followed by several hits of the other therapy. This finding is known as the Goldie-Coldman hypothesis. However, Goldie et al. conceded that alternation may not be optimal if the therapies are not of equal potency.

Day (1986) relaxed the symmetry assumptions of Goldie et al. (1982) and ran a large number of simulations to consider therapies of different strengths. It was found that in many situations the Goldie-Coldman hypothesis could be improved upon, and in the absence of detailed knowledge of parameter values alternating therapies with the least effective drug being delivered first maximised the probability of cure. This result is known as Day's worst drug first rule. However, if detailed knowledge of parameter values is available, then the therapy schedule can be optimised to provide a more effective therapy than Day's worst drug first rule.

However, Day's worst drug first rule is not universally accepted and other works have arrived at different conclusions. In particular, Katouli and Komarova (2010) revisited the worst drug rule and simulated the evolution of stochastic and deterministic models for all possible treatment regimes to consider which treatment schedules gave the greatest probability of treatment success. They found that often the optimal therapy starts with the stronger drug, but that the weaker drug should be applied for longer. Furthermore, several experimental works have found that the worst drug first rule does not apply for non-small cell lung cancers (Colucci et al., 1997; Gebbia et al., 2003; Fulfaro et al., 2003; Grossi et al., 2007).

However, the work of Goldie et al. (1982) and Day (1986) only considered the probability of a doubly resistant cell existing. Their models ignored the competition between resistance and sensitive cells and the possibility of a tumour losing resistance after cessation of the therapy. Furthermore the work of Day only defined the better drug to be the one with the higher cell kill, rather than considering any other potential mechanism which might make a drug better than another one.

The research of Goldie et al. (1982) and Day (1986) considers scheduling therapy to maximise cell kill and minimise the probability of a doubly resistance cell accumulating. It was assumed that these conditions must be met to maximise the chances of complete tumour eradication. However Hahnfeldt et al. (2003) considered whether a maintenance therapy aimed at restricting a tumour below a non-fatal size might be

more practical than aiming to completely eradicate the tumour. They considered a pair of coupled ordinary differential equations governing the evolution of a sensitive cell population and a resistance cell population, where the sensitive population could proliferate more quickly than the resistant population, and it was found that regularly spaced therapy applications allowed the tumour to "resensitize" to the therapy. Hence they found that a regular, lower dose therapy schedule aimed at maintenance could be more practical than a therapy aiming for tumour eradication; other papers have arrived at similar conclusions, see, for example, Monro and Gaffney (2009) who consider the optimal scheduling of palliative therapies.

6.1.2 The Aims of this Chapter

In this chapter we aim to incorporate resistance to therapy, and the cost of being resistant to therapy, into our previous model for vascular tumour growth and treatment presented in Chapters 4 and 5. We will then perform an analysis of parameters to see how this model behaves in the presence of resistance and consider some of the key clinical questions regarding resistance. In particular we will consider whether the Norton-Simon hypothesis is affected by the inclusion of resistance and test the Goldie-Coldman hypothesis and Day's worst drug first rule when the evolution of the cell types is considered, resensitisation is allowed and possible anti-angiogenic effects are included. We will also investigate how therapy should be scheduled to provide the most practical maintenance therapy.

6.2 Modelling Resistance

We now include resistance into our previous non-dimensional model for vascular tumour growth and treatment as given by Equations (5.2) to (5.6) of the previous chapter. Due to the similarity between this and the previous model we will simply present the non-dimensional model, where we have applied the equivalent non-dimensionalisation to that of Section 5.2.3.

6.2.1 The Model

The Cell Compartments

We begin by considering the different cell compartments in this model. In the previous chapter there were four different non-dimensional cell compartments, which were denoted by P, Q, N, and E representing the number of proliferating, quiescent, necrotic and endothelial cells respectively in the tumour. In this section we consider drug sensitive and drug resistant tumour cells, but assume that the endothelial cells do not exhibit resistance to the therapy. Hence we consider the non-dimensional variables P_s, Q_s, P_r, Q_r, N, and E which will denote the number of sensitive proliferating, sensitive quiescent, resistant proliferating, resistant quiescent, necrotic and endothelial cells respectively.

The Resistant Cells

We now consider how the resistant cells behave, and in particular how their behaviour differs from that of the sensitive cells. We assume that there is a cost, ω, of being resistant, so that resistant proliferating cells proliferate a factor $(1-\omega)$ slower than an equivalent sensitive proliferating cell.

We also assume that a population of sensitive proliferating cells randomly mutates to become resistant at a non-dimensional rate εP_s, and a population of resistant cells randomly mutates to lose resistance at a non-dimensional rate $\overline{\varepsilon} P_r$.

The Chemotherapy

In the previous chapter we showed that chemotherapy saturation can significantly affect the response of the tumour to the therapy and provides a possible explanation for the results of Browder et al. (2000) who found that an "anti-angiogenic" scheduling of chemotherapy was more effective than a "conventional" schedule. However, the modelling of saturation requires the inclusion of at least two extra free parameters, namely the half-life of the therapy and the critical chemotherapy concentration in the chemotherapy kill kinetics. To minimise the number of parameters in an already complex model we revert to our original model of chemotherapy delivery presented in Section 5.2, where the chemotherapy concentration is assumed to be low enough to

prevent the action of the therapy saturating and non-dimensional mean chemotherapy concentration in the tumour, $C(t)$, is

$$C(t) = \left(1 - S_{w_4}\left(\tfrac{3(P_r+Q_r+P_s+Q_s)+E}{E}, \alpha_4\right)\right) L(t), \tag{6.1}$$

where $S_w(X, a)$ is the switching function introduced in Section 4.2.1, α_4 is the critical vasculature for the delivery of chemotherapy, w_4 is the sensitivity of the chemotherapy delivery, and $L(t)$ is the intravenous chemotherapy concentration which is defined by the treatment schedule.

However, given the results of the previous chapter we emphasise that this simple model for chemotherapy delivery will only be valid when the half-life of the chemotherapeutic is very short, which would be appropriate for Fluorouracil (5-FU) which has a half-life of 10-15 minutes (White, 2001), and the chemotherapy concentration is sufficiently low that saturation can be neglected.

Having derived an expression for the chemotherapy concentration in the tumour we now consider the effect of the chemotherapy on the tumour. As in Chapter 5 we limit our model to the action of cytotoxic drugs, which only affect actively proliferating cells, and also assume that at clinically relevant concentrations the rate of therapy induced cell kill increases linearly with therapy concentration. We also assume that the resistant cells undergo chemotherapy induced apoptosis a factor σ slower than equivalent sensitive cells.

The Non-Dimensional Model

If all these aforementioned assumptions are incorporated into our previous model, which was presented in Section 5.2.3 of the previous chapter, then our non-dimensional model for the evolution of a tumour undergoing therapy is:

$$\frac{\mathrm{d}P_s}{\mathrm{d}t} = -\Big\{1 + \psi_1\mathcal{S}_1 + \eta\mathcal{S}_2 + \kappa_1 C + \varepsilon\Big\}P_s + \psi_2\left(1 - \mathcal{S}_1\right)Q_s + \bar{\varepsilon}P_r, \tag{6.2}$$

$$\frac{\mathrm{d}Q_s}{\mathrm{d}t} = \Big\{2 + \psi_1\mathcal{S}_1\Big\}P_s - \Big\{\psi_2\left(1 - \mathcal{S}_1\right) + \eta\mathcal{S}_2\Big\}Q_s \tag{6.3}$$

$$\frac{\mathrm{d}P_r}{\mathrm{d}t} = -\Big\{1 - \omega + \psi_1\mathcal{S}_1 + \eta\mathcal{S}_2 + \sigma\kappa_1 C + \bar{\varepsilon}\Big\}P_r + \psi_2\left(1 - \mathcal{S}_1\right)Q_r + \varepsilon P_s \tag{6.4}$$

$$\frac{\mathrm{d}Q_r}{\mathrm{d}t} = \Big\{2(1-\omega) + \psi_1\mathcal{S}_1\Big\}P_r - \Big\{\psi_2\left(1 - \mathcal{S}_1\right) + \eta\mathcal{S}_2\Big\}Q_r, \tag{6.5}$$

$$\frac{\mathrm{d}N}{\mathrm{d}t} = 2\eta\mathcal{S}_2 + 2\kappa_1 C(P_s + \sigma P_r) + \tfrac{2}{3}\kappa_2 C\lambda \log\left(\tfrac{K}{3\mathcal{P}+1.5N+E}\right) E\mathcal{S}_3 - \nu N, \tag{6.6}$$

$$\frac{\mathrm{d}E}{\mathrm{d}t} = (1-\kappa_2 C)\,\lambda \log\left(\tfrac{K}{3\mathcal{P}+1.5N+E}\right) E\mathcal{S}_3, \tag{6.7}$$

where

$$C(t) = (1-\mathcal{S}_4)\,L(t), \qquad \mathcal{S}_i = S_{w_i}\left(\tfrac{3\mathcal{P}+E}{E}, \alpha_i\right), \qquad \max_t L(t) = 1,$$

and for brevity of presentation we have denoted the total live tumour cell population by $\mathcal{P} = P_s + Q_s + P_r + Q_r$.

Having derived our non-dimensional model we now attempt to evaluate the new non-dimensional parameters which have been introduced to our model, namely the cell mutation rates, ε and $\overline{\varepsilon}$, the partial resistance, σ, and the cost of being resistant, ω.

Parameter Estimation

The mutation rate of normal cells is typically of the order of 1 mutation every 10^{12} replications (Duesberg et al., 2000; Drake et al., 1998). Cancer cells typically have a higher mutation rate than this and mutation rates between 1 mutation every 10^3 and 10^8 replications have been observed (Duesberg et al., 2000; Tomlinson et al., 1996). However mathematical models for the mutation of cancer cells typically assume that the mutation rate of cancer cells is 1 mutation every 10^6 to 10^8 replications (Goldie et al., 1982; Goldie and Coldman, 1998; Sawyers, 2005; Jackson and Loeb, 1998). Assuming that 1 mutation occurs every 10^6 replications and that mutations occur during the proliferative rather than quiescent stage of the cell cycle corresponds to taking the mutation rates to be $\varepsilon = \overline{\varepsilon} = 10^{-6}$, although we consider the affect of varying the mutation rates in Section 6.4.

To estimate the value of σ, the partial resistance of the resistant cells, we relate it to the resistive index, RI, which is defined by

$$\mathrm{RI} = \frac{(\mathrm{IC}_{50})_r}{(\mathrm{IC}_{50})_s}$$

where $(\mathrm{IC}_{50})_r$ is the chemotherapy concentration causing 50% inhibition of the growth of the resistant cells, and $(\mathrm{IC}_{50})_s$ is the chemotherapy concentration causing 50% inhibition of the growth of the sensitive cells (Scappini et al., 2004). Recall that sensitive proliferating cells are killed by chemotherapy of concentration C_s at the rate $\kappa_1\mathrm{C}_s$, and resistant proliferating cells are killed by chemotherapy of concentration

C_r at the rate $\kappa_1 C_r$. Then the fact that $(IC_{50})_r$ and $(IC_{50})_s$ are the chemotherapy concentrations which cause a 50% inhibition in the growth of the respective cell populations, and at such concentrations chemotherapy is likely to be the dominant effect inhibiting cell proliferation, implies that

$$\sigma\kappa_1(IC_{50})_r \approx \kappa_1(IC_{50})_s,$$

and re-arranging this we can relate the partial resistance of the resistant cells to the resistive index thus

$$\sigma \approx \frac{1}{RI}.$$

Hence our parameter σ is aproximately the reciprocal of the resistive index. *In vitro* measurements of the resistive index of leukemia cells have been recorded to be as low as 1, but the resistive index of other cells lines have been recorded to be at least 20 (Scappini et al., 2004). This implies that the parameter σ may vary significantly between different tumours and different therapies and could take any value throughout the range $0 \leq \sigma \leq 1$.

To estimate the value of ω, the cost of being resistant, we use the relative doubling times of resistant tumours. *In vitro* myeloma (cancer of white blood cells) cells have been observed to increase their mean doubling time by approximately 10% following their acquisition of resistance (Dalton et al., 1986; Bellamy et al., 1991). Hence for these cell lines and therapy the cost of being resistant is slight.

However, human lung cancer lines *in vitro* have exhibited an increase in mean doubling time of approximately 63% (Davidson et al., 2004; Gautam and Bepler, 2006). So for these cell lines and therapy the cost of being resistant is high. Furthermore, it is possible that the cost of being resistant in other cell lines might be so high that it prevents a significant resistant population from becoming established; in which case resistant cells with an extremely high cost of resistance would exist, but this high cost of resistance would not be readily observed. This implies that the parameter ω may vary significantly between different tumours and therapies and could take any value throughout the range $0 \leq \omega \leq 1$.

We now consider the treatment schedule.

Treatment Schedule

Recall that in Section 5.3 of the previous chapter we found that for a continuous therapy to be effective it is necessary to apply the therapy for at least a few cell cycle

times. To optimise the chemotherapy effectiveness, but minimise the total amount of chemotherapy delivered, we will apply the therapy continuously for 5 days. This therapy application will then be followed by a rest phase, the duration of which will be varied in our analysis and we will repeat this therapy application followed by a rest phase a number of times. When comparing different therapy schedules the same number of therapy applications will be delivered, to ensure that the schedules are comparably toxic, but in different comparisons we may take a different number of therapy applications. The exact number of therapy applications in any given comparison will be outlined in the text.

Numerical Methods for Simulating the Treatment of the Tumour

We now consider how to simulate the evolution of our tumour. As in Section 5.2.6 of the previous chapter we simulate the evolution of our model using an adaptive linear multi-step method. We note that the time scale for tumour recession during treatment may be much faster then the time scale of unperturbed tumour growth, so again we optimise our adaptive linear stepping for stiff systems. We also prescribe a maximum time step size to ensure that each application of the therapy is resolved.

Initial Conditions

We now consider the initial conditions which we should take in our model for the treatment of a vascular tumour which exhibits resistance. As in Section 5.2.4 of the previous chapter these initial conditions should represent a tumour which has just began to undergo treatment, and hence must represent a tumour which has grown to a clinically detectable size.

To generate such initial conditions we again simulate the evolution of our model, as given by Equations (6.2) to (6.7), in the absence of any therapy, starting with an avascular tumour at saturation which has just begun to undergo angiogenesis and finishing with a tumour has grown to half its maximum size as limited by Gompertzian saturation. To do this we require starting values which represent an avascular tumour at saturation which has just begun to undergo angiogenesis. We take these from Section 4.2.3 of Chapter 4, coupled with the assumption that there are no resistant

cells in the avascular tumour, to obtain the following starting values:

$$P_s(0) = 82,000, \qquad Q_s(0) = 620,000, \qquad P_r(0) = 0,$$
$$Q_r(0) = 0, \qquad N(0) = 440,000, \qquad E(0) = 1.$$

These starting values are used to initiate our model in the absence of therapy which allows us to calculate the initial conditions which then are then used in our model in the presence of therapy.

In the absence of any therapy our model still depends upon the cost of being resistant, ω, but is independent of the partial resistance, σ. To investigate how sensitive our initial conditions are to the cost of being resistant we calculate and compare the corresponding initial conditions for the range of values of ω outlined above, for the mutation rates $\varepsilon = \overline{\varepsilon} = 10^{-6}$. The remaining parameter values are as given in Table 4.2 for the 25% growth fraction tumour. The initial conditions we should take in our resistance model depend upon ω as shown in the log plot in Figure 6.1.

It can be seen in Figure 6.1 that as the cost of resistance is increased, a smaller resistant population becomes established. Whilst the sensitive cell population is robust to changes in ω, the resistant cell population is highly sensitive to changes in ω. In particular there is approximately a 200-fold difference in the number of live resistant cells, $P_r + Q_r$, when $\omega = 0$ compared to $\omega = 1$. This is clearly highly significant and the initial conditions we should take in our model should therefore depend upon ω. Hence, for any given value of ω we will perform a simulation to calculate the corresponding initial conditions using the methodology outlined above.

6.2.2 Sensitivity Analysis

We now perform a sensitivity analysis to investigate how our model depends upon the new parameters which have been introduced. Note that in Section 5.2.8 of the previous chapter we found that the therapy can target the tumour using two distinct mechanisms, either by acting as a traditional chemotherapeutic or by exploiting the angiogenesis-therapy feedback loop, and we identified parameter values for which the therapy uses each mechanism. However, it is not known how the inclusion of resistance and the longer therapy application duration now used might affect the mechanism by which the therapy treats the tumour. In particular, the longer therapy application now being applied is likely to alter the parameter values for which each mechanism is utilised. Hence we begin by taking broad, clinically relevant parameters

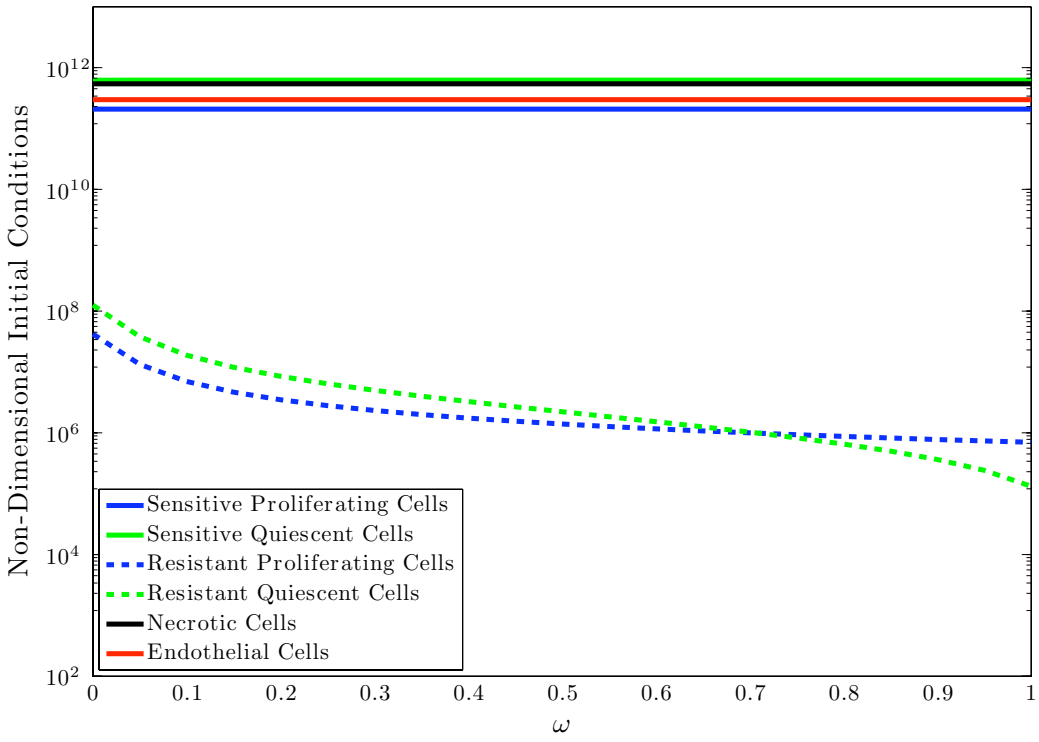

Figure 6.1: The initial conditions in our model including resistance as a function of the cost of being resistant, ω, for the parameter values as outlined in the text, as governed by Equations (6.2) to (6.7). These initial conditions are generated by simulating the evolution of the tumour in the absence of any therapy until the tumour reaches half its maximum size as allowed by Gompertzian saturation (see text for details).

and do not deliberately seek to identify treatment mechanisms yet. Educated by our previous parameter estimation in Section 5.2.4 and Section 6.2.1 we begin by taking the parameter values outlined in Table 6.1.

Also note that during our parameter estimation in Section 6.2.1 we found that both the partial resistance, σ, and the cost of being resistant, ω, are free parameters which may vary significantly from tumour to tumour and therapy to therapy. It is expected that the behaviour of the tumour and the onset of resistance will strongly and jointly depend upon both these parameters and so we now vary them jointly and observe the behaviour of the resulting tumour.

Parameter	Description	Value
κ_1	Sensitivity of proliferating cells to chemotherapy	5
κ_2	Sensitivity of endothelial cells to chemotherapy	25
ε	The mutation rate at which cells randomly acquire resistance	10^{-6}
$\overline{\varepsilon}$	The mutation rate at which cells randomly lose resistance	10^{-6}
The application period	The duration of the therapies	5 days
The rest period	The rest period between therapies	9 days

Table 6.1: The non-dimensional parameter values initially used in our sensitivity analysis.

The Joint Sensitivity of the Tumour Upon σ and ω

The volume of live sensitive cells in the tumour, as defined by $\frac{3(P_s+Q_s)}{0.66}10^{-6}\,\mathrm{mm}^3$, the volume of live resistant cells in the tumour, as defined by $\frac{3(P_r+Q_r)}{0.66}10^{-6}\,\mathrm{mm}^3$, and the total volume of live tumour cells in the tumour as functions of the resistive parameters σ and ω for the parameter values given in Table 6.1 are shown in Figure 6.2.

In Figure 6.2(c) it can be seen that cure is possible for most values of the resistance parameters, σ and ω, however the therapy fails due to the onset of resistance for a region of parameter values which partitions the parameter plane.

For parameter values above and to the right of the region where the therapy fails due to resistance, i.e. for therapies with a relatively high cost of being resistant and to which the resistant cells are relatively highly susceptible, it can be seen in Figure 6.2 that whilst the total tumour volume is small there is a small residual population of sensitive cells. For these parameter values the resistant cells have a relatively high proliferative cost to being resistant, and a relatively low benefit to being resistant, and so the sensitive cells have a competitive advantage over the resistant ones and no resistant population becomes established. By considering the evolution of the different cell populations (results not shown) it can be confirmed that in this region the therapy is acting as a traditional chemotherapeutic so that the tumour undergoes exponential-like decay whilst the therapy is being applied, and then recovers during the rest periods in between applications of the therapy. A small

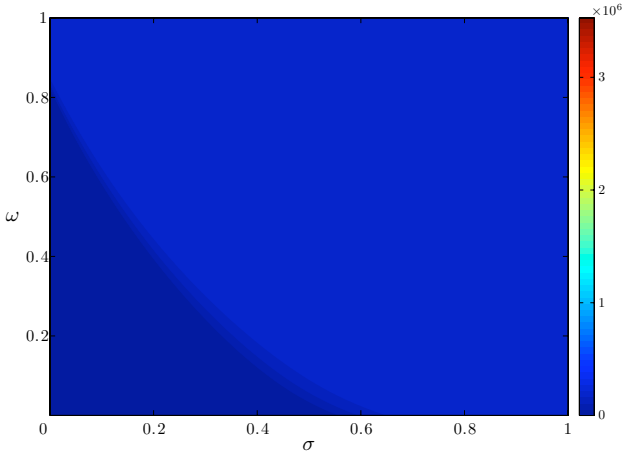

(a) Sensitive Tumour Cells.

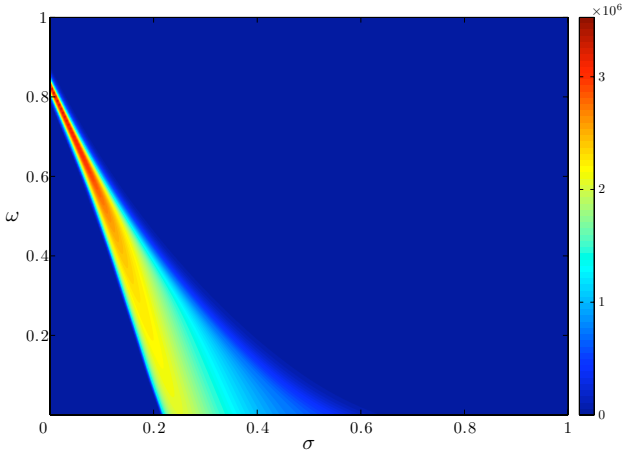

(b) Resistant Tumour Cells.

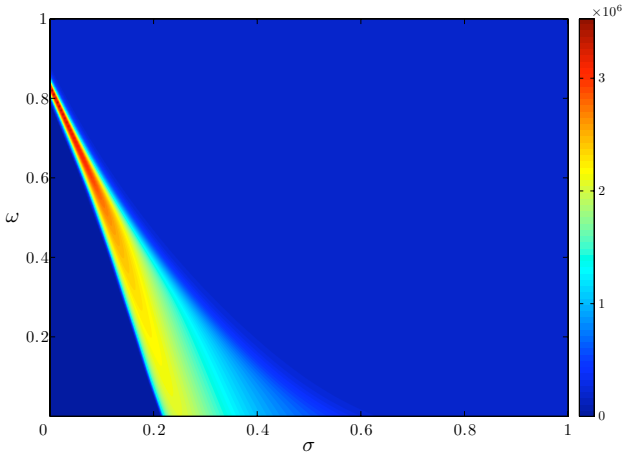

(c) Total Live Tumour Cells.

Figure 6.2: The volume of cells present in our 25% growth fraction tumour (in mm^3) upon cessation of the tenth application of therapy as a function of the partial resistance, σ, and the cost of being resistant, ω, for our 25% growth fraction tumour and the other parameter values outlined in Table 6.1, as governed by Equations (6.2) to (6.7).

sensitive cell population remains because the cell cycle specific drug cannot target the quiescent cells directly and so complete tumour eradication is difficult.

The therapy fails when the resistant cells are more resistant to the therapy, i.e. have a lower value of σ, and/or have a lower cost of being resistant, i.e. have lower values of ω. Since the therapy is now less effective at treating the resistant cells, and/or the resistant cells have a lower cost of being resistant, the therapy fails to effectively target the resistant cells and a significant resistant population becomes established and can grow despite the applications of the therapy.

It is also found that if the resistant cells are even more resistant to the therapy, i.e. have a lower value of σ, and/or have an even lower cost of being resistant, i.e. have a lower value of ω, then the therapy becomes effective again and tumour cure is possible, which is counter-intuitive. By considering the evolution of the different cell populations (results not shown) it is found that in this region the therapy is now so poor at targeting the resistant cells that when the therapy is applied it gives the resistant cells a competitive advantage over the sensitive cells and a resistant cell population quickly becomes established. Once this resistant population has become established each application of therapy is more effective at treating the endothelial cells than the tumour cells, and then each application of the therapy undervascularises the tumour which results in the upregulation of angiogenesis. With angiogenesis upregulated the endothelial cells are then primed for the next application of therapy and there is a compounding effect whereby each application of the therapy targets the endothelial cells, but also primes the tumour for the next application of therapy. Hence the therapy can now use resistance to exploit the angiogenesis-therapy feedback loop which was identified in Section 5.2.8 of the previous chapter. Note that here the therapy is using resistance to exploit the angiogenesis-therapy feedback loop because once resistance is established the therapy becomes better at targeting the endothelial cells than the resistant tumour cells. For these parameter values the therapy is unable to provide a significant anti-angiogenic effect in the absence of this resistance.

Note that for the therapy to use resistance to exploit the angiogenesis-therapy feedback loop requires the establishment of a resistant population in the tumour. Since tumour cells typically exhibit higher cell mutation rates than non-cancerous cells (Boehm et al., 1997) a resistant population will typically become established in a tumour more readily than in non-cancerous cells. Hence we would expect tumour tissue to be more susceptible to a therapy which uses resistance to exploit the angiogenesis-therapy feedback loop than non-cancerous tissue, and so we would

expect it to be possible to successfully target a tumour by using resistance to exploit the angiogenesis-therapy feedback loop without providing a prohibitively toxic effect to the non-cancerous tissue.

It can be confirmed that there are parameter values where the therapy is providing an effective anti-angiogenic therapy by reconsidering these results when the therapy provides no anti-angiogenic effect, i.e. when $\kappa_2 = 0$ and the other parameter values are given in Table 6.1. The volume of live sensitive cells in the tumour, as defined by $\frac{3(P_s+Q_s)}{0.66}10^{-6}\,\text{mm}^3$, the volume of live resistant cells in the tumour, as defined by $\frac{3(P_r+Q_r)}{0.66}10^{-6}\,\text{mm}^3$, and the total volume of live cells in the tumour as functions of σ and ω for the other parameter values given in Table 6.1 are shown in Figure 6.3. It can be seen that when the therapy fails it does so because of the onset of resistance. This occurs when σ and ω are both low, i.e. when the resistant cells are highly resistant to the therapy but with a low cost of being resistant. Comparing Figures 6.2(c) and 6.3(c) it can be seen that the region of parameter values for which the therapy uses resistance to exploit the angiogenesis-therapy feedback loop is very similar to the region for which the therapy completely fails when it provides no anti-angiogenic effect. This highlights how important the anti-angiogenic affect of the therapy is and that it should be considered when designing therapy schedules. In particular it can be seen in Figure 6.2 that when the therapy provided a moderate anti-angiogenic effect it performs best when using resistance to exploit the angiogenesis-therapy feedback loop, which requires relatively low values of both σ and ω. However, in Figure 6.3 it can be seen that these are the worst parameter values when the therapy provides no anti-angiogenic affect.

In this section we have found that therapies with fixed chemotherapy kill rates can either provide effective cure as a traditional chemotherapeutic, fail due to the onset of resistance, or provide an effective therapy by exploiting the angiogenesis-therapy feedback loop, and that which of these situations occurs depends upon the values of the resistance parameters σ and ω. To allow us to consider each of these mechanisms in our later analysis we now identify parameter values where the therapy acts as a traditional chemotherapeutic, which are presented in Table 6.2, fails because of the onset of resistance, which are presented in Table 6.3, and uses resistance to exploit the angiogenesis therapy feedback loop, which are presented in Table 6.4.

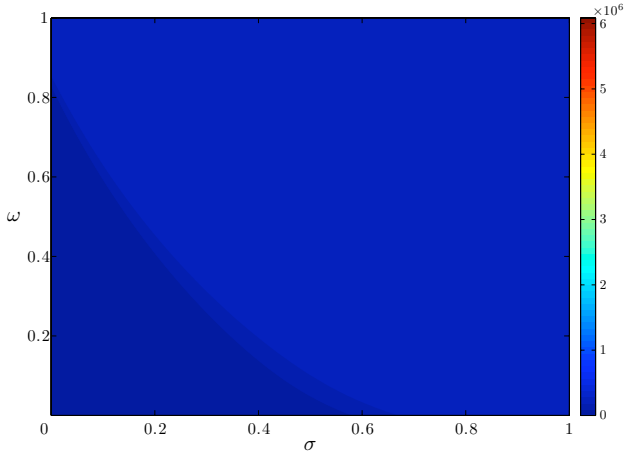

(a) Sensitive Tumour Cells.

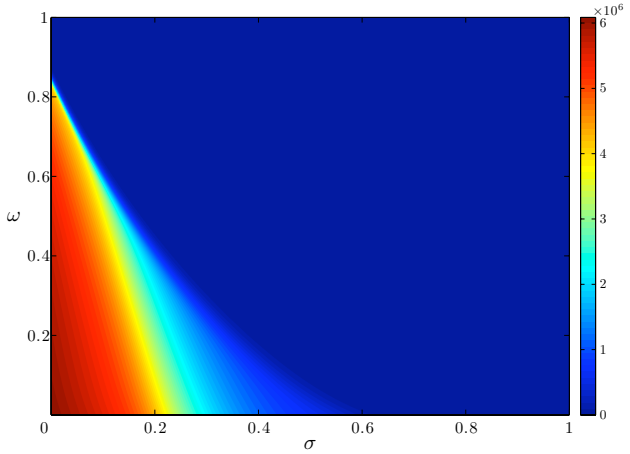

(b) Resistant Tumour Cells.

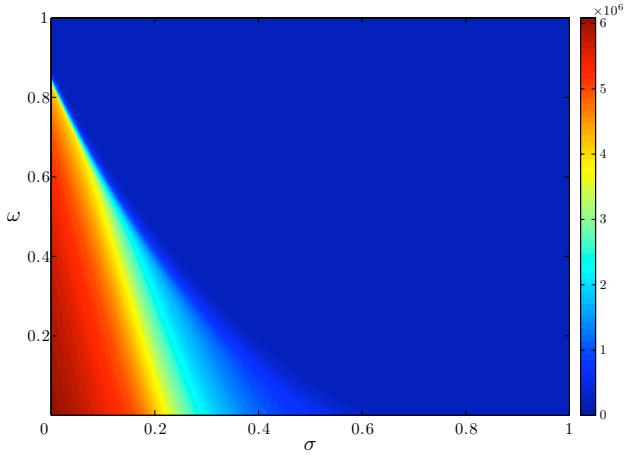

(c) Total Live Tumour Cells.

Figure 6.3: The volume of cells present in our 25% growth fraction tumour (in mm^3) upon cessation of the tenth application of therapy as a function of the partial resistance, σ, and the cost of being resistant, ω, for our 25% growth fraction tumour and the other parameter values outlined in Table 6.1, except for $\kappa_2 = 0$, as governed by Equations (6.2) to (6.7).

Parameter	Description	Value
κ_1	Sensitivity of proliferating cells to chemotherapy	5
κ_2	Sensitivity of endothelial cells to chemotherapy	25
ε	The mutation rate at which cells randomly acquire resistance	10^{-6}
$\overline{\varepsilon}$	The mutation rate at which cells randomly lose resistance	10^{-6}
The application period	The duration of the therapies	5 days
The rest period	The rest period between therapies	9 days
σ	The partial resistance	0.35
ω	The cost of being resistant	0.35

Table 6.2: The non-dimensional parameter values for which our therapy acts as a traditional chemotherapeutic.

Parameter	Description	Value
κ_1	Sensitivity of proliferating cells to chemotherapy	5
κ_2	Sensitivity of endothelial cells to chemotherapy	25
ε	The mutation rate at which cells randomly acquire resistance	10^{-6}
$\overline{\varepsilon}$	The mutation rate at which cells randomly lose resistance	10^{-6}
The application period	The duration of the therapies	5 days
The rest period	The rest period between therapies	9 days
σ	The partial resistance	0.08
ω	The cost of being resistant	0.6

Table 6.3: The non-dimensional parameter values for which the therapy fails because of the onset of resistance.

Parameter	Description	Value
κ_1	Sensitivity of proliferating cells to chemotherapy	5
κ_2	Sensitivity of endothelial cells to chemotherapy	25
ε	The mutation rate at which cells randomly acquire resistance	10^{-6}
$\overline{\varepsilon}$	The mutation rate at which cells randomly lose resistance	10^{-6}
The application period	The duration of the therapies	5 days
The rest period	The rest period between therapies	9 days
σ	The partial resistance	0.15
ω	The cost of being resistant	0.15

Table 6.4: The non-dimensional parameter values for which the therapy uses resistance to exploit the angiogenesis-therapy feedback loop.

6.3 The Norton-Simon Hypothesis (with Resistance)

In Section 5.3 of the previous chapter we validated the Norton-Simon hypothesis, that dose dense therapies provide more effective cell kill than dose sparse therapies. We now consider whether this conclusion is affected by the inclusion of resistance and how the dose density of the therapy affects the onset and evolution of resistance. To do this we simulate the evolution of our model whilst alternating the dose density of the therapy and we will begin by using parameters for which the therapy fails because of the onset of resistance. To ensure that all the therapy schedules considered are similarly toxic to the non-cancerous cells we will deliver ten applications of the chemotherapy in each therapy schedule. We will consider the Norton-Simon hypothesis in the case where the therapy fails because of the onset of resistance. Hence we take parameter values in Table 6.3 and the other parameter values presented in Table 4.2, though with variation of the rest phase. The resultant volume of the live cell compartments in the tumour at the end of the tenth application of therapy as a function of the rest phase is shown in Figure 6.4.

It can be seen that for very dose dense therapies, with rest periods of less than three days or so, the therapy eradicates the tumour and the fact that the endothelial

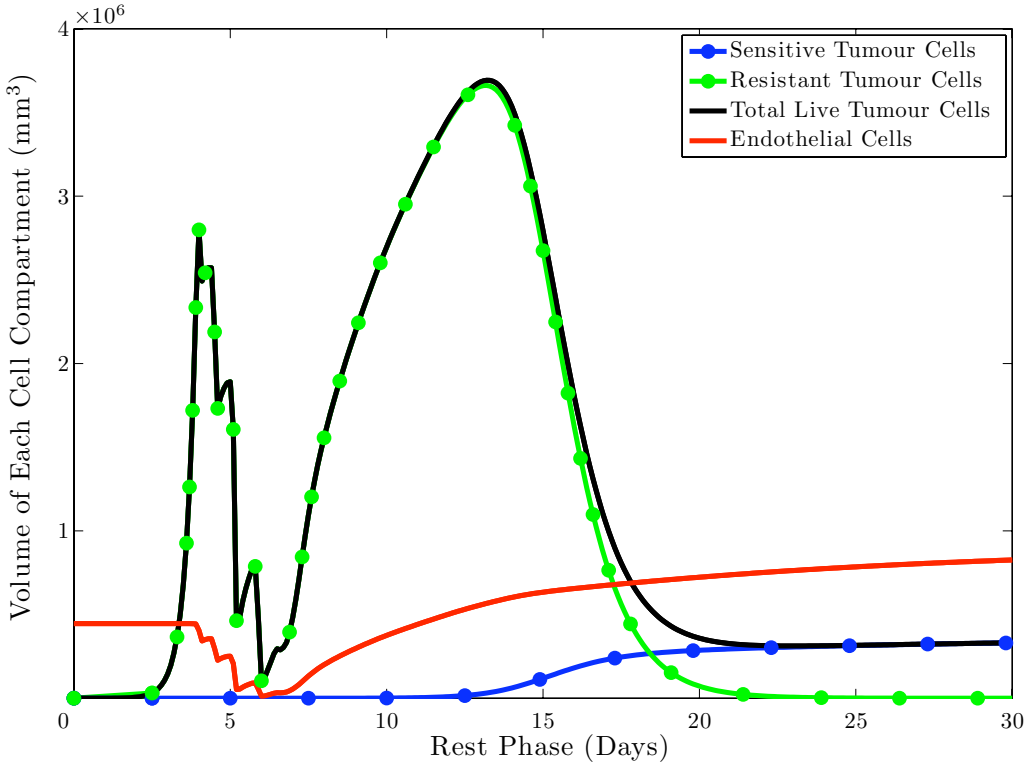

Figure 6.4: The volumes of the live cell compartments in our 25% growth fraction tumour after the tenth application of therapy as a function of the rest phase between application of therapy for the other parameter values given in Tables 4.2 and 6.3, as governed by Equations (6.2) to (6.7). Plot generated for a large number of discrete values of the rest period and then linearly interpolated.

cell population is unaffected by the therapy shows that the therapy is acting as a traditional chemotherapeutic. As the therapy is made less dense it becomes less effective and there is then a small range of rest phases, of about three to six days, where the therapy fails as a traditional chemotherapeutic and a resistant population becomes established. However, there is a local optimal rest phase of approximately six days where the therapy is relatively poor at treating the resistant cells, but relatively good at treating the endothelial cells so that the therapy is effective at exploiting the angiogenesis-therapy feedback loop. The fact that the angiogenesis-therapy feedback loop can only be exploited for a relatively narrow range of rest phases and that oscillations are observed in this region suggest that the angiogenesis-therapy feedback loop is more sensitive to the rest phase when resistance is being exploited than it was in Section 5.3.1 when resistance was not considered. Increasing the rest phase further,

from approximately six days up to approximately thirteen days, results in the therapy losing its ability to use resistance to exploit the angiogenesis-therapy feedback loop. Increasing the rest phase further still, past twenty days or so, results in a tumour which consists largely of sensitive rather than resistant cells and a smaller tumour is observed following the application of the therapy because the larger sensitive portion of the tumour allows more of the tumour to be targeted by the therapy.

Hence there is broad agreement between our model and the Norton-Simon hypothesis. Decreasing the rest phase did always lead to a more potent therapy, however the potential to use resistance to exploit the angiogenesis-therapy feedback loop and the fact that resistant cells cannot always be treated means that it is not always desirable to apply the most potent therapy. In particular, using resistance to exploit the angiogenesis-therapy feedback loop requires the therapy to be sufficiently impotent for it to fail to target the resistant cells, but potent enough to target the endothelial cells. Hence increasing the rest phase, which makes the therapy less potent, could drive a better balance between these two effects and lead to a more effective therapy (in Figure 6.4 the balance between these two effects occurs at the locally optimal rest phase of approximately 6 days).

Furthermore, if tumour cure is not possible then a more dose sparse, less potent therapy, might be desirable to use cellular competition to prevent the onset of resistance. With the onset of resistance prevented it may be possible to schedule a maintenance therapy, which may not be possible if a population of resistant cells had become established.

6.4 The Resistance of Endothelial Cells

In Section 6.2.2 we identified the potential of using resistance to allow a chemotherapeutic to exploit the angiogenesis-therapy feedback loop. It is possible that this result relies upon the often made assumption that endothelial cells do not acquire resistance. We now consider whether this result is affected by the allowance of endothelial cell resistance and we begin by considering the probability that there are no resistant endothelial cells present.

6.4.1 The Probability of Endothelial Cell Resistance

We begin by quantifying the probability that there are no endothelial cells present. If this probability is suitably small then we will have explicitly justified the assumption that the resistance of endothelial cells can be neglected.

The Model

Defining ε_e to be the spontaneous mutation rate at which endothelial cells acquire resistance per replication, the probability of there being no resistant endothelial cells present, p_0, after n cell divisions is

$$p_0 = (1 - \varepsilon_e)^n.$$

Assuming that cell proliferation dominates the growth of endothelial cells, then the number of cell divisions after time t will be

$$n = E(t) - E(0). \tag{6.8}$$

Hence the probability of there being no resistant endothelial cells present after time t is

$$p_0(t) = (1 - \varepsilon_e)^{(E(t)-E(0))}. \tag{6.9}$$

Note that the death of endothelial cells means that Equation (6.8) will actually underestimate the number of endothelial cell divisions and so Equation (6.9) will overestimate the probability of there being no resistant endothelial cells present.

The Mutation Rate of Endothelial Cells

To evaluate Equation (6.9) we require an estimate of the mutation rate of endothelial cells. The mutation rate specifically of endothelial cells has not been widely considered and whilst it has been noted that endothelial cells are more genetically stable than tumour cells, it is not clear whether they should be more or less genetically stable than other non-cancerous cells. In order to estimate the likely magnitude of the endothelial cell mutation rate, ε_e, we now consider the mutation rates of normal non-cancerous cells.

Duesberg et al. (2000) found the mutation rate of normal diploid cells to correspond to $\varepsilon_e = 10^{-12}$, and Drake et al. (1998) found the mutation rates of normal cells

to correspond to $\varepsilon_e = 5 \times 10^{-11}$. Whereas higher mutation rates corresponding to $\varepsilon_e = 2 \times 10^{-7}$ have also been reported (Jackson and Loeb, 1998). Given this range of cell mutation rates we now consider whether the resistance of endothelial cells can ever be *a priori* neglected.

The Probability of No Resistant Endothelial Cells Existing

We now calculate the probability that there are no resistant endothelial cells present in the absence of any therapy by simulating the evolution of the tumour, using the methodology outlined in Section 6.2.1, and inputting the results of the simulation into our equation for the probability of there being no endothelial cells present, Equation (6.9). Note that even in the absence of any therapy our model depends upon the cost of being resistant, ω. However, the probability of there being no resistant endothelial cells present is expected to only weakly depend upon the value of ω, and so for this calculation we set $\omega = 0.5$. Then the probability of there being no resistant endothelial cells in the absence of any therapy as a function of tumour volume for different values of the endothelial cell mutation rate, ε_e, for the parameter values in Table 4.2 is shown in Figure 6.5.

It can be seen that for the range of endothelial cell mutation rates which are clinically relevant, i.e. values up to and including $\varepsilon_e = 10^{-12}$, it is not guaranteed that the endothelial cell population will contain no resistant cells. Furthermore, for some clinically relevant mutation rates, $\varepsilon_e = 10^{-8}, 10^{-10}$ for example, it is almost certain that at least one resistant endothelial cell will be present. This is despite choosing a form for $p_0(t)$ which underestimates the probability of there being a mutation and ignoring the potential for mutations to occur after the therapy has started. Hence we should not *a priori* assume that no resistant endothelial cells will exist. Given this we now consider whether a therapy can still use resistance to exploit the angiogenesis-therapy feedback loop when the endothelial cells can also acquire resistance.

6.4.2 A Tumour with Resistant Endothelial Cells

The Model

We include the resistance of endothelial cells in a similar way to that used to include resistant tumour cells, which gave the model governed by Equations (6.2) to (6.7). We let the non-dimensional number of sensitive and resistant endothelial cells be denoted

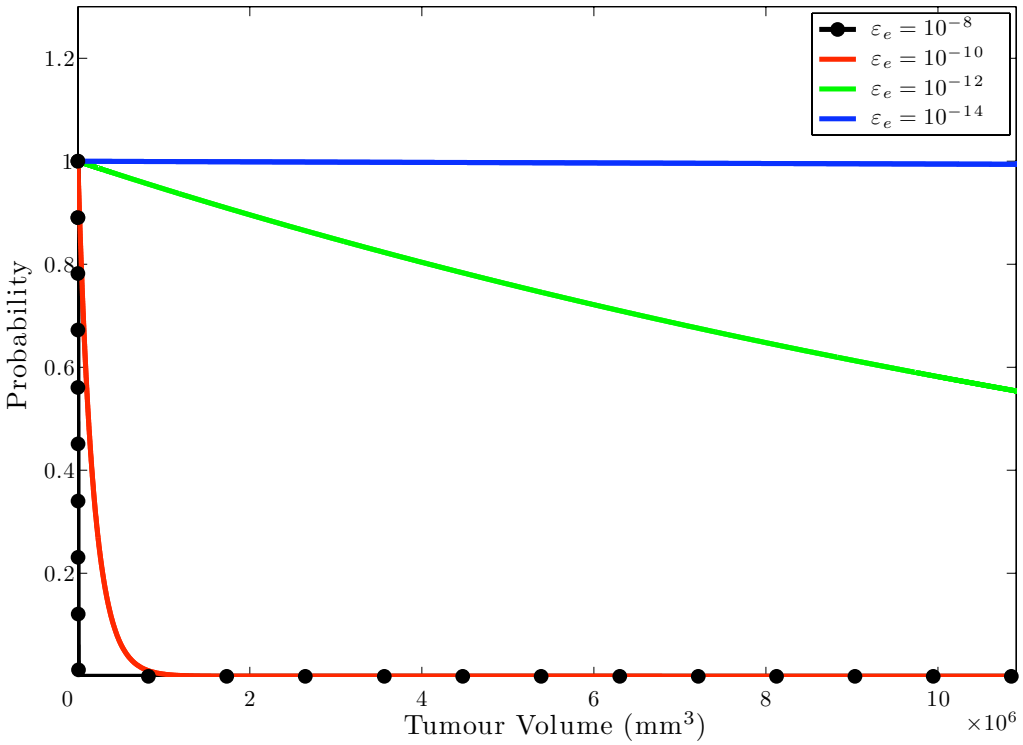

Figure 6.5: The probability of there being no resistant endothelial cells in our modelled tumour, as governed by Equations (6.2) to (6.7), in the absence of any therapy, as a function of tumour volume for different values of the endothelial cell mutation rate, ε_e, and the other parameter values as outlined in Table 4.2.

by E_s and E_r respectively. Then recalling that we found an expression for the fraction of endothelial cells which are proliferating in Section 5.2.4 we can generalise this to give the following expression for the fraction of sensitive endothelial cells which are proliferating

$$\phi = \frac{60}{15.9\log(2)}\left(\frac{\mathrm{d}E_s}{\mathrm{d}t}\right)_{\mathrm{un}},$$

where $\left(\frac{\mathrm{d}E_s}{\mathrm{d}t}\right)_{\mathrm{un}}$ is the unperturbed growth rate of the sensitive endothelial cell population. We also assume that sensitive endothelial cells mutate to acquire resistance at a rate ε_e per cell cycle, and each cell cycle takes $\frac{60}{15.9\log(2)}$ non-dimensional time units, hence the non-dimensional rate at which sensitive endothelial cells mutate to acquire resistance is $\frac{15.9\log(2)\varepsilon_e}{60}$ per proliferating cell per unit time. Therefore the rate at which the population of sensitive endothelial cells mutates to acquire resistance is

$$\varepsilon_e\left(\frac{\mathrm{d}E_s}{\mathrm{d}t}\right)_{\mathrm{un}}.$$

Similarly, the rate at which resistant endothelial cells mutate to lose resistance is

$$\overline{\varepsilon}_e \left(\frac{\mathrm{d}E_r}{\mathrm{d}t} \right)_{\mathrm{un}},$$

where $\overline{\varepsilon}_e$ is the rate at which resistant endothelial cells mutate to lose resistance per cell cycle. This, coupled with our previously made assumptions concerning resistance which were made in Section 6.2 gives the following model for the evolution of our tumour with the resistance of endothelial cells explicitly considered:

$$\frac{\mathrm{d}P_s}{\mathrm{d}t} = -\Big\{1 + \psi_1 \mathcal{S}_1 + \eta \mathcal{S}_2 + \kappa_1 C + \varepsilon\Big\} P_s + \psi_2 \left(1 - \mathcal{S}_1\right) Q_s + \overline{\varepsilon} P_r, \tag{6.10}$$

$$\frac{\mathrm{d}Q_s}{\mathrm{d}t} = \Big\{2 + \psi_1 \mathcal{S}_1\Big\} P_s - \Big\{\psi_2 \left(1 - \mathcal{S}_1\right) + \eta \mathcal{S}_2\Big\} Q_s \tag{6.11}$$

$$\frac{\mathrm{d}P_r}{\mathrm{d}t} = -\Big\{1 - \omega + \psi_1 \mathcal{S}_1 + \eta \mathcal{S}_2 + \sigma\kappa_1 C + \overline{\varepsilon}\Big\} P_r + \psi_2 \left(1 - \mathcal{S}_1\right) Q_r + \varepsilon P_s \tag{6.12}$$

$$\frac{\mathrm{d}Q_r}{\mathrm{d}t} = \Big\{2(1-\omega) + \psi_1 \mathcal{S}_1\Big\} P_r - \Big\{\psi_2 \left(1 - \mathcal{S}_1\right) + \eta \mathcal{S}_2\Big\} Q_r, \tag{6.13}$$

$$\frac{\mathrm{d}N}{\mathrm{d}t} = 2\eta \mathcal{P} \mathcal{S}_2 + 2\kappa_1 C(P_s + \sigma P_r) + \tfrac{2}{3}\kappa_2 C \lambda \log\left(\tfrac{K}{3\mathcal{P}+1.5N+E_s+E_r}\right)(E_s + \sigma E_r)\mathcal{S}_3 - \nu N, \tag{6.14}$$

$$\frac{\mathrm{d}E_s}{\mathrm{d}t} = \Big\{(1 - \kappa_2 C - \varepsilon_e)E_s + \overline{\varepsilon}_e(1-\omega)E_r\Big\} \lambda \log\left(\tfrac{K}{3\mathcal{P}+1.5N+E_s+E_r}\right) \mathcal{S}_3, \tag{6.15}$$

$$\frac{\mathrm{d}E_r}{\mathrm{d}t} = \Big\{(1 - \sigma\kappa_2 C - \overline{\varepsilon}_e)(1-\omega)E_r + \varepsilon_e E_s\Big\} \lambda \log\left(\tfrac{K}{3\mathcal{P}+1.5N+E_s+E_r}\right) \mathcal{S}_3, \tag{6.16}$$

where

$$C(t) = \left(1 - \mathcal{S}_4\right) L(t), \qquad \mathcal{S}_i = S_{w_i}\left(\tfrac{3\mathcal{P}+E_s+E_r}{E_s+E_r}, \alpha_i\right),$$
$$\max_t L(t) = 1, \qquad \mathcal{P} = P_s + Q_s + P_r + Q_r.$$

Numerical Methods for Simulating the Treatment of the Tumour

As in Section 6.2.1 we simulate the evolution of our model using an adaptive linear multi-step method where the adaptive linear stepping is optimised for stiff systems and a maximum time step size is prescribed which ensures that each application of the therapy is resolved.

Initial Conditions

As before our initial conditions should represent a tumour which has grown to a clinically detectable size. To generate such initial conditions we again simulate our

tumour in the absence of any therapy, starting with an avascular tumour at saturation which has just begun to undergo angiogenesis and finishing with a tumour at half its maximum size as limited by Gompertzian saturation. To do this we require starting values which represent an avascular tumour at saturation which has just begin to undergo angiogenesis. We take these from Section 4.2.3, coupled with the assumption that there are no resistant cells in an avascular tumour, to obtain the following starting values in our initial condition generation:

$$P_s(0) = 82,000, \qquad Q_s(0) = 620,000, \qquad P_r(0) = 0, \qquad Q_r(0) = 0,$$
$$N(0) = 440,000, \qquad E_s(0) = 1, \qquad E_r(0) = 0.$$

Results

We are investigating whether resistance can still be used to exploit the angiogenesis-therapy feedback loop when the resistance of endothelial cells is included. Hence we take our resistance parameter values from Table 6.4, and the other parameter values from Table 4.2, and then the volume of the different cell compartments at the end of the tenth application of therapy for different values of the endothelial cell mutation rate, ε_e, are shown in Figure 6.6. It can be seen that when $\varepsilon_e = \overline{\varepsilon}_e = 10^{-6}$, which is the same mutation rate as for the tumour cells, the therapy performs significantly worse than when $\varepsilon_e = \overline{\varepsilon}_e << 10^{-6}$. In fact if the long time behaviour of the model is considered it is found that the therapy fails when $\varepsilon_e = \overline{\varepsilon}_e = 10^{-6}$, but successfully exploits the angiogenesis-therapy feedback loop for the smaller values of the endothelial cell mutation rates.

Considering the growth curves of the tumour compartments (results not shown) it can be seen that when the endothelial cell mutation rates are much smaller than the tumour cell mutation rates, a significant resistant population of tumour cells becomes established in the period before the resistance becomes established in the endothelial cells. This allows the angiogenesis-therapy feedback loop to be exploited before endothelial cell resistance becomes significantly established and whilst there are resistant endothelial cells present, there is a greater proportion of resistant tumour cells and so the tumour is still primed to exploit the angiogenesis-therapy feedback loop.

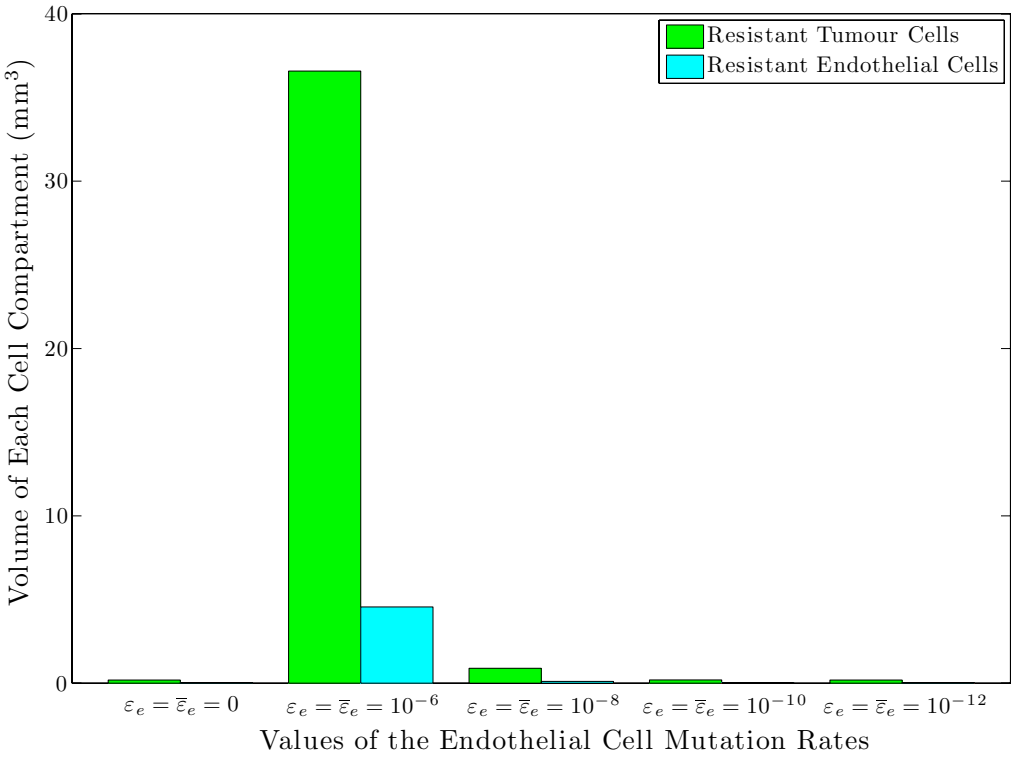

Figure 6.6: The volume of cells in our 25% growth fraction tumour upon completion of the tenth application of chemotherapy for different values of the endothelial cell mutation rates and the other parameter values as outlined in Tables 4.2 and 6.4. Cell populations which are present in too smaller volume to be readily seen are not labelled in the legend.

Conclusions

In this section we investigated whether neglecting the resistance of endothelial cells is necessary for the therapy to be able to use resistance to exploit the angiogenesis-therapy feedback loop. We found that in tumours undergoing therapy we would expect there to be at least one resistant endothelial cell present, so that the resistance of endothelial cells cannot be *a priori* neglected, but including the resistance of endothelial cells did not prevent the exploitation of the angiogenesis-therapy feedback loop in protocol scheduling. If the endothelial cells mutate more slowly than the tumour cells, then it was found that resistance becomes established within the tumour before the endothelial cell population and that this is sufficient to enable the therapy to exploitation of the angiogenesis-therapy feedback loop. Given that tumour cells are typically observed to have mutation rates which are orders of magnitude larger

than normal cells (Drake et al., 1998; Duesberg et al., 2000) we conclude that our results concerning the use of resistance to exploit the angiogenesis-therapy feedback loop when endothelial cell resistance was ignored would still be valid if endothelial cell resistance was included. Furthermore, since our results and conclusions are not significantly affected by the modelling of endothelial cell resistance, we do not consider this effect in our further work.

6.5 Double Resistance

Multiple therapies are often applied in an attempt to prevent the onset of resistance (Goldie et al., 1982). Furthermore, the Goldie-Coldman hypothesis and Day's worst drug first rule both concern the joint application of two distinct chemotherapies. We now derive a model for the application of, and resistance to, two distinct chemotherapies.

6.5.1 The Model

The assumptions of our double therapy model will be equivalent to the assumptions of our single therapy model, albeit with the obvious generalisations. We refer to the two therapies as therapy 1 and therapy 2, and then generalising the model of Section 6.2 to consider the application of two therapies we obtain the non-dimensional system:

$$\begin{aligned}\frac{\mathrm{d}P_s}{\mathrm{d}t} = &-\Big\{1+\psi_1\mathcal{S}_1+\eta\mathcal{S}_2+\kappa_{11}C_1+\kappa_{12}C_2+\varepsilon_1+\varepsilon_2\Big\}P_s\\ &+\psi_2\left(1-\mathcal{S}_1\right)Q_s+\overline{\varepsilon}_1P_{r1}+\overline{\varepsilon}_2P_{r2},\end{aligned} \tag{6.17}$$

$$\frac{\mathrm{d}Q_s}{\mathrm{d}t} = \Big\{2+\psi_1\mathcal{S}_1\Big\}P_s-\Big\{\psi_2\left(1-\mathcal{S}_1\right)+\eta\mathcal{S}_2\Big\}Q_s, \tag{6.18}$$

$$\begin{aligned}\frac{\mathrm{d}P_{r1}}{\mathrm{d}t} = &-\Big\{1-\omega_1+\psi_1\mathcal{S}_1+\eta\mathcal{S}_2+\sigma_1\kappa_{11}C_1+\kappa_{12}C_2+\overline{\varepsilon}_1+\varepsilon_2\Big\}P_{r1}\\ &+\psi_2\left(1-\mathcal{S}_1\right)Q_{r1}+\varepsilon_1P_s+\overline{\varepsilon}_2P_{r12}\end{aligned} \tag{6.19}$$

$$\frac{\mathrm{d}Q_{r1}}{\mathrm{d}t} = \Big\{2(1-\omega_1)+\psi_1\mathcal{S}_1\Big\}P_{r1}-\Big\{\psi_2\left(1-\mathcal{S}_1\right)+\eta\mathcal{S}_2\Big\}Q_{r1}, \tag{6.20}$$

$$\begin{aligned}\frac{\mathrm{d}P_{r2}}{\mathrm{d}t} = &-\Big\{1-\omega_2+\psi_1\mathcal{S}_1+\eta\mathcal{S}_2+\kappa_{11}C_1+\sigma_2\kappa_{12}C_2+\varepsilon_1+\overline{\varepsilon}_2\Big\}P_{r2}\\ &+\psi_2\left(1-\mathcal{S}_1\right)Q_{r2}+\overline{\varepsilon}_1P_{r12}+\varepsilon_2P_s\end{aligned} \tag{6.21}$$

$$\frac{\mathrm{d}Q_{r2}}{\mathrm{d}t} = \Big\{2(1-\omega_2)+\psi_1\mathcal{S}_1\Big\}P_{r2}-\Big\{\psi_2\left(1-\mathcal{S}_1\right)+\eta\mathcal{S}_2\Big\}Q_{r2}, \tag{6.22}$$

$$\frac{\mathrm{d}P_{r12}}{\mathrm{d}t} = -\Big\{(1-\omega_1)(1-\omega_2) + \psi_1\mathcal{S}_1 + \eta\mathcal{S}_2 + \sigma_1\kappa_{11}C_1 + \sigma_2\kappa_{12}C_2 + \overline{\varepsilon}_1 + \overline{\varepsilon}_2\Big\}P_{r12} + \psi_2\left(1-\mathcal{S}_1\right)Q_{r12} + \varepsilon_1 P_{r2} + \varepsilon_2 P_{r1} \tag{6.23}$$

$$\frac{\mathrm{d}Q_{r12}}{\mathrm{d}t} = \Big\{2(1-\omega_1)(1-\omega_2) + \psi_1\mathcal{S}_1\Big\}P_{r12} - \Big\{\psi_2\left(1-\mathcal{S}_1\right) + \eta\mathcal{S}_2\Big\}Q_{r12}, \tag{6.24}$$

$$\frac{\mathrm{d}N}{\mathrm{d}t} = 2\eta\mathcal{S}_2\mathcal{P} + \tfrac{2}{3}(\kappa_{21}C_1 + \kappa_{22}C_2)\lambda\log\left(\tfrac{K}{3\mathcal{P}+1.5N+E}\right)E\mathcal{S}_3 - \nu N + 2\kappa_{11}C_1\Big\{P_s + P_{r2} + \sigma_1(P_{r1}+P_{r12})\Big\} + 2\kappa_{12}C_2\Big\{P_s + P_{r1} + \sigma_1(P_{r2}+P_{r12})\Big\} \tag{6.25}$$

$$\frac{\mathrm{d}E}{\mathrm{d}t} = \left(1-\kappa_{21}C_1 - \kappa_{22}C_2\right)\lambda\log\left(\tfrac{K}{3\mathcal{P}+1.5N+E}\right)E\mathcal{S}_3, \tag{6.26}$$

where $$C_i(t) = \left(1-\mathcal{S}_4\right)L_i(t), \qquad \mathcal{S}_i = S_{w_i}\left(\tfrac{3\mathcal{P}+E}{E}, \alpha_i\right), \qquad \max_t L(t) = 1,$$

$$\mathcal{P} = P_s + Q_s + P_{r1} + Q_{r1} + P_{r2} + Q_{r2} + P_{r12} + Q_{r12},$$

where P_s, Q_s, P_{r1}, Q_{r1}, P_{r2}, Q_{r2}, P_{r12}, Q_{r12}, N, and E are the non-dimensional number of sensitive proliferating cells, sensitive quiescent cells, proliferating cells which are resistant to therapy 1 only, quiescent cells which are resistant to therapy 1 only, proliferating cells which are resistant to therapy 2 only, quiescent cells which are resistant to therapy 2 only, proliferating cells which are resistant to both therapies, quiescent cells which are resistant to both therapies, necrotic cells, and endothelial cells respectively. Furthermore, ω_i is the cost of being resistant to therapy i, κ_{1i} is the rate at which sensitive tumour cells are killed by therapy i, κ_{2i} is the relative rate at which endothelial cells are killed by therapy i, σ_i is the partial resistance to therapy i, ε_i and $\overline{\varepsilon}_i$, are the rates at which cells mutate to acquire and lose resistance to therapy i respectively, and $L_i(t)$ is the intravenous chemotherapy concentration of therapy i which is defined by the treatment schedule.

Note that since the doubly resistant cells must undergo two mutations before they become established it is not immediately obvious that they will be sufficiently abundant to be modelled as a continuum. We will explicitly check the initial size of the doubly resistant population later when calculating our initial conditions to confirm that a continuum model is appropriate.

Parameter Estimation

Given our parameter estimation of Section 6.2.1 we assume that the partial resistance to therapy i, σ_i, and the cost of being resistant to therapy i, ω_i, are both highly

variable and can take the range of values $0 \leq \sigma_i \leq 1$, and $0 \leq \omega_i \leq 1$. As before we also take the cell mutation rates to be $\varepsilon_i = 10^{-6}$ and $\overline{\varepsilon}_i = 10^{-6}$.

Therapy Schedules

Following on from our result of the previous Chapter, that therapies should be delivered for at least a few cell cycle times, in this section therapy will always be applied continuously for 5 days, then followed by a rest period of 9 days, but the number and order of the therapy applications will be varied. Note that if n total applications of therapy are to be applied and there are two candidate chemotherapies, then there are 2^n possible therapy schedules. For even a relatively small value of n this is clearly more schedules than it is desirable to consider explicitly. Instead we will initially consider a smaller number of therapy schedules, but identify which particular schedules should be investigated further to identify the key trends in the tumour response.

To consider even a small number of different therapy schedules it is desirable to introduce a notation to define the schedules. Here we will use square brackets and the relevant sequence of ones and twos to define the schedule, so that the therapy denoted by

$$\mathcal{T} = [1 \quad 2],$$

is the schedule where therapy 1 is applied first, and then therapy 2 is applied second, and then the therapy is ceased.

Numerical Methods for Simulating the Treatment of the Tumour

As in Section 6.2.1 we simulate the evolution of our model using an adaptive linear multi-step method where the adaptive linear stepping is optimised for stiff systems and a maximum time step size is prescribed which ensures that each application of the therapy is resolved.

Initial Conditions

In Section 6.2.1 we found that varying the cost of being resistant had a significant effect on the initial conditions that should be taken in our single therapy model. Given this we anticipate that the cost of being resistant to each therapy will have a significant affect on the initial conditions we should take in our double therapy model.

So as before we will generate new initial conditions for each choice of the parameters ω_1 and ω_2, and again we do this by simulating the evolution of our tumour in the absence of any therapy with the following starting values:

$$\begin{aligned} &P_s(0) = 82,000, \quad P_{r1}(0) = 0, \quad P_{r2}(0) = 0, \quad P_{r12}(0) = 0, \quad N(0) = 440,000, \\ &Q_s(0) = 620,000, \quad Q_{r1}(0) = 0, \quad Q_{r2}(0) = 0, \quad Q_{r12}(0) = 0, \quad E(0) = 1. \end{aligned}$$

Once the tumour in the absence of any therapy has grown to half its maximum size, as given by Gompertzian saturation, we will extract the corresponding cell distributions from this model and take them to be the initial conditions in our double therapy model.

As discussed in the derivation of our model, we now confirm that the initial size of our doubly resistant population is sufficiently large to be modelled as a continuum. For the cost of being resistant $\omega_1 = \omega_2 = 0.2$ we find that the corresponding initial conditions for our doubly resistant population are

$$P_{r12} = 65 \qquad Q_{r12} = 128, \tag{6.27}$$

(rounded to the nearest integer), which we consider large enough to be modelled as a continuum.

6.5.2 Preventing Resistance

Having derived our model for the treatment of a vascular tumour by a combination of two chemotherapies we now consider how applying a double therapy effects the onset of resistance compared to a single therapy. To isolate the affect of introducing a second therapy we will initially consider two non-cross resistant therapies which are of equal strength, partial resistance and cost of being resistant. We are investigating whether a double therapy reduces the onset of resistance and so apply two therapies where each would fail because of resistance when applied singularly and take them each to have the parameter values given by Table 6.3. We will then compare the results of applying ten applications of a single therapy versus ten applications of a double therapy, and in particular we will consider the following treatment schedules:

$$\begin{aligned} \mathcal{T}_1 &= [1 \quad 1 \quad 1 \quad 1 \quad 1 \quad 1 \quad 1 \quad 1 \quad 1 \quad 1], \\ \mathcal{T}_2 &= [1 \quad 2 \quad 1 \quad 2 \quad 1 \quad 2 \quad 1 \quad 2 \quad 1 \quad 2]. \end{aligned} \tag{6.28}$$

The different cell populations at the end of the final application of therapy for these two treatment schedules are shown in Figure 6.7. It can be seen that the single therapy schedule leads to a tumour which consists almost entirely of cells which are resistant to that therapy, whereas the alternating double therapy results in a much smaller tumour which predominantly consists of cells which are sensitive to both therapies.

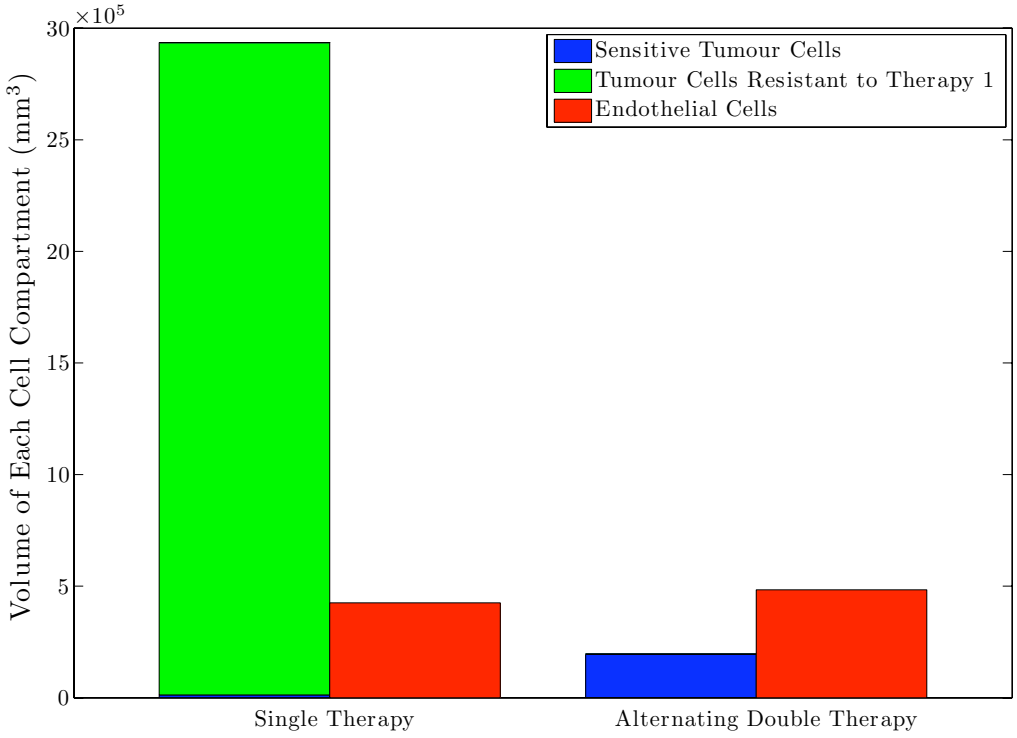

Figure 6.7: The volume of cells in our 25% growth fraction tumour after the final application of therapy for the two therapy schedules defined by Schedules (6.28) for the parameter values given by Tables 6.3 and 4.2, as governed by Equations (6.17) to (6.26). Cell populations which are present in too smaller volume to be readily seen are not labelled in the legend.

The results of Figure 6.7 are for specific and deliberate choices of the partial resistances, and the costs of being resistant. To consider how widely the double therapy provides an improved therapy over the single therapy we now set the partial resistances to be equal, so that $\sigma_1 = \sigma_2 = \sigma$, and the cost of being resistant to be equal, so that $\omega_1 = \omega_2 = \omega$, and vary them jointly throughout the range $0 \leq \sigma \leq 1$ and $0 \leq \omega \leq 1$. We then consider the improvement achieved by delivering the double therapy rather than the single therapy, which we define to be the decrease in the

total volume of live tumour cells in the tumour when delivering the schedule $\mathcal{T}_2$ compared to $\mathcal{T}_1$ as defined by Schedules (6.28). For the chemotherapy kill rates defined in Table 6.3 this gives the results in Figure 6.8.

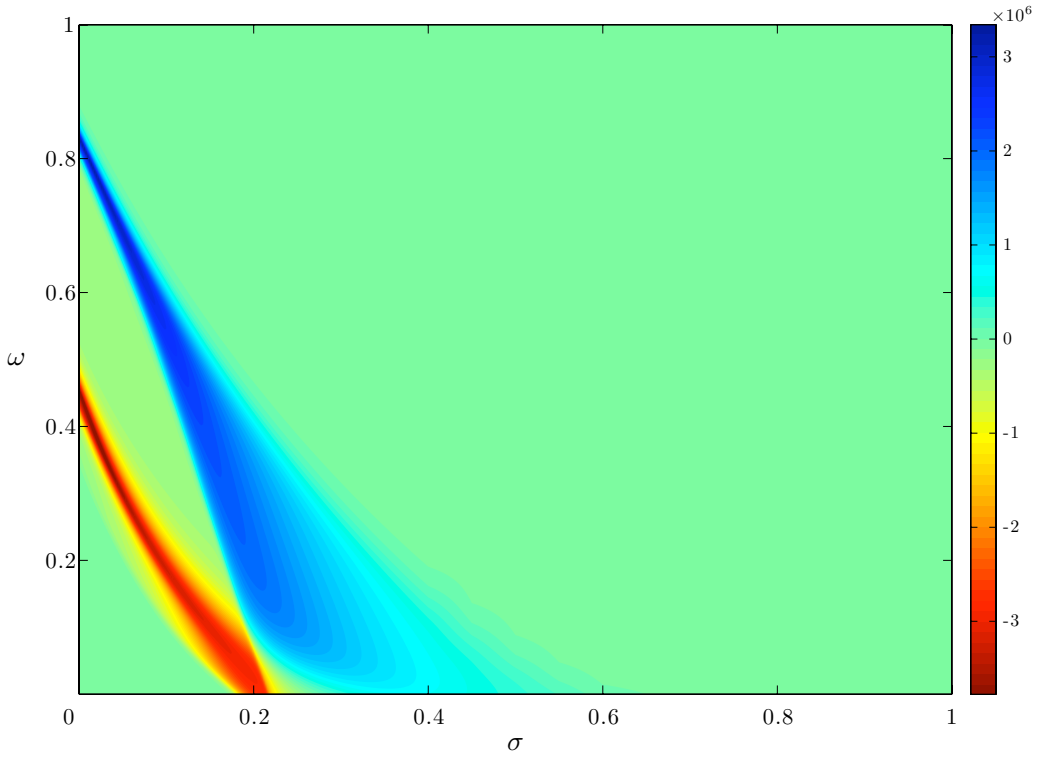

Figure 6.8: The improvement in the volume of live tumour cells in the tumour (in mm^3) as defined in the text, when applying the double therapy compared to the single therapy, defined by Schedules (6.28), after the final application of therapy for the parameter values outlined in the text, which is governed by Equations (6.17) to (6.26).

Comparing Figure 6.2(c) to Figure 6.8 it can be seen that for the values of the resistance parameters where the single therapy provides successful cure whilst acting as a traditional chemotherapeutic, applying an alternating double therapy is equally effective at treating the tumour. Considering the evolution of the growth curves in detail (results not shown) it can be confirmed that the double therapy still acts as a traditional chemotherapeutic.

Furthermore, in the region where the single therapy fails due to the onset of resistance, the alternating double therapy provides a significant improvement over the single

therapy. The reason for this is shown in Figure 6.7, where it can be seen that when the single therapy is applied the resulting tumour eventually consists of cells which are resistant to that therapy. These resistant cells are sufficiently resistant for a resistant population to accumulate and cause the therapy to fail. However, when the alternating double therapy is applied the resulting tumour consists primarily of sensitive cells, which are susceptible to the therapy. The alternating double therapy can then target these sensitive cells and the resultant tumour upon the cessation of the final application of therapy is much smaller than the equivalent tumour following the single therapy.

Comparing Figure 6.2(c) to Figure 6.8 we also find that there is a set of parameter values for which the single therapy uses resistance to exploit the angiogenesis-therapy feedback loop and the alternating double therapy performs significantly worse than the single therapy. By considering the evolution of the single and double therapies for these parameter values in more detail (results not shown) it is found that a single therapy provides effective tumour cure by using resistance to exploit the angiogenesis-therapy feedback loop, however an alternating double therapy either prevents, or delays, a significant resistant population from becoming established so that the angiogenesis-therapy feedback loop either cannot, or is slower to, be exploited.

The results of this section demonstrate that when a single therapy fails because of onset of resistance a double therapy can be a significantly more effective than a single therapy. However when a single therapy which uses resistance to exploit the angiogenesis-therapy feedback loop is applied, applying a double therapy can provide a significantly less effective therapy than a single therapy.

We consider this in more detail in the next section, where we consider the Goldie-Coldman hypothesis.

6.6 The Goldie-Coldman Hypothesis

We now consider the Goldie-Coldman hypothesis, which states that when double therapies are applied the most effective therapy is achieved by alternating the non-cross resistant therapies as quickly as possible. We do this by applying six applications of therapy 1, and six applications of therapy 2, but varying how quickly the therapies are alternated; as a control we also consider twelve applications of a single therapy.

Therefore we consider the following treatment schedules

$$\begin{aligned}
\mathcal{T}_3 &= [1 \quad 1 \quad 1 \quad 1 \quad 1 \quad 1 \quad 1 \quad 1 \quad 1 \quad 1 \quad 1 \quad 1], \\
\mathcal{T}_4 &= [1 \quad 1 \quad 1 \quad 1 \quad 1 \quad 1 \quad 2 \quad 2 \quad 2 \quad 2 \quad 2 \quad 2], \\
\mathcal{T}_5 &= [1 \quad 1 \quad 1 \quad 2 \quad 2 \quad 2 \quad 1 \quad 1 \quad 1 \quad 2 \quad 2 \quad 2], \\
\mathcal{T}_6 &= [1 \quad 1 \quad 2 \quad 2 \quad 1 \quad 1 \quad 2 \quad 2 \quad 1 \quad 1 \quad 2 \quad 2], \\
\mathcal{T}_7 &= [1 \quad 2 \quad 1 \quad 2 \quad 1 \quad 2 \quad 1 \quad 2 \quad 1 \quad 2 \quad 1 \quad 2].
\end{aligned} \tag{6.29}$$

We will consider the Goldie-Coldman hypothesis in the case where the single therapy successfully acts as a traditional chemotherapeutic, fails because of the onset of resistance, and uses resistance to exploit the angiogenesis-therapy feedback loop. We begin by considering the case where the single therapy successfully acts as a traditional chemotherapeutic.

The Goldie-Coldman Hypothesis When the Single Therapy Acts as a Traditional Chemotherapeutic

We begin by considering the behaviour when each therapy acts as a traditional chemotherapeutic when applied singly. Hence we let therapy 1 and therapy 2 each take the parameter values given in Tables 6.2 and 4.2. It is then found that the tumour response to the double therapies is identical to the single therapy (results not shown). Hence when the single therapy successfully acts as a traditional chemotherapeutic applying a double therapy and altering the scheduling of that double therapy has no affect on the effectiveness of the therapy.

The Goldie-Coldman Hypothesis When the Corresponding Single Therapy Fails Because of the Onset of Resistance

We now consider the behaviour of the scheduling when the single therapy fails because of the onset of resistance. We let therapy 1 and therapy 2 each take the parameter values given in Tables 6.3 and 4.2, and the resultant cell populations upon cessation of the final application of therapy for the therapy schedules defined by Schedules (6.29) are shown in Figure 6.9. It can be seen that when the single therapy fails because of the onset of resistance, the double therapies are much less susceptible to resistance. Furthermore, alternating the therapies quickly completely prevents the onset of resistance for these parameter values.

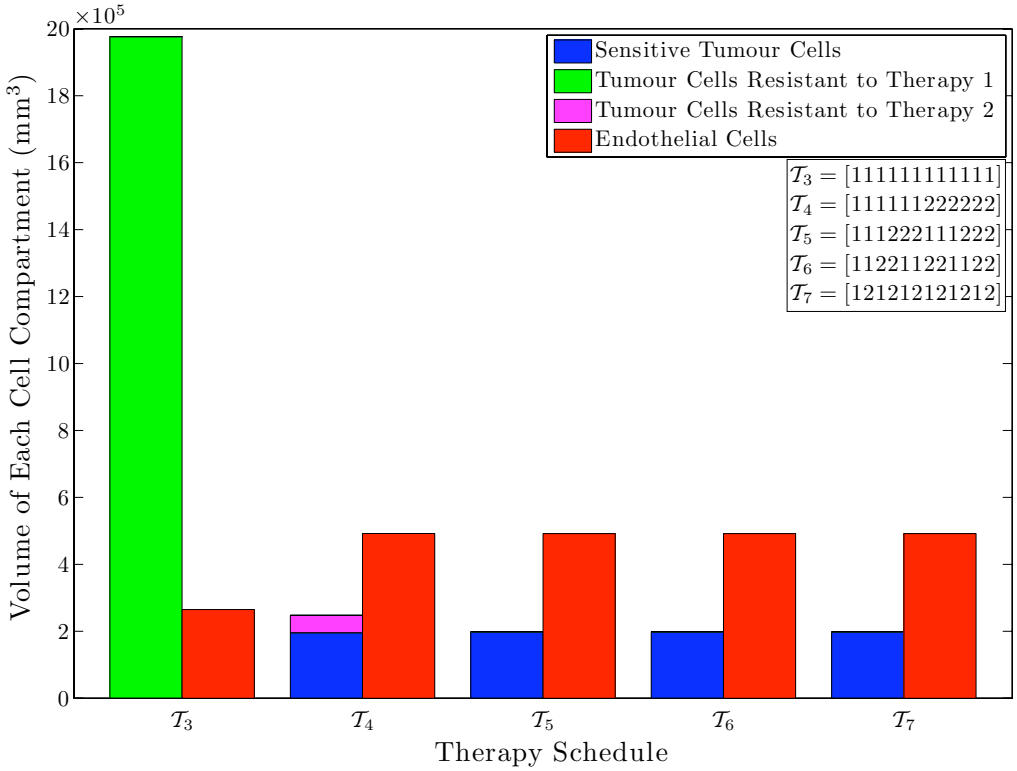

Figure 6.9: The volume of cells in our 25% growth fraction tumour after the final application of therapy for the therapy schedules defined by Schedules (6.29), for the parameter values given in Tables 6.3 and 4.2, as governed by Equations (6.17) to (6.26). Cell populations which are present in too smaller volume to be readily seen are not labelled in the legend.

The Goldie-Coldman Hypothesis When the Corresponding Single Therapy Exploits the Angiogenesis-therapy Feedback Loop

We now consider the behaviour when the single therapy uses resistance to exploit the angiogenesis-therapy feedback loop. We let therapy 1 and therapy 2 each take the parameter values given in Tables 6.4 and 4.2 and then the cell populations upon cessation of the final application of therapy for the therapy schedules defined by Schedules (6.29) are shown in Figure 6.10. It can be seen that the single therapy successfully uses resistance to exploit the angiogenesis-therapy feedback loop, but the double therapies cannot exploit the angiogenesis-therapy feedback loop sufficiently to provide tumour clearance. Furthermore, the more quickly the therapies are alternated the less successful the therapy becomes.

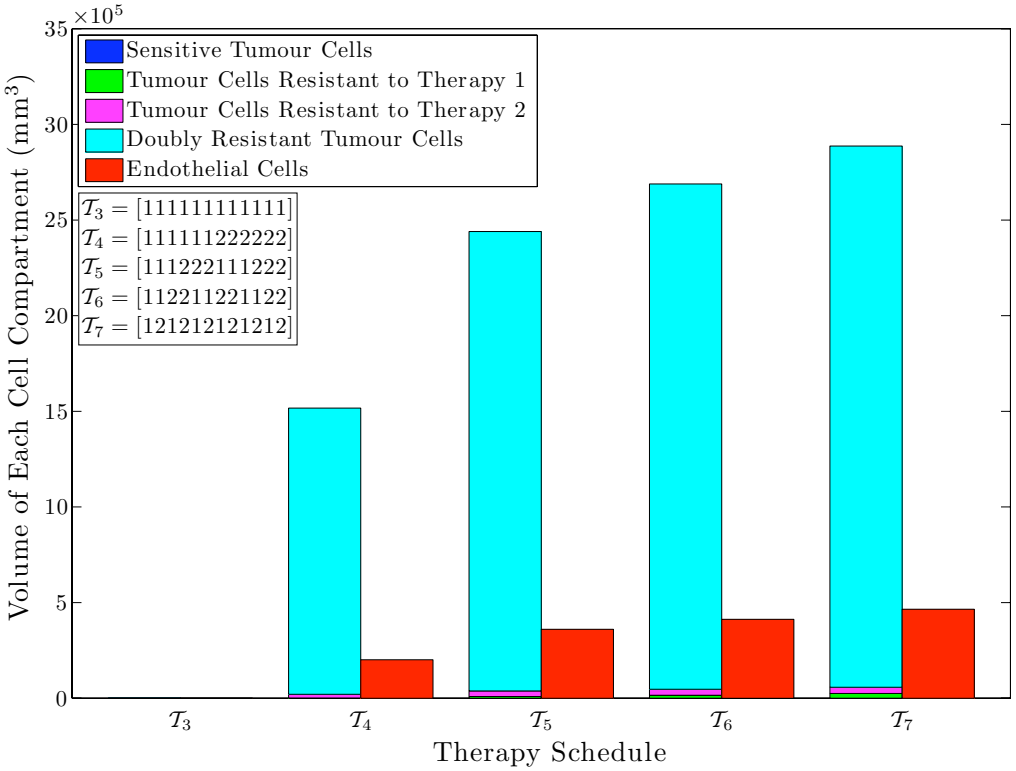

Figure 6.10: The volume of cells in our 25% growth fraction tumour after the final application of therapy for the therapy schedules defined by Schedules (6.29) for the parameter values given in Tables 6.3 and 4.2, as governed by Equations (6.17) to (6.26).

Conclusions

In this section we have found agreement with the Goldie-Coldman hypothesis and found that to minimise the onset of resistance a double non-cross resistant therapy should be applied and alternated as quickly as possible. In each of our situations the double therapy suffered less from resistance than the single therapy and quickly alternating the double therapy minimised the onset of resistance.

If the single therapy can successfully treat the tumour by acting as a traditional chemotherapeutic without being inhibited by the presence of any resistant cells, then applying a double therapy does not improve therapy; since the presence of resistance cells does not inhibit the single therapy minimising the onset of resistance is superfluous.

Furthermore, if the single therapy uses resistance to exploit the angiogenesis-therapy

feedback loop, then applying a double therapy significantly inhibits the effectiveness of the therapy and can even lead to complete failure of the therapy. The reason for this being that for such therapies resistance is utilised to allow the therapy to exploit the angiogenesis-therapy feedback loop. Minimising resistance reduces the possibility of exploiting the angiogenesis-therapy feedback loop and the therapy is actually made less effective.

However, if the single therapy fails because of the onset of resistance then applying a double therapy minimises the onset of resistance, and alternating the therapy as quickly as possible optimises the double therapy.

Hence we have found that whilst applying an alternating double therapy and alternating between the applications of therapy quickly does minimise the effect of resistance on the tumour, this is not always beneficial. When the single therapy fails because of the onset of resistance applying a double therapy provides a significant improvement over the single therapy. However, when the single therapy successfully exploits the angiogenesis-therapy feedback loop applying a double therapy can result in therapy failure. This highlights how non-trivial the application of a double compared to a single therapy is, and that there is no general rule governing whether a single or double therapy should be applied when the therapy mechanism is unknown. The optimal schedule can only be designed given information concerning the mechanism the therapy is using to treat the tumour.

Having considered the Goldie-Coldman hypothesis, we now consider Day's worst drug first rule.

6.7 Day's Worst Drug First Rule

Day (1986) only considered the cell kill of a therapy as a measure of its effectiveness, however there are four mechanisms by which one therapy could be nominally better than another; it could either be better at targeting tumour cells (by having a higher value of κ_1), better at targeting endothelial cells (by having a higher value of κ_2), better at targeting resistance cells (by having a higher value of σ), or have a higher cost of being resistant (by having a higher value of ω). Section 6.2 highlighted that for given parameter values the chemotherapy can either be successful as a traditional chemotherapeutic, fail because of the onset of resistance, or successfully use resistance to exploit the angiogenesis-therapy feedback loop. Hence to fully consider Day's worst

drug first rule would require the consideration of an undesirably large number of configurations. To reduce the size of this task we begin by considering whether the results of our Goldie-Coldman based analysis from the previous section, Section 6.6, can be generalised to yield conclusions corresponding to Day's worst drug first rule. We begin by considering the case where both drugs successfully act as a traditional chemotherapeutic when applied singly.

Day's Worst Drug First Rule when both Therapies Act As Traditional Chemotherapeutics

In Section 6.6 we found that when two therapies both successfully act as a traditional chemotherapeutic when applied singly, with no significant resistant population becoming established, then there is no benefit to applying a double therapy compared to a single therapy. Applying both therapies and alternating them might minimise the chance of a resistant cell population forming, but since the therapy is not limited by the onset of resistance this provides no improvement over a single therapy.

So our previous results imply that when considering two therapies which each successfully act as a traditional chemotherapeutic when applied singly, applying a double therapy will give no improvement over applying a single therapy. Clearly applying a single therapy of the better therapy will be more effective than applying a single therapy of the worse therapy, and so the results in Section 6.6 imply that when there are two candidate therapies for the treatment of a tumour, and each therapy can provide effective tumour cure whilst acting as a traditional chemotherapeutic without failing due to resistance, then only the better therapy should be applied.

This conclusion, which has been extrapolated from the results of the previous section, can be validated by our model. By simulating the evolution of a number of tumours for different parameter values and therapy schedules we find that the results of our model concur with this conclusion (results not shown).

Day's Worst Drug First Rule when both Therapies Use Resistance To Exploit the Angiogenesis-Therapy Feedback Loop

In Section 6.6 we found that when two therapies both successfully use resistance to exploit the angiogenesis-therapy feedback loop when applied as a single therapy, then a single rather than a double therapy should be applied. Whilst a double therapy would minimise the onset of resistance, it is the onset of resistance which is required

to allow the tumour to successfully exploit the angiogenesis-therapy feedback loop and so reducing resistance makes the therapy less effective.

So the conclusions of our previous section imply that when considering two therapies that each use resistance to exploit the angiogenesis-therapy feedback loop when applied as a single therapy, only a single therapy should be used. In this case, clearly the therapy which is most effective at exploiting the angiogenesis-therapy feedback loop should be the one which is applied. However because the therapy is using resistance to exploit the angiogenesis-therapy feedback loop, rather than acting as a traditional chemotherapeutic, the therapy which is most effective at exploiting the angiogenesis-therapy feedback loop may not be nominally the "better" therapy. The therapy most effective at exploiting the angiogenesis-therapy feedback loop will be the therapy which is worst at preventing the onset of a resistant cell population and the best at targeting the endothelial cells. To promote the onset of resistance the best therapy here will have the lower partial resistance, σ, and cost of being resistant, ω, and to target the endothelial cells via the angiogenesis-therapy feedback loop the better therapy will have a higher kill rate of endothelial cells, κ_2, but a lower kill rate of tumour cells, κ_1.

This conclusion, which has been extrapolated from the results of the previous section, can be explicitly validated by our model. By simulating the evolution of a number of tumours for different parameter values and therapy schedules we find that the results of our model concur with this conclusion (results not shown).

6.7.1 Day's Worst Drug First Rule when One of the Therapies Fails because of Resistance

In Section 6.6 we found that if two therapies of equal strength are available to treat the tumour and each fails because of resistance when applied singly, then to prevent the onset of resistance the therapies should be applied jointly and alternated as quickly as possible. However it is not clear how this result generalises when these therapies are not of equal strength.

We now consider Day's worst drug first rule when one of the therapies fails because of the onset of resistance. To do this we will apply two asymmetric therapies where therapy 1 fails because of the onset of resistance when used as a single therapy and hence takes the parameter values given in Table 6.3. Therapy 2 will have similar parameter values to therapy 1, but we will alter each of the parameters, κ_{12}, κ_{22}, σ_2,

and ω_2, in turn and see how the response of the tumour depends upon the therapy schedule. Having considered the Goldie-Coldman hypothesis in Section 6.6 and found that if a double therapy is being used, then to minimise the onset of resistance it should be alternated as quickly as possible we now consider the following therapy schedules:

$$\begin{aligned}
\mathcal{T}_9 &= [1 \quad 2 \quad 1 \quad 2 \quad 1 \quad 2 \quad 1 \quad 2 \quad 1 \quad 2 \quad 1 \quad 2], \\
\mathcal{T}_{10} &= [2 \quad 1 \quad 2 \quad 1 \quad 2 \quad 1 \quad 2 \quad 1 \quad 2 \quad 1 \quad 2 \quad 1], \\
\mathcal{T}_{11} &= [1 \quad 1 \quad 1 \quad 1 \quad 1 \quad 1 \quad 1 \quad 1 \quad 1 \quad 1 \quad 1 \quad 1], \\
\mathcal{T}_{12} &= [2 \quad 2 \quad 2 \quad 2 \quad 2 \quad 2 \quad 2 \quad 2 \quad 2 \quad 2 \quad 2 \quad 2].
\end{aligned} \tag{6.30}$$

To consider the effectiveness of the therapy we will compare the resulting tumour volume at the end of the last application of therapy and we begin by considering the case where the tumour cells exhibit different sensitivities to the therapies.

Varying κ_{12}

We begin by altering κ_{12}, which determines the sensitivity of proliferating cells to therapy 2. In particular we consider the range of values $2.5 \leq \kappa_{12} \leq 10$ and let the other parameters value for therapy 2 be as given in Table 6.3. Figure 6.11 then shows the volume of live cells in the tumour at the end of the final application of therapy as a function of κ_{12} for the different therapy schedules defined by Schedules (6.30).

It can be seen in Figure 6.11 that the double therapies consistently provide significant tumour growth inhibition, but not complete cure, and the worst drug first double therapy is always the best therapy. Considering the evolution of the different cell populations in detail (results not shown) it can be seen that the worst drug first therapy outperforms the best drug first therapy simply because the former ends with the stronger therapy. By considering the evolution of the tumour when an odd number of therapies are applied (results not shown) we find that rather than depending upon the first therapy the optimal therapy is actually the best drug last schedule.

In Figure 6.11 one may also observe that there is a value of κ_{12}, approximately $\kappa_{12} = 3.7$, where the worst drug only therapy schedule is reasonably effective. By considering the response of the tumour to this therapy in more detail (results not shown) it is found that this is the value of κ_{12} for which the worst drug only schedule can exploit the angiogenesis-therapy feedback loop. However, for other values of

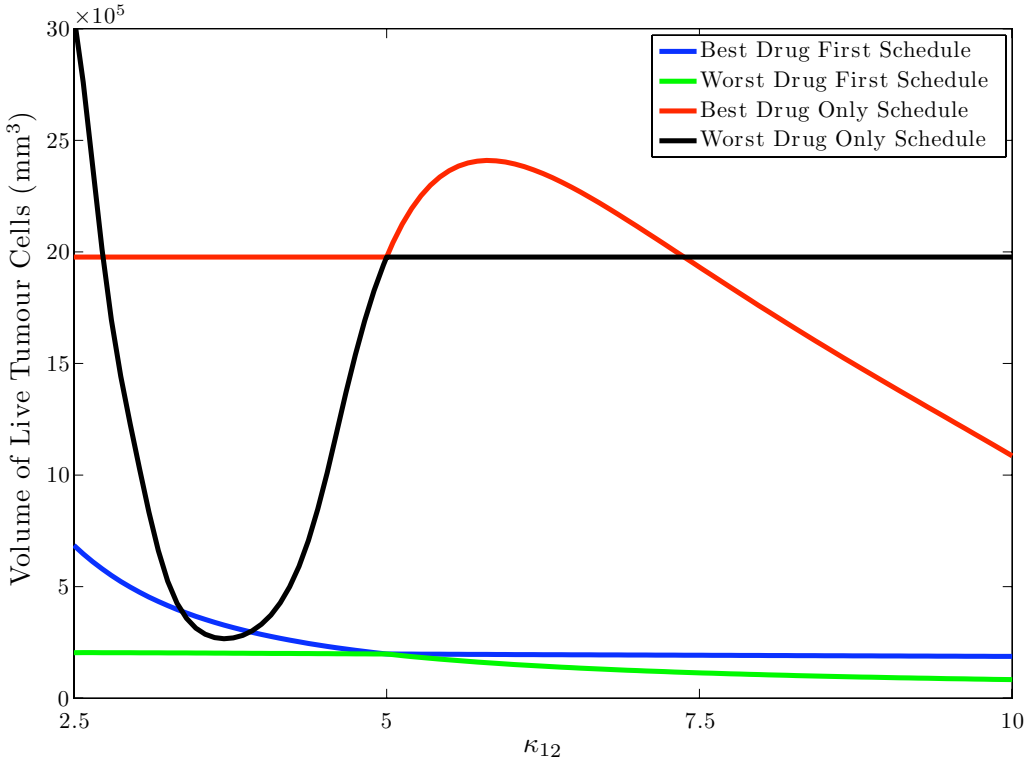

Figure 6.11: The volume of cells in our 25% growth fraction tumour after the final application of therapy for the schedules defined by Schedules (6.30), as a function of κ_{12} for the other parameter values listed in Tables 6.3 and 4.2, as governed by Equations (6.17) to (6.26). Plot generated for a large number of discrete values of κ_{12} and then linearly interpolated.

κ_{12} the single therapies perform poorly, either because they fail due to the onset of resistance, or because they are too impotent to treat the tumour.

Note that in Figure 6.11 the gradients of our lines are discontinuous at $\kappa_{12} = 5$. The reason for this is actually due to a discontinuity in our definition of which is the best therapy and which is the worst therapy. Having taken $\kappa_{22} = 5$ and varied κ_{12} we have labelled therapy 2 as the best therapy when $\kappa_{12} < 5$ and therapy 1 as the best therapy when $\kappa_{12} > 5$. Hence the response of our tumour is continuous to variations in the parameter values, but our labelling of the line is discontinuous.

Varying κ_{22}

We now alter the sensitivity of the endothelial cells to therapy 2 by considering κ_{22} throughout the range $10 \leq \kappa_{22} \leq 50$ and letting the other parameters concerning therapy 2 be as given in Table 6.3. The volume of live cells in the tumour at the end of the final application of therapy as a function of κ_{22} for the therapy Schedules (6.30) and the other parameter values given by Tables 6.3 and 4.2 is shown in Figure 6.12.

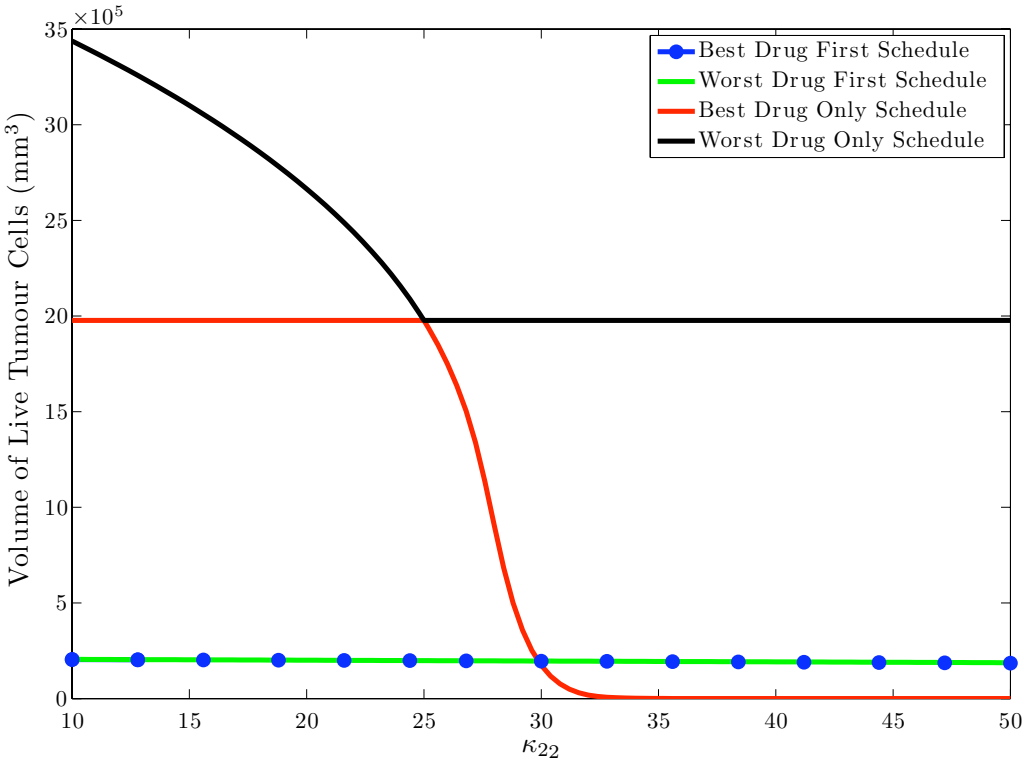

Figure 6.12: The volume of cells in our 25% growth fraction tumour after the final application of therapy for the therapy Schedules (6.30), as a function of κ_{22}, for the other parameter values listed in Table 6.3, as governed by Equations (6.17) to (6.26). Plot generated for a large number of discrete values of κ_{22} and then linearly interpolated.

In Figure 6.12 it can be seen that the alternating double therapies consistently provide successful tumour inhibition, but not complete tumour cure. Furthermore, the effectiveness of the double therapy and whether the best or worst drug should be applied first appears to be independent of how potent the therapy is at targeting the

endothelial cells. The reason for this is that when a double therapy is applied the drugs act together as traditional chemotherapeutics so that no significant resistant cell population becomes established and the angiogenesis-therapy feedback loop is not exploited. Since the double therapy does not use any anti-angiogenic effect to treat the tumour, altering the strength of the anti-angiogenic component of the therapy has no effect on the tumour.

In Figure 6.12 it can also be seen that for lower values of κ_{22} the worst drug only therapy performs poorly. The reason for this is that the therapy fails because of the onset of resistance and so the tumour grows to the size which can be supported by the local vasculature. Decreasing κ_{22} reduces the anti-angiogenic affect of the therapy, which results in a larger population of endothelial cells and hence a larger tumour. However, if κ_{22} is taken to be large enough then the therapy becomes a potent enough anti-angiogen for the angiogenesis-therapy feedback loop to be exploited and the best drug only therapy becomes the most effective.

Note that again there is a point of discontinuous gradients at $\kappa_{22} = 25$ as our definition of which is the best and worst therapies switch over.

Varying σ_2

We now alter the partial resistance of therapy 2. In particular we vary the value of σ_2 about the value previously considered, $\sigma_2 = 0.08$, and consider the values in the range $0 \leq \sigma_2 \leq 0.2$ and letting the other parameters concerning therapy 2 be as given in Table 6.3. The volume of live cells in the tumour at the end of the final application of therapy as a function of σ_2 for the different therapy Schedules (6.30) and the other parameter values given by Tables 6.3 and 4.2 is shown in Figure 6.13. It can be seen that for very low values of σ_2, so that the tumour cells are very resistant to therapy 2, applying the worst drug only as a single therapy provides an effective therapy. By considering the growth dynamics in more detail (results not shown) it is found that for these parameter values the resistant cells are sufficiently resistant to the therapy for the angiogenesis-therapy feedback loop to be exploited; in which case this provides the best therapy. However, as the cells become more resistant to the therapy, i.e. as σ_2 is increased, the single therapy fails because of resistance. However, if σ_2 is increased further still then eventually the best drug only therapy does not suffer from resistance and is as effective as the alternating therapies.

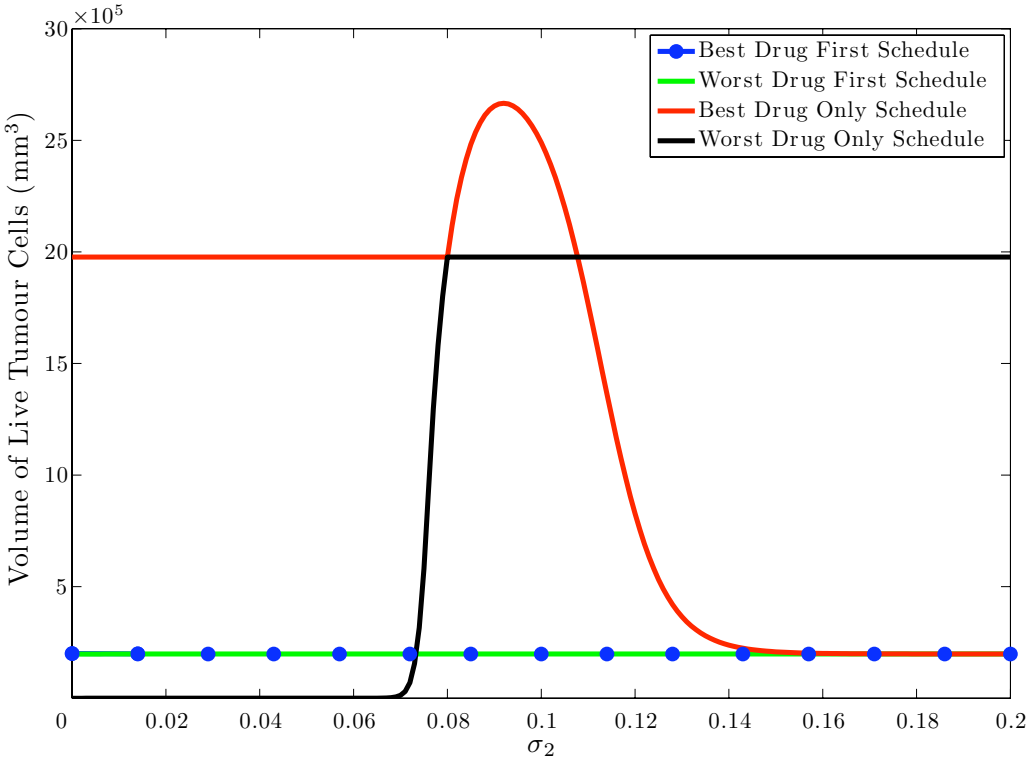

Figure 6.13: The volume of cells in our 25% growth fraction tumour after the final application of therapy for the therapy schedules defined by Schedules (6.30), as a function of σ_2 for the other parameter values listed in Tables 6.3 and 4.2, as governed by Equations (6.17) to (6.26). Plot generated for a large number of discrete values of σ_2 and then linearly interpolated.

Again we find when the therapies are alternated, applying the best drug first or the worst drug first does not affect the therapy. The reason for this is that alternating the therapies prevents a resistant population from becoming established, and so the partial resistance of the resistant cells has no affect on the tumour.

Note that again there is a point of discontinuous gradients at $\sigma_2 = 0.08$ as our definition of which is the best and worst therapies switch over.

Varying ω_2

We now vary the cost of being resistant to therapy 2. In particular we vary the value of ω_2 about the value previously considered, $\omega_2 = 0.6$, and consider the values in the range $0.3 \leq \omega_2 \leq 1$ and let the other parameters concerning therapy 2 be as given

in Table 6.3. Then the volume of live cells in the tumour at the end of the final application of therapy as a function of ω_2, for the different therapy Schedules (6.30) and the other parameter values given by Tables 6.3 and 4.2 are shown in Figure 6.14.

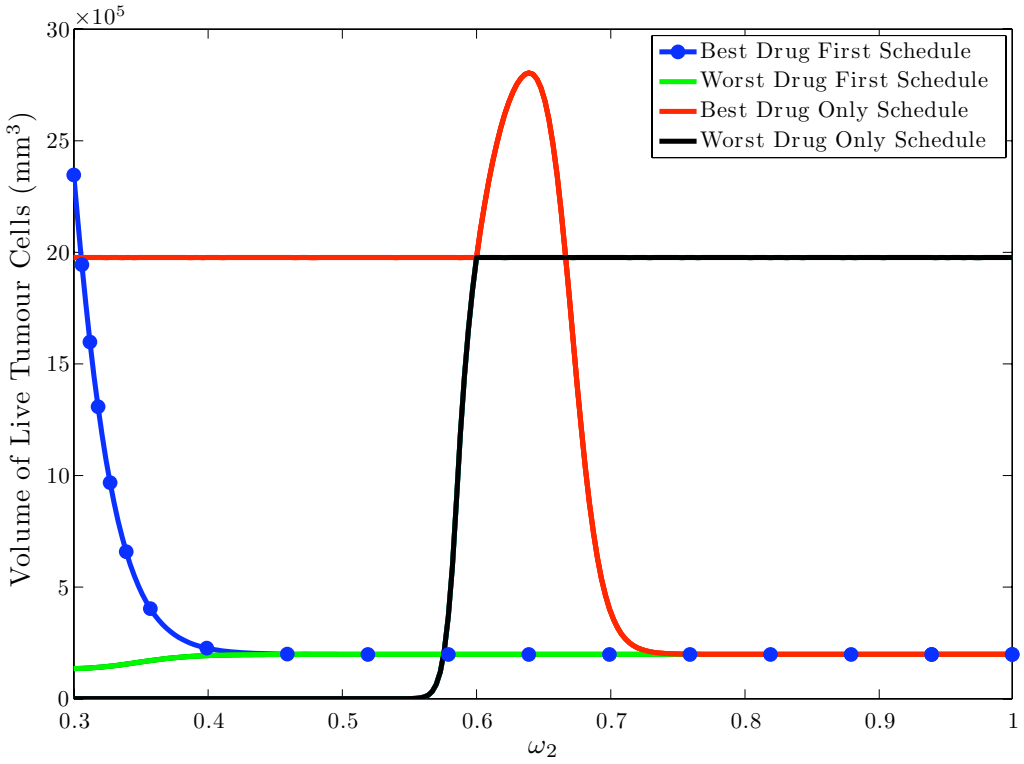

Figure 6.14: The volume of cells in our 25% growth fraction tumour after the final application of therapy for the schedules defined by Schedules (6.30), as a function of ω_2 for the other parameter values listed in Table 6.3 and 4.2, as governed by Equations (6.17) to (6.26). Plot generated for a large number of discrete values of ω_2 and then linearly interpolated.

In Figure 6.14 it can be seen that for very low values of ω_2, so that the cost of being resistant to therapy 2 is very low, the worst drug only schedule provides the most effective therapy schedule. Investigating the tumour behaviour in this region in more detail (results not shown) it is found that if the cost of being resistant to therapy 2 is very low, then a population of cells which are resistant to therapy 2 becomes established which allows the worst drug only schedule to use resistance to exploit the angiogenesis-therapy feedback loop. Equally, if the cost of being resistant to therapy 2 is very high, then resistance to therapy 2 cannot become established and the best

drug only schedule can successfully act as a traditional chemotherapeutic. However, for intermediary values of the cost of being resistant to therapy 2 both single schedules fail due to the onset of resistance.

It can also be seen that if ω_2 is taken to be very low then the best drug first schedule performs poorly. Investigating the tumour behaviour in this region in more detail (results not shown) it is found that if the cost of being resistant to therapy 2 is extremely low the tumour will eventually consist of cells which are all resistant to therapy 2, then even when a double therapy is applied. However the application of a double, rather than single, therapy increases the duration between applications of therapy 2 and in fact the applications of therapy 2 are now too sparse for the therapy to use resistance to exploit the angiogenesis-therapy feedback loop. Instead, for all therapy schedules an application of therapy 1 successfully acts as a traditional chemotherapeutic, but applications of therapy 2 are largely ineffective. Hence any application of therapy 2 in a double schedule effectively gives the tumour a longer recovery period until the next application of therapy 1. It appears that for low values of ω_2 the worst drug first schedule is significantly outperforming the best drug first, however this is simply because the worst drug first schedule is being recorded at the end of an effective hit of therapy, but the best drug first schedule is being recorded at the end of an ineffective hit of therapy. It is this inconsistency which makes one schedule appear more effective than the other and if an odd number of applications is applied then it can be confirmed that the better alternating schedule is the therapy 1 last schedule.

Note that again there is a point of discontinuous gradients at $\omega_2 = 0.6$ as our definition of which is the best and worst therapies switch over.

Conclusions

In this section we were seeking to test Day's worst drug first rule, which states that when a double non-cross resistant therapy is being applied the worst drug should be applied first.

We found that if both therapies act as traditional chemotherapeutics and can cure the tumour without the appearance of a significant resistant population when applied singly, then only a single schedule of the most potent drug should be applied.

We also found that if both therapies use resistance to exploit the angiogenesis-therapy feedback loop when applied singly, then only a single schedule of the drug which is best at exploiting the angiogenesis-therapy feedback loop should be applied.

If one of the therapies fails because of the onset of resistance then we have demonstrated that there is not one general rule which leads to an effective therapy. Alternating the therapies was successful at preventing the onset of resistance, although the onset of resistance is unavoidable if the cost of being resistant to the therapies is extremely low; however preventing resistance did not always lead to the optimal therapy. We have found that there are circumstances where applying a single therapy allowed it to successfully use resistance to exploit the angiogenesis-therapy feedback loop and provide the best therapy, but we also found circumstances where applying a single therapy meant that it failed because of the onset of resistance and resulted in the worst therapy.

We also found that when the double therapies were more effective at treating the tumour than the single therapies, the worst drug first schedule did not perform significantly better than the best drug first therapy. In cases where the worst drug first schedule appeared to perform better this was merely as a result of this schedule also being the best drug last schedule. Hence, overall the two alternating therapies are similarly effective, however whichever schedule has most recently received the better drug will appear to perform better.

These results highlight how non-trivial the derivation of general rules concerning therapy application are and have also illustrated situations where Day's worst drug first rule does not appear to apply.

6.8 Applying a Traditional Chemotherapeutic in Conjunction with Another Therapy which Exploits the Angiogenesis-Therapy Feedback Loop

We now consider the application of a therapy which acts as a traditional chemotherapeutic when applied singly, in conjunction with another therapy which exploits the angiogenesis-therapy feedback loop when applied singly. In such a configuration it is not clear which drug should be labelled the better drug and so Day's worst drug first rule becomes ambiguous. To determine the optimal therapy, we will take therapy 1 to be the traditional chemotherapeutic when applied singly, with parameter values

given by Table 6.2, and therapy 2 to be a therapy which uses resistance to exploit the angiogenesis-therapy feedback loop when applied singly, with parameter values given by Table 6.4. We will consider the two alternating double therapies beginning with either the traditional chemotherapeutic or the therapy which uses resistance to exploit the angiogenesis-therapy feedback loop, and the two single therapies where only the traditional chemotherapeutic or the therapy which uses resistance to exploit the angiogenesis-therapy feedback loop are applied, which are the therapy Schedules (6.30) with our new definition of therapies 1 and 2. The cell populations upon cessation of the final application of therapy are shown in Figure 6.15.

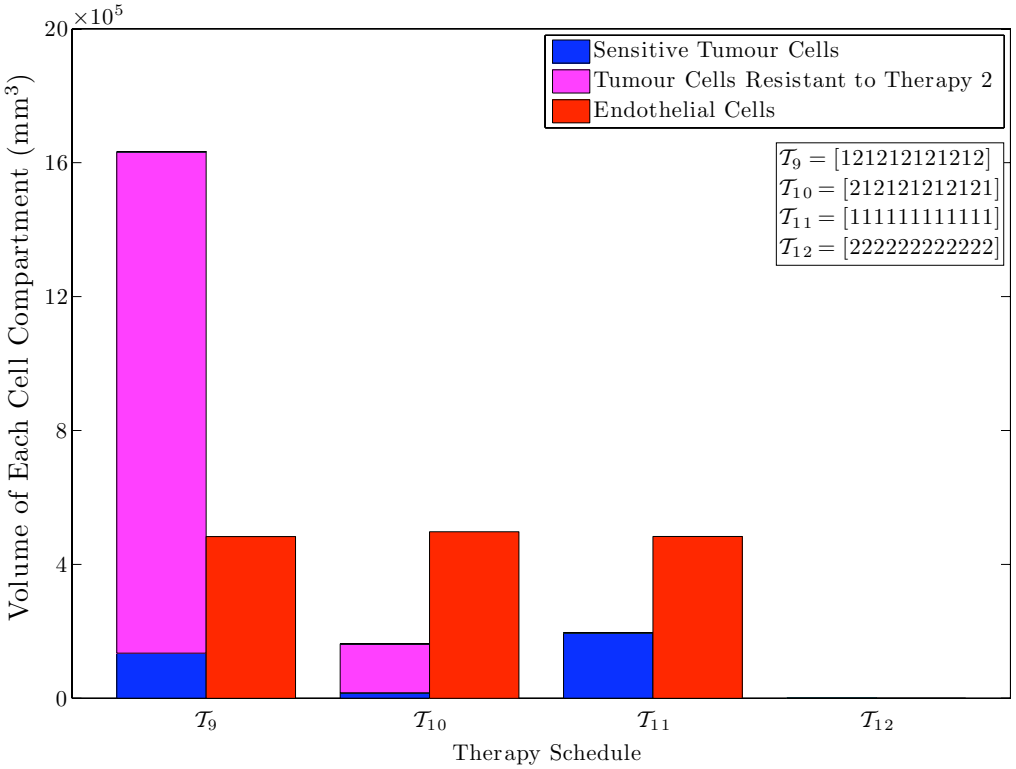

Figure 6.15: The volume of cells present in our 25% growth fraction tumour after the final application of therapy for the therapy schedules defined by Schedules (6.30), when therapy 1 takes the parameter values outlined in Table 6.2 and therapy 2 takes the parameter values outlined in Table 6.4, as governed by Equations (6.17) to (6.26). Cell populations which are present in too smaller volume to be readily seen are not labelled in the legend.

It can be seen that the optimal therapy is the single therapy which uses resistance to exploit the angiogenesis-therapy feedback loop. By considering the evolution of the

tumour in more detail (results not shown) it is found that the other therapies are less successful than this single therapy because to exploit the angiogenesis-therapy feedback loop it is vital that the applications of the therapy under-vascularise the tumour. This will then upregulate angiogenesis which in turn makes the tumour more susceptible to the next hit of therapy. Ensuring that the therapy under-vascularises the tumour is fundamental to the compounding effect which makes the angiogenesis-therapy feedback loop successful. However administering a traditional chemotherapeutic, which predominately targets the tumour cells, in between applications of the angiogenesis-therapy feedback loop exploiting therapy actually serves to over-vascularise the tumour. Hence the actions of these two therapies are mutually inhibitory and sufficiently so that the double therapies are less successful than applying the angiogenesis-therapy feedback loop exploiting therapy singly.

However, if the therapy which acts as a traditional chemotherapeutic is made more potent by setting $\kappa_{11} = 20$, and the therapy which exploits the angiogenesis-therapy feedback loop is made less potent, by setting $\kappa_{22} = 18$, and all other parameters remain unchanged, then the single therapy consisting only of the traditional chemotherapeutic becomes the best schedule, as can be seen in Figure 6.16.

We have found that the double therapies are less effective than the single therapies, because the actions of the single therapies are mutually exclusive and so the therapies do not compliment each other. However, it could be hypothesised that if both therapies are extremely potent, then a single application of either therapy might be sufficiently effective to alter the quality of the tumour's vasculature and overcome the mutual exclusiveness of the therapies. To consider this we apply a highly potent traditional chemotherapeutic with tumour cell kill rate $\kappa_{11} = 20$, and a highly potent angiogenesis-therapy feedback loop exploiter with endothelial cell kill rate $\kappa_{22} = 50$, and leave all the other parameters unchanged. Then the cell populations upon cessation of the final application of therapy for therapy Schedules (6.30) are shown in Figure 6.17.

In Figure 6.17 is can be seen that both single therapies are more effective than either double therapy. This demonstrates that even if each therapy is extremely potent, the mutually inhibitory nature of traditional chemotherapies and angiogenesis-therapy feedback loop exploiting drugs mean that scheduling them to provide an effective double therapy is a highly non-trivial task. In fact our work suggests that any double therapy is likely to perform worse than the better of the single therapies.

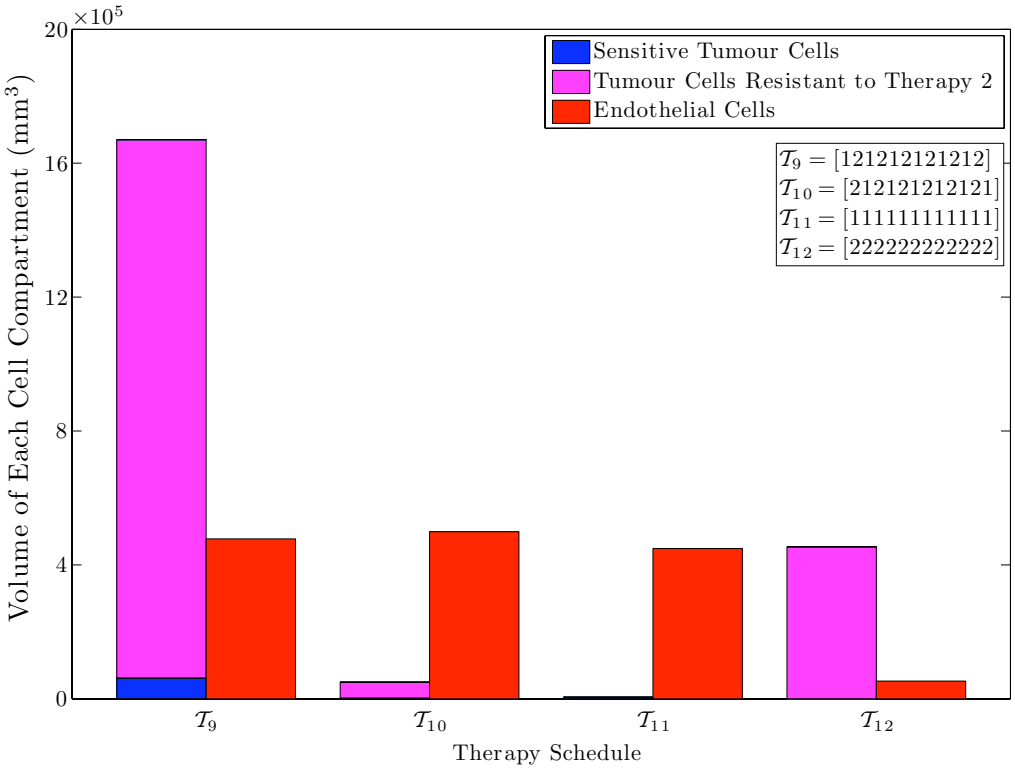

Figure 6.16: The volume of cells in our 25% growth fraction tumour after the final application of therapy for the therapy schedules defined by Schedules (6.30), for the parameter values outlined in the text as governed by Equations (6.17) to (6.26). Cell populations which are present in too smaller volume to be readily seen are not labelled in the legend.

6.9 Conclusions

In this chapter we incorporated resistance into our model for vascular tumour growth and treatment. Our goal was to then use this model to consider whether the inclusion of resistance alters how therapy should be scheduled and in particular whether the results of our model agree with the general rules for therapy scheduling, such as the Norton-Simon hypothesis, the Goldie-Coldman hypothesis, and Day's worst drug first rule. We also aimed to consider whether a maintenance therapy schedule could provide a more practical treatment than attempting tumour eradication.

We successfully included resistance and the cost of being resistant into our model. Our sensitivity analysis of Section 6.2.2 then showed that the resistance parameters can be chosen so that the therapy experiences one of three responses: it can either

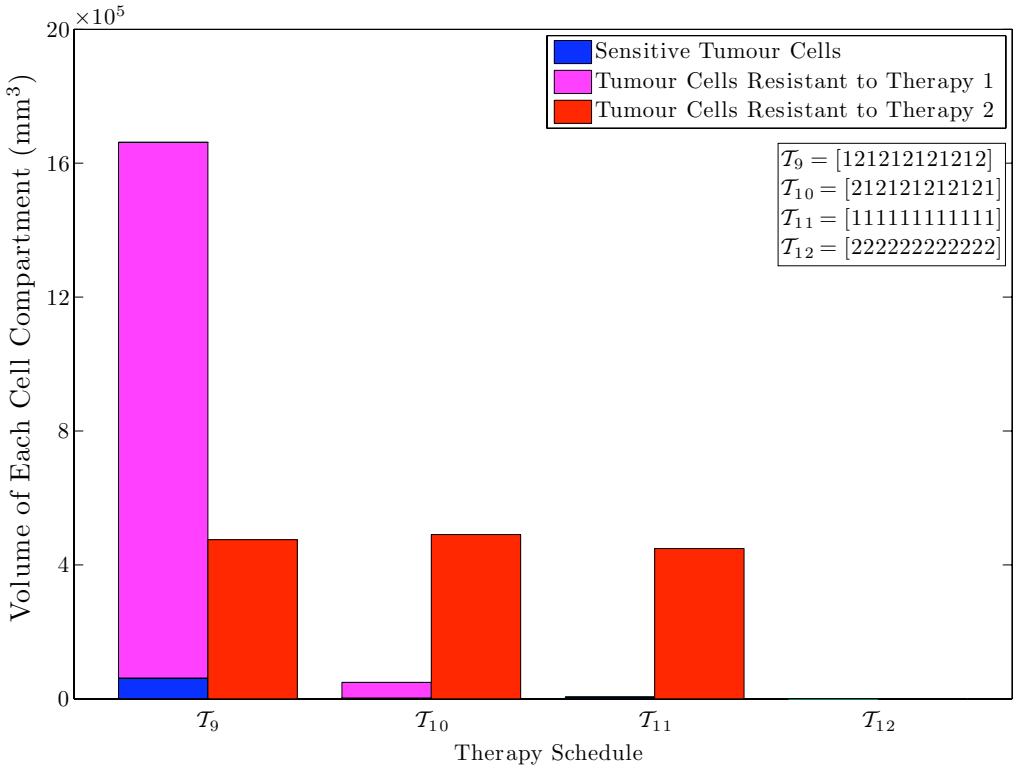

Figure 6.17: The volume of cells present in our 25% growth fraction tumour after the final application of therapy for the therapy schedules defined by Schedules (6.30) for the parameter values outlined in the text, as governed by Equations (6.17) to (6.26). Cell populations which are present in too smaller volume to be readily seen are not labelled in the legend.

treat the tumour by acting as a traditional chemotherapeutic; it can fail because of the onset of resistance; or it can treat the tumour using resistance to exploit the angiogenesis-therapy feedback loop. (Note that in Section 5.2.7 we found that the therapy can exploit the angiogenesis-therapy feedback loop without using tumour cell resistance; this will still be true when tumour cell resistance is included and was not investigated in this chapter.)

In Section 6.3 we considered the Norton-Simon hypothesis, which says that dose dense therapy schedules are more effective than dose sparse ones. In particular we investigated this when the therapy fails because of the onset of resistance. It was found that dose densing made the therapy more potent, which tended to make the therapy act like a traditional chemotherapeutic. In fact for our parameter values, taking very short rest phases made the therapy potent enough to target even the resistant cell

population. Making the therapy increasingly less dense resulted in the therapy failing because of the onset of resistance, then using resistance to exploit the angiogenesis-therapy loop, and finally failing due to lack of potency. This highlights that dose densing makes the therapy more potent as a traditional chemotherapeutic, but this does not always provide a better therapy. In particular, no general rule concerning dose densing can be asserted unless the therapy is sufficiently well understood that it is known by which mechanism the therapy is targeting the tumour.

Whilst considering the Norton-Simon hypothesis we also found that very dose sparse therapies could potentially provide a more effective maintenance therapy than dose dense therapies. This is because dose sparse therapies can be sufficiently potent to eradicate a significant proportion of the tumour when applied, but not potent enough to give a competitive advantage to the resistant cells and so a significant resistant population does not become established. Furthermore, the long rest phase in between applications of very dose sparse therapies is likely to make them more tolerable for the patient. The finding that maintenance therapies should be more dose sparse is in agreement with the results of Hahnfeldt et al. (2003) and Monro and Gaffney (2009).

To check that our results were not reliant upon the neglect of endothelial cell resistance we then modelled the resistance of the endothelial cell population. It was found that despite the endothelial cells having significantly lower mutation rates than the tumour cells, some resistant endothelial cells would be expected to exist in a clinically relevant tumour. Hence the resistance of endothelial cells cannot be *a priori* neglected. However, when the resistance of endothelial cells was included into our model the fact that endothelial cells have a significantly lower mutation rate than to tumour cells was sufficient for the exploitation of the angiogenesis-therapy feedback loop.

We then generalised our model to consider the application of double non-cross resistant therapies of chemotherapy. In Section 6.6 we used this to consider the Goldie-Coldman hypothesis, which states that to minimise the onset of resistance a double therapy should be applied and the therapies should be alternated quickly, and a summary of our results is presented in Table 6.5.

Our model did find that applying a double therapy and alternating it quickly was effective at minimising the onset of resistance, but this did not always give the best therapy. For example if the therapies are each capable of treating the tumour by acting as a traditional chemotherapeutic when applied as a single therapy, without

Therapy Mechanism	Does the Goldie-Coldman hypothesis, that alternating the therapies minimises resistance, hold?	The best therapy schedule
A successful traditional chemotherapeutic	No	The single therapy
The therapy fails because of resistance	Yes	The quickly alternating double therapy
Exploits the angiogenesis-therapy feedback loop	Yes	The single therapy

Table 6.5: A summary of our results concerning the Goldie-Coldman hypothesis.

failing due to the onset of resistance, then the stronger of the two therapies should be applied singly. Furthermore, if the therapies are capable of treating the tumour by using resistance to exploit the angiogenesis-therapy feedback loop, then preventing resistance by applying a double therapy leads to a worse therapy, and possibly even complete failure of the therapy. However, applying a double therapy and alternating it quickly was effective when the therapies fail because of the onset of resistance. This again highlights that general rules concerning the scheduling of the therapy should only be applied if the mechanism the therapy uses to treat the tumour is known.

Finally in Section 6.7 we considered Day's worst drug first rule and a summary of our results is presented in Table 6.6. Again it was found that in several circumstances the best single therapy was the optimal therapy, however this optimal therapy can only be delivered if detailed knowledge of the therapy mechanism and tumour response are known. If the optimal therapy cannot be confidently predicted then the double therapies were more reliable than the single therapies in the sense that they were less prone to suffer complete therapy failure. However when one therapy acts as a traditional chemotherapeutic when applied singly, and the other uses resistance to exploit the angiogenesis-therapy feedback loop when applied singly, the action of the drugs was found to be mutually inhibitory and applying a double therapy resulted in a much poorer therapy than applying the more effective single therapy. When the best drug first and the worst drug first therapies were compared there was often no difference between them, and what difference was observed was primarily due to

which drug was delivered last, rather than first. This again highlights that general rules concerning therapy treatment can only be applied when the mechanisms the therapy is uses to target the tumour are known, and applying the general rules in the incorrect setting can actually lead to a less effective therapy.

Therapy Mechanisms	Does Day's worst drug first rule hold?	The best therapy schedule
Both therapies are traditional chemotherapeutics	No	The more effective single therapy
Both therapies exploit the angiogenesis-therapy feedback loop	No	The more effective single therapy
When one therapy fails because of resistance	Not always	Depends upon parameter values
When one therapy is a traditional chemotherapeutic and the other exploits the angiogenesis-therapy feedback loop	No	The more effective single therapy

Table 6.6: A summary of our results concerning Day's worst drug first rule.

Chapter 7

Summary and Future Work

7.1 Summary

In Chapter 2 we considered the often made assumption that the concentration of any nutrient or drug within an avascular tumour spheroid is radially symmetric. Whilst this assumption has been made in many mathematical models of avascular tumour growth, the justification for it is often implicit and inferred from the fact that avascular tumours are typically observed to grow as spheroids. We explored the validity of this assumption and when it no longer holds by building a model for the radially averaged mean nutrient concentration and the perturbation away from this mean nutrient concentration within an avascular tumour spheroid. We then evaluated this model for a number of different nutrient and nutrient flux configurations when the rate of nutrient uptake saturates. It was found that the condition that the nutrient or drug diffuses at least two cell widths into the tumour is sufficient for the nutrient or drug to be assumed to be radially symmetric. This is because diffusion is a stabilising effect and two cells widths is sufficiently far for diffusion to well mix the nutrient so that the nutrient concentration can be approximated by its radially averaged mean value.

Since a continuum model for tumour growth is unlikely to be appropriate for a nutrient or drug which diffuses less than two cell widths into the tumour, we have shown that when a continuum model is appropriate the nutrient concentration can be assumed to be radially symmetric. However, our analysis may not be valid for chemotherapeutic drugs, for which the rate of drug uptake may not necessarily saturate, and so our work has not shown that the concentration of such drugs can be *a priori* taken to be radially symmetric.

7.1. SUMMARY

In Chapter 3 we considered the interaction between a growing avascular tumour spheroid and the surrounding vasculature. In particular we investigated how the distance between the surface of the tumour spheroid and the neighbouring capillaries varies as the tumour grows. An oxygen delivery argument showed that the 2 mm gap between the tumour and neighbouring vasculature observed following tumour implantation into a test animal's cornea must be unique to that setting. The cornea is an uniquely large region of avascular tissue and if an avascular tumour grows elsewhere then a gap of this size between the tumour and vasculature would put an impossibly large strain on the vasculature network. Such a configuration is therefore impossible.

We then utilised our results of Chapter 2 to build a multi-compartment model for the growth of an avascular tumour and its interaction with the neighbouring vasculature in the absence of a basal membrane, which particularly represents the growth of a micrometastasis. It was found that when the non-cancerous cells proliferate less quickly than the cancerous cells, which is typically the case, the gap between the tumour and neighbouring vasculature initially closes; a result which was confirmed by a simple scaling argument. Once the tumour has grown to a larger size the re-establishment of a gap between the tumour and vasculature would not require an impossibly large rate of non-cancerous cell proliferation, however there is no obvious mechanism which would upregulate non-cancerous cell proliferation to the required extent and a number of biologically motivated mechanisms were tested and found to not be sufficient. From this we conclude that once the tumour has grown to a reasonable size (about 200 μm in radius) there will be no significant gap between the tumour and neighbouring vasculature and the surrounding capillaries will effectively lie on the surface of the tumour. More generally, noting that the initial gap between the initiating tumour and the capillary bed is of the order of the inter-capillary distance, even in the presence of a basal membrane, these studies highlight that the numerous mathematical and computational models based on the cornea implant experiments are not sufficiently general for modelling carcinogenesis.

In Chapters 4, 5, and 6 we derived a multi-compartment model for vascular tumour growth, included the application of chemotherapy, and included therapy resistance respectively. Having derived our multi-compartment model for vascular tumour growth we chose some of our model's parameters by performing a literature search in combination with an asymptotic and steady state analysis. We then estimated the remaining

parameters by performing an analysis of parameters whereby parameters were chosen so that the corresponding tumour growth dynamics were suitably realistic.

Having included the application of therapy and evaluated the chemotherapy based parameters we discovered that the therapy can be effective via one of two mechanisms: it can either act as a traditional chemotherapeutic, or it can exploit the angiogenesis-therapy feedback loop. To exploit the latter the therapy should be more potent at targeting the endothelial cells than the tumour cells. Then each application of the therapy under-vascularises the tumour, which up-regulates angiogenesis, which then makes the tumour more susceptible to the next application of endothelial cell targeting therapy. It was found that the therapy which exploits the angiogenesis-therapy feedback loop was often the more effective therapy. This is because the endothelial cells recover more slowly than the tumour cells following an application of therapy, so that the system recovers more slowly following an endothelial cell targeting therapy than a traditional chemotherapeutic, the fact that therapies which exploit the angiogenesis-therapy feedback loop have a compounding effect whereby each application of therapy treats the tumour but also primes the tumour for the next application of therapy also contributed to making them effective.

We then considered whether the Norton-Simon hypothesis applies to therapies which utilise these identified treatment mechanisms. It was found that for both therapies which act as a traditional chemotherapeutic and those which exploit the angiogenesis-therapy feedback loop, and for both discrete and continuous applications of therapy, dose densing the therapy did cause more effective cell kill. More dose therapies allowed higher chemotherapy concentrations, or therapies with shorter rest phases, which were more intensive and provided a more effective therapy despite the application time of the therapy being reduced. However, we did find one important caveat to this, that the therapy must be applied for at least a few cell cycle times in duration. This is required so that the therapy is applied for sufficient time for all the proliferating cells to be targeted, and for all the quiescent cells to be recruited back into the cell cycle and then targeted.

However, we also found that dose dense therapies are more likely to give a competitive advantage to the resistance cells and cause a resistant population to become established within the tumour. Hence if tumour cure is impossible, or a maintenance therapy is sought, then the therapy should be relatively dose sparse. Then each application of the therapy can prune the tumour and maintain it at a non-fatal size, but the therapy is never intense enough to drive the onset of resistance.

We then considered the work of Browder et al. (2000) who showed that chemotherapy can effectively treat drug-resistant tumours, so that the chemotherapy must be providing an anti-angiogenic effect. Furthermore, they found that an "anti-angiogenic" therapy schedule was more effective than a "conventional" therapy schedule. Whilst Browder et al.'s work exemplifies the possibility of using traditional chemotherapies to provide an effective anti-angiogenic effect, we actually found that the difference between the effectiveness of their "anti-angiogenic" and "conventional" therapy schedules was probably due to the action of the chemotherapy saturating. Hence we found that Browder et al.'s results comparing "anti-angiogenic" and "conventional" therapy schedules can actually be phrased more generally; that if the action of the chemotherapy saturates, then the duration of the rest phase between applications of therapy should be comparable to the half-life of the chemotherapeutic. Then the therapy concentration can be constantly topped up to provide continual significant cell kill, but with minimal toxicity.

Upon including resistance into our model we found that the therapy can fail because of the onset of resistance, but resistance also creates another mechanism by which the therapy can provide an effective treatment, namely the therapy can use resistance to exploit the angiogenesis-therapy feedback loop. To do this the therapy should be potent enough to give a competitive advantage to the resistant cells. Then a resistant population will become established in the tumour and once this happens, and for certain parameter values, the therapy will be more potent at targeting the endothelial cells than the resistant tumour cells and the therapy can exploit the angiogenesis-therapy feedback loop in the manner previously outlined.

We then considered whether the Goldie-Coldman hypothesis and Day's worst drug first rule applied for these therapy mechanisms. If the total amount of therapy delivered is held constant, so that the therapies are comparably toxic, it was found that when two single therapies act as a traditional chemotherapeutic or fail because of the onset of resistance, the Goldie-Coldman hypothesis held and alternating the therapy quickly was effective at preventing the onset of resistance. However, if both therapies are unaffected by resistance then applying both as a double therapy was not beneficial and applying the stronger single therapy was optimal. If both therapies failed because of resistance when applied singly we did not find Day's worst drug first rule to hold and instead we found that the perceived effectiveness of the therapy was more dependent upon which drug was delivered last. However when one

of the therapies exploits the angiogenesis-therapy feedback loop applying an alternating double therapy was not appropriate. Whilst the Goldie-Coldman hypothesis was correct in the sense that applying a double therapy prevented the onset of resistance, the therapy requires the onset of resistance to exploit the angiogenesis-therapy feedback loop, and so applying an alternating therapy led to a worse therapy schedule and even complete therapy failure. Furthermore we found that if one therapy acts as a traditional chemotherapeutic, and the other exploits the angiogenesis-therapy feedback loop, then the mechanisms of these therapies are mutually inhibitory and applying them jointly led to a worse therapy than applying either of them singly.

We also showed that these conclusions would be unaffected by the explicit consideration of endothelial cell resistance. The fact that endothelial cells are more genetically stable than tumour cells, and therefore less likely to mutate to acquire resistance, is sufficient for therapy to be able to use resistance to exploit the angiogenesis-therapy feedback loop. The reason for this being that resistance becomes established in the tumour cells much more quickly than in the endothelial cells, and so there is a time window where the tumour consists largely of resistant cells, but the endothelial cells consist largely of sensitive cells, and the angiogenesis-therapy feedback loop can be effectively exploited in this window.

Overall we have found that there is potentially another mechanism by which a therapy can provide an effective treatment, namely it can use resistance to exploit the angiogenesis-therapy feedback loop. However, if the therapy uses this mechanism then many of the typical therapy scheduling rules, particularly the Goldie-Coldman hypothesis and Day's worst drug first rule, do not apply. Furthermore following them can lead to complete therapy failure. This highlights how non-trivial the problem of therapy scheduling is. Furthermore, if the mechanisms by which the therapies treat the tumour, or whether the therapy fails because of resistance, are known then rules concerning how the therapies should be applied can be found. However this requires a good understanding of how the therapy and the tumour interact and in the absence of such knowledge there is not one therapy schedule which will be effective for all therapies. In fact, the best therapy schedule for a traditional chemotherapeutic is typically the worst therapy schedule for a therapy which uses resistance to exploit the angiogenesis-therapy feedback loop. This highlights how difficult it is to schedule general therapies with the intention of completely eradicating the general tumour.

This suggests that maintenance therapies which intend to manage, rather than completely eradicate, the tumour might be more practical. In which case relatively dose

sparse therapies should be applied which do not give a significant competitive advantage to the resistant cells and give the tumour sufficient time to resensitise to the therapy in between applications of the therapy.

7.2 Future Work

Our model in Chapter 2 only considered the radial symmetry of nutrients and drugs for which the rate of nutrient, or drug, uptake saturates and does so quickly. This is certainly true for oxygen and is expected to be valid more generally for nutrients which are required for cell growth, because cells have evolved to be very good at uptaking such nutrients, but may not be valid for a general chemotherapeutic drug, which highlights the opportunity for future work.

In Chapters 4, 5, and 6 we considered how chemotherapy should be scheduled to obtain the most effective tumour treatment. In particular, one aspect of chemotherapy scheduling we considered was how to schedule the therapy to provide the best maintenance therapy, by which we mean a therapy which keeps the tumour below some non-fatal size rather than trying to completely eradicate it. A similar investigation could be undertaken to consider what the best palliative therapy schedule is, i.e. if a tumour cannot be eradicated how should therapy be delivered to limit its progression to the greatest extent.

Another extension which could be performed to the work of Chapters 4, 5, and 6 is the consideration of spatial effects. Since vascular tumours have been observed to be highly spatially inhomogeneous we have not attempted to model any spatial aspect of the tumour. Instead we averaged the behaviour of the tumour across the entire tumour. Spatial effects could be included in a future model and the results of the model in this thesis could be tested against the results of the spatial model to investigate whether spatial effects are significant.

A major area of future work would be the experimental testing of our theoretical assumptions and results. For example, in Chapter 3 we concluded that for an established *in vivo* avascular tumour the neighbouring capillaries effectively lie on the surface of the tumour. Whilst there are *in vivo* images which show that a 2 mm gap between the tumour and neighbouring capillaries, such as that seen following an intra-cornea implant, there has been no explicit experimental study of how the distance between the tumour and neighbouring capillaries behaves as the tumour grows.

Whether the neighbouring capillaries do actually lie of the surface of the tumour, as predicted by our model, or whether there is a gap, albeit a smaller one than the 2 mm gap observed in the intra-cornea experiments, between the capillaries and tumour could be explicitly investigated. Furthermore, if the capillaries are found to lie on the surface of the tumour then a detailed study of how quickly the gap closes would allow our model to infer what proliferation kinetics the non-cancerous cells undergo as the tumour grows.

The other major area of this thesis which would benefit from detailed experimental testing is our model for the growth and response of a vascular tumour, which was presented in Chapters 4, 5, and 6. Care has been taken to ensure that all the assumptions in our model are biologically reasonable and some, such as the use of Michaelis-Menten proliferation kinetics, have been tested in other works, and the results of our model have been tested against observed experimental results, both in the presence and absence of therapy. However, the field would still benefit from detailed experimental investigations. Initially tumour spheroids could be grown in culture and the observed growth of these spheroids could be analysed to estimate the parameter values in our model corresponding to the grown spheroids. While it is straightforward to match empirical growth curves as they simply increase and saturate, exploring whether the current modelling frameworks presented here, and in the literature more generally, are capable of predicting tumour dynamics in the presence of multiple distributions of cytotoxins remains to be explored. This also offers the opportunity for iterative cycles of model refinement and testing which is critical for the integrity of next generation simulations.

Existing clinical trials tend to use protocols that are more complicated than the idealised ones considered here, and there is ample scope for assessing existing data from real trials in modelling frameworks to assess whether the qualitative trends predicted *in silico* can be observed in current data. When, or perhaps if, a simulation based discovery platform addressing protocol scheduling is validated against *in vitro* data and also appears to be consistent with trends in existing clinical trials data, there is then scope for iterations of model validation and *in vivo* experiments as well as an increasing application in developing insight for clinical trials. The fact the latter occurs with even the simple models of today, as proudly highlighted in a number of Nortons clinical trials, emphasises the importance of embarking on a cycle of modelling refinement by iterative comparison with empirical studies.

Appendix A

Simplifying the Numerical Scheme of Chapter 2

A.1 Simplifying the Numerical Scheme for Test Function 2

We begin by integrating Equations (2.29) and (2.30) for the coefficients $\alpha_{n,m}$ and $\beta_{n,m}$. Here we are able to use the orthogonality of the trigonometric functions to simplify our calculations. Upon substituting the test function given in Equation (2.41) into the integral equation for $\alpha_{n,m}$, Equation (2.29), and recalling the orthogonality properties of the trigonometric functions we find that

$$\alpha_{n,m} = 0 \qquad \forall\, n, m.$$

Similarly, upon substituting this test function into the integral equation for $\beta_{n,m}$, Equation (2.30), and recalling the orthogonality properties of the trigonometric functions, we find that

$$\beta_{n,m} = \begin{cases} \dfrac{\pi(1-{r_*}^3)}{3} \displaystyle\int_0^{2\pi} \sqrt{\tfrac{2n+1}{2\pi}\tfrac{(n-63)!}{(n+63)!}} P_n^{63}(\cos(\phi)) \sin(63\phi)\, \mathrm{d}\phi & \text{if } m = 63, \\ 0 & \text{if } m \neq 63, \end{cases} \qquad \forall\, n. \tag{A.1}$$

So for this test function most of the $\beta_{n,m}$ coefficients are zero, except for the coefficients $\beta_{n,63}$ which now contain a single integral. Here we calculate this single integral numerically using the inbuilt matlab function quadl with an absolute error tolerance of 10^{-9}, which implements an adaptive Lobatto quadrature method. This then gives us an approximation to $\beta_{n,63}$ which we denote by $\beta'_{n,63}$.

A.1. SIMPLIFYING THE NUMERICAL SCHEME FOR TEST FUNCTION 2

Having shown that most of the coefficients in our Laplace series are zero we find that our numerical approximation to the perturbed flux becomes

$$\widetilde{h}'(\theta,\phi) = \sum_{n=63}^{N} \beta'_{n,63} Y_{s_{n,63}}(\theta,\phi).$$

The condition that the relative mean square error in the numerical approximation to the perturbed flux must be less than 1%, as given by Equation (2.38), then becomes

$$\int_0^{2\pi}\int_0^{\pi} \left(\sum_{n=63}^{N} \frac{3\beta'_{n,63}}{1-r_*^3} Y_{s_{n,63}}(\theta,\phi) - \sin(63\theta)\sin(63\phi) \right)^2 \sin\phi \, \mathrm{d}\phi \, \mathrm{d}\theta < \frac{\pi}{25}. \qquad \text{(A.2)}$$

To evaluate this double integral we apply the trapezium rule twice to obtain a repeated trapezium rule quadrature method. We implement this $(63k)^2$ quadrature points, evenly spaced in θ and ϕ, and increase k until the relative change in approximation to the double integral is less than 10^{-4}.

From Equation (A.1) it can be seen that the quantities of $3\beta_{n,63}/(1-r_*^3)$ are actually independent of r_* and it follows that Condition (A.2) is also independent of r_*. Hence, having approximated $\beta_{n,63}$ by numerically integrating Equation (A.1) and satisfied Condition (A.2) for the first value of r_*, we can immediately rescale these results to obtain suitable approximations of $\beta_{n,63}$ for any other value of r_*.

Having found $\beta'_{n,63}$ and ensured that Condition (A.2) is satisfied we obtain the following numerical approximation to the perturbation

$$\widetilde{c}'(r,\theta,\phi) = -\sum_{n=63}^{N} \frac{r^n}{n} \beta'_{n,63} Y_{s_{n,63}}(\theta,\phi),$$

and for a given value of r the maximum value of the perturbation is found to satisfy

$$\max_{\theta,\phi} |\widetilde{c}'(r,\theta,\phi)| = \left(\frac{1-r_*^3}{3}\right) \max_{\theta,\phi} \left| \sum_{n=63}^{N} \frac{r^n}{n} \frac{3\beta'_{n,63}}{1-r_*^3} Y_{s_{n,63}}(\theta,\phi) \right|. \qquad \text{(A.3)}$$

Note that as before the absolute value on the right hand side of this equation is independent of r_*. Hence we only need calculate this maximum value once and we can then rescale our result to obtain the maximum value of the perturbation for other values of r_*.

We now approximate the maximum value of the absolute value on the right hand side of Equation (A.3) numerically and to do this we define

$$L_k(r) = \max\left\{ \left| \sum_{n=63}^{N} \frac{r^n}{n} \frac{3\beta'_{n,63}}{1-r_*^3} \sqrt{\tfrac{(2n+1)}{2\pi}\tfrac{(n-63)!}{(n+63)!}} P_n^{63}\left(\cos\tfrac{p\pi}{63k}\right) \right| \middle| 0 \le p \le 63k \right\},$$

where $L_k(r)$ is related to the maximum observed value of the perturbation, $M_k(r)$ as defined by Equation (2.39), thus

$$L_k(r) = \frac{3}{1-r_*^3} M_k(r).$$

Again Equation (A.1) shows that $L_k(r)$ is independent of r_*.

We previously used Condition (2.40) to ensure that the maximum value of the perturbation is suitably approximated. That condition for $M_k(r)$ gives rise to the following condition for $L_k(r)$

$$\max_{0\le r\le 1} |L_{k+1}(r) - L_k(r)| < \frac{3\overline{c}(1)}{10^4(1-r_*^3)}.$$

Notice that the left hand side of this equation is independent of r_* but the right hand side depends upon r_*. So we will increase k until this condition is satisfied for all the values of r_* being considered. Noting that

$$\min\left\{ \left(\frac{3\overline{c}(1)}{1-r_*^3} \right) 10^{-4} \middle| r_* \in \{0.83, 0.92, 0.85, 0.9, 0.95\} \right\} = 2.5 \times 10^{-6} \quad (2\,\text{s.f.}),$$

we find that we must increase k until

$$\max_{0\le r\le 1} |L_{k+1}(r) - L_k(r)| < 2.5 \times 10^{-6},$$

and once this condition is satisfied we can approximate the maximum value of the perturbation by

$$\max_{\theta,\phi} |\widetilde{c}(r,\theta,\phi)| = \left(\frac{1-r_*^3}{3} \right) L_{k+1}(r).$$

A.2 Simplifying the Numerical Scheme for Test Function 3

Upon substituting the test function given in Equation (2.42) into the integral equation for $\alpha_{n,m}$, Equation (2.29), we find that it is possible to separate the double integral into two single integrals where the θ integral is

$$\int_0^{2\pi} \sin\left\{ 63\left(\theta + \tfrac{\sin(10\theta)}{20} \right) \right\} \cos(m\theta)\, \mathrm{d}\theta.$$

However, the periodicity of the trigonometric functions can be used to show that this integral is zero for all n, so that

$$\alpha_{n,m} = 0, \quad \forall\, n,\, m.$$

Similarly, the θ integral in the double integral for $\beta_{n,m}$, as given by Equation (2.30), is

$$I_\theta = \int_0^{2\pi} \sin\left\{63\left(\theta + \tfrac{\sin(10\theta)}{20}\right)\right\} \sin(m\theta)\, \mathrm{d}\theta.$$

The symmetry of this integral's integrand about the point $\theta = \pi$ can then be used to show that

$$I_\theta = \begin{cases} 2\displaystyle\int_0^{\pi} \sin\left\{63\left(\theta + \tfrac{\sin(10\theta)}{20}\right)\right\} \sin(m\theta)\, \mathrm{d}\theta & \text{when } m \text{ odd}, \\ 0 & \text{when } m \text{ even}. \end{cases}$$

Given this, our integral equation for $\beta_{n,m}$ becomes

$$\beta_{n,m} = \begin{cases} 2\left(\dfrac{1-r_*^3}{3}\right) \displaystyle\int_0^{\pi}\int_0^{\pi} \frac{3\widetilde{h}(\theta,\phi)}{1-r_*^3} Y_{C_{n,m}}(\theta,\phi)\, \mathrm{d}\theta\, \mathrm{d}\phi & \text{when } m \text{ odd}, \\ 0 & \text{when } m \text{ even}. \end{cases}$$

Notice from Equation (2.42) that $3\widetilde{h}(\theta,\phi)/(1-r_*^3)$ is independent of r_* and so it is only necessary to evaluate the integral in this expression once and the result can be used to find the value of $\beta_{n,m}$ corresponding to any other value of r_*. Here we calculate this double integral numerically by splitting it into two single integrals and evaluating each one using the inbuilt matlab function quadl with an absolute error tolerance of 10^{-9}, which implements an adaptive Lobatto quadrature method. This then gives us an approximation to $\beta_{n,63}$ which we denote by $\beta'_{n,63}$.

Also notice that for this test function the condition that the relative mean square difference between the perturbed flux and the numerical approximation to the perturbed flux must be less than 1%, as given by Equation (2.38), becomes

$$\int_0^{2\pi}\int_0^{\pi} \left(\sum_{n=1}^{N} \sum_{k=0}^{\lfloor \frac{n}{2}+1 \rfloor} \frac{3\beta'_{n,2k+1}}{1-r_*^3} Y_{s_{n,2k+1}}(\theta,\phi) - \frac{3\widetilde{h}(\theta,\phi)}{1-r_*^3} \right)^2 \sin\phi\, \mathrm{d}\phi\, \mathrm{d}\theta < \frac{\pi}{25}, \qquad \text{(A.4)}$$

where $\lfloor x \rfloor$ is the floor function which rounds a number down to its next smallest integer.

To evaluate this double integral we apply the trapezium rule twice to obtain a repeated trapezium rule quadrature method. We implement this $(63k)^2$ quadrature points, evenly spaced in θ and ϕ, and increase k until the relative change in approximation to the double integral is less than 10^{-4}.

Recalling that $3\beta_{n,2k+1}/(1-r_*^3)$ and $3\widetilde{h}(\theta,\phi)/(1-r_*^3)$ are both independent of r_* we find that N is also independent of r_*. So again we only need to calculate the value of N for the first value of r_* and we have found it for any value of r_*.

Having found $\beta'_{n,2k+1}$, our numerical approximations to $\beta_{n,2k+1}$, and having found N and having ensured that Condition (A.4) is satisfied we find that our numerical approximation to the perturbation is given by

$$\widetilde{c}'(r,\theta,\phi) = -\sum_{n=0}^{N}\sum_{k=0}^{\lfloor \frac{n}{2}+1\rfloor} \frac{r^n}{n}\beta'_{n,2k+1}Y_{s_{n,2k+1}}(\theta,\phi),$$

and the maximum value of the numerical approximation to the perturbation is

$$\max_{\theta,\phi}|\widetilde{c}'(r,\theta,\phi)| = \left(\frac{1-r_*^3}{3}\right)\max_{\theta,\phi}\left|\sum_{n=0}^{N}\sum_{k=0}^{\lfloor \frac{n}{2}+1\rfloor} \frac{r^n}{n}\frac{3\beta'_{n,2k+1}}{(1-r_*^3)}Y_{s_{n,2k+1}}(\theta,\phi)\right|.$$

The absolute value on the right hand side of this equation is independent of r_* and so we only need calculate its maximum value once and we can then scale our result to obtain the maximum value of the perturbation for any value of r_*. As before we approximate the maximum value of this absolute value by defining

$$L_k(r) = \max\left\{\left|\sum_{n=0}^{N}\sum_{k=0}^{\lfloor \frac{n}{2}+1\rfloor} \frac{r^n}{n}\frac{3\beta'_{n,2k+1}}{(1-r_*^3)}Y_{s_{n,2k+1}}\left(\frac{p\pi}{63k},\frac{q\pi}{63k}\right)\right| \middle| 0\le p\le 63k, 0\le q\le 63k\right\},$$

and increasing k until the error in this maximum is acceptably small and Condition (2.40) is satisfied so that

$$\max_{0\le r\le 1}|L_{k+1}(r)-L_k(r)| < 2.5\times 10^{-6}.$$

Once this condition is satisfied we approximate the maximum value of the perturbation by

$$\max_{\theta,\phi}|\widetilde{c}'(r,\theta,\phi)| = \left(\frac{1-r_*^3}{3}\right)L_{k+1}(r).$$

Appendix B

Details of Parameter Estimations

B.1 The Parameters in Chapter 3

B.1.1 Estimating the Value of A

We estimate A, the maximum rate at which colorectal cells undergo mitosis, by relating it to the doubling time of colorectal cancer cells. Under optimal conditions we assume that a tumour of volume $V(t)$, a function of time, only consists of proliferating cancer cells and that cell mitosis dominates cell necrosis. Then to leading order the evolution of the tumour volume will be governed by:

$$\begin{aligned} \frac{\mathrm{d}V}{\mathrm{d}t} &= AV, \\ \implies \quad V(t) &= V(0)e^{At}. \end{aligned}$$

Letting t_2 be the doubling time of the tumour, so that $V(t_2) = 2V(0)$, we find that

$$\begin{aligned} e^{At_2} &= 2, \\ \implies \quad A &= \frac{\log 2}{t_2}. \end{aligned}$$

Finally, substituting in $t_2 = 135$ hours we find that $A = 1.4 \times 10^{-6} s^{-1}$.

B.2 The Parameters in Chapter 4

B.2.1 Estimating the Value of $\widehat{K}$

To estimate the value of $\widehat{K}$ we assume that we have 3×10^{12} cells in total, of which X are viable cells, $3 \times 10^{12} - X$ are necrotic cells, and we neglect the contribution

of any endothelial cells. Then the total volume of the live cell compartment is $X\frac{V_L}{\mathcal{V}}$ and the volume of the necrotic compartment is $(3\times10^{12}-X)\,\frac{V_N}{\mathcal{V}}$. Recalling that we previously took the necrotic fraction of our tumour to be 0.25 we find that we should choose X so that:

$$\frac{(3\times10^{12}-X)\,V_N}{XV_L+(3\times10^{12}-X)\,V_N}=\frac{1}{4}.$$

Recalling that we have previously found that $\frac{V_N}{V_L}=0.5$ this becomes:

$$\begin{aligned}\frac{(3\times10^{12}-X)}{2X+3\times10^{12}-X}&=\frac{1}{4},\\ \Longrightarrow\qquad X&=\frac{9}{5}\times10^{12}.\end{aligned}$$

Hence there are $\frac{9}{5}\times10^{12}$ live cells in the tumour, $\frac{6}{5}\times10^{12}$ necrotic cells in the tumour, and the non-dimensional carry capacity of the tumour's host is:

$$\begin{aligned}\widehat{K}&=\frac{\mathcal{V}}{V_E}\left(\tfrac{9}{5}\times10^{12}\tfrac{V_L}{\mathcal{V}}+\tfrac{6}{5}\times10^{12}\tfrac{V_N}{\mathcal{V}}\right),\\ &=7.2\times10^{12}.\end{aligned}$$

Bibliography

B. Alberts, D. Bray, J. Lewis, M. Raff, K. Roberts, and J. D. Watson, editors. *Molecular Biology of the Cell*. Garland Publishing Inc,US, 2002.

W. R. Amberson. The influence of oxygen tension upon the resporation of unicellular organisms. *Biological Bulletin*, 55:79–91, 1928.

M. Andreef, D. W. Goodrich, and A. B. Pardee. Cell proliferation, differentiation and apoptosis. In: D. W. Kufe and J. F. Holland (eds.), Cancer Medicine, 6th ed., Hamilton, Ontario (Canada): BC Decker, 2000.

G. Arfken and H. Weber. *Mathematical Methods for Physicists*. Amsterdam; London: Elsevier Academic, sixth edition, 2005.

D. Balding and D. L. S. McElwain. A mathematical model of tumour-induced capillary growth. *Journal of Theoretical Biology*, 114:53–73, 1985.

S. Begley. Rethinking the war on cancer. *Newsweek*, 2008.

W. T. Bellamy, W. S. Dalton, M. C. Gleason, T. M. Grogan, and J. M. Trent. Development and characterization of a melphalen-resistant human multiple myeloma cell line. *Cancer Research*, 51:995–1002, 1991.

C. M. Bender and S. A. Orzag. *Advanced Mathematical Methods for Scientists and Engineers*. McGraw and Hill Book Company, 1978.

R. Bicknell, C. E. Lewis, and N. Ferrara. Introduction. In: R. Bicknell, C. E. Lewis and N. Ferrara (eds.) Tumour angiogenesis, Oxford University Press, 1997.

T. Boehm, J. Folkman, T. Browder, and M. S. O'Reilly. Antiangiogenic therapy of experimental cancer does not induce acquired drug resistance. *Nature*, 390:404–407, 1997.

T. Browder, C. E. Butterfield, B. M. Kraling, B. Shi, B. Marshall, M. S. O'Reilly, and J. Folkman. Antiangiogenic scheduling of chemotherapy improves efficacy against experimental drug-resistant cancer. *Cancer Research*, 60:1878–1886, 2000.

D. L. Buckley, J. D. Bui, M. I. Phillips, and S. J. Blackband. MRI measurement of cell volume fraction in the perfused rat hippocampal slice. *Magnetic Resonance in Medicine*, 42(3):603–607, 1999.

A. C. Burton. Rate of growth of solid tumours as a problem of diffusion. *Growth*, 30: 157–176, 1966.

H. M. Byrne and M. A. J. Chaplain. Mathematical models for tumour angiogenesis: Numerical simulations and nonlinear wave solutions. *Bulletin of Mathematical Biology*, 57(3):461–486, 1995.

P. Carmeliet and R. K. Jain. Angiogenesis in cancer and other diseases. *Nature*, 407: 249–257, September 2000.

P. Carmeliet, V. Ferreira, G. Breier, S. Pollefeyt, L. Kieckens, M. Gertsenstein, M. Fahrig, A. Vandenhoeck, K. Harpal, C. Ederhardt, C. Declercq, J. Pawling, L. Moons, D. Collen, W. Risau, and A. Nagy. Abnormal blood vessel development and lethality in embryos lacking a single VEGF allele. *Nature*, 380:435–439, 1996.

J. J. Casciari, S. V. Sotirchos, and R. M. Sutherland. Mathematical modelling of microenvironment and growth in EMT6/Ro multicellular tumour spheroids. *Cell Proliferation*, 25:1–22, 1992.

M. A. J. Chaplain. The mathematical modelling of tumour angiogenesis and invasion. *Acta Biotheoretica*, 43(4):387–402, 1995.

M. A. J. Chaplain. Mathematical modelling of angiogenesis. *Journal of Neuro-Oncology*, 50(1):37–51, 2000.

M. A. J. Chaplain and A. M. Stuart. A model mechanism for the chemotactic response of endothelial cells to tumour angiogenesis factor. *Mathematical Medicine and Biology*, 10(3):149–168, 1993.

M. A. J. Chaplain, S. M. Giles, B. D. Sleeman, and R. J. Jarvis. A mathematical analysis of a model for tumour angiogenesis. *Journal of Mathematical Biology*, 33: 744–770, 1995.

V. P. Collins, R. K. Loeffler, and H. Tivey. Observations on growth rates of human tumors. *The American Journal of Roentgenology, Radium Therapy & Nuclear Medicine*, 76:988–1000, 1956.

G. Colucci, V. Gebbia, D. Galetta, F. Riccardi, S. Cariello, and N. Gebbia. Cisplatin and cinorelbine followed by ifosfamide plus epirubicin vs the opposite sequence in advanced unresectable stage III and metastatic stage IV non-small-cell lung cancer: a prospective randomized study of the Southern Italy Oncoloy Group (GOIM). *British Journal of Cancer*, 76(11):1509–1517, 1997.

W. S. Dalton, B. G. M. Durie, D. S. Alberts, J. H. Gerlach, and A. E. Cross. Characterization of a new drug-resistant human myeloma cell line that expresses P-glycoprotein. *Cancer Research*, 46:5125–5130, 1986.

J. D. Davidson, L. Ma, M. Flagella, S. Geeganage, L. M. Gelbert, and C. A. Slapak. An increase in the expression of ribonucleotide reductase large subunit 1 is associated with gemcitabine resistance in non-small cell lung cancer lines. *Cancer Research*, 64:3761–3766, 2004.

R. S. Day. Treatment sequencing, asymmetry and uncertainty: Protocol strategies for combination chemotherapy. *Cancer Research*, 46:3876–3885, 1986.

B. Dome, S. Paku, B. Somlai, and J. Timar. Vascularization of cutaneous melanoma involves vessel co-option and has clinical significance. *Journal of Pathology*, 197(3): 355–362, 2002.

C. Donnellan. *Confronting Cancer*. Independence Educational Publishers, 2003.

J. W. Drake, B. Charlesworth, D. Charlesworth, and J. F. Crow. Rates of spontaneous mutation. *Genetics*, 148:1667–1686, 1998.

P. Duesberg, R. Stindl, and R. Hehlmann. Explaining the high mutation rates of cancer cells to drug and multidrug resistance by chromosome reassortments that are catalyzed by aneuploidy. *Proceedings of the National Academy of Sciences*, 97 (26):14295–14300, 2000.

R. E. Durand and E. Sham. The lifetime of hypoxic human tumour cells. *International Journal of Radiation Oncology • Biology • Phyics*, 42:711–715, 1998.

E. Fait, W. Malkusch, S. H. Gnoth, C. Dimitropoulou, A. Gaumann, C.J. Kirkpatrick, T. Junginger, and M. A. Konerding. Microvascular patterns of the human large intestine: Morphometric studies of vascular parameters in corrosion casts. *Scanning Microscopy*, 12(4):641–651, 1998.

N. Ferrara, K. Carver-Moore, H. Chen, M. Dowd, L. Lu, K. S. O'Shea, L. Powell-Braxton, K. J. Hilan, and M. W. Moore. Heterozygous embryonic lethality induced by targeted inactivation of the VEGF gene. *Nature*, 380:439–442, 1996.

J. Folkman and M. Hochberg. Self-regulation of growth in three dimensions. *Journal of Experimental Medicine*, 138:745–753, 1973.

J. Folkman and R. Kalluri. Tumour angiogenesis. In: D. W. Kufe, R. E. Pollock, R. R. Weichselbaum, R. C. Bast Jr., J. F. Holland and E. Frie III (eds.), Cancer Medicine, 6th ed., Hamilton, Ontario (Canada): BC Decker., 2003.

C. E. Freter and M. C. Perry. *The Chemotherapy Source Book*, chapter Principles of Chemotherapy, pages 30–36. Philadelphia; London: Wolters Kluwer Lippincott Williams and Wilkins, 4^{th} edition, 2008.

J. P. Freyer. Decreased mitochondrial function in quiescent cells isolated from multicellular tumor spheroids. *Journal of Cellular Physiology*, 176:138–149, 1998.

J. P. Freyer and R. M. Sutherland. Proliferative and clonogenic heterogeneity of cells from EMT6/Ro multicellular spheroids induced by the glucose and oxygen supply. *Cancer Research*, 46:3513–3520, 1986.

D. Fukmura and R. K. Jain. Tumor microvasculature and microenvironment: Targets for anti-angiogenesis and normalization. *Microvasculature Research*, 2007.

F. Fulfaro, M. R. Valerio, G. Badalamenti, N. Gebbia, and A. Russo. Antiblastic drug combinations with ifosfamide: an update. *Oncology*, 65 (suppl 2):21–30, 2003.

R. A. Gatenby. A change of strategy in the war on cancer. *Nature*, 459:508–509, 2009.

A. Gautam and G. Bepler. Suppression of lung tumor formation by the regulartory subunit of ribonucleotide reductase. *Cancer Research*, 66(13):6497–6502, 2006.

F. Gavosto and A. Pileri. *The Cell Cycle and Cancer*, chapter Cell Cycle of Cancer Cells in Man, pages 97–128. Marcel Dekker, New York, 1971.

V. Gebbia, D. Galetta, M. Caruso, F. Verderame, G. Pezzella, M. Valdesi, N. Borsellino, G. Pandolfo, E. Durini, M. Rinaldi, M. Loizzi, N. Gebbia, R. Valenza, M. L. Tirrito, F. Varvara, and G. Colucci. Gemcitabine and cisplatin versus vinorelbine and cisplatin versus ifosfamide+gemcitabine vinorelbine and cisplatin followed by ifosfamide and gemcitabine in stage IIIb-IV non small cell lung carcinoma: a prospective randomized phase III trial of the Gruppo Oncologico Italia Meridionale. *Lung Cancer*, 39(2):179–189, 2003.

J. H. Goldie. *The Chemotherapy Source Book*, chapter Drug Resistance, pages 21–29. Philadelphia; London: Wolters Kluwer Lippincott Williams and Wilkins, 4^{th} edition, 2008.

J. H. Goldie and A. J. Coldman. A mathematical model for relating the drug sensitivity of tumours to their spontaneous mutation rate. *Cancer Treatment Reports*, 63(11-12):1727–1733, 1979.

J. H. Goldie and A. J. Coldman. *Drug Resistance in Cancer*. Cambridge University Press, 1998.

J. H. Goldie, A. J. Coldman, and G. A. Gudauskas. Rationale for the use of alternating non-cross-resistant chemotherapy. *Cancer Treatment Reports*, 66(3):439–449, 1982.

B. Gompertz. On the nature of the function expressive of the law of human mortality, and on a new mode of determining the value of life contingencies. *Philosophical Transactions of the Royal Society of London*, 115:513–585, 1825.

M. R. Green. Targeting targeted therapy. *The New England Journal of Medicine*, 350(21):2191–2193, 2004.

K. Groebe, S. Erz, and W. Mueller-Klieser. Glucose diffusion coefficients determined from concentration profiles in EMT06 tumor spheroids incubated in radioactively labeled L-glucose. *Advances in Experimental Medicine and Biology*, 46:619–625, 1994.

F. Grossi, M. Aita, A. Follador, C. Defferrari, A. Brianti, G. Sinaccio, and O. Belvedere. Sequential, alternating, and maintenance/consolidation chemotherpay in advanced non-small cell lung cancer: a review of the literature. *The Oncologist*, 12:451–464, 2007.

J. Grote, R. Sussking, and P. Vaupel. Oxygen diffusivity in tumour tissue (ds-carcinoma) under temperature conditions within the range of 20-40 °C. *European Journal of Physiology*, 372:37–42, 1977.

N. Gunduz. Cytokinetics of tumour and endothelial cells and vascularization of lung metastases in C3H/He mice. *Cell and Tissue Kinetics*, 14:343–363, 1981.

R. D. Guzy and P. T. Schumacker. Oxygen sensing by mitochondria at complex III: The paradox of increased reactive oxygen species during hypoxia. *Experimental Physiology*, 91:807–819, 2006.

M. Gyllenberg and G. F. Webb. Quiescence as an explanation of gompertzian tumour growth. *Growth Development and Aging*, 53:25–33, 1989.

P. Hahnfeldt, D. Panigraphy, J. Folkman, and L. Hlatky. Tumour development under angiogenic signaling: A dynamical theory of tumour growth, treatment response and postvascular dormancy. *Cancer Research*, 59:4770–4775, 1999.

P. Hahnfeldt, J. Folkman, and L. Hlatky. Minimizing long-term tumor burden: The logic for metronomic chemotherapeutic dosing and its antiangiogenic basis. *Journal of Theoretical Biology*, 220:545–554, 2003.

M. Haji-Karim and J. Carisson. Proliferation and viability in cellular spheroids of human origin. *Cancer Research*, 38:1457–1464, 1978.

D. Hanahan and R. A. Weinberg. The hallmarks of cancer. *Cell*, 100:57–70, 2000.

L. Hlatky and E. Alpen. Two-dimensional diffusion limited system for cell growth. *Cell and Tissue Kinetics*, 18(8):597–611, 1985.

E. W. Hobson. *The Theory of Spherical and Ellipsoidal Harmonics*. New York, 1955.

J. Holash, P. C. Maisonpierre, D. Compton, P. Boland, C. R. Alexander, D. Zagzag, G. D. Yancopoulos, and S. J. Wiegand. Vessel cooption, regression, and growth in tumors mediates by angiopoietins and VEGF. *Science*, 284(5422):1994–1998, 1999.

M. J. Holmes and B. D. Sleeman. A mathematical model of tumour angiogenesis incorporating cellular traction and viscoeslastic effects. *Journal of Theoretical Biology*, 202:95–112, 2000.

R. A. Hromas, J. A. North, and C. P. Burns. Decreased cisplatin uptake by resistant L1210 leukemia cells. *Cancer Letters*, 36:197–201, 1987.

I. Ishiwata, C. Ishiwata, M. Soma, D. R. Naik, H. Hashimoto, T. Sudo, and H. Ishikawa. Effect of tumour angiogenesis factor on proliferation of endothelial cell and tube formation. *Virchows Archiv -A: Pathological Anatomy and Histopathology*, 417:473–476, 1990.

A. L. Jackson and L. A. Loeb. The mutation rate and cancer. *Genetics*, 148:1483–1490, 1998.

J. P. Jaffrézou, G. Chan, G. E. Durán, J. S. Kühl, and B. I. Sikic. Mutation rates and mechanisms of resistance to etoposide determined from fluctuation analysis. *Journal of the National Cancer Institute*, 86(15):1132–1158, 1994.

S. W. Johnson, D. W. Shen, I. Paston, M. M. Gottesman, and T. C. Hamilton. Cross-resistance, cisplatin accumulation, and platinum-DNA adduct formation and removal in cisplatin-sensitive and -resistant human hepatoma cell lines. *Experimental Cell Research*, 226:133–139, 1996.

A. A. Katouli and N. L. Komarova. The worst drug rule revisted: A mathematical modelling of cyclic cancer treatments. *Bulletin of Mathematical Biology*, 2010.

R. S. Kerbel. Tumour angiogenesis: past, present and the near future. *Carcinogenesis*, 21(3):505–515, 2000.

A. A. Khalil, M. R. Horsmas, and J. Overgaard. The importance of determining necrotic fraction when studying the effect of tumour volume on tissue oxygenation. *Acta Oncologica*, 34:297–300, 1995.

K. J. Kim, L. Bing, J. Winer, M. Armanini, N. Gillet, H. S. Phillips, and N. Ferrara. Inhibition of vascular endothelial growth factor-induced angiogenesis suppresses tumour growth *in vivo*. *Nature*, 362:841–844, 1999.

L. J. Kleinsmith. *Principles of Cancer Biology*. Pearson Benjamin Cummings, 2006.

A. G. Knudson. Two genetic hits (more of less) to cancer. *Nature Reviews Cancer*, 1:157–162, 2001.

M. A. Konerding, E. Fait, and A. Gaumann. 3D microvascular architecture of precancerous lesions and invasive carcinomas of the colon. *British Journal of Cancer*, 84(10):1354–1362, 2001.

F. Kozusko and Z. Bajzer. Combining gompertzian growth and cell population dynamics. *Mathematical Biosciences*, 185:153–167, 2003.

A. Krogh. The number and distribution of capillaries in muscles with calculations of the oxygen pressure head necessary for supplying the tissue. *The Journal of Physiology*, 52(6):409–415, 1919.

S. Kusama, J. S. Spratt, W. L. Donegan, F. R. Watson, and C. Cunningham. The gross rate of growth of human mammary carcinoma. *Cancer*, 30:594–599, 1972.

A. K. Laird. Dynamics of tumor growth. *British Journal of Cancer*, 18:490–502, 1964.

A. K. Laird. Dynamics of relative growth. *Growth*, 29:249–263, 1965.

A. K. Laird, S. A. Taylor, and A. D. Barton. Dynamics of normal growth. *Growth*, 29:233–248, 1965.

J. Landry, J. P. Freyer, and R. M. Sutherland. Shedding of mitotic cells from the surface of multicell spheroids during growth. *The Journal of Cellular Physiology*, 106(23), 1981.

J. Landry, J. P. Freyer, and R. M. Sutherland. A model for the growth of multicellular spheroids. *Cell and Tissue Kinetics*, 15(6):585–594, 1982.

K. E. A. LaRue, M. Khalil, and J. P. Freyer. Microenvironmental regulation of proliferation in multicellular spheroids is mediated through differential expression of cyclin-dependent. *Cancer Research*, 64:1621–1631, 2004.

L. W. Law. Origin of the resistance of leukaemic cells to folic acid antagonists. *Nature*, 169:628–629, 1952.

W. P. Leenders, B. Kusters, and R. M. de Wall. Vessel co-option: How tumors obtain blood supply in the absence of sprouting angiogenesis. *Endothelium*, 9(2):83–87, 2002.

C. K. N. Li. The glucose distribution in 9L rat brain multicell tumour spheroids and its effect on cell necrosis. *Cancer*, 50(10):2066–2073, 2006.

S. H. Lin. Oxygen diffusion in a spheroid cell with non-linear uptake kinetics. *Journal of Theoretical Biology*, 60:449–457, 1976.

Y. A. Luqmani. Mechanisms of drug resistance in cancer chemotherapy. *Medical Principles and Practice*, 14 (Suppl. 1):35–48, 2005.

S. E. Luria and M. Delbrück. Mutations of bacteria from virus sensitivity to virus resistance. *Genetics*, 28(6):491–511, 1943.

P. Marini, S. Denzinger, D. Schiller, S. Kauder, S. Welz, R. Humphreys, P. T. Daniel, V. Jendrossek, W. Budach, and C. Belka. Combined treatment of colorectal tumours with agonistic TRAIL receptor antibodies HGS-ETR1 and HGS-ETR2 and radiotherapy: Enhanced effects in vitro and dose-dependent growth delay in vivo. *Oncogene*, 25:5145–5154, 2006.

J. A. McCredie, W. R. Inch, J. Kruuc, and T. A. Watson. The rate of tumour growth in animals. *Growth*, 29:331–347, 1965.

D. L. S. McElwain. A re-examination of oxygen diffusion in a spherical cell with michaelis-menten oxygen uptake kinetics. *Mathematical Biosciences*, 71:255–267, 1978.

R. G. McKinell, R. E. Parchment, A. O. Perantoni, and G. B. Pierce. *The Biological Basis of Cancer*. Cambridge University Press, 1998.

M. L. Mendelsohn. The growth fraction: A new concept applied to tumors. *Science*, 132:1496, 1960.

F. Michor, Y. I. Iwasa, and M. A. Nowak. Dynamics of cancer progression. *Nature Reviews Cancer*, 4(3):197–205, March 2004.

R. S. J. Midgley and D. J. Kerr. ABC of colorectal cancer: Adjuvant therapy of colorectal cancer: Adjuvant therapy. *British Medical Journal*, 321:1208–1211, 2000.

P. Mistry, L. R. Kelland, S. Y. Loh, G. Abel, B. A. Murrer, and K. R. Harrap. Comparison of cellular accumulation and cytotoxicity of cisplatin with that of tetraplatin and amminedibutyratodichloro(cyclohexylamine)platinum(IV) (JM221) in human ovarian carcinoma cell lines. *Cancer Research*, 52:6188–6193, 1992.

H. C Monro and E. A. Gaffney. Modelling chemotherapy resistance in palliation and failed cure. *Journal of Theoretical Biology*, 257:292–302, 2009.

W. Mueller-Klieser. Three-dimensional cell cultures: from molecular mechanisms to clinical applications. *American Journal of Physiology*, 273:1109–1123, 1997.

W. Mueller-Klieser. Tumour biology and experimental therapeutics. *Critical Reviews in Oncology Hematology*, 36(123-139), 2000.

A. Murray and T. Hunt. *The Cell Cycle: An Introduction*. Oxford University Press, 1994.

L. Norton. A Gompertzian model of human breast cancer growth. *Cancer Research*, 48:7067–7071, 1988.

L. Norton. Conceptual and practical implications of breast tissue geometry: Toward a more effective, less toxic therapy. *The Oncologist*, 10:370–381, 2005.

L. Norton and R. Simon. Growth curve of an experimental solid tumour following radiotherapy. *Journal of the National Cancer Institute*, 58:1735–1741, 1977a.

L. Norton and R. Simon. Tumour size, sensitivity to therapy and design of treatment schedules. *Cancer Treatment Reports*, 61(7):1307–1317, 1977b.

L. Norton, R. Simon, H. D. Brereton, and A. E. Bogden. Predicting the course of Gompertzian growth. *Nature*, 264:542–545, 1976.

P. L. Olive, C. Vikse, and M. J. Trotter. Measurement of oxygen diffusion distance in tumor cubes using a fluorescent hypoxia probe. *International Journal of Radiation Oncology • Biology • Phyics*, 22(3):397–402, 1992.

O. Oudar. Spheroids: relation between tumour and endothelial cells. *Critical Reviews in Oncology Hematology*, 36:99–106, 2000.

H. M. Patt and M. E. Blackford. Quantitative studies of the growth response of the krebs ascites tumor. *Cancer Research*, 14:391–396, 1954.

M. C. Perry. *The Chemotherapy Source Book*. Lippincott, Williams, and Wilkins, 2007.

A. Persidis. Cancer multidrug resistance. *Nature Biotechnology*, 17:94–95, 1999.

D. A. Rew and G. D. Wilson. Cell production rates in human tissues and tumours and their significance. part II: Clinical data. *European Journal of Surgical Oncology*, 26 (405-417), 2000.

D. B. Rubin, E. A. Drab, and K. D. Bauer. Endothelial cell subpopulations in vitro: cell volume, cell cycle, and radiosensitivity. *The Journal of Applied Physiology*, 67 (4):1585–1590, 1989.

B. Saltin, G. Blomqvist, J. H. Mitchell, R. L. Johnson Jr., K. Wildenthal, and C. B. Chapman. Response to exercise after bed rest and after training. *Circulation*, 38, 1968.

C. L. Sawyers. Calculated resistance in cancer. *Nature*, 11(8):824–825, 2005.

B. Scappini, S. Gatto, F. Onida, C. Ricci, V. Divoky, W. G. Wierda, M. Andreef, L. Dong, K. Hayes, S. Verstovsek, H. M. Kantarjian, and M. Beran. Changes associated with the development of resistance to imatinib (STI571) in two leukemia cell lines expressing p210 Bcr/Abl protein. *Cancer*, 100(7):1459–1471, 2004.

J. A. Schetz. *Fundamentals of Fluid Mechanics*. New York; Chichester: Wiley, 1999.

B. P. Schneider and G. W. Sledge Jr. Drug insight: VEGF as a therapeutic target for breast cancer. *Nature Clinical Practice Oncology*, 4(3):181–189, 2007.

D. Shweiki, A. Itin, D. Soffer, and E. Keshet. Vascular endothelial growth factor induced by hypoxia may mediate hypoxia-initiated angiogenesis. *Nature*, 359:843–845, 1992.

D. Shweiki, M. Neeman, A. Itin, and A. Keshet. Induction of vascular endothelial growth factor expression by hypoxia and by glucose deficiency in multicell spheroids: Implications for tumor angiogenesis. *Proceedings of the National Academy of Sciences*, 92:768–772, 1995.

H. E. Skipper, F. M. Schabel Jr., and W. S. Wilcox. Experimental evaluation of potential anticancer agents XIII. on the criteria and kinetics associated with "curability" of exerperimental leukemia. *Cancer Chemotherapy Reports*, 35:1–111, 1964.

A. Strain and A. M. Diehl, editors. *Liver Growth and Repair*. London: Chapman & Hall, 1998.

W. P. Summers and R. E. Handschumacher. The rate of mutation of L5178Y asparagine-dependent mouse leukemia cells to asparagine independence and its biological consequences. *Cancer Research*, 33:1775–1779, 1973.

I. F. Tannock. The relation between cell proliferation and the vascular system in transplanted mouse mammary tumour. *British Journal of Cancer*, 22:258–273, 1968.

I. F. Tannock. Tumour physiology and drug resistance. *Cancer and Metastasis Reviews*, 20:123–132, 2001.

M. J. Tindall and C. P. Please. Modelling the cell cycle and cell movement in multicellular tumour spheroids. *Bulletin of Mathematical Biology*, 69(1147-1165), 2007.

M. J. Tindall, C. P. Please, and M. J. Peddie. Modelling the formation of necrotic regions in avascular tumours. *Mathematical Biosciences*, 211:34–55, 2008.

I. P. M. Tomlinson, M. R. Novelli, and W. F. Bodmer. The mutation rate and cancer. *Proceedings of the National Academy of Sciences*, 93:14800–14803, 1996.

N. M. Tsoukais, D. Goldman, A. Vadapalli, R. N. Pittman, and A. S. Popel. A computational model of oxygen delivery by hemoglobin-based oxygen carriers in three-dimensional microvascular networks. *Journal of Theoretical Biology*, 248: 657–674, 2007.

M. Tubiana. The kinetics of tumour cell proliferation and radiotherapy. *British Journal of Radiology*, 44:325–347, 1971.

O. Warburg. On the origin of cancer cells. *Science*, 123(3191):309–314, February 1956.

B. A. Warren and P. Shublik. The growth of the blood supply to melanoma transplants in the hamster cheek pouch. *Laboratory Investigation*, 15(2):464–478, 1966.

E. Weiss. Adenosine triphosphate and other requirements for the utilization of glucose by agents of the psittacosis-trachoma group. *Journal of Bacteriology*, 90(1):243–253, 1965.

P. Wesseling, D. J. Ruiter, and P. C. Burger. Angiogenesis in brain tumors; pathobiological and clinical aspects. *Journal of Neuro-Oncology*, 32(3):253–265, 1997.

A. White, P. Handler, E. L. Smith, R. L. Hill, and I. R. Lehman. *Principles of Biochemistry*. New York: McGraw-Hill, 1978.

R. M. White. Correct fluorouracil (5-FU) half-life comparator for a 5-FU prodrug plus a dihydropyrimidine dehydrogenase inhibitor. *Journal of Clinical Oncology*, 19(11):2970, 2001.

www.cancer.gov. Fact sheet 7.42: Angiogenesis inhibitors in the treatment of cancer. National Cancer Institute, May 2002.

www.cancer.gov. Fact sheet: Bevacizumab (avastin) for treatment of solid tumors: Questions and answers. National Cancer Institute, 2005.

www.cancer.gov. Fact sheet 7.49: Targeted cancer therapies: Questions and answers. National Cancer Institute, June 2006a.

www.cancer.gov. Fact sheet 7.18: Gene therapy for cancer: Questions and answers. National Cancer Institute, August 2006b.

www.who.int. Cancer - quick cancer facts, Last checked 23 July 2010. World Health Organization. URL `http://www.who.int/cancer/en/`.

E. D. Yorke, Z. Fuks, L. Norton, W. Whitmore, and C. C. Ling. Modelling the development of metastases from primary and locally recurrent tumors: Comparison with a clinical data base for prostatic cancer. *Cancer Research*, 33:2987–2993, 1993.